Numerical Analysis of Lithosphere Deformation

By

Jichun Sun, B.Sc.

A thesis submitted for the degree of Doctor of Philosophy
at the University of London

Department of Geological Sciences
University College London

1992

ProQuest LLC.
789 East Eisenhower Parkway
P.O. Box 1346
Ann Arbor, MI 48106 – 1346

Abstract

This thesis comprises several studies in the modelling of lithosphere deformation, using an improved thin viscous sheet model. The lithosphere is represented by a thin viscous sheet with power-law viscosity, which is deformed by external forces as surface forces and also by buoyancy forces arising through density heterogeneities. The lithosphere is in isostatic equilibrium and the effects of a lithospheric root or anti-root are incorporated. The thickness of the lithosphere, when perturbed by deformation, tends to be restored to the initial value by thermal processes which can be approximated mathematically.

The model is then used to test some hypotheses relating to the tectonics of the Tibetan Plateau. The results show that the late E-W extension of the Tibetan Plateau is probably associated with recent uplift of the plateau due to the detachment of the lower part of the thickened lithosphere, which is denser than the asthenosphere.

Three instances of continental extension leading in some circumstances to rifting have also been studied, with the mantle playing a different role in each of them: a) Airy type of compensation is assumed during extension, so that the subsidence of the top surface is totally balanced by the ascent of the Moho (or crustal anti-root); b) the subsidence of the top surface is partly compensated by the lithospheric anti-root, as well as the crustal anti-root; c) mantle upwelling elevates the lithosphere and causes initial doming. The results suggest, among other things, that currently active continental rifts, where the rifting had not been predated by initial doming, have developed along preexisting weak belts.

Acknowledgements

My study in Britain has been sponsored jointly by the State Education Commission of China, the late Sir Y. K. Bao, and the British Council.

This work has been carried out under the direct supervision of Professor S.A.F. Murrell, who is responsible for many of the ideas in the thesis. Without his help, both academically and personally, this work could not have been completed.

I thank Professor N. J. Price, who is also my supervisor, for both his criticism and encouragement. Due to his retirement, I could not see him regularly, but my discussion with him has always been stimulating and rewarding.

I am also grateful for the help of Professor M. Audley-Charles and Dr. P. Meredith on a number of difficult occasions during my study. My thanks also go to Dr. R. Hall who allowed me to use the computer facilities of his group to process some of the diagrams in my thesis.

During my stay in UCL, I obtained from Mr. Y. Hu the help I could get nowhere else. My work could have been more difficult but for his advice.

With my research I have been helped by many other members in the Department of Geological Sciences, and by the staff in UCL Computer Centre Advisory. It is not possible to list their names here. I am deeply in debt to them. Their memory and friendship I will cherish all my life.

Table of Contents

List of Tables

List of Figures

Chapter 1. Introduction

§1.1 The problem

The purpose of this work is to investigate by numerical methods the long-term and large-scale deformation of the continental lithosphere in the framework of plate tectonics.

The fundamental assumption of plate tectonics is that the Earth's surface shell is made up of a number of rigid plates that are in relative motion and that deform mainly at their edges. These plates consist of low density continental parts which are permanently resident at the Earth's surface, and higher-density oceanic parts which have only a finite residence time (~ 120 Ma) at the Earth's surface. Oceanic lithosphere is constantly being formed at spreading centres and destroyed by subduction at oceanic margins. At the oceanic spreading centres, narrow bands of seismicity define plate boundaries where the deformation is restricted and is specified completely by the relative horizontal motion of the plates on either side. At the subduction zones, however, the deformation of the surface plates and of the subducting lithosphere is complex. On the other hand, continents exhibit deformation that is distributed over horizontal distances that far exceed the plate thickness. Zones of large deformation such as the Himalayan mountain belt and the Tibetan Plateau indicate that continental plates may not be rigid as is frequently assumed in plate tectonic studies, at least not at their convergent zones. Moreover the deformation within the wide bands of continental seismicity is not specified by the relative motion of the rigid plates on either side (e.g., England & Jackson, 1989). Clear

indications that horizontal extension perpendicular to the trend of the mountain range is actually taking place despite the fact that the crust on either side of the range is under compression have been observed by Dalmayrac & Molnar (1981) in the Andes and by Molnar & Tapponnier (1978) in Tibet.

Many methods, each of which has advantages and disadvantages, have been used to simulate the deformation of the continental lithosphere. The deformation of lithosphere rocks is complicated, as it depends on their composition, structure, temperature, pressure, strain-rate, and so forth. To simulate this process, simplifications must be made. There are several ways of doing this, one of which is to represent the long term and large scale deformation of continental lithosphere by a thin viscous sheet (e.g., England & McKenzie, 1982).

In this thesis, a new thin viscous sheet model is derived and used to analyze the shortening and extension of continental lithosphere, namely

A. The deformation of continental lithosphere in convergent plate collision zones, as exemplified by the Himalayan mountain belt and the Tibetan Plateau.

B. Continental extension which may be localized, leading to rifting, or distributed, resulting in structures such as the Basin and Range in the U.S.A..

§ 1.2 Arrangement of the thesis.

In Chapter 2, the basic theory of plate tectonics, the driving forces of plate motion and deformation, and the current methodology of numerical modelling are reviewed.

In Chapter 3, a new thin viscous sheet model for lithosphere deformation is derived and discussed in order to clarify aspects of the physics of continental deformation.

Chapter 4 reviews the tectonics of the Himalayan mountain belt and the Tibetan Plateau, and the existing related modelling is compared with the new model.

In Chapter 5 the new thin viscous sheet model is applied to the evolution of the Tibetan Plateau.

Chapter 6 reviews continental extension tectonics and pertinent studies on numerical modelling.

Chapter 7 models the extension of continental lithosphere due to boundary displacements and buoyancy forces, using the new thin viscous sheet model.

In Chapter 8, a summary of this work is given, the difficulties in encountered are examined, and some suggestions are given in respect of further research.

Chapter 2. A review of lithosphere deformation

§ 2.1 Plate tectonics

The theory of plate tectonics describes the interactions of lithosphere plates and the consequences of these interactions.

The lithosphere is depicted as the strong, solid outermost shell of the earth. It has enduring resistance to a deviatoric stress of the order of a few hundred bars to one kilobar. The asthenosphere, which directly underlies the lithosphere, can be defined as a layer which has no enduring resistance to deviatoric stress. The boundary between them is gradual and is approximately an isotherm. The Earth material is not chemically different across the boundary. The asthenosphere is thought to be partially (~ 1%) molten.

The basic concept of plate tectonics is that the lithosphere is divided into a small number of nearly rigid plates, like curved caps on a sphere, which are moving over the asthenosphere. Most of the deformation which results from the plate motion, such as stretching, folding or shearing, takes place at the edges or boundaries of plates. The plate boundaries are of three types:

A. Along divergent or constructive boundaries, plates are moving away from each other. At such boundaries new plate material at high temperature, derived from the mantle, is added to the lithosphere. The divergent plate

boundary is represented by the mid-ocean ridge system, along the axis of which new plate material is produced.

B. Along convergent boundaries, also described as consuming or destructive, plates are approaching each other. Most such boundaries are represented by the oceanic trench - island arc system of subduction zones where the oceanic part of one of the convergent plates descends into the mantle and is destroyed. The downgoing plate often penetrates the mantle to depths as much as 700 km. Oceanic plates have only a finite residence time (in the order of 100 Ma) at the Earth's surface. Collision zones occur at convergent boundaries when the continental parts of converging plates come into contact.

C. Along conservative boundaries lithosphere is neither created nor destroyed. The plates move laterally past each other. These plate boundaries are represented by transform faults, of which the San Andreas fault in California, U.S.A. is a famous example.

Adjacent plates move relative to each other at rates which may be as high as 15 cm/year.

Heat is lost from the mantle by convection processes mostly through the cooling of the advecting oceanic plates. Thus oceanic plates are hot and thin at spreading centres, and cold and thick at subduction zones. Continental plates are thick and relatively cold (depending on recent thermal events such as stretching).

§ 2.2 The origin of tectonic stress in the lithosphere

The lithosphere is the relatively strong outer layer of the Earth which supports substantial deviatoric stresses, in contrast to the asthenosphere and deeper parts of the earth where the stress differences are small as a result of creep at the high prevailing temperatures. The deformation of lithosphere is the result of tectonic stresses. There are two primary categories of stresses, renewable and non-renewable types (Bott, 1982). Stress systems of renewable type are those which persist, as a result of the continued presence and re-application of the causative boundary or body forces, even though the strain energy is being progressively dissipated. The two main examples are stress systems arising from plate boundary forces and from isostatically compensated surface loads. Stress systems of non-renewable type are those which can be dissipated by release of the strain energy initially present. Bending stresses, membrane stresses and thermal stresses are of this type. Tectonic stresses in the lithosphere are effectively caused by renewable stresses, being a combination of different sources (Bott & Kusznir, 1984). They originate from two types of force: plate boundary forces and intraplate body forces.

Plate boundary forces

The various types of possible driving and resistive forces that may act on a plate have been summarized by Forsyth & Uyeda (1975) and Bott & Kusznir (1984). These are as follows.

A. The slab-pull force acting on a subducting plate and resulting from the negative buoyancy of the cooler, denser lithosphere of the sinking slab. It

comprises two parts. The first part is caused by the temperature difference between the subducting slab and the mantle, and the second part is due to the elevation of the olivine-spinel phase change within the slab compared with the mantle. This phase change occurs at depths of 300-400 km. The latter part is of about half the magnitude of the former one. This force is potentially the largest of the plate boundary forces, but is partly counteracted by resistances produced by sinking, downbending and collision. Bott & Kusznir estimate a magnitude of 0-50 MPa for this force.

B. The subduction suction force, originally recognized by Elsasser (1971) and named the 'trench suction force', is caused by the effect of subduction on the overlying plate, and is estimated to be around 20 MPa in magnitude. The nature of this force is not very clear. Both the slab-pull and the subduction-suction forces will produce tensional deviatoric stresses in adjacent lithosphere, provided that the resistance forces are sufficiently low.

C. Resisting forces due to friction at subduction zones. This force partly balances the slab pull.

D. The ridge-push force, which acts at ocean ridges, helping to force the plates apart and causing lateral compression within the adjacent ocean plates. This is a buoyancy force arising from the mass of hotter, less dense material making up the ridge, and is calculated to be 20-30 MPa in magnitude. Again, it is made up of two parts: the pushing of the upwelling mantle material and the tendency of newly formed plate to spread away from the ridge due to gravity.

An alternative approach to ridge-push force has been given by Price et al. (1988) in which gravity-glide of the whole lithosphere is involved. Ridge-push force is the major driving force for plate motion in this approach. Price et al. (1988) also explained how gravity-glide mechanism can cause the initiation of subduction and rifting. This theory gives a straightforward solution to otherwise difficult problems. For example, the formation of the Zagros mountain belt can be easily explained by ridge-push in the form of gravity-glide (Vita-Finzi, 1991). A key element in this theory is the existence of a strong layer working as a stress guide and causing large differential stresses in the lithosphere under gravity-glide ridge push. In this thesis, because I assume that the lithosphere is a homogeneous thin viscous sheet the gravity-glide mechanism has not been incorporated.

E. The mantle drag force, which is the viscous force acting on the base of a moving plate. Because of the relatively low viscosity of the asthenosphere, this force is considered to be small compared to the plate boundary forces. This force is commonly believed to be resisting plate motion (e.g. Richardson et al., 1979).

F. Resisting forces are also produced at ocean ridges and at transform faults. The former is due to the limited strength of the ridge crust, which requires some force to tear apart. The latter is due to the friction of the two sides at shallow part and the shearing of ductile mantle at deeper part. These appear to be small compared with the resistance at convergent plate boundaries.

The previously discussed forces are exerted on continental lithospheres as surface forces. Body forces due to gravity, although acting vertically, will induce horizontal pressure gradients, which can drive horizontal flow in the case of horizontal density contrast. Isostatically compensated variations in the crustal thickness are the simplest form of horizontal density variations and are the most common source of buoyancy forces in continuum models. The characteristic time for isostatic adjustment is short (in the order of 0.01 - 0.1 Ma) compared to the time scale of orogeny (~ 10 Ma) as attested by measurements of isostatic rebound and by the fact that isostatic compensation prevails on a regional scale (e.g., Jacobs et al., 1974). However, an isostatically compensated mountain range is not in hydrostatic equilibrium and will tend to spread and collapse laterally unless restrained by appropriate stress depending on the strength of the crust and lithosphere. The body forces are often called buoyancy forces. Buoyancy forces acting on large elevated plateaus are comparable in magnitude to tectonic forces associated with plate motion (Fleitout & Froidevaux, 1983; Froidevaux & Ricard, 1987; Ekstrom & England, 1989; England & Jackson, 1989). Thus deformation in regions of high elevated plateau represents the combined effect of the tectonic and the buoyancy forces.

§ 2.3 The state of stress in plates

The state of stress in the lithosphere can be speculated about based on the boundary forces. Some simple situations, which ignore the many possible complications which may occur, are generalized by Bott & Kusznir (1984) as follows:

(1). A plate which has ocean ridges on opposite sides should be in compression throughout as a result of the ridge push acting on opposite sides (Figure 2.3-1A). Example: present African plate with ridges to east and west.

(2). A plate with an ocean ridge on one side and a subduction zone on the opposite side would be expected to show a stress system which grades from compression at the ridge to tension adjacent to the subduction zone, assuming the driving forces are mainly balanced by mantle drag (Figure 2.3-1B,C). Examples: Pacific plate with slab pull force on one side and ridge push on the other; South American plate with trench suction force on one side and ridge push on the other.

(3). If subduction occurs on the opposite sides of an essentially continental plate, then the trench suction force acting on opposite sides of a plate with small overriding resistance should cause the whole plate to be subjected to lateral deviatoric tension (Figure 2.3-1D). This situation does not exist at the present stage of plate evolution, but may have applied during the early Mesozoic when Pangaea formed a large continental plate with subduction occurring on opposite sides. This stress, interacting with continental hot spot activity, may have caused the break-up of Pangaea during the Mesozoic.

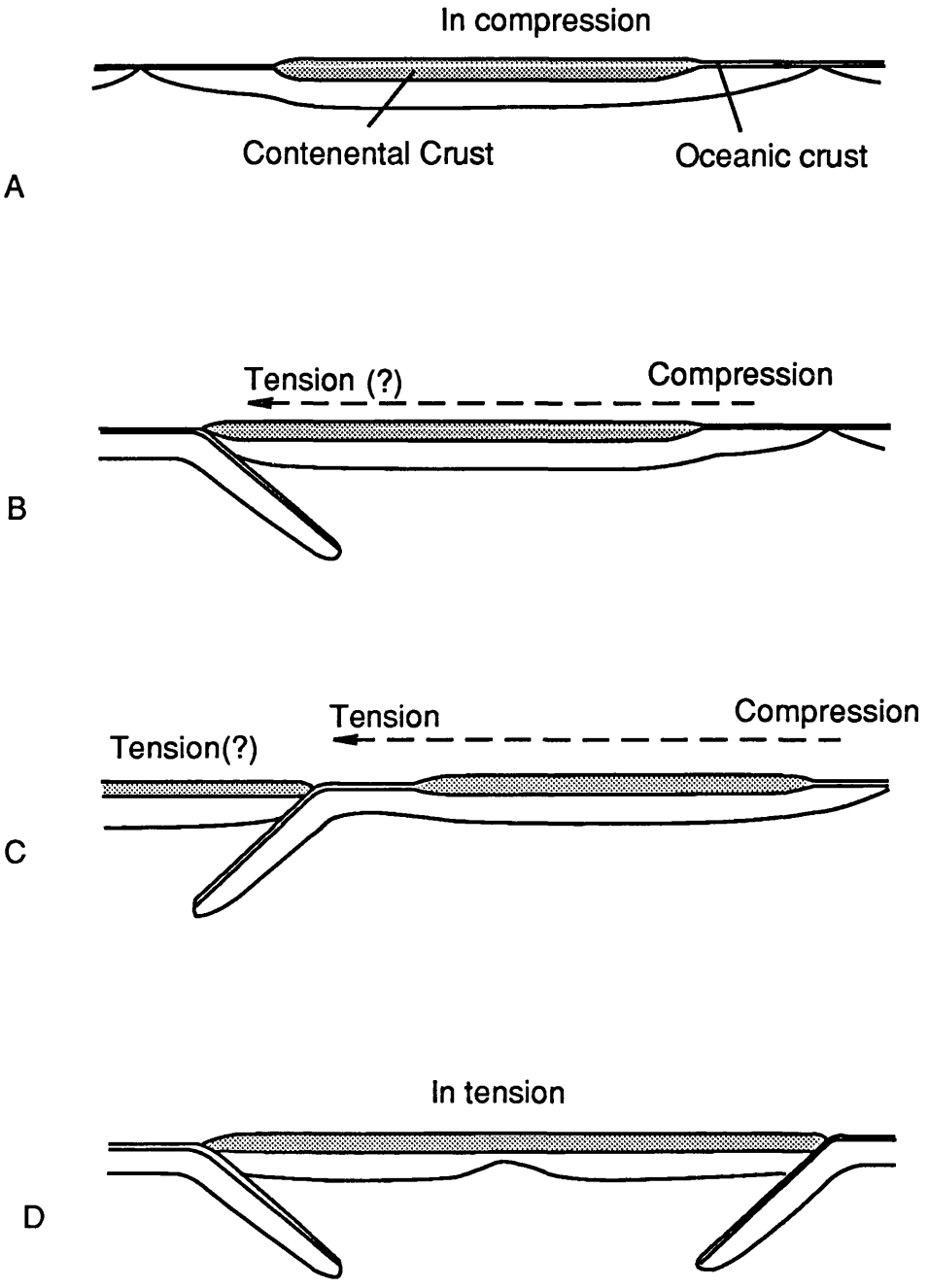

Figure 2.3-1 The expected state of stress in the lithosphere (after Bott & Kusznir, 1984).

§ 2.4. Numerical modeling and the continuum approach

The behaviour of the Earth is governed by the basic laws of mathematics, physics and chemistry. Therefore any theory about the tectonic evolution of the earth must comply with these basic laws, no matter how much other evidence supports this theory.

However, many geological problems are too complicated to be decided by physical intuitions or simple arguments.

Numerical modelling work has been developed to solve such problems. Numerical modelling in Geodynamics uses mathematical methods and physical laws to study, with some assumptions and simplifications, the tectonics of the Earth. It has at least two purposes. The first is to physically evaluate the validity or feasibility of hypotheses and discriminate between them. The second is to make predictions, e.g., if some assumptions are true, then certain conclusions are inevitable..

The importance of numerical modelling work has been demonstrated in the history of Plate Tectonics. The concept of continental drift was put forward by Frank B. Taylor in 1910 and was further developed by Alfred Wegener beginning in 1912. However, although convincing qualitative (primarily geological) arguments had been put forward by some authors (e.g., Alexander du Toit, 1937) to support continental drift, almost all earth scientists opposed the hypothesis until a sound physical explanation was available. The opposition was mainly based on arguments concerning the apparent rigidity of mantle shown by the propagation of seismic waves, and the lack of an adequate driving mechanism.

The fluid behaviour of the mantle was established quantitatively by N. A. Haskell in 1935 when modelling the post-glacial isostatic rebound in Scandinavia by treating the mantle as a viscous fluid. Haskell found the uplift can be explained if the viscosity of mantle is about 10^{20}Pas. Although this is a very large value, it leads to a fluid behaviour for the mantle over long periods of geological time.

The driving mechanism for continental drift is a more fundamental problem. Wegener suggested that either tidal forces or forces associated with the rotation of the earth caused the motion of the continents. Jeffreys (1924) showed that the value of this force is not sufficient. Other mechanisms had to be provided. Now we know that continental drift is the result of plate tectonics caused by mantle convection.

So numerical modelling plays an important role in the Earth sciences. In this thesis we use numerical modelling to investigate the deformation of continental lithosphere.

Because of the limitations of mathematical theories and of computational capacity, most investigations of the mechanics of continental deformation have treated the lithosphere as a continuous medium (e.g., Bird & Piper, 1980; England & McKenzie 1982, 1983; Lin & Parmentier, 1990).

It appears that earthquakes in regions of continental deformation account, in most cases, for over 30% and, in some cases, for almost 100% of the strain of the upper crust (Jackson & Mckenzie 1988; Ekström & England 1989). It might, therefore, seem inappropriate to treat continental

deformation as a continuum phenomenon. The question is whether the deformation of the continents may be approximated by that of a continuous medium.

The scale of continental deformation is large. Active regions have horizontal dimensions that are several times the thickness of the lithosphere, and many times the crustal thickness. Using continuum mechanics to investigate the behaviour of deforming continental lithosphere involves assuming that the discontinuities represented by faults and shear zones are small compared with the thickness of the lithosphere. If this assumption is correct, then the continuum approach to the mechanics of the continental lithosphere may be a reasonable one.

The occurrence of earthquakes shows that, at some scale, the deformation must be treated as discontinuous. The point is that the seismic zone is only 10 - 15 km thick, and only for $M > 6.0$ earthquakes is the strike of the active fault greater than this. Most earthquake ($M < 7.0$) faults have dimensions less than 10 km x 100 km approximately. An approach that treats the continents as continuous will not provide all the answers on all observable scales; on the other hand, the simple physical arguments that follow from treating the lithosphere as being continuous on the large scale have given some useful insights to the mechanics of the continents.

Hence, although the deformation may be intermittent in time and discontinous in space, there is both necessity and justification to approximate it by continuum method in the long term and at the large scale. There have been few attempts to use non-continuum approaches in numerical modelling. In 1991 Bird & Kong announced the first fully converged solution

incorporating realistic fault networks. Experimental modelling has been often used to investigate deformation involving discontinuities (i.e., faults). For example, Tapponnier et al. (1982) studied the faulting produced in a layered plasticine block being penetrated by a rigid indenter, and compared it with the large faulting system in East Asia. Davy et al. (1990) made similar experiments, and argued that the the existence of undeformed regions in the midst of otherwise penetrative deformation could arise naturally from a fractal style of continental faulting, and that these regions were not necessarily strong.

§ 2.5 The two types of numerical models

Having made the assumption of continuity, the numerical analysis is usually carried out in two dimensions. Fully three dimensional models are ideal but so far few attempts have been made to investigate that way because of the huge amount of computing involved (more discussion concerning this can be found in Bird 1989). There are mainly two types of two dimensional numerical models: those that investigate in the vertical section, and those that investigate in the horizontal domain.

The planes studied in the vertical section models are usually chosen to be perpendicular to the major structural lines such as the strike of rift valleys. They usually make the plane strain assumption (e.g., Wang et al., 1982, Lin & Parmentier, 1990), which assumes a) that displacement normal to the plane in study is zero, and b) that the stresses and strains do not vary in the direction normal to the plane. This is probably the mostly widely used type of model. Models of this type have been used to study crust and mantle deformation processes in various tectonic circumstances including

rifting (e.g., Zuber & Parmentier, 1986, Lin & Parmentier, 1990), subduction (e.g., Wdowinski et al., 1989, 1991), continental collision (e.g., Wang et al., 1982), etc..

The horizontal models are less used than the vertical section models. Most investigators working in the horizontal domain make use of the thin-sheet approximation (e.g., Bird & Piper 1980). In this approximation, stresses acting on the top and base of the lithosphere are assumed to be negligible, as are the surface slopes, so shear stress on horizontal planes within the lithosphere are negligible compared with the other components of the stress tensor. Under these conditions, one principal stress is vertical, and is equal to the weight per unit area of overlying rock. Neglecting shear stresses on horizontal planes is equivalent to assuming that the top of the lithosphere is not displaced horizontally relative to its base; the behaviour of the system then depends on the vertical averages of the stresses acting within the lithosphere.

The assumption that the top of the lithosphere is not displaced appreciably with respect to its base may seem to be not realistic considered in the light of field observation. Thin sheet model is effectively "pure shear" model, in which a vertical reference line remains vertical during deformation. All thrusts and normal faults do contain such components of shear, and there is abundant evidence in the fabrics of rocks deformed in the ductile regime that they have undergone sub-horizontal shear. However, provided that the continuum hypothesis is tenable for a given region, a distributed set of thrust or normal shear zones produces horizontal displacement of the top of the lithosphere with respect to its base that is small compared with the total shortening or extension.

Another challenge to the thin sheet model is the possibility of channel flow in the lower crust. Materials migrate horizontally through the weak layer of the lower crust under pressure differences and the Moho topography is thereby smoothed (Kusznir & Matthews, 1988; Bird, 1991; Kruse et al., 1991). This process is very much wavelength-dependent, with medium wavelength topography decaying fastest (Kusznir & Matthews, 1988). Since long-wavelength Moho topography is not readily removed by channel flow, the thin sheet model is not invalidated in large-scale lithosphere deformation studies. Although the thin sheet model has many shortcomings, and Bird (1989) has introduced a more realistic by complicated model to replace it, it still appeals to numerical modellers due to its simplicity. For example, Buck (1991) still makes the thin sheet assumption in studying the mode of rifting.

Both types of models have advantages and disadvantages. The former one is suitable to study the vertical distribution of stress and strain. It can use vertically varying rheology more easily, and is therefore clearer physically. The latter one illustrates the horizontal distribution of deformation, and this is ofter important in geology.

In Chapter 3, a model in the horizontal domain for the deformation of lithosphere is derived based on the thin sheet assumption. The lithosphere is of power-law viscous rheology. It is subjected to both boundary surface forces and the intraplate body forces due to lateral density contrast. In Chapters 4, 5, 6 and 7, the model is compared with existing ones and used to investigate large scale deformation, in particular, the shortening and extension, of continental lithosphere.

Chapter 3. A General thin viscous sheet model

This chapter comprises six parts. § 3.1 deals with the thermal processes associated with lithosphere deformation. § 3.2 deals with the rheology of the lithosphere. § 3.3 derives the governing mechanical equations for the deformation, which must take into account body forces as well as external tectonic forces. The lithosphere during deformation is taken to be in an isostatic state. § 3.4 gives the equations for calculating the evolution of the surface layer, Moho layer and the lower boundary of the lithosphere in isostatic equilibrium during deformation. § 3.5 discusses the effect of erosion and sedimentation. § 3.6 discusses some special cases to clarify the physics of the model. § 3.7 introduces the numerical method used to solve the equations.

§ 3.1 The thermal processes:

The thickness of the lithosphere is affected by thermal processes as well as mechanical processes. Thermal processes always tend to restore the thickness of lithosphere to a thermally stable one, if the thickness is changed by a mechanical perturbation. There is no analytic solution to this problem because of the moving boundary between the lithosphere and the underlying asthenosphere (which can only sustain weak shear stresses and in which heat is transferred principally by convection). McKenzie (1978) and England & Sonder (1989) gave two approximate solutions to the thermal problem of a thinned lithosphere. However neither of them took into account

the sharp contrast between the thermal behaviour of the lithosphere and of the asthenosphere, and neither of them can be applied to the case of a thickened lithosphere. In this work I have derived an approximate solution based on the following four approximations:

A. Although heat transfer in the asthenosphere is primarily convective, it is represent effectively as a conductive process with a large and constant value for the effective thermal conductivity (k') and diffusivity (κ'). In addition, the effective heat conduction is taken as totally vertical.

B. The temperature in both lithosphere and asthenosphere is approximated as a piecewise linear function of depth, with $\overline{dT/dz}$ in the lithosphere >> $\overline{dT/dz}$ in the asthenosphere, where $\overline{dT/dz}$ is the mean value of dT/dz, at any time, $\overline{dT/dz}$ is related to the thickness of the lithosphere (Figure 3.1-1).

C. The thermal conductivity (k) and the diffusivity (κ) of the lithosphere are taken as uniform and constant.

D. As with the previous works, heat generated in the lithosphere or asthenosphere is neglected.

In an ideal lithosphere (thermally stable, solid lines in Figure 3.1-1), heat input equals output, so by Fourier's law

$$k' \frac{(T_A - T_L)}{A_o} = k \frac{T_L}{L_o}$$

i.e.,

$$k' = k \frac{A_o T_L}{L_o (T_A - T_L)} \qquad (3.1\text{-}1)$$

in which Ao is the normal equilibrium thickness of the asthenosphere, Lo is the equilibrium thickness of the lithosphere, T_L is the temperature of the

lower boundary of the lithosphere, and T_A that of the lower boundary of the asthenosphere.

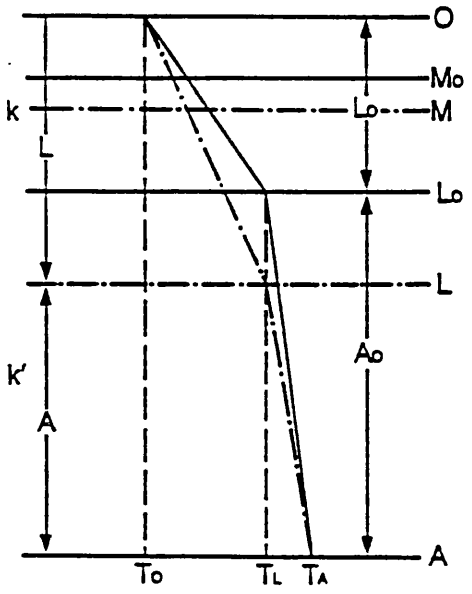

Figure 3.1-1. Temperature distribution in the thermally stable lithosphere and asthenosphere (solid line) and the deformed lithosphere and asthenosphere (dashed line). To, T_L and T_A are the temperature of the top surface, the base of the lithosphere, and the base of the asthenosphere respectively. Lo and Ao are the thickness of thermally stable lithosphere and asthenosphere respectively. L and A are the thickness of the deformed lithosphere and asthenosphere respectively. k and k′ are the conductivity of the lithosphere and the asthenosphere respectively.

At any time (dashed lines in Figure 3.1-1), the heat quantity inside the lithosphere and asthenosphere is (assuming ρ, the density, and c, the specific heat capacity in the lithosphere is the same as in the asthenosphere)

$$Q=\frac{1}{2}\rho cLT_L+\frac{1}{2}\rho cA(T_L+T_A)$$

so

$$\frac{dQ}{dt}=\frac{1}{2}\rho cT_A\frac{dA}{dt}=-\frac{1}{2}\rho cT_A\frac{dL}{dt} \qquad (3.1\text{-}2)$$

The difference between heat input and output of the lithosphere is

$$k'\frac{(T_A-T_L)}{A}-k\frac{T_L}{L}$$

(which, using (3.1-1))

$$=\frac{Ao}{Lo}k\frac{T_L}{A}-k\frac{T_L}{L}$$

$$=k\frac{T_L}{Lo}(\frac{Ao}{A}-\frac{Lo}{L})$$

$$=k\frac{T_L}{Lo}(\frac{Ao}{Ao+Lo-L}-\frac{Lo}{L}) \qquad (3.1\text{-}3)$$

This difference is equal to the rate of variation of the quantity of heat inside the lithosphere and asthenosphere, so

$$-\frac{1}{2}\rho cT_A\frac{dL}{dt}=k\frac{T_L}{Lo}(\frac{Ao}{Ao+Lo-L}-\frac{Lo}{L})$$

and finally, the rate of thermal thickening or thinning of a lithosphere with a thickness L is

$$\frac{dL}{dt}=\frac{k}{\rho c}\frac{2T_L}{LoT_A}(\frac{Lo}{L}-\frac{Ao}{Ao+Lo-L}) \qquad (3.1\text{-}4)$$

In a non-dimensional form this can be expressed as an incremental relationship between lithosphere thickness changes $\Delta(\frac{L}{Lo})$ and time step $\Delta(\frac{t}{t_o})$.

$$d(\frac{L}{Lo})=H(\frac{Lo}{L}-\frac{Ao}{Ao+Lo-L})d(\frac{t}{t_o}) \qquad (3.1\text{-}5)$$

where $H=\frac{2kT_L}{\rho cLoT_AUo}=\frac{2\kappa T_L}{LoT_AUo}$, $t_o=\frac{Lo}{Uo}$, and Uo is a scaling factor for the typical horizontal velocity of displacement in the lithosphere. In this

problem, Uo is chosen as 5 cm/year.

According to Carslaw & Jaeger [1959,(Appendix VI)], the thermal diffusivity for average rock is 1.18×10^{-6} m^2s^{-1}. Because the temperature gradient at the top surface is about three times the average temperature gradient of the lithosphere, it would be reasonable to assume that the average diffusivity of the lithosphere, κ, is $3 \times 1.18 \times 10^{-6}$ m^2s^{-1}. So if Uo=5cm/year, then H=0.04.

From the formula, it can be seen that dL/dt=0 when L=Lo, dL/dt>0 when L<Lo, and dL/dt<0 when L>Lo. So this new formula is at least qualitatively correct, although it is still very primitive.

The formula can be tested (not calibrated, unfortunately) in the following way: suppose a lithosphere with stable thickness L_o is thickened or thinned mechanically to thickness L simultaneously, then the thermal process will begin to restore L to L_o. The calculated relative thickness L/L_o against time t is shown in Figure 3.1-2. It is seen that thinned lithosphere restores faster than thickened lithosphere, and those with smaller initial thickness restore faster than those with bigger initial thickness. This is in line with our general understanding of the thermal process. It also shows that with L_o=100 km, in 60 Ma L is restored to within more than 95 % of its initial thickness, L_o, which agrees with McKenzie's conclusion that thermal anomalies of stretched lithosphere die out in the order of 60 Ma.

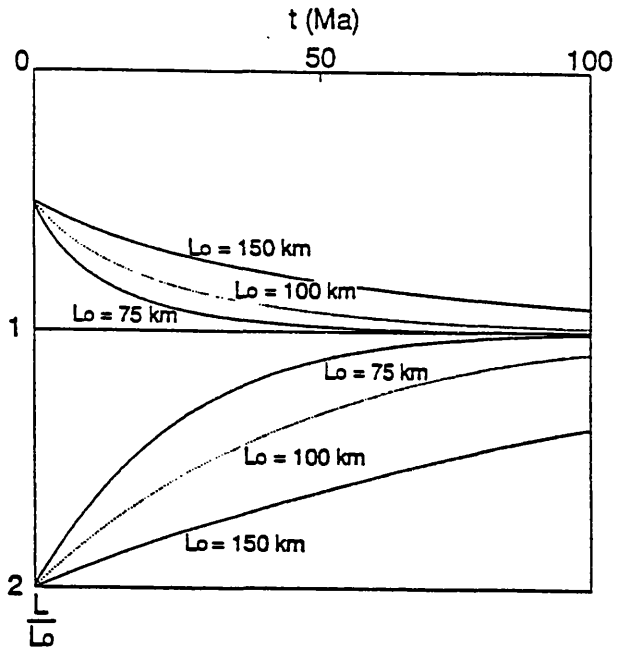

Figure 3.1-2 The thermal restoration process as calculated using the derived formula and assumed parameters.

§ 3.2 The rheology of the lithosphere

In the first part of this section, I introduce a previously used (e.g., England & McKenzie, 1982) formulation of the average stress and strain-rate relation of the lithosphere, which is based on the assumption that the strength of the lithosphere is controlled by the temperature-dependent part

of the lithosphere. In the second part of this section, I give a new formula describing the stress and strain-rate relation, which takes into account not only the strength of the temperature-dependent part of the lithosphere, but also the upper part of the lithosphere where deformation is in the form of brittle failure. Both types of formulation will be used in the later part of this thesis.

The upper crust deforms in a discontinuous manner by faulting. Although faults are prominent in the surface geological record, they represent only the failure of the outermost, brittle layer of the lithosphere, and not necessarily that of the lithosphere as a whole. The response of the lithosphere to applied forces is largely controlled by the rheology of the strongest portion of the lithosphere. Laboratory determinations of the rheology of olivine and other minerals representative of the crust and upper mantle indicate that at high temperatures they deform by power law creep according to a law like

$$\dot{\varepsilon} = C(\sigma_1 - \sigma_3)^n \exp(\frac{-Q}{R\vartheta}) \qquad (3.2\text{-}1)$$

in the range of conditions likely to apply to the deformation of the continental lithosphere. C is a constant of the material, σ_1 and σ_3 are the greatest and the least principle stresses, ϑ is the absolute temperature, R is the gas constant and Q is the activation energy for the relevant deformation mechanism. Rewriting (3.2-1), we have

$$\sigma_1 - \sigma_3 = \frac{1}{C} \cdot \exp(\frac{Q}{nR\vartheta}) \dot{\varepsilon}^{1/n}$$

$$= B \cdot \dot{\varepsilon}^{1/n} \qquad (3.2\text{-}2)$$

where $B = \frac{1}{C} \cdot \exp(\frac{Q}{nR\vartheta})$. B is therefore a measure of the strength of the

Earth material. If the vertical gradient of horizontal velocity is negligible, the above equation can be replaced by an average stress and strain-rate relation for the whole lithosphere in the form of

$$\sigma_1 - \sigma_3 = \bar{B} \cdot \dot{\varepsilon}^{1/n} \qquad (3.2\text{-}3)$$

where $\bar{B}$ averages, throughout the lithosphere, the temperature dependent parts of equation 3.2-2. Among other factors, $\bar{B}$ is dependent on the vertical temperature distribution in the lithosphere. But having made the linear assumption in § 3.1 for the temperature profile, $\bar{B}$ can be treated as constant to a first order of approximation. The problem may now be formulated in terms of the deformation of a homogeneous power law material that is assumed to be isotropic and incompressible.

The above treatment assumes that the strength of the lithosphere lies in the temperature-dependent portion in the lower crust or upper mantle, and was first used in England & McKenzie (1982). However, the strength of the shallower part of the lithosphere may also be important. Sonder and England (1986) suggest this strength may be included to some extent by increasing the exponent in the power-law rheology. Here I use another approach to include the strength of upper layer of lithosphere in the simple rheology formulation. A more detailed analysis follows.

In the lower crust and upper mantle, the strength of Earth material declines exponentially as temperature T increases. It also depends on the melting temperature and therefore increases, but much less rapidly, with pressure. At shallow depth (low temperatures and pressures) there is a brittle-ductile transition, and in the surface layer of the lithosphere deformation is dominated by cataclasis and fracture, for which the strength is lower than the plastic flow strength. In this brittle layer the strength

is nearly independent of temperature but increases with pressure in an approximately linear fashion. (See Murrell 1986 for further discussion) So the strength of the Earth material increases with depth to a maximum value, then decreases exponentially. I am aware that the definition of "strength" is different at the shallow and deep depth and the shallower part of the lithosphere can not be completely represented by power-law viscous material, but for simplicity, the two parts are treated in the same way. I assume that the depth of maximum strength is determined by a critical temperature, Tc. Above the depth Lc with critical temperature Tc, the strength increases linearly as pressure increases with depth, and below that depth strength decreases exponentially as temperature increases with depth, as shown in Figure 3.2-1.

Let B_{max} and B_{omax} be the maximum strength in deformed and in normal equilibrium lithosphere respectively, and Lc and Loc be the corresponding depths in the lithosphere at which the strength reaches its maximum value. Because the maximum strength varies in the same ratio as the depth of critical temperature, then

$$B_{max} \approx B_{omax}\frac{Lc}{Loc}$$

and furthermore, approximately, the new average "strength" is given by

$$\bar{B} = \bar{B}o\frac{Lc}{Loc}$$

If the deformation is vertically uniform, then

$$\frac{Lc}{Loc} = \frac{L}{Lo}$$

So, finally

$$\bar{B} = \bar{B}o\frac{L}{Lo} \qquad (3.2\text{-}4)$$

This formula shows that the average strength is increased (or decreased) by the same ratio as the lithosphere is mechanically thickened (or thinned). So a thickened lithosphere is stronger not only because there is a larger thickness to resist deformation but also because the average strength is increased as well. For a thinned lithosphere, the reverse is the case. This is of course a simplification. The true value of $\bar{B}$ may be between $\bar{B}o$ and $\bar{B}o\frac{L}{Lo}$.

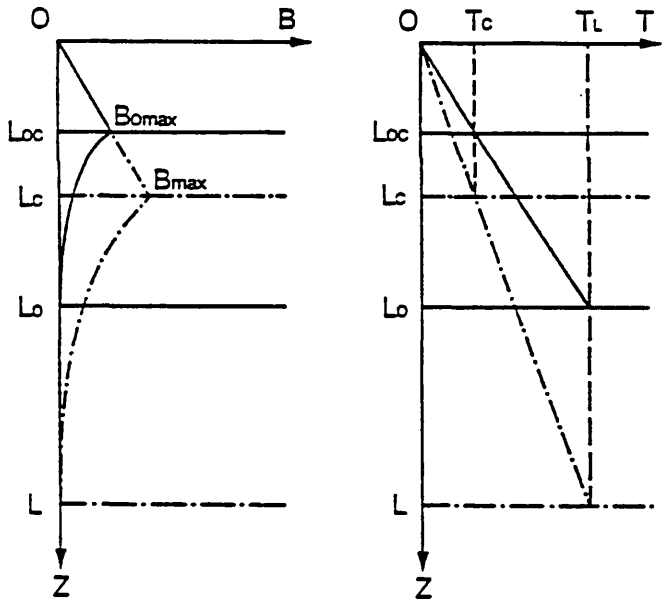

Figure 3.2-1 The strength (A) and the temperature distribution (B) of the initial (solid line) and deformed (dashed line) lithosphere.

The thickness-related average strength formulation can also be justified empirically. In the case of continental shortening it provides an alternative mechanism for limiting the continental thickening (the common explanation for the limit is the buoyancy force from the high gravity potential due to crustal thickening, but Fleitout & Froidevaux [1982] have demonstrated that thickened lithosphere does not necessarily tend to extend). In the case of continental extension, it partly simulates the effect of the failure of the brittle layer on the average strength of the whole lithosphere, which is otherwise not represented in the viscous sheet model.

Now the problem is reduced to the deformation of a thin viscous sheet of power-law viscosity, with constant or thickness related strength parameter $\bar{B}$.

To be applicable in a general numerical analysis, the strength and strain rate relationship may be generalized as

$$\tau_{ij}=B\dot{E}^{(1/n-1)}\dot{\varepsilon}_{ij} \qquad (3.2\text{-}5)$$

in which $\dot{E}$ is the square root of the second invariant of the strain rate tensor, and τ_{ij} and $\dot{\varepsilon}_{ij}$ are the components of the stress and strain-rate tensors respectively (See Ranalli [1987] for more details).

§ 3.3 The mechanical equations:

In this section, I give the results of my derivation of new equations describing the deformation of the lithosphere under buoyancy forces as well as external forces. One advantage of the equations to be derived is that

they allow the asthenosphere to have different densities from the lithosphere mantle, whereas in previous studies of numerical modelling in the horizontal domain making use of the thin sheet assumption compensation is achieved within the lithosphere so that the asthenosphere does not come into the model. Another improvement is that they can be applied to the lithosphere covered by water or loose sediments. The whole derivation is independent of previous studies, although it too is based on the thin sheet assumptions, which are

A. The rheology of the lithosphere is vertically averaged .

B. The deviatoric stress is also vertically averaged.

C. For mathematical convenience, shear stress in the vertical direction is neglected so that the weight of every vertical column is totally supported by the underlying asthenosphere. The lithosphere is in isostatic state.

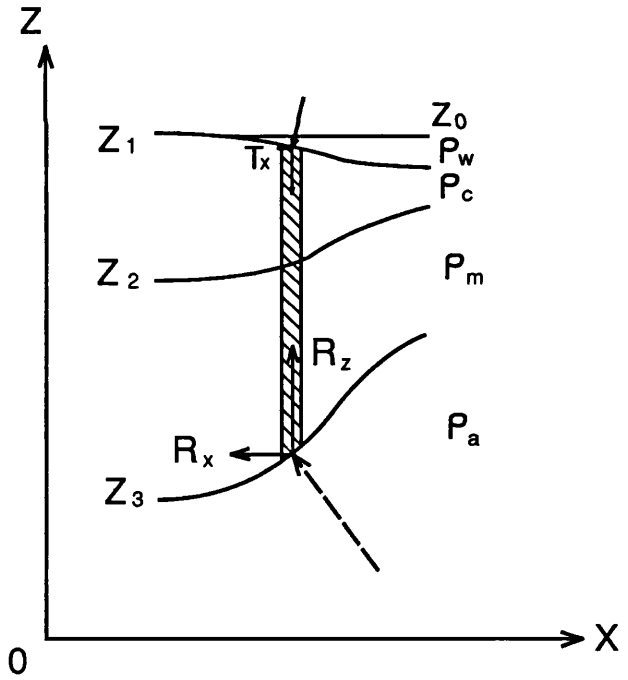

Figure 3.3-1. Part of the lithosphere under study.

Referring to Figure 3.3-1, consider a vertical column element in a thin

viscous sheet covered by water. In the x-direction, for equilibrium, we have

$$\frac{\partial}{\partial x}\left(\int^{L}\sigma_x dz\right) + \frac{\partial}{\partial y}\left(\int^{L}\tau_{xy} dz\right) + T_x + R_x = 0 \qquad (3.3\text{-}1)$$

where R_x is the x component of the force exerted by the asthenosphere on the bottom of the lithosphere, T_x is that exerted by the water on the top of the lithosphere, and L is the thickness of the lithosphere.

Let $\tau_x = \sigma_x - \frac{1}{3}(\sigma_x+\sigma_y+\sigma_z)$,

$\tau_y = \sigma_y - \frac{1}{3}(\sigma_x+\sigma_y+\sigma_z)$

then $\sigma_x = 2\tau_x + \tau_y + \sigma_z$, and $\sigma_y = 2\tau_y+\tau_x+\sigma_z$. Substituting these into eq.(3.3-1) we obtain

$$\frac{\partial}{\partial x}\left[\int^{L}(2\tau_x+\tau_y)dz\right] + \frac{\partial}{\partial y}\left(\int^{L}\tau_{xy} dz\right) + \frac{\partial}{\partial x}\left(\int^{L}\sigma_z dz\right) + T_x + R_x = 0 \qquad (3.3\text{-}2)$$

in which $\frac{\partial}{\partial x}\left(\int^{L}\sigma_z dz\right) = \int^{L}\frac{\partial}{\partial x}\sigma_z dz + \frac{\partial Z_1}{\partial x}\sigma_z\Big|_{Z=Z1} - \frac{\partial Z_3}{\partial x}\sigma_z\Big|_{Z=Z3}$

where Z_1 is the level of the top of the lithosphere, and Z3 that of the bottom of the lithosphere, measured relative to a compensation level deep in the asthenosphere. σ_z is zero on the top of lithosphere,

$$\frac{\partial Z_1}{\partial x}\sigma_z\Big|_{Z=Z1} = -T_x$$

$$\frac{\partial Z_3}{\partial x}\sigma_z\Big|_{Z=Z3} = R_x$$

So eq.(3.3-2) becomes

$$\frac{\partial}{\partial x}\left[\int^{L}(2\tau_x+\tau_y)dz\right] + \frac{\partial}{\partial y}\left(\int^{L}\tau_{xy} dz\right) + \int^{L}\frac{\partial}{\partial x}\sigma_z dz = 0$$

where $\sigma_z = -\int_{z}^{Z_o}\rho g dz$

in which Zo is the level of the water surface measured in the same way as Z_1 and Z_3.

Calculating $\int^L \frac{\partial}{\partial x}\sigma_z dz$, making use of assumption C., we have

$$\int^L \frac{\partial}{\partial x}\sigma_z dz = - \int^L (\rho_c-\rho_w)g\frac{\partial Z_1}{\partial x} - \int_{Z3}^{Z2} (\rho_m-\rho_c)g\frac{\partial Z_2}{\partial x}$$

in which Z_2 is the level of the Moho surface measured in the same way as Z_1 and Z_3. Applying assumption B., then we obtain the equation for force equilibrium (in the x-direction)

$$\frac{\partial}{\partial x}[L(2\tau_x+\tau_y)]+ \frac{\partial}{\partial y}(L\tau_{xy})- (\rho_c-\rho_w)gL\frac{\partial Z_1}{\partial x} -(\rho_m-\rho_c)g(L-s)\frac{\partial Z_2}{\partial x} = 0 \qquad (3.3\text{-}3)$$

in which s is the thickness of the crust. According to the definition of strain-rate and making use of eq.3.2-5, we have

$$\tau_{xy}= \bar{B}\dot{E}^{(1/n-1)}\frac{1}{2}(\frac{\partial v}{\partial x} + \frac{\partial u}{\partial y}) \qquad (3.3\text{-}4)$$

$$\tau_x = \bar{B}\dot{E}^{(1/n-1)}\frac{\partial u}{\partial x} \qquad (3.3\text{-}5)$$

$$\tau_y = \bar{B}\dot{E}^{(1/n-1)}\frac{\partial v}{\partial y} \qquad (3.3\text{-}6)$$

where u and v are the velocities in the x and y direction respectively. Substituting equations (3.3-4), (3.3-5) and (3.3-6) into eq.(3.3-3), rearranging the equation, then we have

$$2\frac{\partial^2 u}{\partial x^2} + \frac{1}{2}\cdot\frac{\partial^2 u}{\partial y^2} = - \frac{3}{2}\frac{\partial^2 v}{\partial x\partial y} - \frac{\dot{E}^{(1-1/n)}}{L\bar{B}}[(2\frac{\partial u}{\partial x} + \frac{\partial v}{\partial y})\frac{\partial}{\partial x}(L\bar{B}\dot{E}^{(1/n-1)})$$
$$+ \frac{1}{2}(\frac{\partial u}{\partial y} + \frac{\partial v}{\partial x})\frac{\partial}{\partial y}(L\bar{B}\dot{E}^{(1/n-1)})]+ \frac{\dot{E}^{(1-1/n)}}{L\bar{B}}[(\rho_c - \rho_w)gL\frac{\partial Z_1}{\partial x} +(\rho_m -\rho_c)(L- s)\frac{\partial Z_2}{\partial x}]$$

(3.3-7)

It is more convenient to express it in a non-dimensional form. Let $L=\mathit{L}L_o$, $x=\mathit{x}L_o$, $y=\mathit{y}L_o$, $Z_1=Z_1L_o$, $Z_2=Z_2L_o$, $u=\mathit{u}u_o$, $v=\mathit{v}u_o$, $\bar{B}=\mathit{B}\bar{B}_o$, $\dot{E}=\dot{\mathit{E}}\cdot\frac{u_o}{L_o}$, then eq.(3.3-7) becomes

$$2\frac{\partial^2 u}{\partial x^2}+\frac{1}{2}\cdot\frac{\partial^2 u}{\partial y^2}=-\frac{3}{2}\frac{\partial^2 v}{\partial x\partial y}-\frac{\dot{E}^{(1-1/n)}}{LB}\left[\left(2\frac{\partial u}{\partial x}+\frac{\partial v}{\partial y}\right)\frac{\partial}{\partial x}\left(LB\dot{E}^{(1/n-1)}\right)\right.$$
$$\left.+\frac{1}{2}\left(\frac{\partial u}{\partial y}+\frac{\partial v}{\partial x}\right)\frac{\partial}{\partial y}\left(LB\dot{E}^{(1/n-1)}\right)\right]+A\frac{\dot{E}^{(1-1/n)}}{LB}\left[\left(1-\frac{\rho_w}{\rho_c}\right)\frac{\partial Z_1}{\partial x}+\left(\frac{\rho_m}{\rho_c}-1\right)\left(1-\frac{s}{L}\right)\frac{\partial Z_2}{\partial x}\right] \tag{3.3-8a}$$

where we define $A=\rho_c g\frac{L_o^{((1/n)+1)}}{u_o^{1/n}\,\bar{B}_o}$. (3.3-9)

Similarly, in the y direction, the equation for force equilibrium in a non-dimensional form is

$$2\frac{\partial^2 v}{\partial y^2}+\frac{1}{2}\cdot\frac{\partial^2 v}{\partial x^2}=-\frac{3}{2}\frac{\partial^2 u}{\partial x\partial y}-\frac{\dot{E}^{(1-1/n)}}{LB}\left[\left(2\frac{\partial v}{\partial y}+\frac{\partial u}{\partial x}\right)\frac{\partial}{\partial y}\left(LB\dot{E}^{(1/n-1)}\right)\right.$$
$$\left.+\frac{1}{2}\left(\frac{\partial u}{\partial y}+\frac{\partial v}{\partial x}\right)\frac{\partial}{\partial x}\left(LB\dot{E}^{(1/n-1)}\right)\right]+A\frac{\dot{E}^{(1-1/n)}}{LB}\left[\left(1-\frac{\rho_w}{\rho_c}\right)\frac{\partial Z_1}{\partial y}+\left(\frac{\rho_m}{\rho_c}-1\right)\left(1-\frac{s}{L}\right)\frac{\partial Z_2}{\partial y}\right] \tag{3.3-8b}$$

In eq.(3.3-8a,b), if $\bar{B}=\bar{B}_o$, then $B=1$; if $\bar{B}=\frac{L}{L_o}\bar{B}_o$, then $B=L$.

The final terms in equations (3.3-8a), (3.3-8b) containing the factor A express the effect gravitational forces can have on the horizontal deformation of the lithosphere.

From its definition, it can be seen that A is a measure of the inverse of the average lithosphere strength, and the variation of its value is primarily due to the variation of $\bar{B}$. To put a constraint on the value of A,

the relationship between the value of A and the equivalent viscosity of the lithosphere is given below.

From eq.3.2-5, the equivalent viscosity of the thin sheet of the lithosphere at the beginning of deformation is

$$\frac{\tau_{ij}}{\dot{\varepsilon}_{ij}} = \bar{B}o\dot{E}^{(1/n-1)} \qquad (3.3\text{-}10)$$

Using eq.(3.3-9), eq.(3.3-10) becomes

$$\frac{\tau_{ij}}{\dot{\varepsilon}_{ij}} = \rho_c g \frac{L_o^{((1/n)+1)}}{u_o^{1/n} A} \dot{E}^{(1/n-1)} \qquad (3.3\text{-}11)$$

With n = 3, u_o = 5cm/year, L_o=100km, ρ_c = 2900kg/m^3, g = 9.8m/s^2, the equivalent viscosity is about $\frac{10^{22}}{A}$ Pas at a strain rate of $10^{-12}s^{-1}$, and about $\frac{10^{24}}{A}$ Pas at a strain rate of $10^{-15}s^{-1}$. So the value of A typically ranges from 1 to 100. England and Mckenzie (1982, 1983) have introduced a similar scaling factor Ar, which they call the Argand number. Their definition of the Argand number is

$$Ar = \rho_c g \frac{L_o^{((1/n)+1)}}{u_o^{1/n} B}(1- \frac{\rho_c}{\rho_m})$$

So for the same lithosphere the relationship between Ar and A is

$$Ar = A(1- \frac{\rho_c}{\rho_m}) \qquad (3.3\text{-}12)$$

It may be more appropriate to call A the re-defined Argand number. But for simplicity, A is just called the A number in this thesis.

The equations (3.3-8a) and (3.3-8b) show that the horizontal flow due to gravity is contributed by the topography of both the upper surface and

the Moho surface of the lithosphere. For continental lithosphere in isostatic equilibrium, the two effects usually partly cancel each other because shortening causes the subsidence of the Moho surface and the elevation of the upper surface of the lithosphere while stretching causes the elevation of the Moho surface and the subsidence of the upper surface of the lithosphere (provided that the crustal thickness s is no less than 18 km, see McKenzie 1978 and Murrell 1986). If the top elevation is totally compensated by a crustal root in the mantle, the effect of the top topography will dominate and thickened lithosphere will tend to extend under gravity. If, however, the top elevation is compensated not only by a crustal root in the mantle but also by a lithosphere root in the asthenosphere, there will be the possibility that the effect of the Moho topography dominates and that the lithosphere which has been thickened by shortening is in general compression under gravity forces. This result is in line with that of Fleitout & Froidevaux (1982), who studied the effect of density heterogeneities in the lithosphere. Because the variation of the top surface and of the Moho is the major source of lithosphere density heterogeneities, the mechanical equations given in this section describe the role of density heterogeneities more directly than the method of Fleitout & Froidevaux (1982), and can be used more easily in large-scale numerical modelling of lithosphere deformation.

The above equations are for the part of the lithosphere covered with water or sediment. The deformation of the part of lithosphere without water coverage is also described by the above equations by taking $\rho_w = 0$. The effect of sedimentation will be discussed further in § 3.5.

§ 3.4 Vertical displacement during deformation.

When a lithospheric plate is stretched or shortened, the elevation of its top surface, Moho surface, and lower boundary will usually change. McKenzie (1978) has calculated the basin subsidence caused by instantaneous stretching followed by thermal cooling. But because of the instantaneous stretching assumption McKenzie's formula is not suitable for this thesis. Later Jarvis & McKenzie (1980) studied basin subsidence caused by finite-rate stretching, but the solution is derived for stretched lithosphere only, and it is not convenient for a study in which not only the thermal process but also the mechanics of lithosphere extension or shortening are of concern. In this section I derive simple formulae describing the step-by-step changing of the three surfaces (top surface, Moho surface, and the lower boundary of lithosphere) of the lithosphere subjected to mechanical deformation and also thermal restoration, which are valid for both lithosphere shortening and extension. Before deriving the equations describing the vertical displacement of the three surfaces, I define the term "equivalent density" used in this thesis.

The density of earth material is determined by three factors: its composition, temperature, and pressure. It decreases with temperature (due to thermal expansion) and increases with pressure (due to compressibility). It has been found through various studies including seismology (e.g., Bolt & Uhrhammer, 1975) that the earth's density increases with depth, i.e., the effect of increased pressure overrides the effect of increased temperature on density. However, the amount of calculated vertical displacements due to lithosphere shortening or extension are very similar whether or not compressibility is allowed for (see Appendix for the derivation), and

therefore in calculating the vertical displacement during lithosphere deformation it is acceptable to assume that the earth material is incompressible and assign to the crust, lithosphere mantle and asthenosphere densities calculated according to temperature alone. This is the so-called "equivalent density" approach used in this thesis. Similar treatment has been used in many works (e.g., McKenzie, 1978) without proper explanation.

Now I present my derivation of the equations describing the evolution of the levels of the upper surface (Z1), the Moho surface (Z2) and the base of lithosphere (Z3) during deformation. The compensation depth is fixed relative to mean sea level (MSL, =Zo). In the following derivation, ρ_c, ρ_m and ρ_a denote the average equivalent densities of the crust, of the lithosphere mantle, and of the asthenosphere.

Because of isostatic equilibrium,

$$\frac{d}{dt}[\rho_w(Z_o-Z_1) + \rho_c s + \rho_m(L - s) + \rho_a Z_3] = 0 \qquad (3.4\text{-}1)$$

For the crust, the volume does not change during deformation (the effect of erosion is not included here), so

$$\frac{d}{dt} s = - s(\frac{\partial u}{\partial x} + \frac{\partial v}{\partial y}) \qquad (3.4\text{-}2)$$

For the upper mantle component of the lithosphere, however, the volume does change (due to thermal processes) and

$$\frac{d}{dt}(L - s) = - (L - s)(\frac{\partial u}{\partial x} + \frac{\partial v}{\partial y}) + f(L) \qquad (3.4\text{-}3)$$

in which $$f(L)=\frac{2\kappa T_L}{L_o T_A}(\frac{L_o}{L}-\frac{A_o}{A_o+L_o-L}) \qquad (3.4\text{-}4)$$

f(L) is the effect of thermal thinning or thickening which have been

derived in § 3.1 by means of the thermal equation.

Solving eq.(3.4-1), (3.4-2) and (3.4-3) together (note $s = Z_1-Z_2$ and $L-s = Z_2-Z_3$), we finally obtain

$$\frac{dZ_1}{dt} = \frac{1}{\rho_a-\rho_w}[L(\rho_m-\rho_a) - s(\rho_m-\rho_c)](\frac{\partial u}{\partial x} + \frac{\partial v}{\partial y}) + \frac{\rho_a-\rho_m}{\rho_a-\rho_w}f(L) \quad (3.4-5)$$

$$\frac{dZ_2}{dt} = \frac{1}{\rho_a-\rho_w}[L(\rho_m-\rho_a) - s(\rho_m+\rho_w-\rho_c-\rho_a)](\frac{\partial u}{\partial x} + \frac{\partial v}{\partial y}) + \frac{\rho_a-\rho_m}{\rho_a-\rho_w}f(L) \quad (3.4-6)$$

$$\frac{dZ_3}{dt} = \frac{1}{\rho_a}[L\rho_m - s(\rho_m-\rho_c)](\frac{\partial u}{\partial x} + \frac{\partial v}{\partial y}) + \frac{\rho_w-\rho_m}{\rho_a-\rho_w}f(L) \quad (3.4-7)$$

§ 3.5 The effect of erosion and sedimentation

On the surface of the lithosphere, materials are eroded from the higher parts and deposited in the lower parts. The speed of erosion is very difficult to estimate, since it depends on the surface topography, the structure and composition of the surface material, the climate, etc. Some models have been designed to study the erosion and excavation process (e.g., Carson & Kirkby, 1972; England & Richardson, 1977; Stuwe, 1991). The process of sedimentation is limited by erosion, and is difficult to describe as well. Besides, the subsided part of lithosphere may be covered by water.

Both erosion and sedimentation are complicated processes. Therefore in numerical analysis of large-scale horizontal lithosphere deformation there is a tendency to neglect these processes (e.g., Vilotte et al., 1982, 1986; England & McKenzie, 1982, 1983; Cohen & Morgan, 1986, Sonder & England, 1989). Both processes cause vertical displacement and therefore may have

great influence on horizontal deformation by changing the buoyancy forces. No work has been done to assess the effect of this omission. In this section, I examine how the omission of sedimentation processes affects the accuracy of the thin sheet model.

Consider first the case of a basin formed by stretching and subsidence. Suppose the sediments are loose, and therefore do not add to the strength of the lithosphere. Adding sediments (including water) has two effects. First, it causes further subsidence, as shown in eq.3.4-6, and therefore also increases the slope of the top surface. Second, it reduces the density contrast across the top boundary of the lithosphere, which decreases the gravitational buoyancy forces. These two effects act against each other and as a result, the effect of sedimentation on horizontal deformation may be small. Now I examine this.

Suppose Z_1, Z_2 and Z_3 represent the level of the top surface, the Moho and the base of a "dry" lithosphere with no sediment on its top. Add water or sediments to this lithosphere and let Z_0, Z_1', Z_2' and Z_3' represent the water surface, the top surface of the lithosphere, the Moho and the base of the lithosphere (Figure 3.5-1).

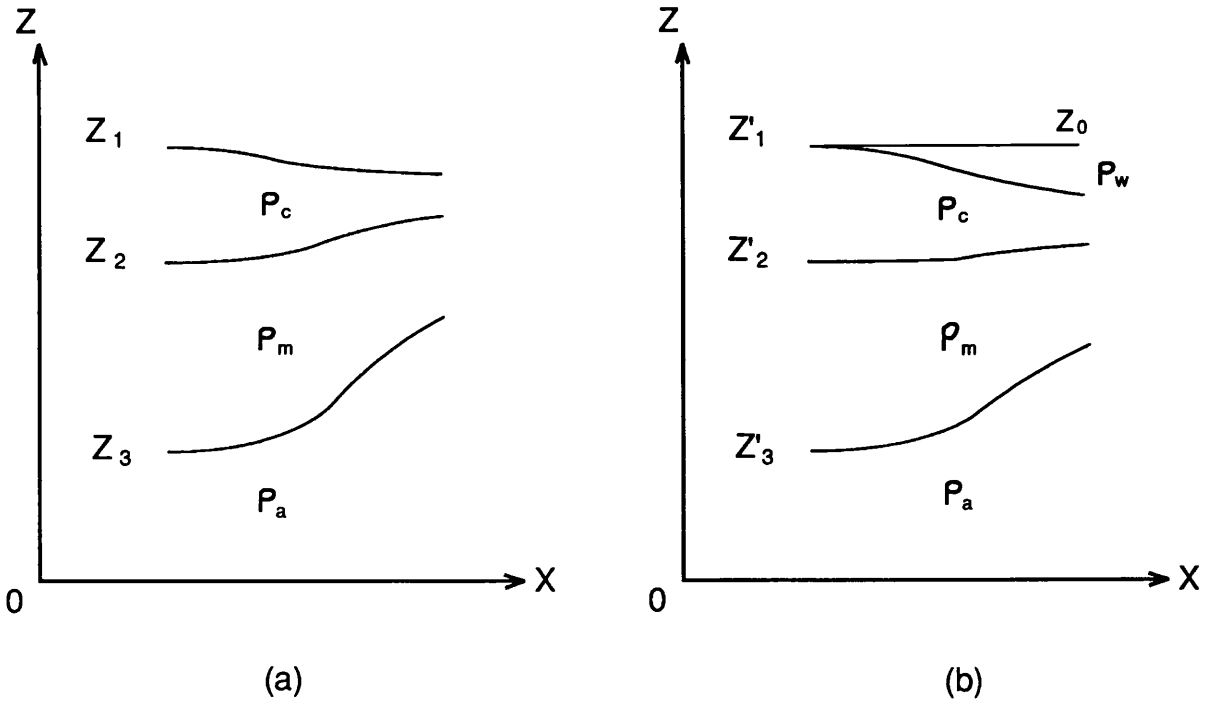

Figure 3.5-1. The deformed lithosphere (a) without and (b) with sediments on the top.

Because of isostasy,

$$\rho_w(Z_0'-Z_1') + \rho_c(Z_1'-Z_2') + \rho_m(Z_2' - Z_3') + \rho_a Z_3' = \text{constant} \qquad (3.5\text{-}1)$$

$$\rho_c(Z_1-Z_2) + \rho_m(Z_2 - Z_3) + \rho_a Z_3 = \text{constant} \qquad (3.5\text{-}2)$$

Subtracting the two equations, we obtain

$$\rho_c(Z_1-Z_1') + (\rho_m-\rho_c)(Z_2 - Z_2') + (\rho_a-\rho_m)(Z_3-Z_3') - \rho_w(Z_0'-Z_1') = 0 \qquad (3.5\text{-}3)$$

Let D be the subsidence caused by the sedimentation, then

$$D = Z_1 - Z_1' = Z_2 - Z_2' = Z_3 - Z_3'$$

and eq.3.5-3 is reduced to

$$\rho_a D - \rho_w(Z_0'-Z_1') = 0 \qquad (3.5\text{-}4)$$

or

$$\rho_a(Z_1-Z_1') - \rho_w(Z_0'-Z_1') = 0 \qquad (3.5\text{-}5)$$

Differentiate eq.(3.5-4) and eq.(3.5-5) with respect to x, then we have

$$\rho_a\frac{\partial D}{\partial x} = -\rho_w\frac{\partial Z_1'}{\partial x} \qquad (3.5\text{-}6)$$

or

$$\rho_a\frac{\partial Z_1}{\partial x} = (\rho_a - \rho_w)\frac{\partial Z_1'}{\partial x} \qquad (3.5\text{-}7)$$

Based on eq.(3.3-3), the horizontal spreading or contracting forces due to gravity before adding the sediment can be expressed as (in x direction)

$$\rho_c gL\frac{\partial Z_1}{\partial x} + (\rho_m-\rho_c)g(L-s)\frac{\partial Z_2}{\partial x} = F_x$$

After adding the sediment, it is

$$(\rho_c-\rho_w)gL\frac{\partial Z_1'}{\partial x} + (\rho_m-\rho_c)g(L-s)\frac{\partial Z_2'}{\partial x} = F_x'$$

For simplicity, in these two equations effective densities are used instead of real densities as a first order approximation.

Now take the difference

$$F_x - F_x' = \rho_c gL\frac{\partial Z_1}{\partial x} + (\rho_m-\rho_c)g(L-s)\frac{\partial Z_2}{\partial x}$$

$$- (\rho_c-\rho_w)gL\frac{\partial Z_1'}{\partial x} - (\rho_m-\rho_c)g(L-s)\frac{\partial Z_2'}{\partial x}$$

$$= \rho_c gL\left(\frac{\partial Z_1}{\partial x} - \frac{\partial Z_1'}{\partial x}\right) + (\rho_m-\rho_c)g(L-s)\left(\frac{\partial Z_2}{\partial x} - \frac{\partial Z_2'}{\partial x}\right) + \rho_w gL\frac{\partial Z_1'}{\partial x}$$

$$= \rho_c gL\frac{\partial D}{\partial x} + (\rho_m-\rho_c)g(L-s)\frac{\partial D}{\partial x} + \rho_w gL\frac{\partial Z_1'}{\partial x}$$

$$= \rho_c g L \frac{\partial D}{\partial x} + (\rho_m - \rho_c) g (L-s) \frac{\partial D}{\partial x} - \rho_a g L \frac{\partial D}{\partial x}$$

$$= \left[\rho_c L + (\rho_m - \rho_c)(L-s) - \rho_a L\right] g \frac{\partial D}{\partial x}$$

$$= \left[L(\rho_m - \rho_a) + s(\rho_c - \rho_m)\right] \left(- g \frac{\rho_w}{\rho_a} \frac{\partial Z_1'}{\partial x}\right)$$

$$= \left[L(\rho_m - \rho_a) + s(\rho_c - \rho_m)\right] \left(- g \frac{\rho_w}{\rho_a} \frac{\rho_a}{\rho_a - \rho_w} \frac{\partial Z_1}{\partial x}\right)$$

$$= \left[L(\rho_m - \rho_a) + s(\rho_c - \rho_m)\right] \frac{g \rho_w}{\rho_w - \rho_a} \frac{\partial Z_1}{\partial x} \qquad (3.5\text{-}8)$$

To get an idea of the magnitude of this difference, let's consider a dry lithosphere with a flat base. Differentiating eq.(3.5-2) with respect to x, we obtain

$$\frac{\partial Z_2}{\partial x} = \frac{\rho_c}{\rho_c - \rho_m} \cdot \frac{\partial Z_1}{\partial x}$$

Therefore the horizontal spreading or contracting force due to gravity before adding the sediments is

$$F_x = \rho_c g L \frac{\partial Z_1}{\partial x} + (\rho_m - \rho_c) g (L-s) \frac{\partial Z_2}{\partial x}$$

$$= \rho_c g L \frac{\partial Z_1}{\partial x} + (\rho_m - \rho_c) g (L-s) \cdot \frac{\rho_c}{\rho_c - \rho_m} \cdot \frac{\partial Z_1}{\partial x}$$

$$= \rho_c g s \cdot \frac{\partial Z_1}{\partial x} \qquad (3.5\text{-}9)$$

Assuming ρ_c=2.9, ρ_m=3.3, ρ_a=3.26, s=0.35L, then

$$\frac{F_x - F_x'}{F_x} = \frac{L(\rho_m - \rho_a) + s(\rho_c - \rho_m)}{\rho_c s} \cdot \frac{\rho_w}{\rho_w - \rho_a}$$

$$= 0.099 \frac{\rho_w}{\rho_a - \rho_w}$$

So the value of F_x-F_x' is one magnitude smaller than F_x (less than 0.1 F_x) in this case, provided that the filling in the depression is mostly water

($\rho w \simeq 1$). When ρw increases, the value of $\frac{Fx - Fx'}{Fx}$ increases as well, as shown in Figure 3.5-2.

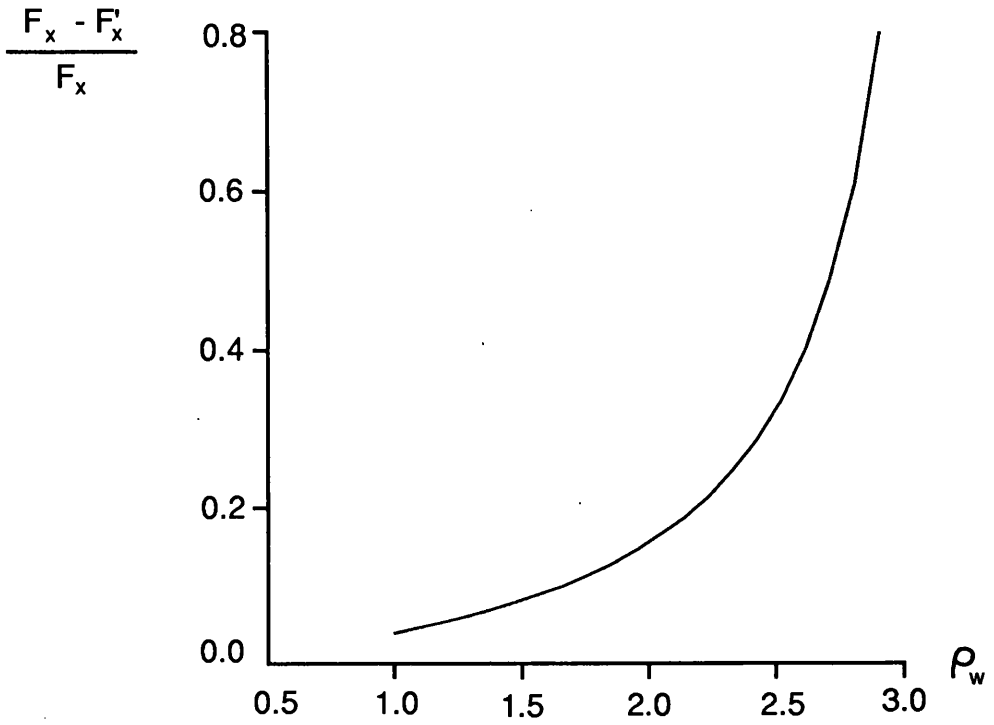

Figure 3.5-2 The effect of sedimentation with increasing sediment density

The above example shows that the effect on the horizontal spreading (or contracting) force due to gravity caused by sedimentation increases as sediment density increases, slowly when $\rho w < 2.0$ but rapidly when $\rho w > 2.5$. If $\rho w = 2.3$, which is probably the upper limit of sediment density, $\frac{Fx - Fx'}{Fx} = 0.24$. The above analysis assumes the depression is completely filled with sediments. In reality, the basin is usually only partly covered, so the effect of sedimentation on horizontal deformation will be less than estimated above.

So it follows from the above analysis that in modelling the horizontal

deformation of lithosphere, the effect of sedimentation is initially small, and can be neglected. It is only in the later stages when the basin has deepened and filled with dense compacted sediments that it becomes a more important factor.

I have made some attempts to assess the effect of erosion on horizontal forces due to gravitational buoyancy effects, but the results from the analysis depend on too many assumptions to be helpful, and they are therefore not included here. It has been suggested that erosion takes place on a similar time scale to the thermal relaxation process (e.g., Murrell, 1986), and in future research it may be necessary to include erosion terms in the governing equations of this kind of models.

§ 3.6 Discussion of the derived equations

So far the necessary equations for a general model have been derived. To clarify the physics in the model, I now present several special cases by giving the effective densities ρ_c, ρ_m and ρ_a particular relative values. All the following discussions are for the case in which there is no erosion or sedimentation (and no surface water, so we put $\rho_w = 0$). And the lithosphere is assumed to be initially flat. Because the difference between the effective density and the real density is very small, for simplicity, effective densities are used instead of real densities in calculating the horizontal buoyancy forces.

Remember the horizontal forces due to gravitational buoyancy effects is expressed as (in the x-direction)

$$F_{xi} = \rho_c g L \frac{\partial Z_1}{\partial x_i} + (\rho_m - \rho_c) g (L-s) \frac{\partial Z_2}{\partial x_i} \qquad (3.6\text{-}1)$$

where x_i = x or y.

Note that $(\frac{\partial u}{\partial x} + \frac{\partial v}{\partial y}) < 0$ means shortening or mechanical thickening and $(\frac{\partial u}{\partial x} + \frac{\partial v}{\partial y}) > 0$ means stretching or mechanical thinning.

A. $\rho_c = \rho_m = \rho_a$

In this case we have a strong uniform lithosphere overlying a weak asthenosphere with the same density as the lithosphere. The lithosphere is therefore neutrally buoyant.

From eq.(3.4-5)

$$\frac{dZ_1}{dt} = 0$$

which means the upper surface of the lithosphere is not changed during the deformation and remains flat. So we have

$$\frac{\partial Z_1}{\partial x_i} = 0 \qquad (3.6\text{-}2)$$

From eq.(3.4-6)

$$\frac{dZ_2}{dt} = s(\frac{\partial u}{\partial x} + \frac{\partial v}{\partial y})$$

From eq.(3.4-7)

$$\frac{dZ_3}{dt} = L(\frac{\partial u}{\partial x} + \frac{\partial v}{\partial y}) - f(L)$$

And from eq.(3.6-1) and eq.(3.6-2)

$$F_x = F_y = 0$$

So for a uniform lithosphere overlying an asthenosphere with the same density, the shortening or stretching will not cause any variation in level

of the upper surface of the lithosphere, and there will be no horizontal flow due to gravity. Only the level of the bottom of the lithosphere is changed by the mechanical and thermal processes. Of course this is only possible if the lithosphere is everywhere in isostatic equilibrium. This situation can not be found on Earth.

B. $\rho_c<\rho_a<\rho_m$ and $\rho_a = \frac{\rho_m(L-s) + \rho_c s}{L}$

This is a lithosphere with a crust of density ρ_c, with lithosphere mantle of density ρ_m, overlying an asthenosphere of density ρ_a. The density of the asthenosphere is equal to the mean density of the lithosphere, so the latter is neutrally buoyant as in case A.

Rewriting $\rho_a = \frac{\rho_m(L-s) + \rho_c s}{L}$, we have

$$L(\rho_m-\rho_a) - s(\rho_m-\rho_c) = 0 \qquad (3.6\text{-}3)$$

Substitute eq.(3.6-3) into eq.(3.4-5), we find, as in case A above,

$$\frac{dZ_1}{dt} = 0$$

And therefore

$$\frac{\partial Z_1}{\partial x} = \frac{\partial Z_1}{\partial y} = 0 \qquad (3.6\text{-}4)$$

From eq.(3.6-1)

$$F_{xi} = (\rho_m-\rho_c)g(L-s)\frac{\partial Z_2}{\partial x_i} \qquad (3.6\text{-}5)$$

where x_i = x or y.

Eq.(3.6-4) shows that the upper surface remains flat during stretching or shortening, as in case A, because the average effective density of the lithosphere is equal to that of the asthenosphere. However, eq.(3.6-5)

shows that because of the density contrast inside the lithosphere, there is horizontal flow due to gravity, contributed by the variation of the Moho surface caused by shortening or stretching, although the upper surface of the lithosphere remains flat. This situation corresponds to a lithosphere with a relatively thin (≈ 18 km, see McKenzie 1978 and Murrell 1986) crust.

C. $\rho_c=\rho_m<\rho_a$ or $\rho_c=\rho_m>\rho_a$

In this case we have a uniform strong lithosphere overlying an asthenosphere with larger or smaller density respectively.

From eq.(3.4-5)

$$\frac{dZ_1}{dt} = (\rho_m/\rho_a - 1)L\left(\frac{\partial u}{\partial x} + \frac{\partial v}{\partial y}\right) + (1-\rho_m/\rho_a)f(L) \qquad (3.6\text{-}6)$$

and from eq.(3.6-1)

$$F_{x_1} = \rho_c g L \frac{\partial Z_1}{\partial x_1} \qquad (3.6\text{-}7)$$

In this case, unlike cases A and B, the free surface (Z_1) no longer remains flat, due to the density contrast between the lithosphere and the asthenosphere. Horizontal flow because of gravity is contributed by the variation in height of the upper surface of the lithosphere. From eq.(3.6-6), it can be seen that thickening causes elevation and thinning causes subsidence of the upper surface of the lithosphere if $\rho_c=\rho_m<\rho_a$, and thickening causes subsidence and thinning causes elevation of the upper surface of the lithosphere if $\rho_c=\rho_m>\rho_a$.

D. $\rho_c<\rho_a<\rho_m$ and $\rho_a < \frac{\rho_m(L-s) + \rho_c s}{L}$ or $\rho_a > \frac{\rho_m(L-s) + \rho_c s}{L}$

The second condition can be rewritten as

$L(\rho_m-\rho_a) - s(\rho_m-\rho_c) > 0$ or $L(\rho_m-\rho_a) - s(\rho_m-\rho_c) < 0$

So from eq.(3.4-5) we see that the elevation or subsidence of the upper surface of the lithosphere caused by stretching or shortening is controlled by the relative value of the average effective density of the lithosphere and that of the asthenosphere. If the average effective density of the lithosphere is higher than that of the asthenosphere, stretching causes the elevation of the upper surface of the lithosphere and shortening causes the subsidence of it, and vice versa. In fact, this conclusion is also valid for the previous cases. For most continental lithosphere, the average effective density is smaller than that of the asthenosphere, i.e., $L(\rho_m-\rho_a) - s(\rho_m-\rho_c) < 0$, because their crustal thicknesses are usually larger than the critical thickness ($\approx$ 18 km).

E. $\rho_c<\rho_m=\rho_a$

In this case we have a strong lithosphere consisting of a crust of lower density ρ_c and a mantle with density equal to that of the asthenosphere.

From eq.(3.4-5)

$$\frac{dZ_1}{dt} = (\rho_c/\rho_a-1)s\left(\frac{\partial u}{\partial x} + \frac{\partial v}{\partial y}\right) \qquad (3.6\text{-}8)$$

From eq.(3.4-6)

$$\frac{dZ_2}{dt} = (\rho_c/\rho_a)s\left(\frac{\partial u}{\partial x} + \frac{\partial v}{\partial y}\right) \qquad (3.6\text{-}9)$$

From eq.(3.4-7)

$$\frac{dZ_3}{dt} = [L + (\rho_c/\rho_a-1)s]\left(\frac{\partial u}{\partial x} + \frac{\partial v}{\partial y}\right) - f(L) \qquad (3.6\text{-}10)$$

From eq.(3.6-1)

$$F_{xi} = \rho_c g L \frac{\partial Z_1}{\partial x} + (\rho_m - \rho_c) g (L-s) \frac{\partial Z_2}{\partial x_i} \qquad (3.6\text{-}11)$$

where x_i = x or y.

In this case, the horizontal flow due to gravity forces is contributed by the topography of both the upper surface and the Moho surface of the lithosphere. From eq.(3.6-8) and eq.(3.6-9) we see that stretching always causes the subsidence of the upper surface and the elevation of the Moho surface of the lithosphere, and shortening always causes the elevation of the upper surface and the subsidence of the Moho surface of the lithosphere. So $\frac{\partial Z_1}{\partial x_i}$ and $\frac{\partial Z_2}{\partial x_i}$ are always of opposite signs, provided that the upper surface and the Moho surface of the lithosphere are flat at the beginning of the deformation.

In this situation, top surface elevation (or subsidence) is completely balanced by Moho surface subsidence (or elevation). This is the assumption made by many authors (e.g., England & McKenzie, 1982, 1983; Cohen & Morgan, 1986; Sonder & England, 1989). It is not a very realistic assumption, and will be discussed further in Chapter 4 and Chapter 5.

§ 3.7 Numerical solution to the equations

The governing equations can not be solved analytically. Numerical methods have to be employed to carry out specific studies.

The mechanical equations have been solved in the present work using the finite difference method on a mesh of 32 by 32(Lo). The derivatives are

approximated by their standard space-centered finite difference forms. e.g.

$$\frac{\partial u}{\partial x} = (u_{i+1,j} - u_{i-1,j})/\ 2\Delta x$$

$$\frac{\partial^2 u}{\partial^2 x} = (u_{i+1,j} - 2u_{i,j} + u_{j-1,j})/\Delta x^2$$

$$\frac{\partial^2 u}{\partial^2 y} = (u_{i,j+1} - 2u_{i,j} + u_{i,j-1})/\Delta y^2$$

$$\frac{\partial^2 u}{\partial x \partial y} = (u_{i+1,j+1} + u_{i-1,j-1} - u_{i+1,j-1} - u_{i-1,j+1})/4\Delta x\Delta y$$

After approximation, the left sides of the mechanical equations are linear combinations of $u_{i,j}$ and $v_{i,j}$, while the right sides (Rx and Ry) are not. So the equations are solved by an iterative procedure: initial estimates are made for u and v, which are used to evaluate Rx and Ry. Then the linear equations of $u_{i,j}$ and $v_{i,j}$ are solved making use of NAG (Numerical Algorithm Group) routine programme libraries. The output value of u is then combined with the old value of u:

$$u_{new} = \alpha \cdot u_{out} + (1-\alpha) \cdot u_{old}$$

and the new value of u is used to evaluate Rx and Ry, and new equations are solved. The above process is iterated until the largest change in either velocity component is less than a desired fraction of the maximum velocity in the system:

$$\frac{|u_{out} - u_{old}|_{max}}{|u_{old}|_{max}} < \beta$$

Eqs.(3.4-5), (3.4-6) and (3.4-7), the formulae for the rate of change of the levels of the three surfaces are used in the approximate non-dimensional form to calculate the value of ΔZ1, ΔZ2 and ΔZ3 after a time span of Δt. The process is then continued to the end of the calculation.

The value of the time step Δt is chosen to satisfy

$$\frac{\Delta t}{|u_{ij}|_{max}+|v_{ij}|_{max}} \leq 1$$

The boundary conditions and the physical properties of the lithosphere used in modelling depend on the nature of the problems, and will be discussed in Chapter 5 and Chapter 7.

Chapter 4. The India-Eurasia collision zone

This chapter gives a brief review of the tectonics of the Himalaya mountain belt and the Tibetan plateau, which is a unique form of continental collision zone. A discussion is also given of some attempts to model this tectonic structure.

When an oceanic plate is subducted beneath continental lithosphere, an Andean type mountain range develops on the edge of the continent. If the subducting plate also contains continental lithosphere, continued underthrusting can result in contraction of the intervening ocean basin, and causes convergence of the continents, bringing them into juxtaposition (i.e., collision). Whereas old oceanic lithosphere is relatively dense and sinks into the asthenosphere, the greater sialic content of continental lithosphere causes it to possess a positive buoyancy with respect to the asthenosphere which prevents its being subducted to any great depth (McKenzie, 1969). Consequently, the arrival of continental lithosphere at a trench results in collision with the overriding continent; rapid relative motion is halted, and other plates reorganize to take up the motion elsewhere. Continued convergence of the two plates results in crustal shortening and thickening.

The Himalaya and the Tibetan plateau has been formed in this way by continental collision of the India plate with Eurasia, which began in Tertiary times. Some other mountain ranges such as the Appalachians, the Caledonides, the Alps and the Urals were also formed by continental collision in earlier times. The Himalaya and the Tibetan Plateau region is the least understood because of the difficulties in the way of geological

and geophysical investigation. Existing knowledge about it is summarized below. Figure 4-1 is a schematic map of the geology of the region.

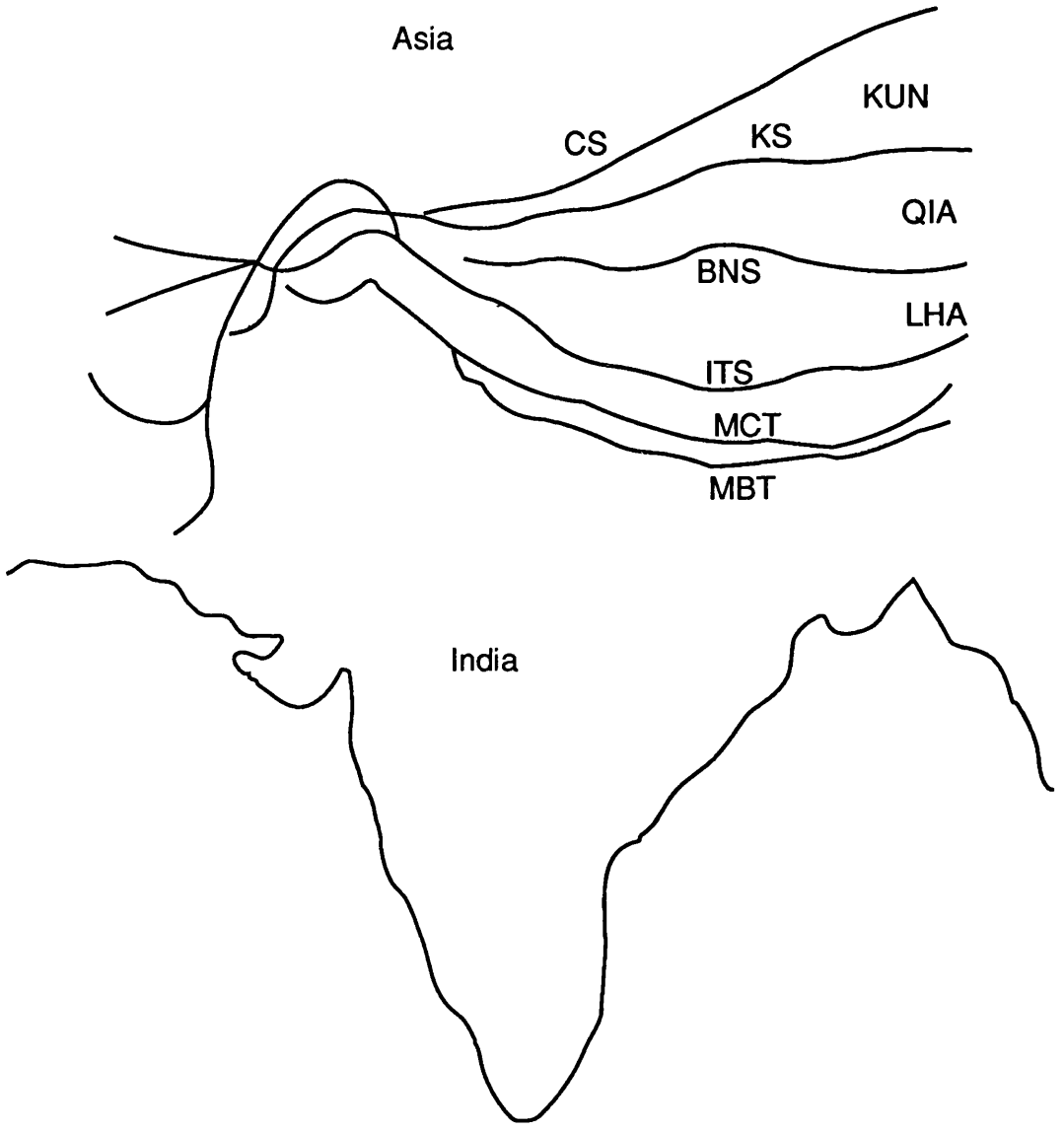

Figure 4-1. The major geologic provinces in the Himalayan mountain belt and the Tibetan plateau (after Allègre et al.,1984).

MBT: Main Boundary Thrust.
MCT: Main Central Thrust.
ITS: Indus Tsangpo Suture (also Indus-Zangbo Suture).
BNS: Bangong Nujiang Suture (also Bangong Suture).
KS: Kokoxili Suture (also Jinsha Suture).
CS: Chilien Suture.

KUN: Kunlun Block.
QIA: Qiangtang block (also Changtang block).
LHA: Lhasa block.

The Himalayan mountain belt is 250-350 km wide and extends for about 3000 km from Afghanistan to Burma. It comprises a series of lithologic and tectonic units which run parallel to the mountain belt and maintain a constant character for great distances. Molnar (1984) and Windley (1985) summarized the geology of Himalaya.

The Lower (or lesser) Himalaya occupies elevations from 1500-3000 m and is thrust over the Sub-Himalaya along the Main Boundary Thrust. The thrust is still active and focal mechanism solutions suggest that the fault plane dips northwards at a shallow angle. The Lower Himalaya consists of Precambrian-Mesozoic low grade metasediments which are overthrust by nappes consisting of gneisses of the Higher Himalaya.

The Higher (or Greater) Himalaya reaches altitudes of over 8000 m and consists of a basement of Precambrian gneiss overlain by Palaeozoic and Mesozoic sediments of Tethyan origin which were originally situated on the northern margin of India. The unit is thrust over the Lower Himalaya along the Main Central Thrust by an amount exceeding 100 km. The unit is intruded by many granites of Miocene age which originated by melting of the lower crust.

The Indus-Zangbo Suture Zone is the major boundary separating the Precambrian India plate from the younger Mesozoic-Cenozoic Trans-Himalaya to the north. The suture, which is a steeply dipping thrust zone, contains Tethyan ophiolites, blueschists and granulites. The ophiolites are not continuous, and in places are replaced by sediments typical of the forearc

environment. Virtually all the material of the Himalayan range, i.e., south of the suture, was once part of the Indian plate and not derived from the Asian plate.

The Trans-Himalaya magmatic belt is situated along the northern margin of the Indus-Zangbo Suture Zone. In the central eastern Himalaya the southern Tibetan plateau with a cover of Palaeozoic and Mesozoic sediments is intruded by the Cretaceous-Eocene Trans-Himalayan granite batholith which formed along an Andean-type plate margin in response to northwards underthrusting of the Tethys Ocean. In the western Himalaya the equivalent unit is an island arc which formed within the Tethys in Mid-Cretaceous times, ultimately to become squeezed between the converging Indian and Asian plates at about 100 Ma ago. This unit is separated by the minor Northern Suture (Bangong-Nujiang Suture) from the Karakorum granite batholith to the north.

§ 4.2 Tibetan Geology

For the purpose of description, the Tibetan Plateau is taken to extend from the south side of the Kun Lun Range to the north side of the Trans-Himalayan magmatic belt. This region is divisible into three micro-continental fragments, the Kun Lun, Changtang and Lhasa Terrains separated by the Jinsha and Bangong Sutures (Chang et al., 1986). Faunal data suggest that the Kun Lun was already part of Laurasia by the Carboniferous, and that the Changtang and Lhasa Terrains were separated from Gondwana in the pre-Permian and Triassic respectively. These terrains were accreted successively northwards to the southern margin of Asia. The Jinsha Suture formed in the late Triassic-early Jurassic and the Banggong Suture in the late Jurassic-early Cretaceous (Lin & Watts, 1988). Palaeomagnetic data

by Patriat & Achache (1984) indicate that the Lhasa Terrain remained stationary through most of the Upper Cretaceous and Eocene, but that it has moved 20°north since the suturing of India to it in the Eocene. The folding and thrusting of Palaeogene red beds across a wide extent of the Tibetan Plateau allows a minimum estimate of overall shortening of 12 percent (Chang et al., 1986).

Neotectonic structures are widespread across the Tibetan Plateau. These are extensional structures which are significantly different in south and north Tibet respectively (Chang et al., 1986; Mercier et al., 1987). South Tibet has extended in an E-W direction on major N-S aligned rifts (Tapponnier et al., 1981). The rate of Quaternary extension is about 1 percent per Ma, corresponding to a "spreading rate" of 1.0±0.6 cm per year (Armijo et al., 1986). In contrast, north Tibet has been able to move more easily eastwards and thus has extended along a conjugate set of NW-SE and NE-SW strike-slip faults (Mercier et al., 1987). The elevation of the Tibetan Plateau is about 4-5 km, and is surprisingly flat.

§ 4.3 Seismicity of the area

Focal mechanism solutions of earthquakes in the Himalaya and the Tibetan Plateau have been generalized by Molnar & Chen (1983) to reveal the present style of faulting. A single event in the Indian Shield to the south is indicative of normal faulting along an E-W striking plane, and is consistent with the extension experienced in this area as a result of the bending of the Indian Shield beneath the Himalaya. Thrust faulting occurs beneath the lower Himalaya, with the fault planes probably dipping north at shallow angles. Thrust faulting gives way to normal faulting on N-S

striking planes in the Higher and Trans-Himalaya, and probably reflects the increased loading of the lithosphere, causing the vertical stress to pass from being the least to the most compressive stress. Most earthquakes in the Tibetan Plateau occurred within 25 km below the surface (Molnar & Chen, 1983; Zhao & Helmberger, 1991). This implies that the Tibetan Plateau is hot and weak, and is not a shield region. It also implies that there is no double-crust structure below Tibet.

§ 4.4 Deep structure of the area

Several models have been proposed to explain the structure of the Tibetan plateau:

a. Powell (1986), Powell & Conaghan (1973, 1975) and Barazangi & Ni (1982) etc. suggested that the Indian crust was thrust under Tibet, so doubling the crustal thickness. According to this model there should be geophysical evidence under northern Tibet of a remnant northward-dipping subducting slab. From palaeomagnetic data, Lin & Watt (1988) conclude that since collision at 40 Ma ago the Lhasa Terrain has moved northwards 2000±600 km; this challenges the underthrusting model for Tibet.

b. Dewey & Burke (1973) and Sengör & Kidd (1979) argued that the thick Tibetan crust was caused by intracrustal N-S shortening. The later geophysical data of Hirn et al. (1984a,b) and the geological information of Chang et al. (1986) support this idea. According to Chang et al. (1986) the Tibetan Plateau has been shortened by at least 40 percent in post-Eocene times, and this allows all the crustal thickening to be explained by

internal deformation. The fact that most earthquakes in Tibetan Plateau occurred with 25 km of depth also implies that there is not double-crust structure below Tibet.

Detailed imaging of crustal structure has come from a 500 km-long seismic traverse across the Himalaya and Tibet in which emphasis was placed on the recording of critical reflections from the Moho (Hirn et al., 1984a,b) The data show that the crustal thickness of the Indian Shield is some 35 km, and that this increases to 55 km beneath the Himalaya and to 70 km under Tibet. The crust mantle boundary, rather than being a sharp contact, occupies a transition zone over a vertical interval of some 12 km. The Moho structure is not smooth, and exhibits a number of steps, some of which are vertical and in some of which there is an overlapping of the Moho at different depths. All steps produce a vertical Moho displacement of less than 20 km. The vertical discontinuities are associated with the Indus-Zangbo suture and the Danqiao ophiolite, and probably indicate that these features are now strike-slip faults associated with indentation tectonics. The stacked Moho segments probably represent the thrust faults which were responsible for the thickening of the Himalaya/Tibet crust. The thickness of these thrust slices is less than 20 km, i.e., considerably less than the normal crustal thickness. This implies that crustal thickening does not take place by simple underthrusting of Indian crust beneath Eurasia in which the Moho is smoothly depressed northwards. Rather, it suggests that thickening has taken place in response to intracontinental thrusting and large scale nappe movement affecting both the crust and uppermost mantle.

A more recent study by Zhu (1991) shows that although the crustal

thickness is around 70 km for the Tibetan Plateau, the thickness of lithosphere is only about 125 km. So the lithosphere has an anomalously high proportion of crust. This may be the result of the loss of mantle at the base of the lithosphere in the later stage of lithosphere shortening and thickening, as suggested by Houseman et al. (1981).

§ 4.5 The kinematic evolution of the Himalaya and the Tibetan plateau

On the basis of stratigraphic and tectonic observations, together with isotope age determinations and palaeomagnetic data, Allegre et al. (1984) proposed a geodynamical model for the evolution of blocks which are now part of the Indian-Asian continent over the past 120-140 Ma at 20 Ma intervals (Figure 4.5-1). The Qiangtang block was sutured to Asia along the Kokoxili suture around 200 Ma ago and some crustal shortening may subsequently have occurred on continental thrusts. Around 140-120 Ma ago, a small ocean basin between the Qiangtang and Lhasa blocks closed. The Lhasa block was sutured to Asia along the Bangong Nujiang Suture (BNS) around 100 Ma. Continental shortening followed along the Gulu and Anduo thrusts. Subduction took place beneath the Lhasa continental margin around 80-60 Ma. The Lingzizong arc volcanics were erupted between 60 and 45 Ma. At 40 Ma continental shortening or obduction took place as the Indian and Asian plates collided along the Indus Tsangpo Suture (ITS). At 20 Ma, the Main Central Thrust (MCT) was the main thrust. At present, thrusting takes place mainly along the Main Boundary Thrust (MBT). India has penetrated about 2000 km into Asia since collision occurred.

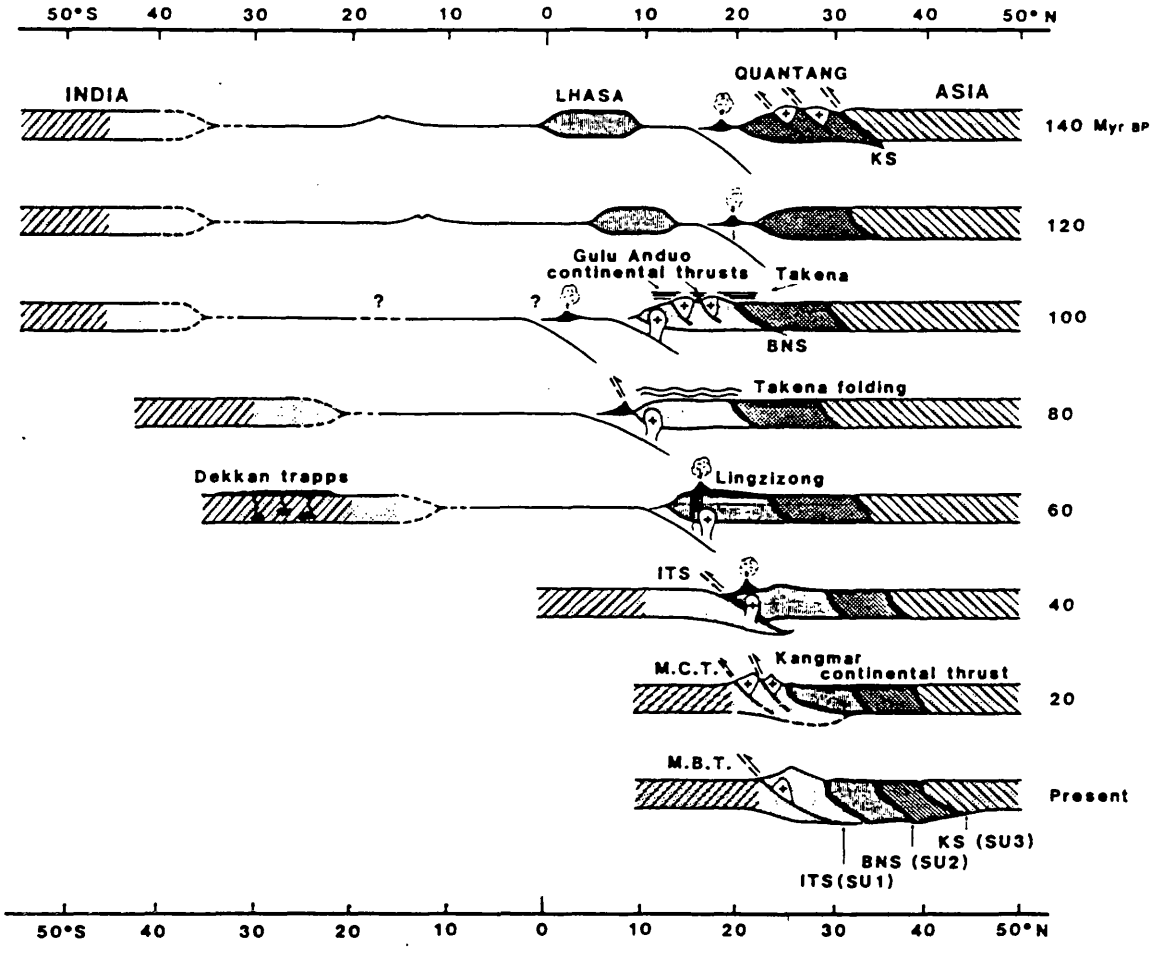

Figure 4.5-1. A reconstruction of Tibet and the Himalayas at 20 Ma intervals from 140 Ma to the present. The Qiangtang block is assumed to have sutured to Asia at about 200 Ma.

140-120 Ma: Small ocean basin between Asia and the Lhasa block closes.
100 Ma: Lhasa block is sutured to Asia along the BNS.
80-60 Ma: Subduction takes place beneath Lhasa continental margin.
40 Ma: Subduction ceases. Continental obduction or shortening takes place as Indian and Asian plates collide.
20 Ma: MCT is the main thrust.
Present: MBT is the main thrust.

(From Allegre et al., 1984)

The Himalayan region is still seismically active, and is undergoing rapid uplift at rates between 0.5 and 4 mm/year and there remains an area of active tectonics within a broad zone stretching some 3000 km north of the mountain chain (Molnar & Chen, 1982). It is estimated that India is still moving northwards at a rate of some 5 cm/year, less than half of which (2 cm/year) is taken up by the convergence in the Himalaya along the MBT (Tapponnier & Molnar, 1977; Armijo et al., 1982).

§ 4.6 The dynamics of the Himalayas and the Tibetan Plateau

A three phase evolutionary scenario for plateaus of high altitudes has been put forward (Froidevaux & Isacks, 1984; Froidevaux & Ricard, 1987). Phase one is the build-up of the high topography through lithosphere thickening. At this stage, maximum compressional stress is horizontal and minimum compressional stress is vertical, therefore lithosphere shortening dominates. As the crust thickens and the topography builds up, the vertical stress grows larger. Phase 2 begins when the vertical stress becomes the intermediate stress. In this stage strike-slip faulting dominates instead of thrusting, and crustal thickening ceases. In phase 3, the vertical stress becomes the maximum compressional stress. Normal faulting dominates, resulting in the extension and thinning of the crust, and the plateau collapses. The different parts of a plateau, owing to differences in elevation, may be in different phases at the same time.

Froidevaux & Ricard (1987) related the three phases to the Andean belt, to western North America, and to the Tibetan Plateau. In western North America extensional tectonics — phase 3 — occurred over the last 40 Ma.

In western South America the Andean belt is mostly under compression and is in phase 1, except between 14°S and 27°S, the Altiplano segment is in phase 2 or 3. The build-up of the Tibetan Plateau started about 40 Ma ago. Currently, Himalaya is in phase 1, where thrusting dominates; Northern Tibet is in phase 2 or 3, where strike-slip faulting has been reported (Armijo et al., 1982) and may absorbs 30 percent of the total convergence between India and Asia (Armijo et al., 1989); Southern Tibet is in phase 3, where normal faulting has been the dominant tectonic regime in Tibet in the last 1.5-2.5 Ma. The rate of Quaternary extension is about 1 percent per Ma, along a 1100-km-long ESE traverse across south Tibet, corresponding to a spreading rate of 1±0.6 cm/year (Armijo et al., 1986). Focal mechanisms of earthquakes in the Tibetan Plateau show that the maximum compressional stress is vertical (Molnar & Chen, 1983).

The evolution from phase 1 to phase 2 is natural, because the vertical compressional stress will normally increase as high topography is built up. The transition from phase 2 to phase 3 is more complicated. It requires that the vertical stress becomes the maximum compressional stress. This can be achieved by a drop of horizontal compressional stress, or an increase in the vertical compressional stress. A change in the horizontal stress can only be attributed to modifications in the configuration or dynamics of the global plate system, whereas changes in vertical stress are produced locally within the lithosphere or just below it (Fleitout & Froidevaux, 1982). The reduction of horizontal stress may be the cause of the extension of western North America, but in the case of the Tibetan Plateau, the convergence between India and Eurasia is still active, therefore the cause of the transition from phase 2 to phase 3 is less clear.

Fleitout & Froidevaux (1982) proposed a simple hypothesis of lithosphere shortening (Figure 4.6-1) which may help to explain the evolution of plateaus. They found that when neglecting thermal processes, the lithosphere may be unstable. A thickened lithosphere will tend to shorten further, because the cold and dense lithosphere root formed through lithosphere thickening generates strong compression in the thickened lithosphere. Both convection experiments (Nataf et al., 1981) and numerical simulation (Houseman et al., 1981) suggest that the cold lithosphere root can detach from the upper layer and sink. When this happens, the state of stress is changed and extension will take the place of contraction. This self-contraction mechanism of lithosphere thickening does not necessarily work, depending on the ratio of crustal and lithospheric thickness, but the detachment of the lithosphere root at the later stage of lithosphere shortening does cause lithosphere uplift and may have caused the transition from phase 2 to phase 3 in the evolution of the Tibetan Plateau. England & Houseman (1988) also attribute the extension of the Tibetan Plateau to the delamination or detachment of a lithosphere mantle root.

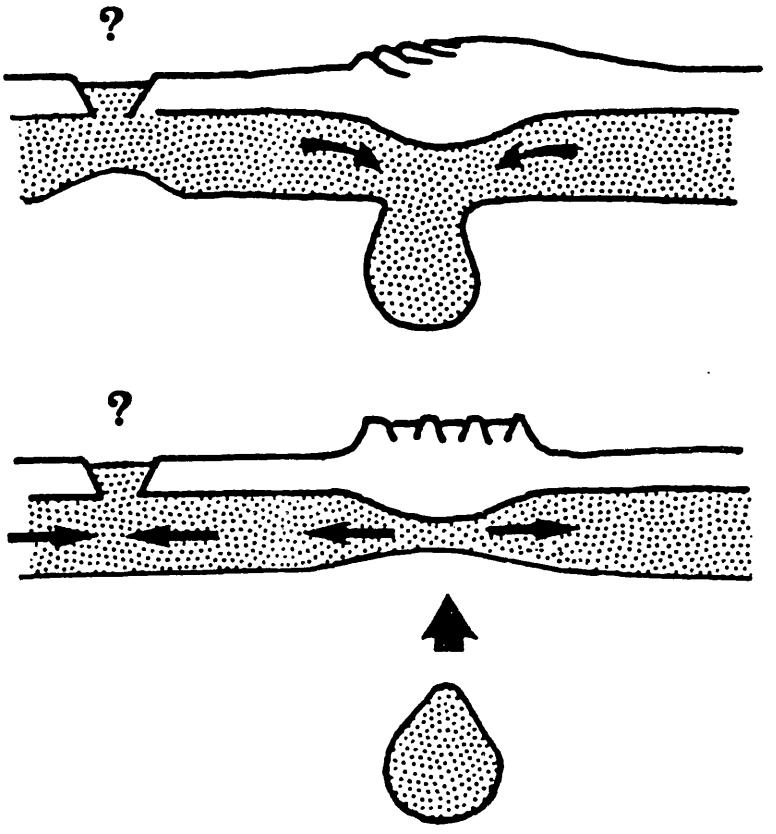

Figure 4.6-1. Schematic picture of the possible time evolution of the lithospheric thickening process. At the top the dense cold lithospheric root generates strong compression in the mountain range. At the bottom the instability has gone further: a cold blob has detached so that rapid uplift is observed in the mountain range, accompanied by extensional tectonics. (From Fleitout & Froidevaux, 1982)

§ 4.7 Existing studies modelling the India-Eurasia collision zone

For the purpose of description, existing efforts to model the India-Eurasia collision may be put into three groups: a) Plane strain analysis in the vertical section across the tectonic strikes, b) models in the horizontal domain with emphasis on faulting, in particular, strike-slip faulting, and c) models in the horizontal domain in which the deforming

plate behaves strictly as a continuum.

a). The first type of model is represented by Wang et al. (1982). They used a two dimensional finite element model to predict the observed data on uplift rate and the gravity anomalies released in the 1980 symposium on the Tibetan Plateau. Among other conclusions, the model predicts that the entire area of Tibet thickens at a rate of 2 mm/year, which contradicts the results from more recent studies (e.g. Tapponnier et al., 1986) which show that the plateau is under extension and subject to net thinning. This is probably due to the plane strain assumption used in the model of Wang et al. (1982) which prohibits displacements traverse to the direction of the collision.

b). The second type of model is represented by the work of Tapponnier & Molnar (1976) and Tapponnier et al. (1982). Their models lay emphasis on strike-slip faulting and the movement of blocks along strike-slip faults. Molnar & Tapponnier (1975) first introduced the idea of using slip-line theory to study the faulting pattern of indented lithosphere. Tapponnier & Molnar (1976) calculated the slip-line fields in plastic media indented by several types of rigid indenters, and compared the slip-lines with the major faults in east Eurasia. They found that the Herat fault, the Altyn Tagh fault, the Kunlun fault, and the Kangting fault can all be compared in sense and trend to the calculated slip-lines in the indented plastic media with indenters of various shapes. Furthermore, a plane indenter can cause tension at large distance, and therefore the Baikal Rift Zone and Shansi Graben may be the consequence of the indentation of Eurasia by India. These findings suggest that most of the tectonics of Asia are caused by the collision of India with Eurasia, and there exists a unifying explanation for the phenomena occurring in continental collision.

There are a number of limitations to this approach, as recognized by Tapponnier et al. (1982). The first is the extreme simplicity of indenter geometries and boundary conditions which are amenable to analytical solutions. The second is that the slip-line field merely provides information on stress and infinitesimal strain, valid for a small instant in geological time. In reality there is finite displacement along strike-slip faults and they almost certainly change their geometry or even their sense of displacement during the long process of at least 40 Ma during which India penetrated over 2000 km into Eurasia. To overcome these limitations, Tapponnier et al. (1982) tested and improved the above hypothesis by experiment, in which a layered plasticine is indented by a rigid indenter. As a result of indentation, strains in the layered plasticine become rapidly localized into narrow shear zones because of strain softening, and these are compared to the faulting system of SE Asia. These ideas are also used to explain the opening of the South China Sea (Tapponnier et al., 1982; Tapponnier et al., 1986).

There is another limitation to the slip-line approach which cannot be overcome by the adoption of the experimental method. The slip-line approach and the above experimental method both assume plane horizontal strain deformation, while it is obvious that there is significant crustal thickening in the formation of the Tibetan Plateau during the collision. This limitation is tackled in the next group of models.

c). The third group of models are represented by the work of Vilotte et al. (1982) and England & McKenzie (1982, 1983). These are models in the horizontal domain solved by numerical methods, assuming continuum behaviour. Both models allow crustal thickening, but the latter has been more cited because it considered the effect of buoyancy forces arising from the

elevation of the top surface due to crustal thickening, and it defined a number (the Argand number) to describe the relative importance of the buoyancy force. My model is similar to this in that I also make the thin sheet assumption and assume a power-law average rheology for the lithosphere. Because of this, a detailed review of England & McKenzie (1982, 1983) is given below.

In the two papers by England & McKenzie (1982, 1983, the second one being a correction to the first), a zone of continental collision is studied using the viscous sheet formulation. The following assumptions were made:

A. The lithosphere is of vertically-averaged rheology.

B. The vertical gradient of deviatoric stress is negligible.

C. The lithosphere is in an isostatic state.

Based on these assumptions, the governing mechanical equation was derived, with a non-dimensional number, Ar, (the Argand number) in it. The Argand number indicates the relative importance of gravitational and tectonic forces, its definition is introduced later in this chapter. When solving the equation, the deforming continental lithosphere was taken to be rectangular with rigid boundaries — zero normal and tangential velocity — except over part of one boundary where material identical to that of the interior flows in at a rate that is a function of position but not of time. Two major conclusions were found. First, the distance affected by the indenting is similar to the length of the indenting boundary. Second, with $Ar > 0$, there is an upper limit to the crustal thickness supportable under compressive boundary conditions. The deformation style transforms from intense compressive strain in the early phase to almost plane strain (phase 2) once the maximum supportable crustal thickness is reached. In fact,

after 30 to 40 Ma of deformation, assuming power law creep plasticity, with $n = 3$, and $Ar \geq 3$, the lateral gravitational flow arising from the thickening is great enough to prevent further thickening.

However, the governing equations appear to have not been correctly derived. When a lithosphere is thickened, the surface of the lithosphere is usually elevated, and this elevation causes increased vertical stress which enables the thickened part of lithosphere to flow laterally. In these two papers, the vertical stress is averaged to show its effect. However, the vertical stress averaged over the thicker part of lithosphere appears to be smaller than that averaged over the thinner part of lithosphere. In the calculation of the average vertical stress, a mathematical mistake was made, and as a result, the averaged stress in thicker lithosphere was incorrectly calculated to be higher than that in thinner lithosphere. The calculation where the mathematical error is found is as follows:

In the process of derivation, there is a formula (England & McKenzie, 1983, eq.(14)):

$$\bar{p} = \bar{\tau}_{zz} + P_o - \frac{g}{L + h} \int_o^{L+h} dz' \int_o^{z'} \rho dz$$

where $\bar{p}$ is the vertically averaged pressure, $\bar{\tau}_{zz}$ is the averaged vertical deviatoric stress, P_o is the pressure at the base of the lithosphere, L is the thickness of the lithosphere without crust, ρ_c and ρ_m are the densities of crust and lower lithosphere respectively. After some algebra with approximation, England & McKenzie (1983) obtained the result

$$\bar{p} = \bar{\tau}_{zz} + \frac{g\rho_m L}{2} + \frac{g\rho_c s^2}{2L}(1-\rho_c/\rho_m)$$

The last term is positive which means a lithosphere with crust has a higher vertically averaged pressure than that without crust.

There is approximation in the process of deriving the above equation. I do not know how the approximation was done, but if the algebra is done without approximation, it is found

$$\bar{p} - \bar{\tau}_{zz} - P_o = -\frac{g}{L+h}\int_o^{L+h} dz' \int_o^{z'} \rho dz$$

$$= -\frac{g}{L+h}\left(\int_o^{L+h-s} \rho_m z dz + \int_{L+h-s}^{L+h} (\rho_m(L+h-s)+\rho_c(z-L-h+s))dz\right)$$

$$= -\frac{g}{L+h}\left(\frac{\rho_m(L+h-s)^2}{2} + s\rho_m(L+h-s) + s\rho_c(s-L-h)\right.$$

$$\left. + \frac{\rho_c((L+h)^2-(L+h-s)^2)}{2}\right)$$

$$= -\frac{g}{L+h}\left(\frac{\rho_m(L+h-s)^2}{2} + s\rho_m(L+h-s) + s\rho_c(s-L-h)\right.$$

$$\left. + s\rho_c(L+h-\frac{s}{2})\right)$$

$$= -\frac{g}{L+h}\left(\frac{\rho_m((L+h)^2-2s(L+h)+s^2)}{2} + \rho_m s(L+h) - \rho_m s^2 + \frac{\rho_c s^2}{2}\right)$$

$$= -g\left(\frac{\rho_m(L+h)}{2} + \frac{s^2(\rho_c-\rho_m)}{2(L+h)}\right)$$

$$= -\frac{\rho_m g L}{2} - \frac{\rho_m g h}{2} + \frac{(\rho_m-\rho_c)gs^2}{2(L+h)}$$

making use of $h = s(1-\rho_c/\rho_m)$, $P_o = \rho_m g L$,

$$\bar{p} = \bar{\tau}_{zz} + \rho_m g L - \rho_m g L/2 - \rho_m g s(1-\rho_c/\rho_m)/2 + (\rho_m-\rho_c)gs^2/2(L+h)$$

$$= \bar{\tau}_{zz} + \frac{\rho_m g L}{2} - \rho_m g s(1-\rho_c/\rho_m)\left(1-\frac{s}{L+h}\right)/2$$

and the last term is now negative rather than positive, which means the vertically averaged pressure of a lithosphere with crust is smaller than that without crust. This error also affects the sign of the Argand number

defined in those papers. In spite of these errors the conclusions in those papers appeared plausible. The incorrectly derived equations were used later in a series of further works (e.g., Cohen & Morgan, 1986; Houseman & England, 1986; Sonder & England, 1989).

There are further differences between this model and the model derived in Chapter 3. The major difference is that England & McKenzie (1982, 1983) assumed that the elevation of the top surface is totally balanced by the crustal root. That means the lithosphere root produced by lithosphere shortening does not play a role in the formation of the plateau. Fleitout & Froidevaux (1982) have shown that this is not the case. Another difference is England & McKenzie (1982,1983) neglected the thermal process, while the model in Chapter 3 contains a formula to estimate the changing of the thickness of mechanically disturbed lithosphere by thermal process.

Cohen & Morgan (1986) and Houseman & England (1986) improved the work of England & McKenzie (1982, 1983) by using the Finite Element Method. These works are mostly concerned with the total strain of Asia caused by indentation. The differences mentioned above still remain.

In Chapter 5 the new thin viscous sheet model that I have derived in Chapter 3 is applied to simulate the evolution of the Tibetan Plateau. Particular attention is paid to the cause of Quaternary extension, i.e., the transition from phase 2 to phase 3, of the evolution of the plateau.

Chapter 5. Application of the thin viscous sheet model to the evolution of the Tibetan Plateau

This chapter comprises five parts. In § 5.1, an analysis is carried out similar to those done by England & McKenzie (1982, 1983) to compare the results, and see if the new model gives significantly different results. In § 5.2, a calculation with more realistic boundary conditions is done, with a decreasing rate of convergence. In § 5.3, the deformation is analyzed with not only a decreasing rate of boundary displacement, but also a weakening lithosphere. In § 5.4, I simulate the effect on the deformation of the plateau of the detachment of part of the lower lithosphere after some period of thickening. A discussion is given in § 5.5.

§ 5.1 The comparison between the new and the previous model.

When a lithosphere is indented at part of its boundary, lithosphere thickening occurs near the indented boundary, and usually the surface Z1 of the thickened lithosphere elevates. The gravitational force arising from this elevation has the effect of resisting further thickening and also dispersing the thickening to wider areas by means of gravitational flow England & McKenzie (1983). Two conclusions were derived by England & McKenzie (1983): A. The area affected by the indentation is on a similar scale to the length of the indenting boundary. So the Tibetan plateau may well be the result of crustal thickening caused by boundary indentation. B. With $Ar > 0$, there is an upper limit to the crustal thickness supportable by boundary indentation. The deformation style transforms from intense

compressive strain in the early phase to almost plane strain once the maximum supportable crustal thickness is reached. Since their derivations have been found to be at fault, I carried out a similar analysis using the same boundary conditions and parameters as were used by England & McKenzie (1983) to investigate if and how their conclusions have been seriously affected. The boundary conditions are shown in Figure 5.1.1. Because of symmetry, only the right-hand half of the area under study is shown. The parameters are listed below.

Initial thickness of the lithosphere	L_o=100 km
Initial thickness of crust	s =35 km
Velocity scaling factor	U_o=5 cm/year
Density of crust	ρ_c=2.95
Density of lower lithosphere	ρ_m=3.30
Density of asthenosphere	ρ_a=3.30
Temperature at lower boundary of lithosphere	T_L=1200°C
Temperature at lower boundary of asthenosphere	T_A=1300°C
Power law exponent in rheological equation	n =3
Thermal diffusivity of the lithosphere	$\kappa = 3.54\times10^{-6} m^2 s^{-1}$

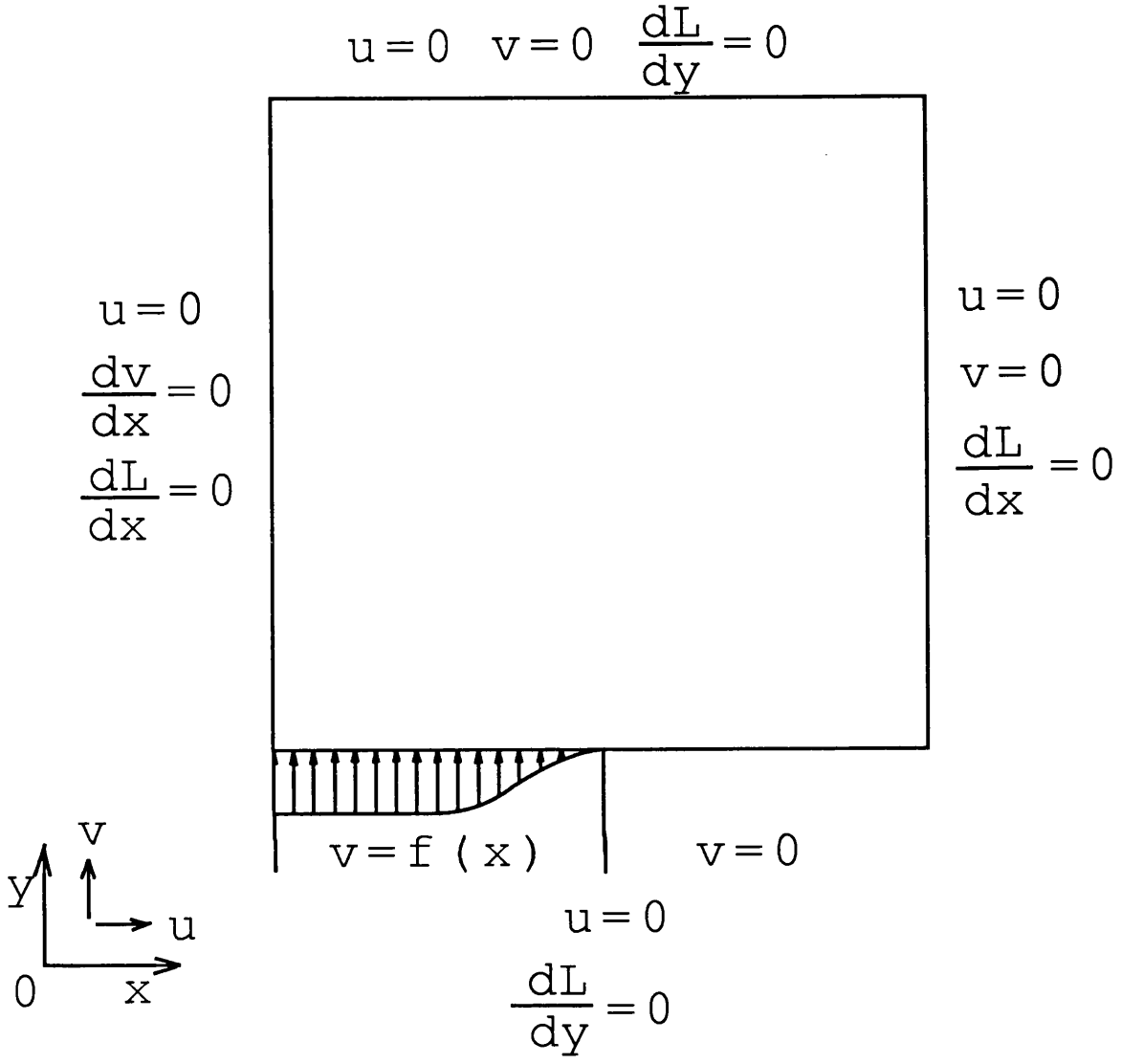

Figure 5.1-1. The general boundary conditions used in studying lithosphere shortening are the same as those used by England & McKenzie (1982, 1983). The function f(x) has the form:

$f(x)=u_{max}$ $\quad 0 \le x \le 8Lo$

$f(x)=u_{max}\cos^2[\frac{\pi}{2}(\frac{x}{8Lo} - 1)]$ $\quad 8Lo \le x \le 16Lo$

where Lo is the initial thickness of the lithosphere.
The area is meshed 32Lo × 32Lo.

Two sets of analyses were carried out with different strength formulations. The first uses a constant average rheology ($\bar{B} = \bar{B}o$), and makes no allowance for thermal processes. It therefore has completely the same boundary conditions and mechanical properties as in the England & McKenzie (1982, 1983) model. Any differences in results would be solely due to the differences in the mechanical equations used.

In all the following figures, the unit of crustal thickness is kilometers and the unit of vertical strain rate is Uo/Lo, where Uo is 5cm/year and Lo is 100 km. So Uo/Lo = $1.7 \times 10^{-14} s^{-1}$.

Figure 5.1-2 and Figure 5.1-3 are the contour maps of the crustal thicknesses and the vertical strain rates with A=30 **(Model 5.1I)** and A=100 **(Model 5.1II)** respectively. With A=30, the deformation style is dominated by the boundary indentation up to 32 Ma. By 40 Ma, the effect of gravitational flow arising from the high elevation is as great as boundary influx, and the maximum thickening occurs almost uniformly in a large area in front of the influxing boundary, including the area with maximum elevation. With A=100, the effect of gravity begins to show after 16 Ma. At 32 Ma, the maximum thickening occurs deep in front of the influxing boundary, and at 40 Ma, the elevated area has one of the least rates of thickening. This case is similar to the one given by England & McKenzie (Figure 9, 1983).

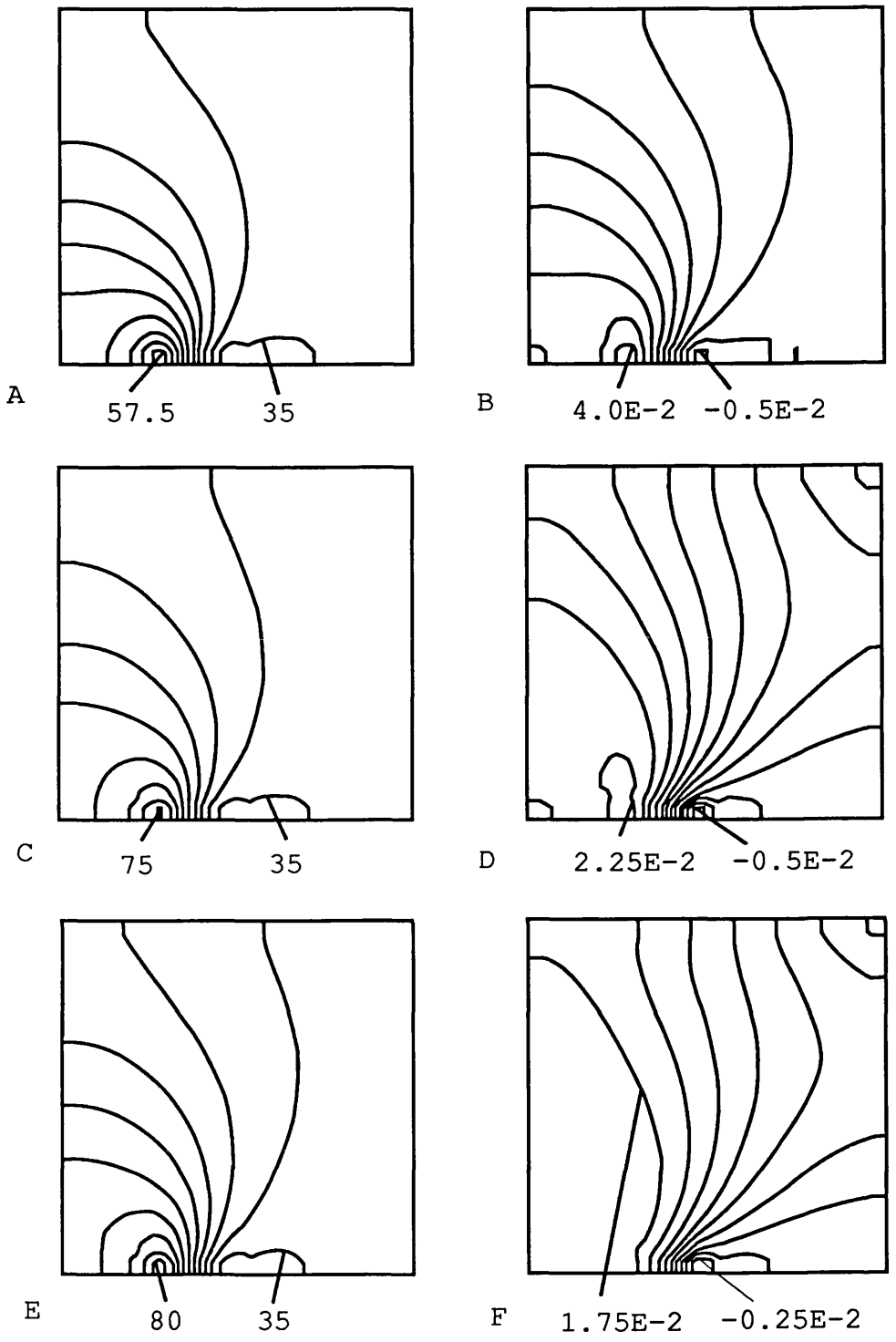

Figure 5.1-2. Contour maps of crustal thickness (A, C, E) and vertical strain rate (B, D, F) of a shortened lithosphere, with A = 30, $\bar{B}=\bar{B}o$, and no thermal processes **(Model 5.1I)**.

A. Time is 16 Ma, contours are from 35 by 2.5 to 57.5 km.
B. Time is 16 Ma, contours are from -0.5E-2 by 0.5E-2 to 4.0E-2 (Uo/Lo).
C. Time is 32 Ma, contours are from 35 by 5 to 75 km.
D. Time is 32 Ma, contours are from -0.5E-2 by 0.25E-2 to 2.25E-2 (Uo/Lo).
E. Time is 40 Ma, contours are from 35 by 5 to 80 km.
F. Time is 40 Ma, contours are from -0.25E-2 by 0.25E-2 to 1.75E-2 (Uo/Lo).

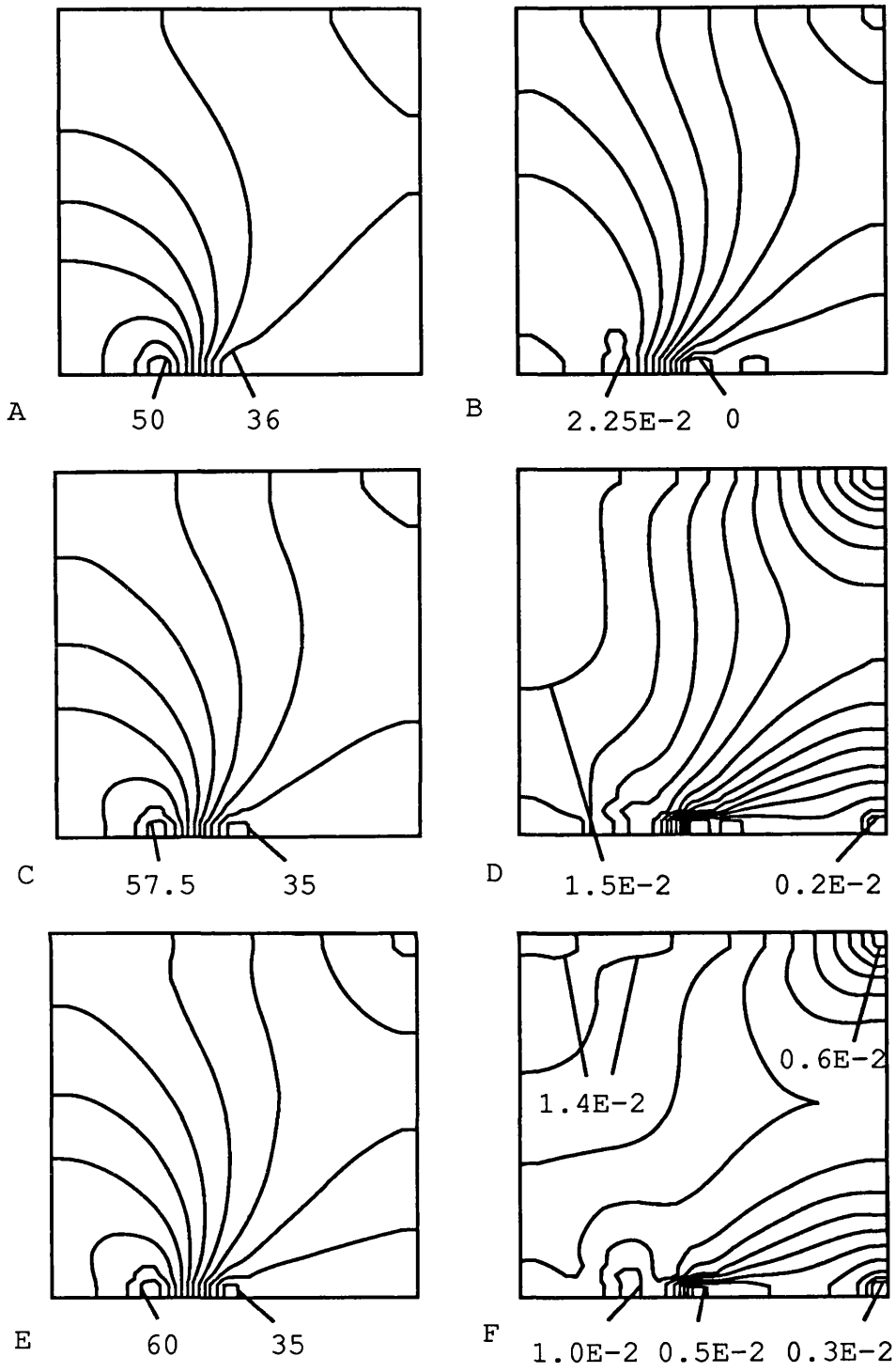

Figure 5.1-3. Contour maps of crustal thickness (A, C, E) and vertical strain rate (B, D, F) of a shortened lithosphere, with A = 100, $\bar{B}=\bar{B}o$, and no thermal processes **(Model 5.1II)**.

A. Time is 16 Ma, contours are from 36 by 2 to 50 km.
B. Time is 16 Ma, contours are from 0 by 0.25E-2 to 2.25E-2 (Uo/Lo).
C. Time is 32 Ma, contours are from 35 by 2.5 to 57.5 km.
D. Time is 32 Ma, contours are from 0.2E-2 by 0.1E-2 to 1.5E-2 (Uo/Lo).
E. Time is 40 Ma, contours are from 35 by 2.5 to 60 km.
F. Time is 40 Ma, contours are from 0.3E-2 by 0.1E-2 to 1.4E-2 (Uo/Lo).

Generally speaking, with constant average strength, the results obtained, although different in details, are consistent with those by England & McKenzie (1983). This may further suggest that conclusions stemming from those works (England, Houseman & Sonder, 1985; Cohen & Morgan, 1986; Sonder & England, 1989) have not been qualitatively invalidated by the involvement of the incorrectly derived equations.

The above calculation does not take into account the thermal processes. As a result, if a crust is thickened from 35 km to 70 km, the lithosphere is thickened from 100 km to 200 km. This is certainly not the case in the Tibetan Plateau, where the thickness of the lithosphere is only about 125 km although the thickness of the crust is in the range of 60 to 70 km. Also, the above calculation treats the buoyancy force due to the thickening of crust as the only factor which opposes further thickening.

The second set of calculations takes into account the thermal restoration process, using eq.(3.1-5). It also uses a thickness-related average strength ($\bar{B} = \bar{B}oL/Lo$) due to the increased depth of the brittle-ductile transition zone (see §3.2), because of which the thickened lithosphere is strengthened and resists further thickening, which provides another mechanism to limit the thickness of the lithosphere under indentation.

Figure 5.1-4 and Figure 5.1-5 show the crustal thickness and vertical strain rates with A=30 **(Model 5.1III),** and 100 **(Model 5.1IV)** respectively allowing for the thermal restoration processes on lithospheric thickness. With A=30, the maximum thickening occurs at the indenting boundary all the

time, and clearly the effect of gravity is not significant. With A=100, the style of deformation is still controlled by the boundary indentation, but by 40 Ma, large thickening has spread further from the indented boundary driven by the gravitational flow arising from high topography. Compared with the corresponding results given by England & McKenzie (Figure 8, Figure 9, 1983), however, the effect of gravitational flow is apparently smaller. The area affected by the indentation is to some extent deeper than in the last set of calculations with $\bar{B}=\bar{B}o$.

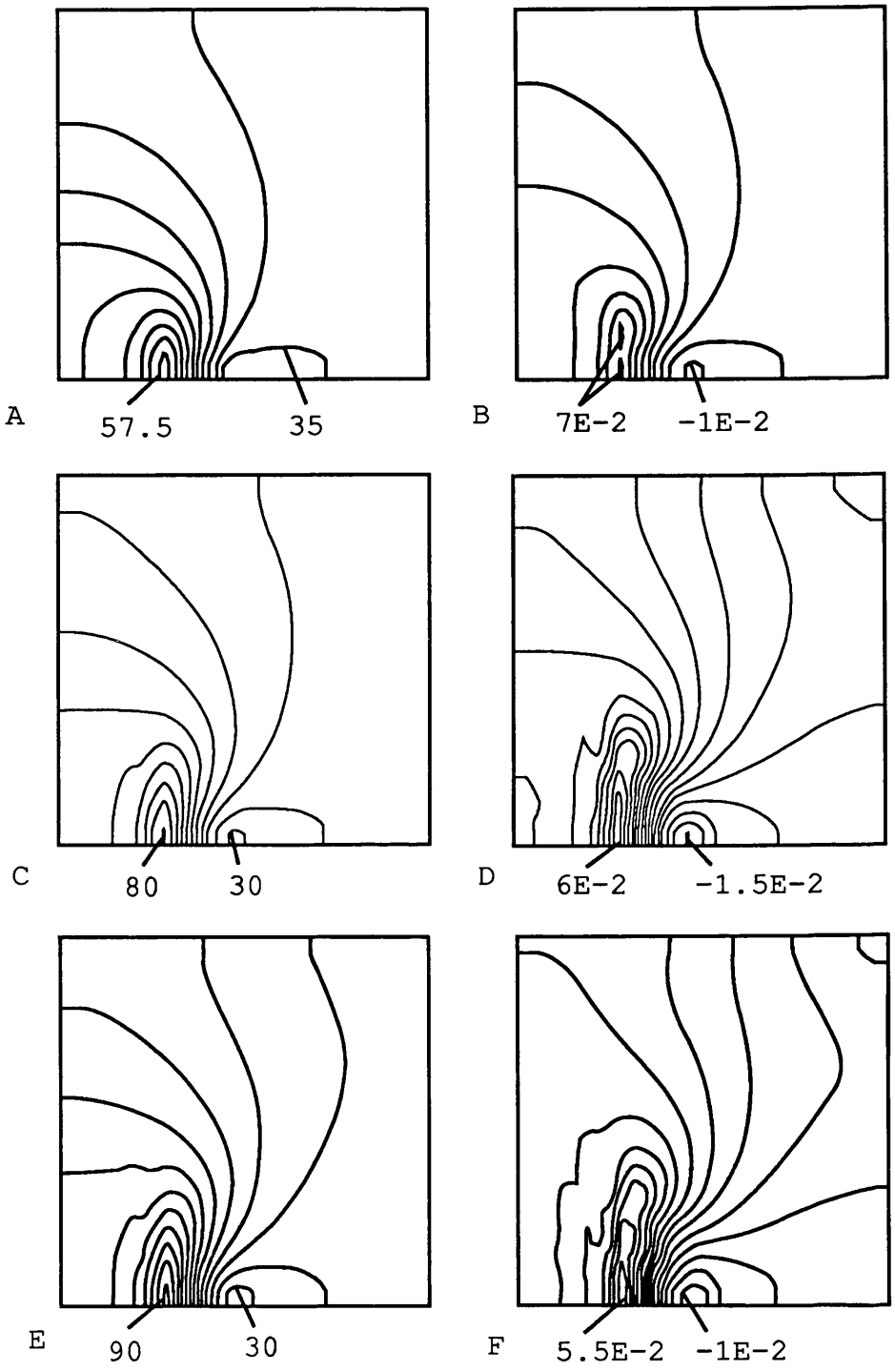

Figure 5.1-4. Contour maps of crustal thickness (A, C, E) and vertical strain rate (B, D, F) of a shortened lithosphere, with A = 30, $\bar{B}$ = $\bar{B}$oL/Lo, and thermal restoration process **(Model 5.1III)**.

A. Time is 16 Ma, contours are from 35 by 2.5 to 57.5 km.
B. Time is 16 Ma, contours are from -1.0E-2 by 1.0E-2 to 7.0E-2 (Uo/Lo).
C. Time is 32 Ma, contours are from 30 by 5 to 80 km.
D. Time is 32 Ma, contours are from -1.5E-2 by 0.5E-2 to 6.0E-2 (Uo/Lo).
E. Time is 40 Ma, contours are from 30 by 5 to 90 km.
F. Time is 40 Ma, contours are from -1.0E-2 by 0.5E-2 to 5.5E-2 (Uo/Lo).

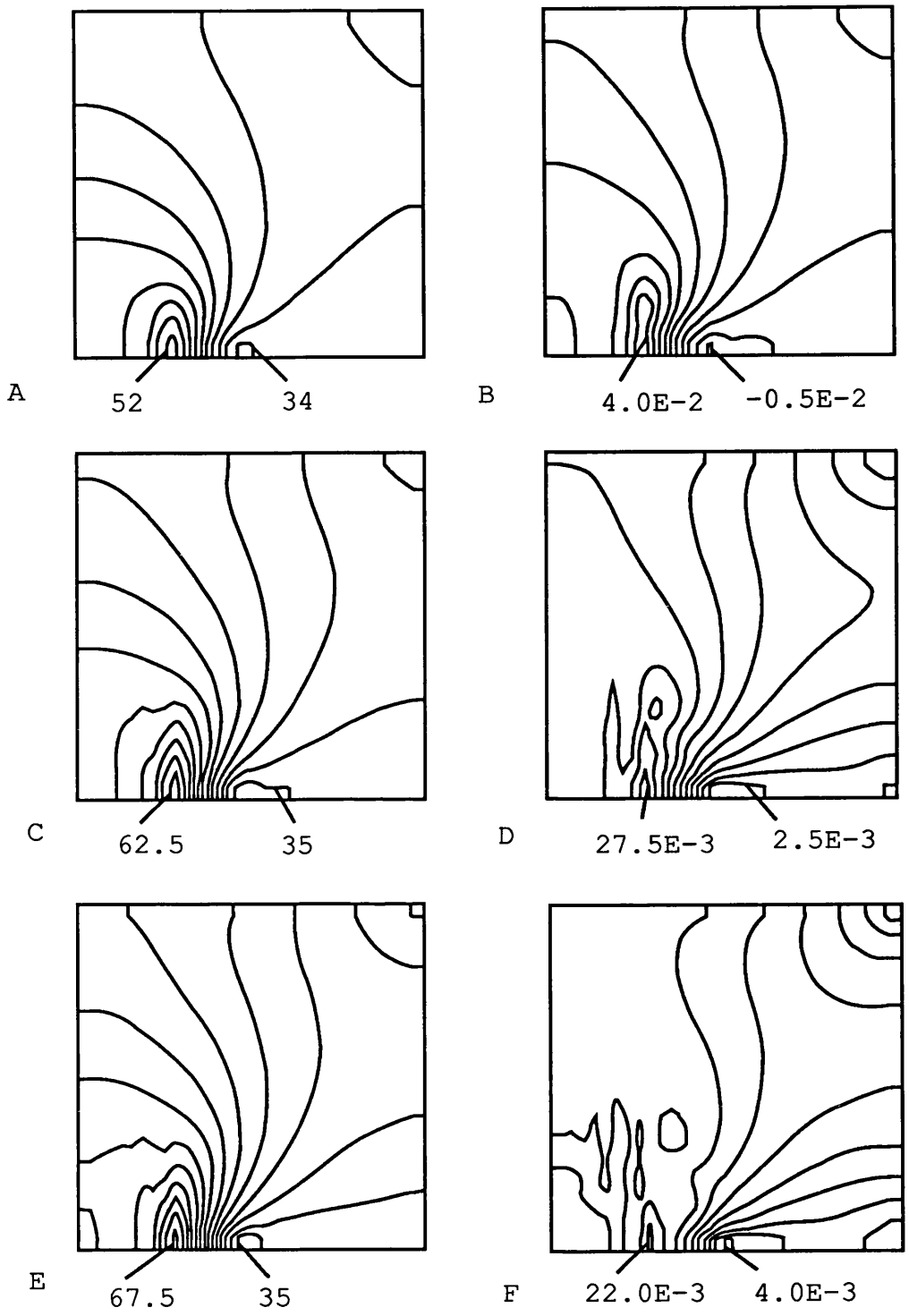

Figure 5.1-5. Contour maps of crustal thickness (A, C, E) and vertical strain rate (B, D, F) of a shortened lithosphere, with A = 100, $\bar{B}$ = $\bar{B}$oL/Lo, and thermal restoration process **(Model 5.1IV)**.

A. Time is 16 Ma, contours are from 34 by 2 to 52 km.
B. Time is 16 Ma, contours are from -0.5E-2 by 0.5E-2 to 4.0E-2 (Uo/Lo).
C. Time is 32 Ma, contours are from 35 by 2.5 to 62.5 km.
D. Time is 32 Ma, contours are from 2.5E-3 by 2.5E-3 to 27.5E-3 (Uo/Lo).
E. Time is 40 Ma, contours are from 35 by 2.5 to 67.5 km.
F. Time is 40 Ma, contours are from 4.0E-3 by 2.0E-3 to 22.0E-3 (Uo/Lo).

§ 5.2 Analysis of the deformation with a decreasing rate of boundary displacement.

In the last section, all the analysis was done with a constant rate of boundary indentation. It is clear from those results that the plateau will not collapse at a later stage of deformation. A possible cause of the extension of plateaus is a reduction in boundary compression. In the case of the Tibetan Plateau palaeomagnetic measurements and geological observations all indicate that the convergence rate between the two continents decreased from 10 cm/year to the present 4.5 cm/year, and about half of the present convergence is taken up by the thrusting in front of the Himalaya (Tapponnier & Molnar, 1977; Armijo et al., 1982). In this section, I model the deformation of the Tibetan Plateau with a decreasing rate of convergence. Three cases are studied. In the first one, the boundary displacement slows down in two stages. In the second one, the boundary displacement was reduced abruptly after initial deformation. In the third one, the lithosphere is of thickness-related average strength ($\bar{B} = \bar{B}oL/Lo$), and the boundary velocity is cut abruptly as in the second case. In all the three cases, the parameters are as listed in § 5.1. The thermal restoration process is included in all the cases.

A. Case one

In this case, u_{max} decreases from 10 cm/year in two stages to 2 cm/year in 40 Ma (Figure 5.2-1). The boundary condition is still as shown in Figure 5.1-1. The lithosphere is of constant average strength with A=30 **(Model 5.2I)**. The two-stage decrease is chosen on speculation of the reason for the slowing down of boundary indentation. The first decrease is between

the time when the two continents first collided with a weak geosyncline in between (see § 4.5 and Murrell 1986) and the time when the trapped geosyncline is fully compressed, and the second decrease is taken to be due to the increased resistance to lithosphere thickening. However, the choice of the pattern of the decrease of indentation rate is found to be not important. If the decrease is uniform, the result is basically the same.

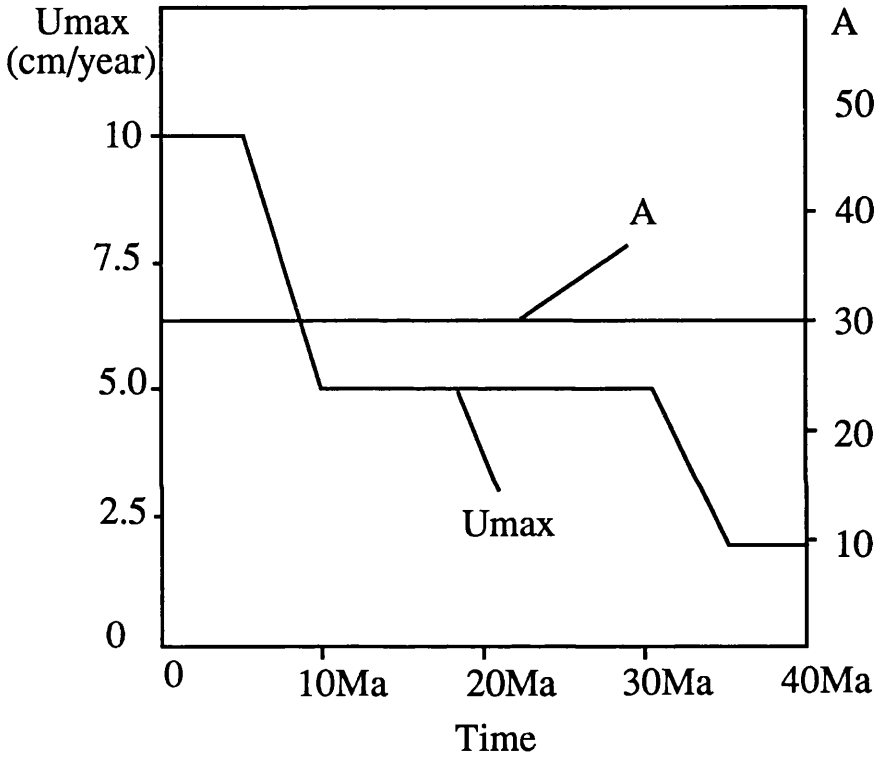

Figure 5.2-1 The A number and the decreasing rate of boundary indentation in **Model 5.2I**.

Results from this calculation shows that at no time is there net thinning over the thickened part of the lithosphere. The crustal thickness and the vertical strain rate after 20, 30 and 40 Ma of deformation is shown in Figure 5.2-2.

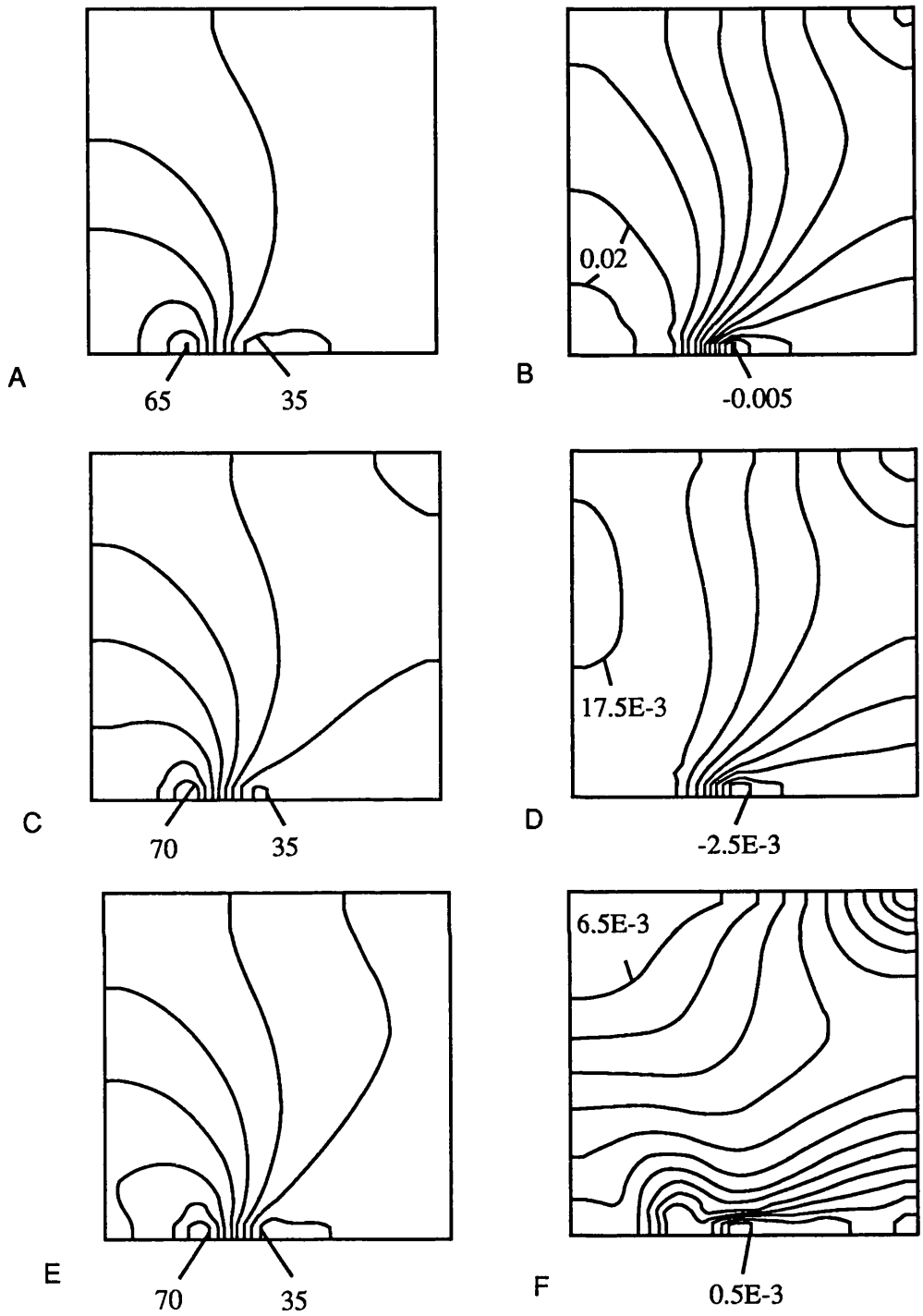

Figure 5.2-2 The crustal thickness (A, C, E) and vertical strain rate (B, D, F) during deformation with decreasing rate of indentation **(Model 5.2I).** A=30. $\bar{B} = \bar{B}o$. Thermal restoration process is considered.

A. Time =20 Ma. Contours are from 35 by 5 to 65 km.
B. Time =20 Ma. Contours are from -0.005 by 0.0025 to 0.02 (Uo/Lo).
C. Time =30 Ma. Contours are from 35 by 5 to 70 km.
D. Time =30 Ma. Contours are from -2.5E-3 by 2.5E-3 to 17.5E-3 (Uo/Lo).
E. Time =40 Ma. Contours are from 35 by 5 to 70 km.
F. Time =40 Ma. Contours are from 0.5E-3 by 0.5E-3 to 6.5E-3 (Uo/Lo).

B. Case two

Since gradual slowing down does not cause net extension, I study a case in which slowing down is abrupt. In this case, u_{max} is maintained at 5 cm/year for 32 Ma and then reduced to 2 cm/year, with A=30 **(Model 5.2II)** and 100 **(Model 5.2III)** respectively. The results after the first 32 Ma deformation are similar to Figure 5.1-2 C,D for A=30 and to Figure 5.1-3 C,D for A=100. Immediately after the abrupt reduction of u_{max}, thickening is still the dominant process, and there is no net thinning at the thickened part of the lithosphere, whether A=30 or A=100 (Figure 5.2-3). After 32 Ma, as long as there is no further reduction of boundary indentation rate, net thinning can not occur. The results are not shown here.

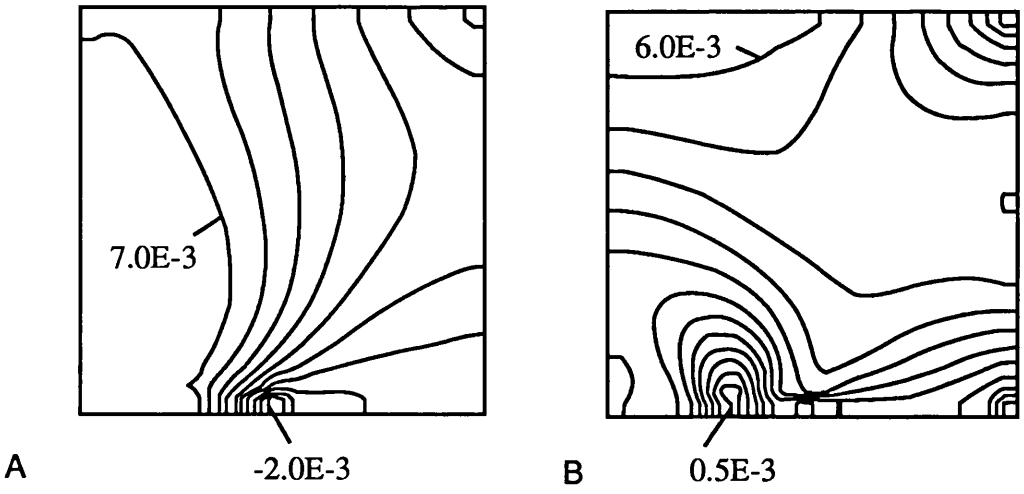

Figure 5.2-3 The vertical strain rates immediately after the reduction of boundary indentation rate to 2 cm/year at the end of 32 Ma constant indentation with u_{max}=5 cm/year. $\bar{B}=\bar{B}o$. Thermal restoration process has been considered.
A. A=30 **(Model 5.2II)**. Contours are from -2.0E-3 by 1.0E-3 to 7.0E-3 (Uo/Lo).
B. A=100 **(Model 5.2III)**. Contours are from 0.5E-3 by 0.5E-3 to 6.0E-3.

C. Case three

In this case the lithosphere is of thickness-related average strength ($\bar{B} = \bar{B}oL/Lo$), and the abrupt cut of u_{max} resulted in net thinning at the thickened part of the lithosphere under some circumstances.

First, the lithosphere with thickness-related strength is indented for 32 Ma with constant boundary velocity u_{max} = 5 cm/year with A = 50 **(Model 5.2IV)** and 90 **(Model 5.2V)** respectively (Figure 5.2-4 and Figure 5.2-5). Then u_{max} is reduced from 5 cm/year to 2 cm/year. In the case with A=50, on the reduction of u_{max}, the vertical strain rate is still positive at the thickened areas, although the thicker part has the smaller thickening rate (Figure 5.2-6A), while with A=90, after the same reduction of u_{max}, the buoyancy force is great enough to override the boundary indentation, and part of the thickened lithosphere has negative vertical strain-rate, that is, the plateau is under net thinning or extension (Figure 5.2-6B).

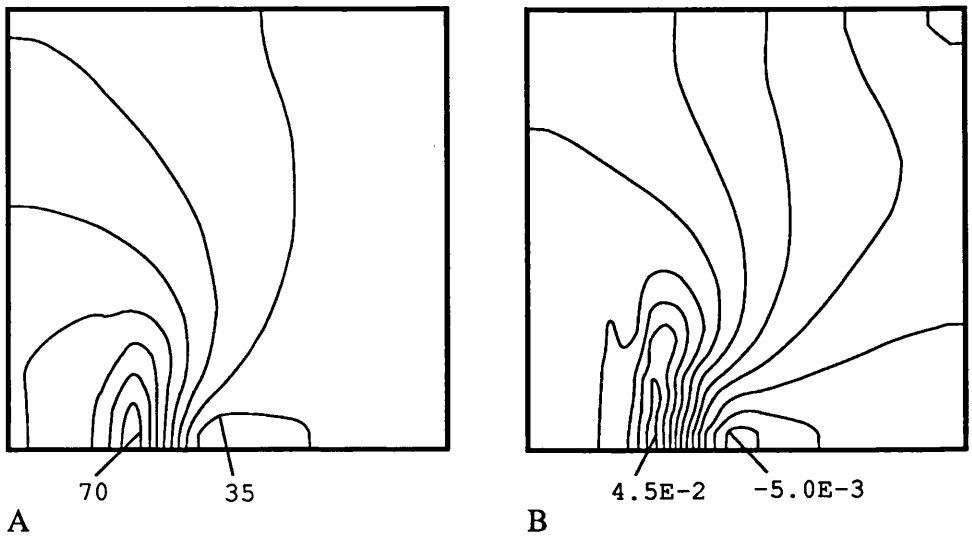

Figure 5.2-4 The crustal thickness and vertical strain rate after 32 Ma constant indentation with u_{max} = 5 cm/year, A = 50, $\bar{B}$ = $\bar{B}$oL/Lo and thermal restoration process **(Model 5.2IV)**.
A. Crustal thickness. Contours are from 35 by 5 to 70 km.
B. Vertical strain rate. Contours are from -0.005 by 0.005 to 0.045 (Uo/Lo).

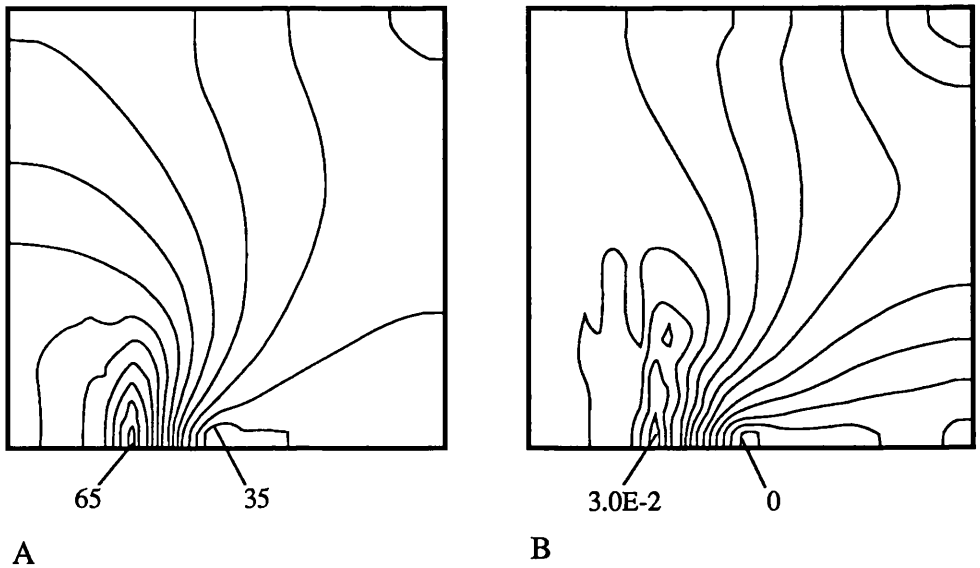

Figure 5.2-5 The crustal thickness and vertical strain rate after 32 Ma constant indentation with u_{max} = 5 cm/year, A = 90, $\bar{B}$ = $\bar{B}$oL/Lo, and with thermal restoration process **(Model 5.2V)**.
A. Crustal thickness. Contours are from 35 by 5 to 65 km.
B. Vertical strain rate. Contours are from 0 by 0.0025 to 0.03 (Uo/Lo).

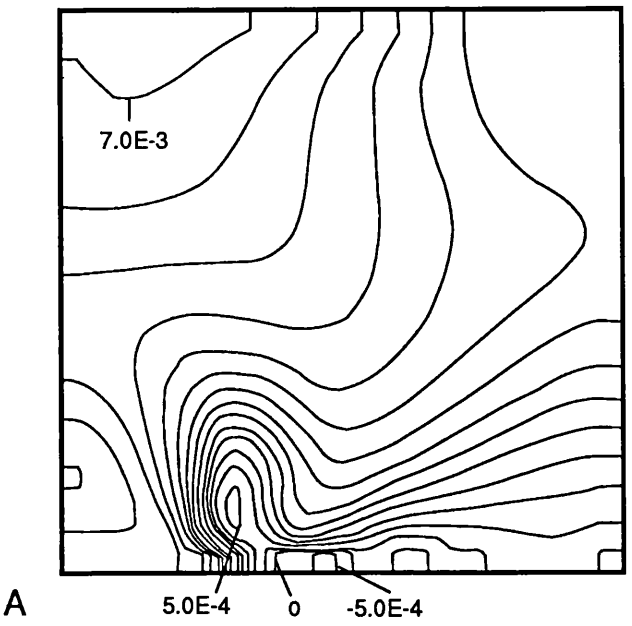

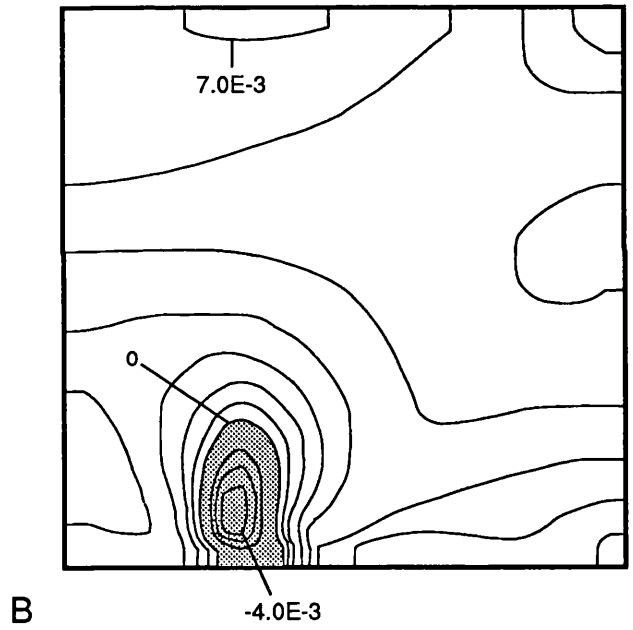

Figure 5.2-6 The vertical strain rates on the reduction of boundary indentation rate to 2 cm/year at the end of 32 Ma constant indentation in Model 5.2IV and Model 5.2V.
A. A=50 **(Model 5.2IV)**. Contours are from 5.0E-4 by 5.0E-4 to 7.0E-3 (Uo/Lo). The vertical strain-rate at the elevated area is very close to 0, and is therefore in phase 2.
B. A=90 **(Model 5.2V)**. Contours are from -4.0E-3 by 1.0E-3 to 7.0E-3 (Uo/Lo). The vertical strain-rate at the elevated area is negative, and therefore extension is under way. This is the only example in this section in which the plateau evolves from phase 2 to phase 3 by reducing the rate of boundary displacement.

The above analysis shows that a reasonable slowing down of indentation does not result in the net thinning of the thickened lithosphere unless the lithosphere is of thickness-related average rheology ($\bar{B} = \bar{B}oL/Lo$). The thickness-related average rheology is valid in geologically fast shortening or extension of lithosphere so that the strong layer is not significantly heated or cooled during deformation. In the case of the Tibetan Plateau, 40 Ma seems to be enough for the strong layer to be affected by heating, and the thickness-related rheology may not be valid. For a plateau formed in a much shorter time than Tibet, reduction in boundary displacement may cause the transition from phase 2 to phase 3.

The analysis in this chapter has been concerned with the transformation of the style of deformation during indentation. There are two processes during deformation acting against each other. One is the boundary indentation, which causes compression and thickening, and the other is the horizontal buoyancy force due to high gravity potential at the elevated area (plateau) near the indenting boundary, which tends to make the lithosphere to flow away from that area. The former is dominant in the beginning, but the latter gradually becomes important too as crustal thickness increases. By reducing the rate of boundary indentation, the balance of the two process may be changed and the effect of gravitational flow may dominate. However, it can be seen from the results that in the case of the Tibetan Plateau, a reasonable reduction of the boundary indentation rate is not enough to change the balance. This result supports the conclusion of England & Houseman (1988) that a reasonable reduction in the rate of boundary displacement could not be the cause of the extension of the Tibetan Plateau.

§ 5.3 The deformation of indented lithosphere with a decreasing rate of boundary displacement and a weakening rheology.

Numerical analysis in § 5.2 shows that under most circumstances reduction of the boundary displacement rate does not cause subsequent extension of the indented and thickened lithosphere. Additional explanations for the extension are either that the lithosphere undergoes a rheological change (due to the heating of the thickened, cooler lithosphere) so that the maximum crustal thickness supportable is reduced or that there has been an uplift of the Tibetan plateau (due to detachment of thickened lithosphere mantle) and the increased gravitational potential causes the E-W extension. Because a larger A number corresponds to weaker lithosphere, the effects of warming up of the lithosphere can be simulated by increasing the value of A at a later stage of deformation.

In this section, the boundary displacement evolves in stages. The lithosphere strength is independent of thickness. Two models are analyzed. In the first one **(Model 5.3I)**, both the boundary rate of displacement and the A number change relatively moderately (Figure 5.3-1), u_{max} from 10 cm/year to 2.5 cm/year, A from 0 to 30. The results after 40 Ma of deformation are shown in Figure 5.3-2. There is local net thinning, but small in both area and magnitude. In the second one **(Model 5.3II)**, u_{max} changes from 10 cm/year in the beginning to 2cm/year in the end, and A increases from 0 to 50 (Figure 5.3-3). The results show significant extension (Figure 5.3-4).

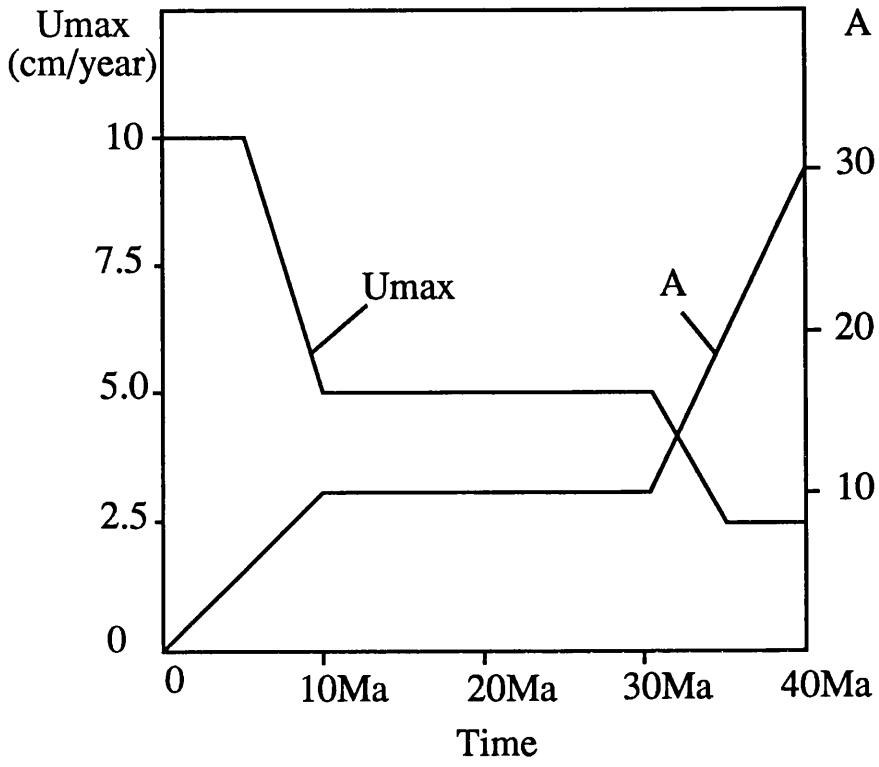

Figure 5.3-1. The boundary velocity and the A number for **Model 5.3I.**

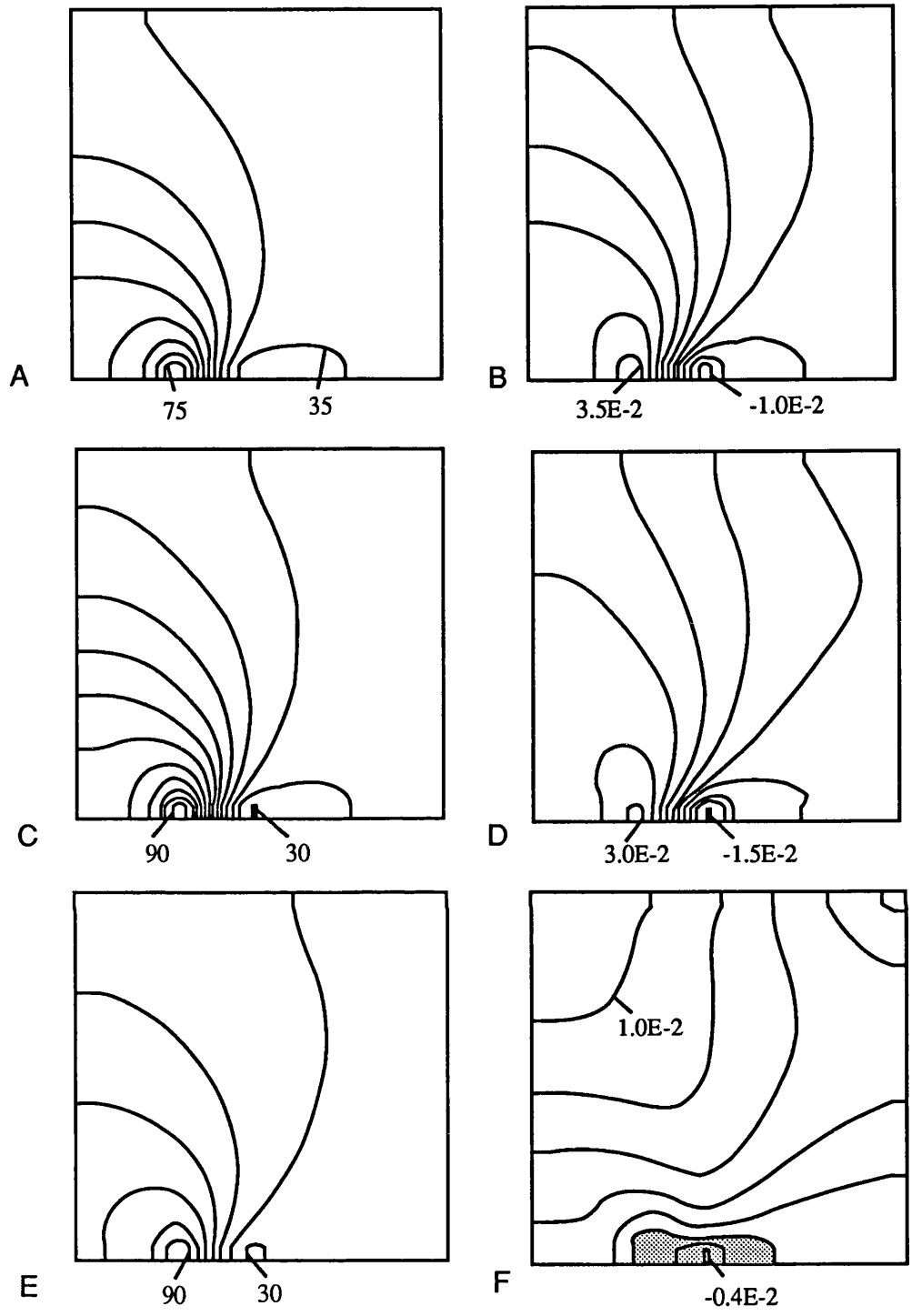

Figure 5.3-2. Crustal thickness (A, C, E) and vertical strain rate (B, D, F) of an indented lithosphere with decreasing boundary velocity and increasing A number as shown in Figure 5.3-1 **(Model 5.3I)**.
A. Time is 30 Ma, contours are from 35 by 5 to 75 (km).
B. Time is 30 Ma, contours are from -1.0E-2 by 0.5E-2 to 3.5E-2 (Uo/Lo).
C. Time is 35 Ma, contours are from 30 by 5 to 90 (km).
D. Time is 35 Ma, contours are from -1.5E-2 by 0.5E-2 to 3.0E-2 (Uo/Lo).
E. Time is 40 Ma, contours are from 30 by 10 to 90 (km).
F. Time is 40 Ma, contours are from -0.4E-2 by 0.2E-2 to 1.0E-2 (Uo/Lo).

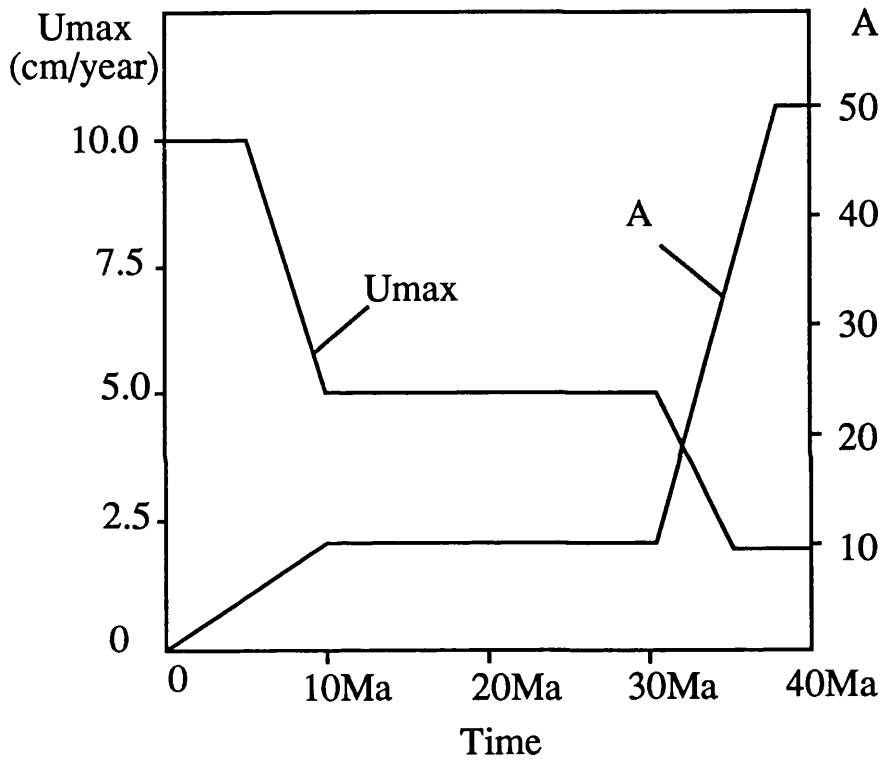

Figure 5.3-3. The boundary velocity and the A number during the deformation in **Model 5.3II.**

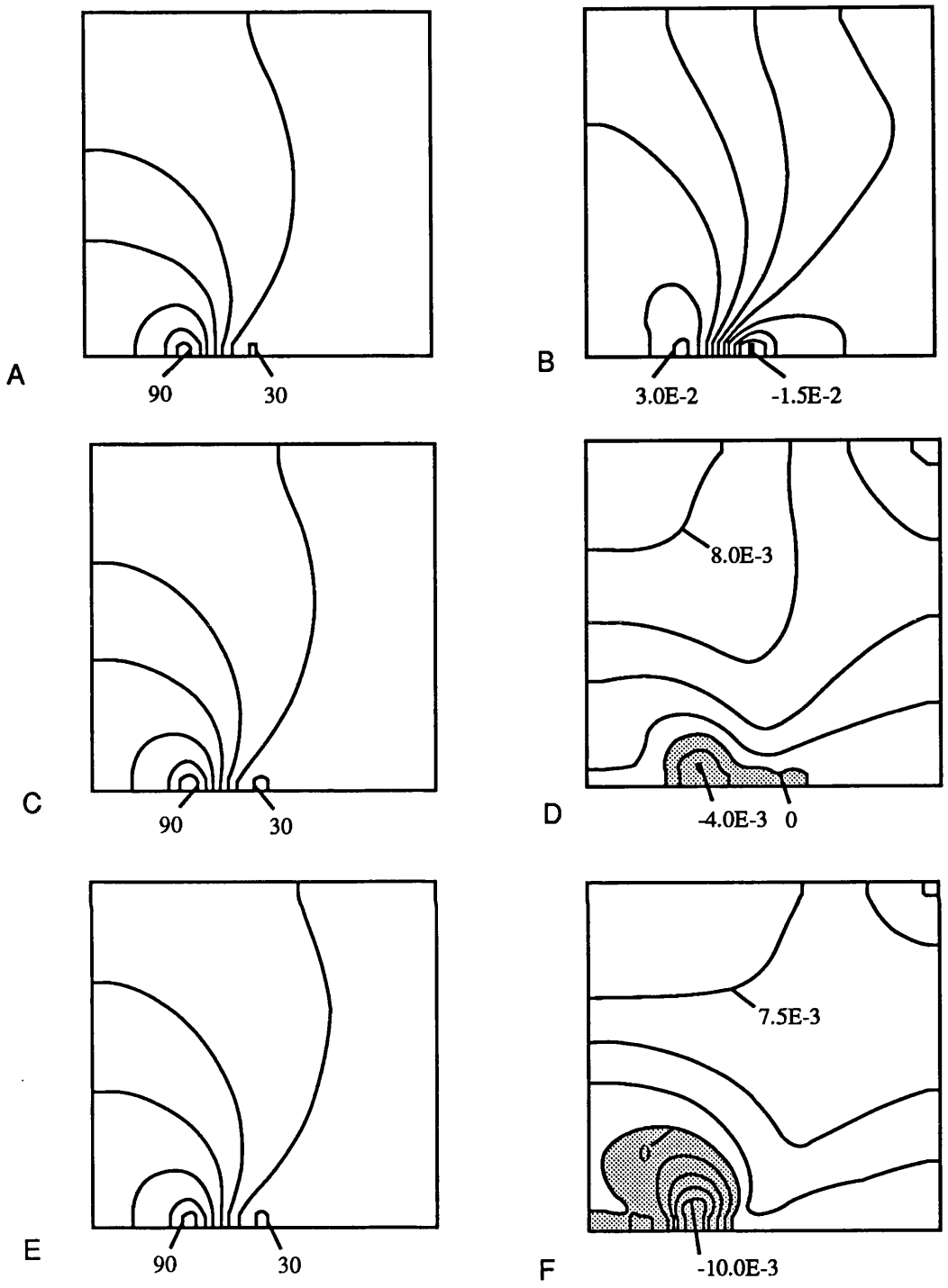

Figure 5.3-4. The crustal thickness (A, C, E) and vertical strain rate (B, D, F) of an indented lithosphere with decreasing boundary velocity and increasing A number as shown in Figure 5.3-3 **(Model 5.3II).**
A. Time is 30 Ma, contours are from 30 by 10 to 90 (km).
B. Time is 30 Ma, contours are from -1.5E-2 by 0.5E-2 to 3.0E-2 (Uo/Lo).
C. Time is 35 Ma, contours are from 30 by 10 to 90 (km).
D. Time is 35 Ma, contours are from -4.0E-3 by 2.0E-3 to 8.0E-3 (Uo/Lo).
E. Time is 40 Ma, contours are from 30 by 10 to 90 (km).
F. Time is 40 Ma, contours are from -10.0E-3 by 2.5E-3 to 7.5E-3 (Uo/Lo).

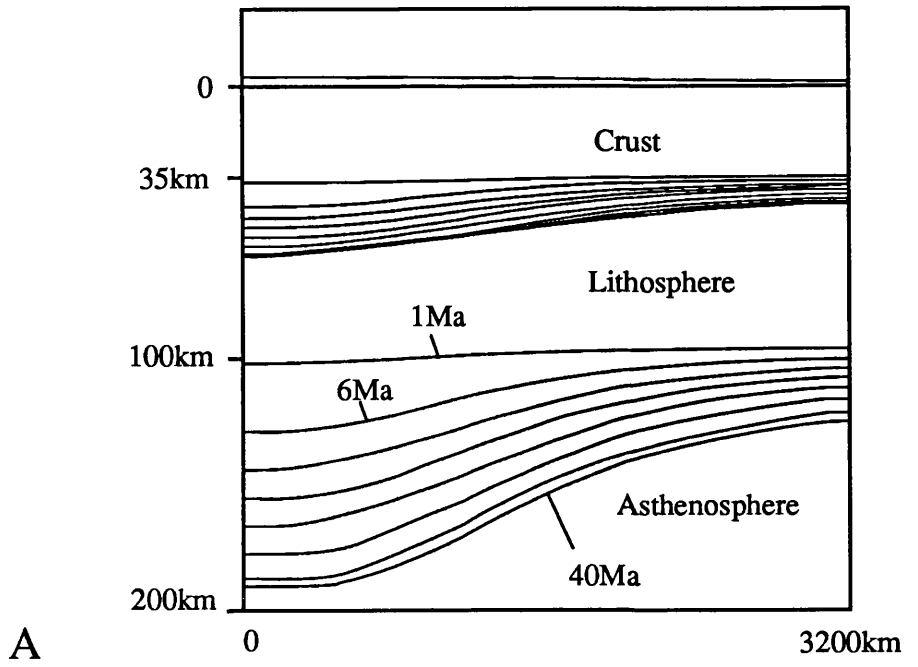

A

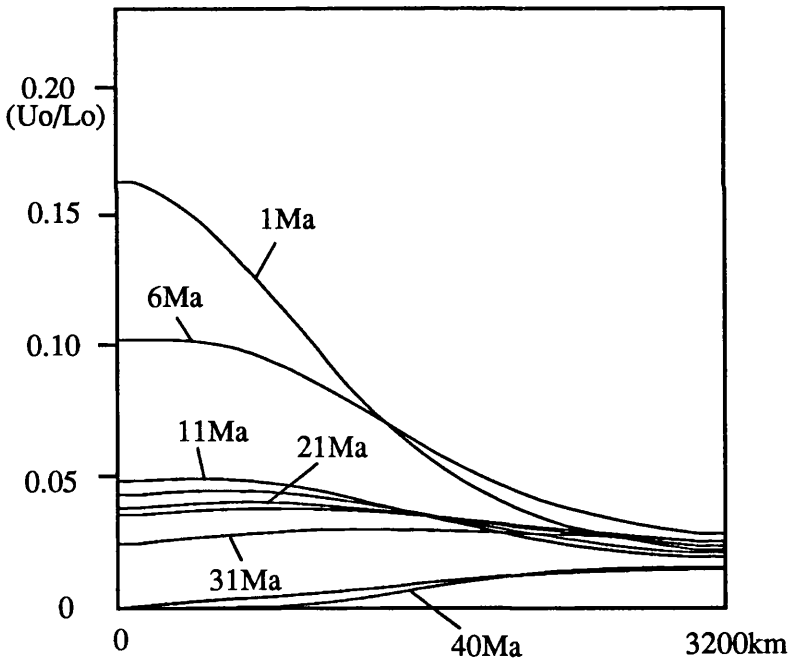

B

Figure 5.3-5. The crustal thickness and the vertical strain rate on the central cross section during the deformation in **Model 5.3II**. Boundary indentation rate decreases and A number increases as shown in Figure 5.3-3. Note how after 36 Ma the vertical strain-rate near the indenting boundary decreases to zero.

The above calculations show that the dramatic weakening of the lithosphere at a late stage in the process of shortening and thickening is effective in causing net extension at a late stage in the deformation. Because the elevation in the fist 10 Ma is not large, the value of A is not important during that stage. It is the increase of A from 10 to 30 **(Model 5.3I)** or 50 **(Model 5.3II)** in the later stage that is of concern. The definition of A is (eq.3.3-9)

$$A = \rho_c g \frac{L_o^{((1/n)+1)}}{u_o^{1/n} \bar{B}_o}.$$

so an increase of A by a factor of 3 or 5 is equivalent to a decrease of strength coefficient by a factor of 3 or 5. The question is whether the amount and the duration of lithosphere shortening is large enough to result in the warming up of the strong layer causing a reduction in its strength.

When a lithosphere is shortened of extended, the thermal gradient is disturbed and therefore will tend to restore itself. Solutions have been given to the thermal cooling process in the case of lithosphere extension (McKenzie, 1978; Jarvis & McKenzie, 1980) but not to the warming process in the case of lithosphere shortening. Here I use an analogy to crudely estimate the possible weakening of shortened lithosphere by a thermal process. England (1983) calculated the increase of strength of stretched lithosphere. It can be seen from the result (England 1983, Fig.3) that if a lithosphere is stretched at a strain-rate of $5 \times 10^{-16} s^{-1}$(Peclet number 10), its average strength will increase by a factor of 5 when the lithosphere has been extended by an amount of 2.5 or 1.8, depending on the activation energy of the strong layer material, and the corresponding time required is about 100 Ma and 55 Ma respectively. If the strain-rate is $2.5 \times 10^{-15} s^{-1}$ (Peclet

number 50), the lithosphere will be extended by a factor of 3 in about 40 Ma, and the strength practically does not increase. Thus, for a lithosphere being stretched by an amount of 2 in 40 Ma, it is reasonable to assume that the increase of average strength by thermal cooling is definitely less than a factor of 5. Because the thermal relaxation time of a plate is proportional to the square of its thickness, the decrease in the average strength of thickened lithosphere by a factor of 5 is not likely to happen within 40 Ma and with the amount of shortening mostly between 0.5 and 1. Therefore the restoration of a disturbed thermal gradient is not likely to be quick enough to cause the weakening of the Tibetan Plateau by a factor of 5 in the last 40 Ma.

The above analysis does not take into account the heat produced in the lithosphere. In fact, the crust is rich in heat-producing elements and thus thickened lithosphere generates more heat, which may account for the heating and weakening of the Tibetan Plateau. It is therefore still possible that the Tibetan Plateau has undergone a major rheological change.

§ 5.4 The deformation of indented lithosphere with decreasing boundary velocity and fast uplift at a late stage due to detachment of part of the lower lithosphere.

In this section another possible cause of the extension of the Tibetan Plateau, the delamination or detachment of part of the lithosphere mantle, is studied.

As the lithosphere thickens by shortening, its bottom descends. The thicker the lithosphere is, the deeper is its lower boundary. The relatively cooler extra lithosphere is effectively denser than the surrounding asthenosphere at the same depth. Both convection experiments (Nataf et al., 1981) and numerical simulation (Houseman et al., 1981) suggest that the cold root of lithosphere can detach and sink into the asthenosphere and result in uplift. Fleitout & Froidevaux (1982) raised this hypothesis but did not simulate it. England & Houseman (1988) modelled the effect of uplift due to detachment, but, as mentioned before, their model assumes that mountain is totally balanced by mountain root and there is some degree of self-contradiction in their treatment of this problem.

In this section, the role of a lithosphere root formed during shortening is included by assigning the asthenosphere a lower equivalent density, the value of which is estimated below.

The ratio between the average equivalent density of the asthenosphere and that of the lithosphere mantle is

$$r = \frac{\frac{1}{2}\left[\rho_m(1-\alpha T_L) + \rho_m(1-\alpha T_L)\right]}{\frac{1}{2}\left[\rho_m(1-\alpha T_L\frac{s}{L}) + \rho_m(1-\alpha T_L)\right]} = \frac{1-\alpha T_L}{1-\frac{1}{2}(1+\frac{s}{L})\alpha T_L}$$

in which ρ_m is the density of mantle material on surface temperature and pressure, α is the thermal coefficient, T_L is the temperature at the lower boundary of the lithosphere, s is the crustal thickness, and L is the thickness of the lithosphere. Taking $\alpha = 3.28 \times 10^{-5}/^{\circ}C$, $T_L = 1250\ ^{\circ}C$, and $\frac{s}{L} = 0.35$, then r= 0.986. So if the average equivalent density of the lithosphere mantle is 3.3, that of the asthenosphere would be 3.254.

The boundary conditions are the same as shown in Figure 5.1-1 and parameters used are listed below (note ρ_a is 3.26 rather than 3.30).

Initial thickness of the lithosphere	Lo=100 km
Initial thickness of crust	s=35 km
Velocity scaling factor	Uo=5 cm/year
Effective Density of crust	ρ_c=2.95
Effective Density of lower lithosphere	ρ_m=3.30
Effective Density of asthenosphere	ρ_a=3.26
Temperature at lower boundary of lithosphere	T_L=1200°C
Temperature at lower boundary of asthenosphere	T_A=1300°C
Power law exponent in rheological equation	n=3
Thermal diffusivity of the lithosphere	$\kappa=3.54\times10^{-6}m^2s^{-1}$

The value of A is 50. The maximum boundary velocity decreases from 10 cm/year to 2 cm/year (Figure 5.4-1). The lithosphere is of constant average strength ($\bar{B}=\bar{B}o$). Thermal restoration process on lithosphere thickness has been considered.

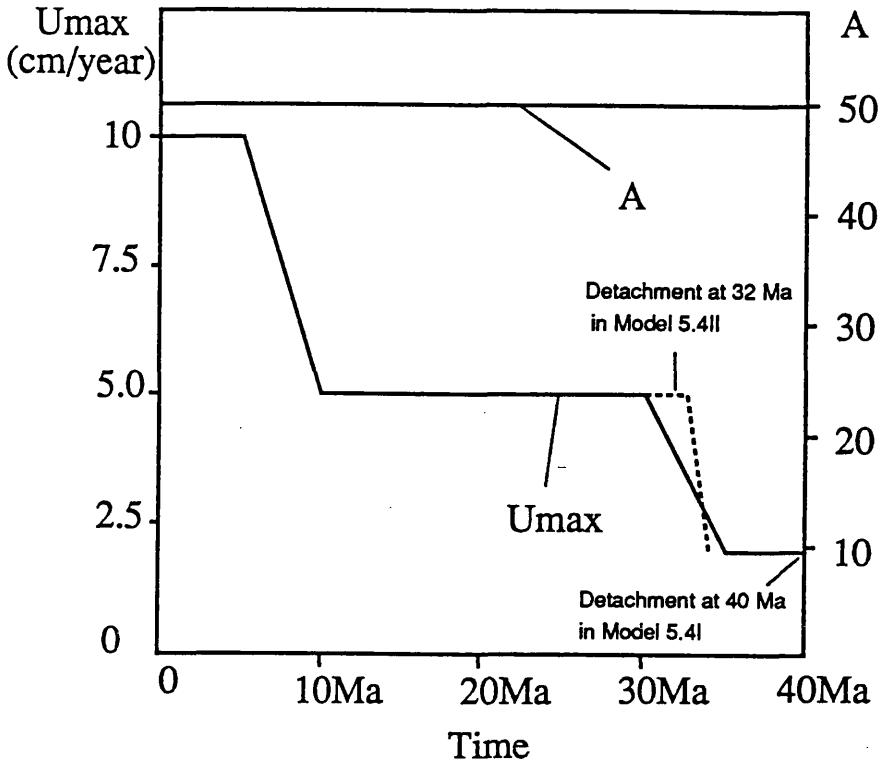

Figure 5.4-1. The A number and the maximum rate of boundary displacement in **Model 5.4I** and **Model 5.4II**.

Two calculations are presented here. In **Model 5.4I**, detachment occurs after the slowing down of indentation, and in **Model 5.4II**, slowing down of the indentation follows the detachment, which results in instant elevation of the plateau.

In **Model 5.4I**, the lithosphere is indented persistently for 40 Ma, with maximum rate of boundary displacement as shown in Figure 5.4-1. The evolution of the crustal thickness and the vertical strain rate is shown in Figure 5.4-2 and Figure 5.4-3. Compared with **Model 5.2I** (Figure 5.2-2), which has the same boundary velocity and lower A number (thus less resistant to lithosphere thickening), the crustal thickness in **Model 5.4I** is larger (up to 15 km) at equivalent times. In the words of Fleitout & Froidevaux (1982), this is because the cold lithosphere root below the thickened

lithosphere generates compressional stress in it and tends to augment thickening. In my model, this is because the thickened lithosphere in **Model 5.4I** sinks more because the asthenosphere has a lower equivalent density than in **Model 5.2I**, thus affecting the slope of the top surface and the Moho surface of the lithosphere, and hence the buoyancy forces. Although expressed differently, the two explanations are physically the same.

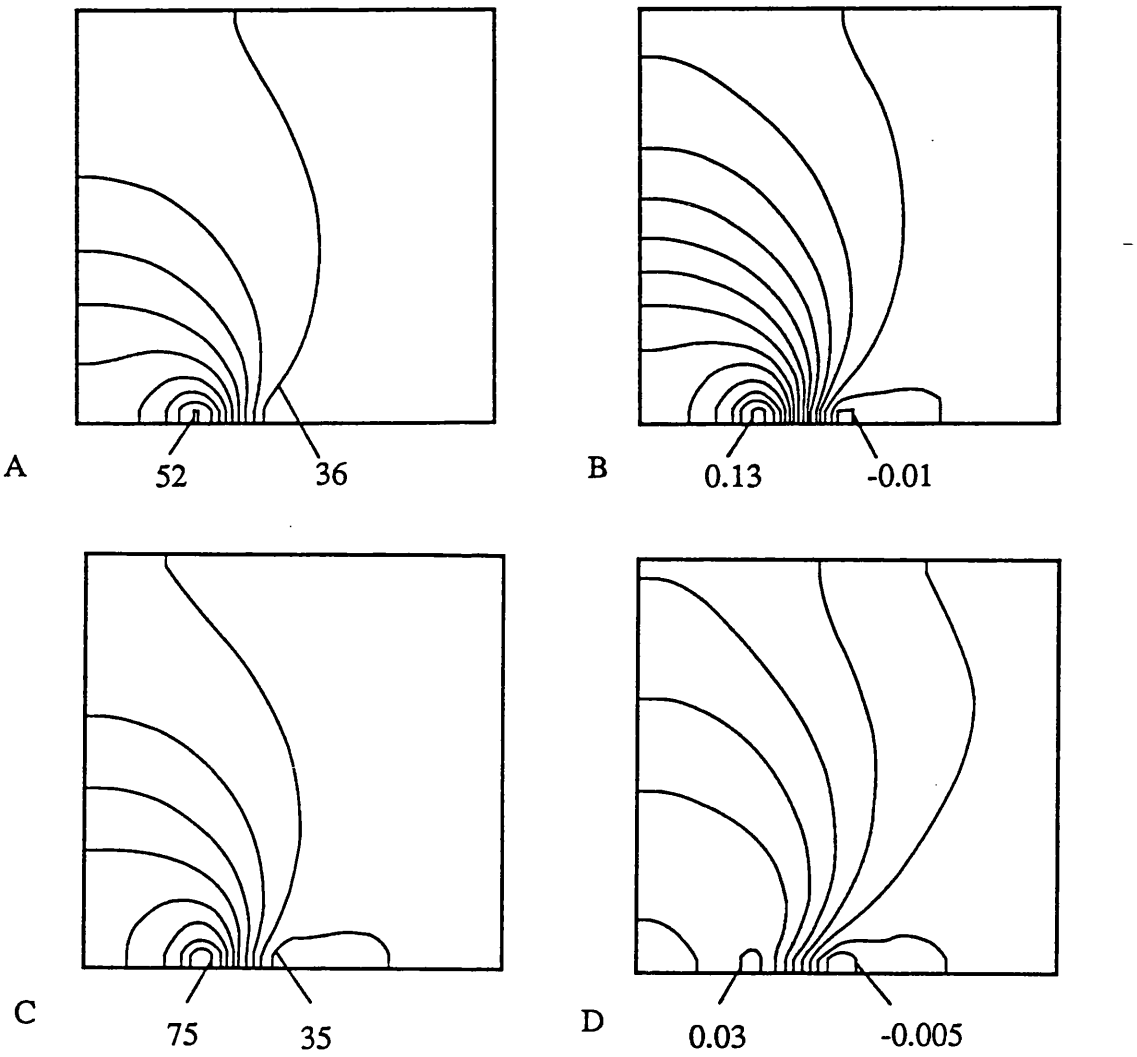

Figure 5.4-2. The crustal thickness (A, C) and the vertical strain rate (B, D) of indented lithosphere with decreasing rate of boundary displacement as shown by the solid line in Figure 5.4-1. A = 50. $\bar{B}=\bar{B}o$. **(Model 5.4I)**
A. Time is 5 Ma, contours are from 36 by 2 to 52 km.
B. Time is 5 Ma, contours are from -0.01 by 0.01 to 0.13 (Uo/Lo).
C. Time is 20 Ma, contours are from 35 by 5 to 75 km.
D. Time is 20 Ma, contours are from -0.005 by 0.005 to 0.03 (Uo/Lo).

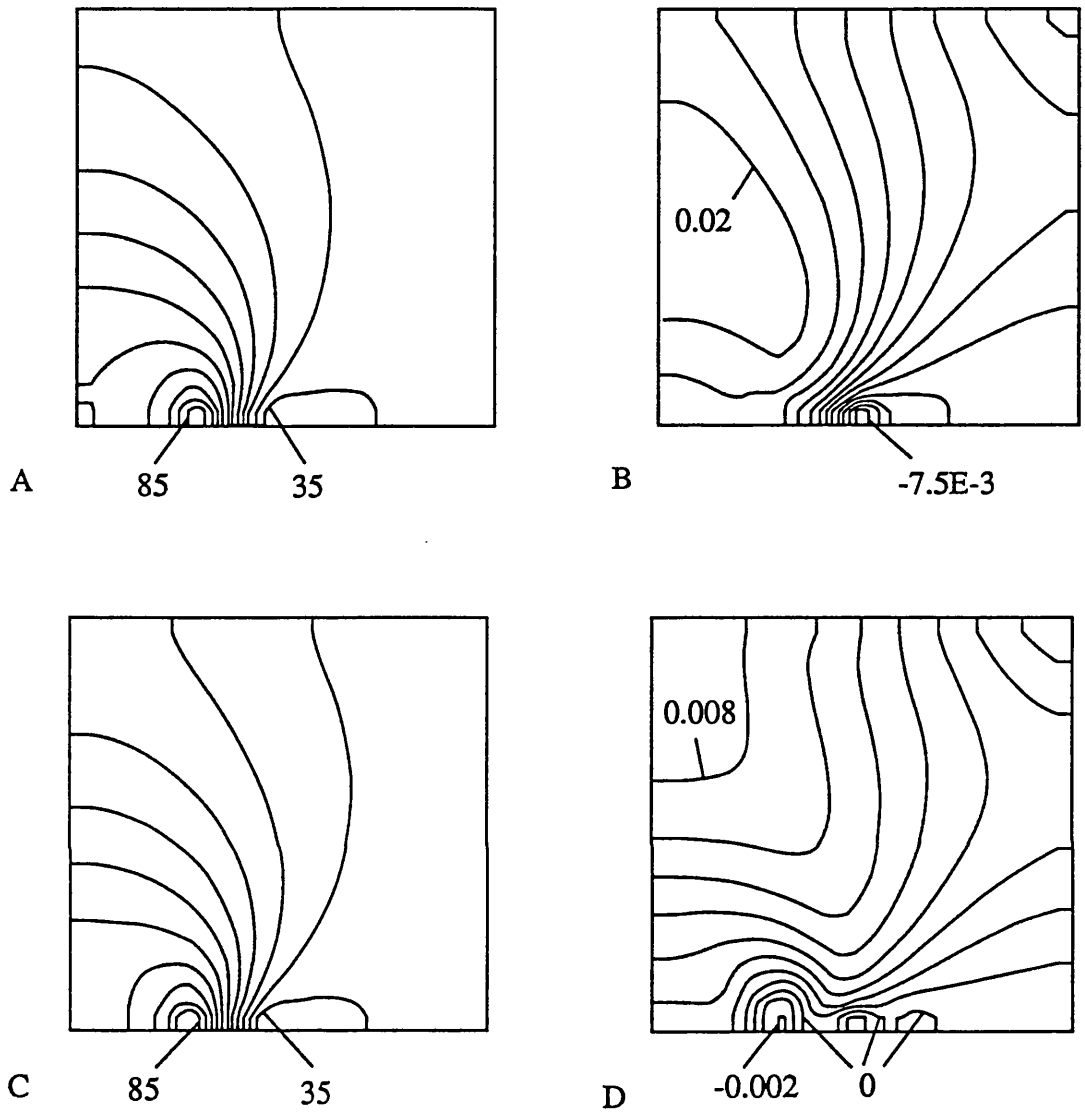

Figure 5.4-3. The crustal thickness (A, C) and the vertical strain rate (B, D) of indented lithosphere with decreasing rate of boundary displacement as shown by the solid line in Figure 5.4-1. A = 50. $\bar{B}=\bar{B}o$. **(Model 5.4I).**
A. Time is 30 Ma, contours are from 35 by 5 to 85 (km).
B. Time is 30 Ma, contours are from -0.0075 by 0.0025 to 0.02 (Uo/Lo).
C. Time is 40 Ma, contours are from 35 by 5 to 85 (km).
D. Time is 40 Ma, contours are from -0.002 by 0.001 to 0.008 (Uo/Lo).

The results shown in this and previous diagrams demonstrate that buoyancy force still resists lithosphere thickening as thickening slowed down at later stage of deformation; and that the equivalent density contrast between the lithosphere mantle and the asthenosphere contributes to lithosphere thickening process as the maximum crustal thickness is 15 km larger than that in Figure 5.2-2.

The evolution of the top surface, the Moho, the base of the lithosphere and the vertical strain-rate in **Model 5.4I** are shown in a more straight forward but less accurate way with isometric plots in Figure 5.4-4 to Figure 5.4-7 respectively.

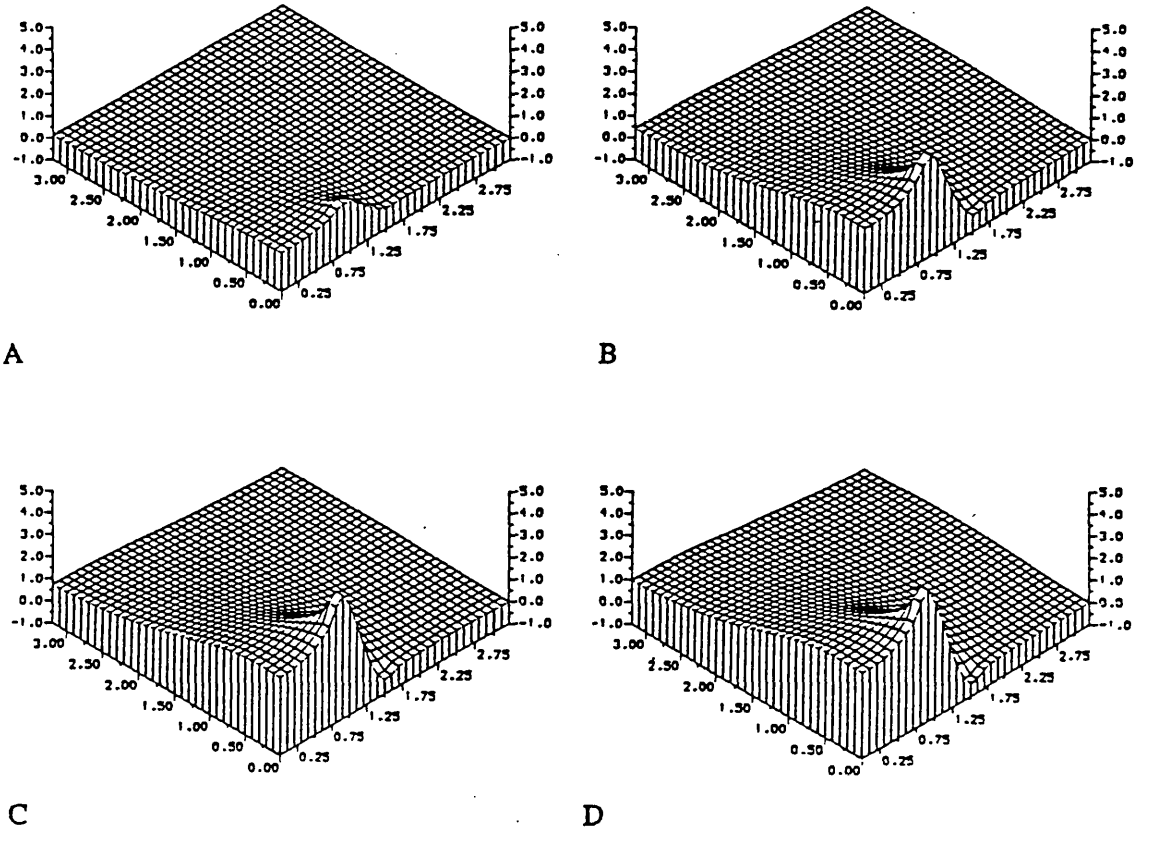

Figure 5.4-4 The evolution of the top surface of the indented lithosphere in **Model 5.4I**. Horizontal unit is 1000 km. Vertical unit is km.
A. 5 Ma.
B. 20 Ma.
C. 30 Ma.
D. 40 Ma.

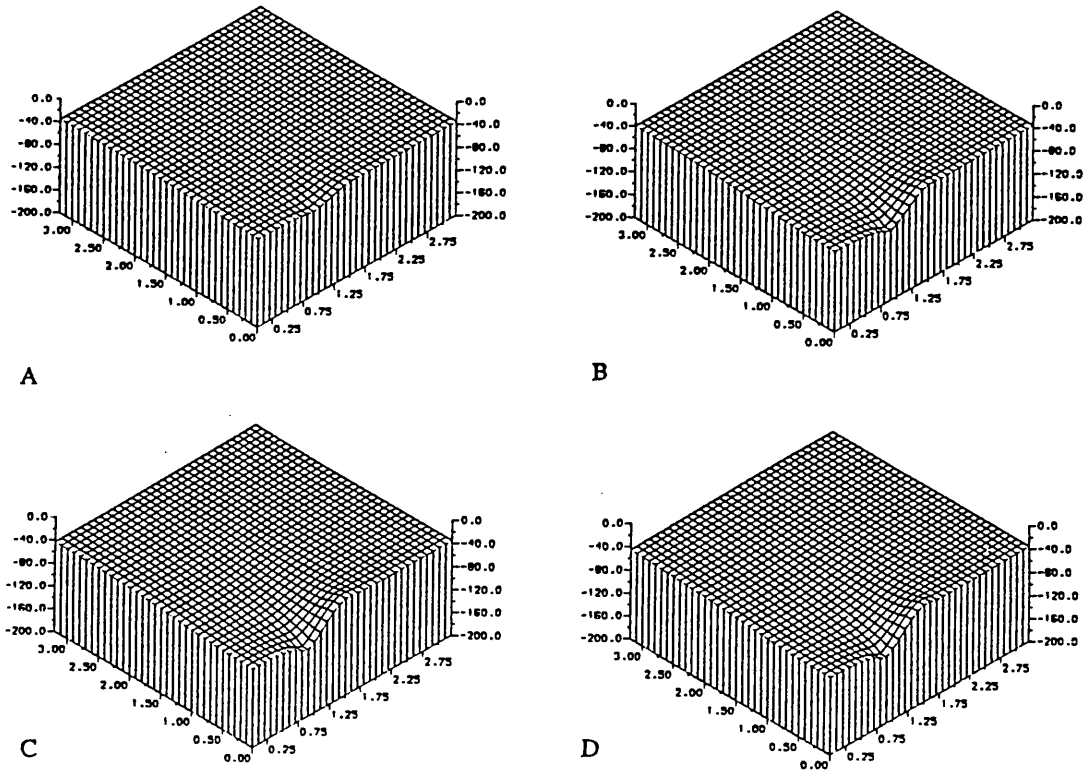

Figure 5.4-5 The evolution of the Moho surface of the indented lithosphere in **Model 5.4I**. Horizontal unit is 1000 km. Vertical unit is km.
A. 5 Ma.
B. 20 Ma.
C. 30 Ma.
D. 40 Ma.

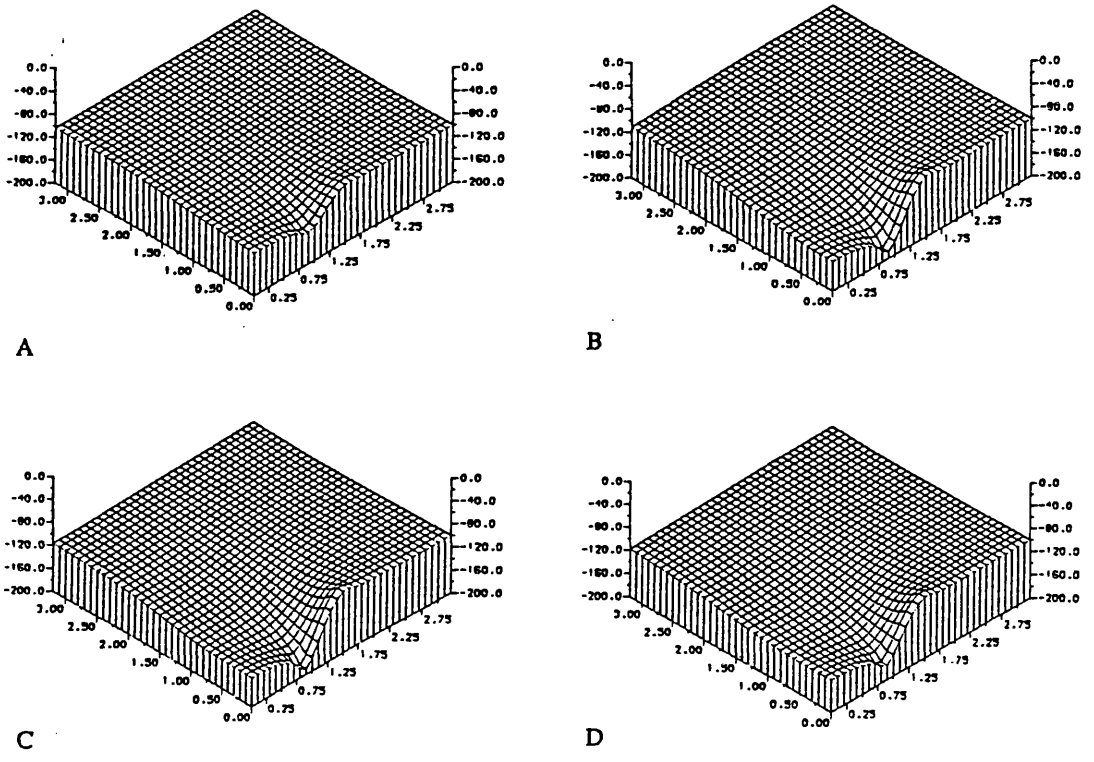

Figure 5.4-6 The evolution of the base of the indented lithosphere in **Model 5.4I**. Horizontal unit is 1000 km. Vertical unit is km. Note how the base is slightly restored upward by thermal process at the later stage.
A. 5 Ma.
B. 20 Ma.
C. 30 Ma.
D. 40 Ma.

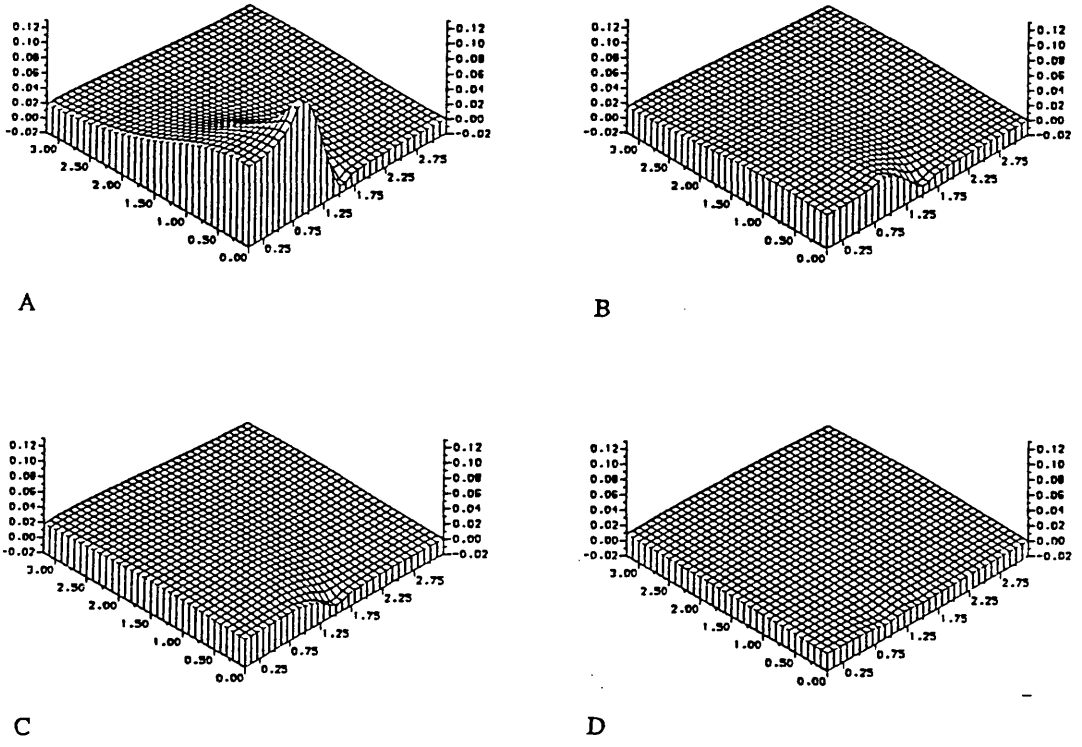

Figure 5.4-7 The evolution of the vertical strain-rate of the indented lithosphere in **Model 5.4I**. Horizontal unit is 1000 km. Vertical unit is Uo/Lo. At later stage, the vertical strain-rate is almost uniform.
A. 5 Ma.
B. 20 Ma.
C. 30 Ma.
D. 40 Ma.

At the end of 40 Ma, the extra thickness of the mantle lithosphere becomes detached at the level of the initial depth of the lithosphere bottom (100 km). Since the lithosphere mantle has larger equivalent density than that of the asthenosphere and the asthenosphere can not sustain long-term deviatoric stress, the detachment results in fast uplift of the lithosphere. So far in this section for simplicity we have been using ρ_a=3.26, which is calculated for a lithosphere with 35 percent crust, although this percentage increases to some extent. However the detachment changes the proportion of the crust dramatically, so the amount of uplift has to be calculated in a different way.

Figure 5.4-8(A) shows the temperature profiles of a column of lithosphere and asthenosphere with thickness L before detachment, and (B) shows the temperature distribution immediately after the extra thickness (L-Lo) falls off (I neglect the temperature gradient inside the asthenosphere). Above the compensation level, the detached lithosphere of a vertical column is replaced by asthenosphere material with the same weight (therefore the same mass), but with higher temperature. The weight of the column above the compensation level is the same, but the volume of the column increases due to the increase of temperature at part of it. The amount of uplift is therefore equal to the the amount of thermal expansion, which is

$$d = \frac{1}{2}\,\alpha\,(T_L - \frac{L_o}{L}T_L)(L-L_o)$$

$$= \frac{\alpha T_L}{2L}(L-L_o)^2 \qquad (5.4\text{-}1)$$

So the uplift of the lithosphere due to the detachment at the end of 40 Ma indentation in **Model 5.4I** is calculated using eq.(5.4-1) and shown in

Figure 5.4-9(A). Indentation continues with u_{max} = 2cm/year and the new vertical strain rate is shown in Figure 5.4-9(B). The uplift due to the detachment and the vertical strain-rate immediately after the detachment are also shown with isometrical plots in Figure 5.4-10. The evolution of crustal thickness and the vertical strain rate along the symmetry plane of the indented lithosphere is shown in Figure 5.4-11.

As seen in Figure 5.4-9, the maximum amount of uplift is 600 m and the maximum thinning rate is 0.0175 (Uo/Lo), which is equivalent to a displacement of 0.0875 cm/Ma across a distance of 100 km, or about 0.96 cm/Ma across a distance of 1100 km. This is equal to the rate of Tibetan extension estimated by Armijo et al. (1986). Hence if the average uplift of the plateau is in the order of 600 m, the overall extension of the Tibetan Plateau would agree well with the extension rate estimated by Armijo et al. (1986).

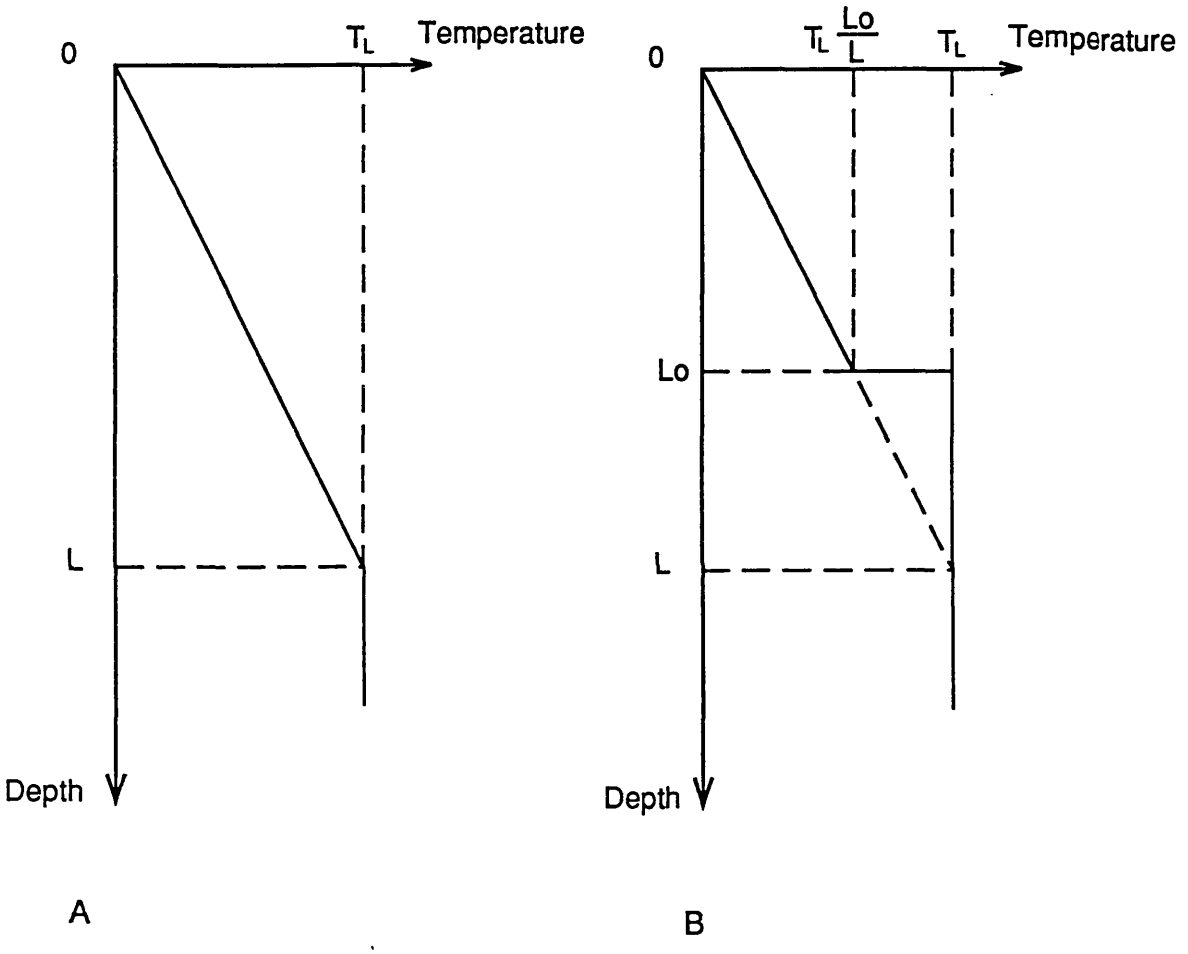

Figure 5.4-8. The vertical distribution of temperature of a column of lithosphere (A) before and (B) after detachment of the lower part of the lithosphere at Lo.

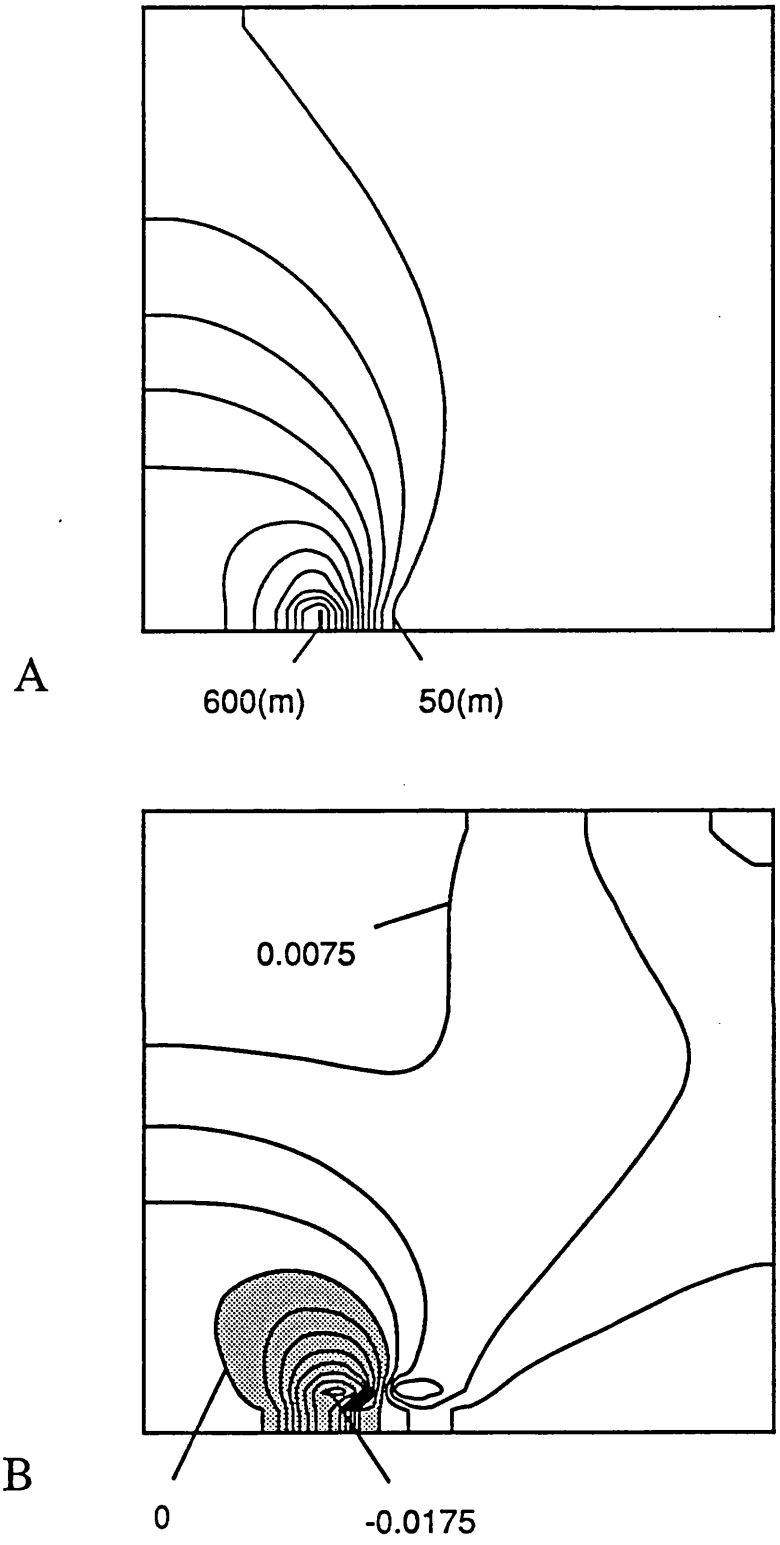

Figure 5.4-9. (A) The contour map of the uplift of the lithosphere due to the detachment of the lower part of the lithosphere at the depth of Lo in **Model 5.4I**, after 40 Ma indentation. Contours are from 50 by 50 to 600 (m). (B). The contour map of the vertical strain rate after the detachment in Model 5.4I. Contours are from -0.0175 by 0.0025 to 0.0075 (Uo/Lo).

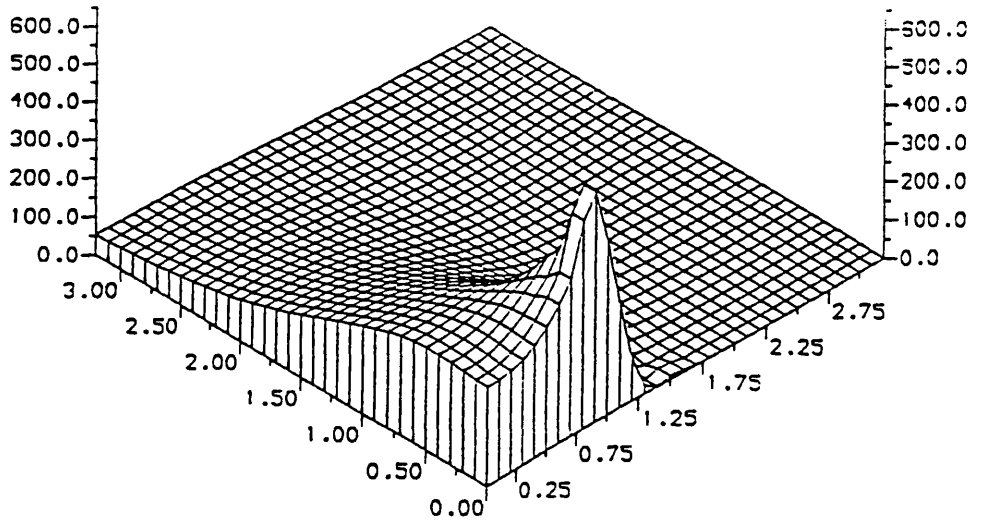

A

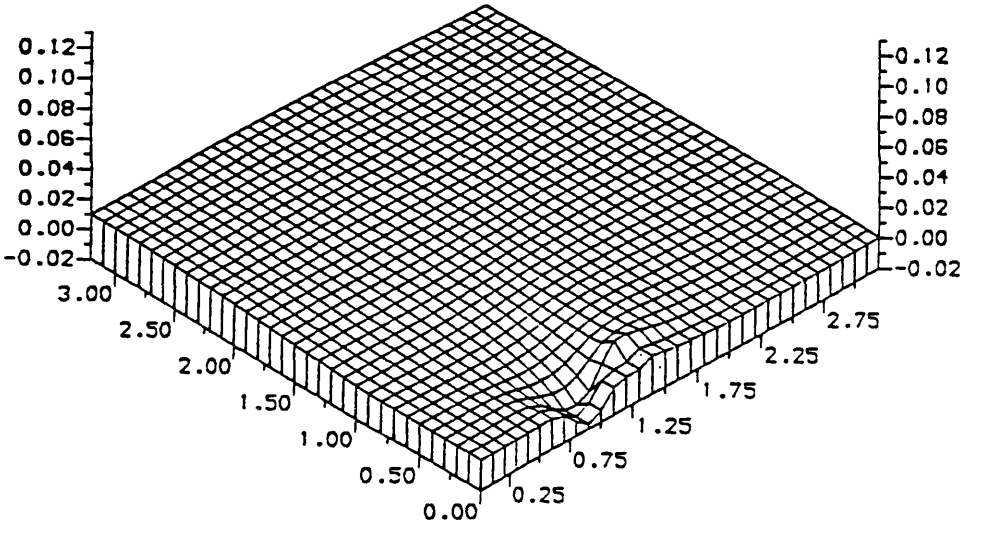

B

Figure 5.4-10. (A) The isometric plot of the uplift of the lithosphere due to the detachment of the lower part of the lithosphere at the depth of Lo, after 40 Ma of indentation with decreasing rate of boundary displacement shown as the solid line in Figure 5.4-1. A=50. $\bar{B}=\bar{B}o$. **(Model 5.4I)** The vertical unit is meter. The horizontal unit is 1000 km.
(B). The isometric plot of the vertical strain rate after the detachment in **Model 5.4I**. The vertical unit is (Uo/Lo). The horizontal unit is 1000 km.

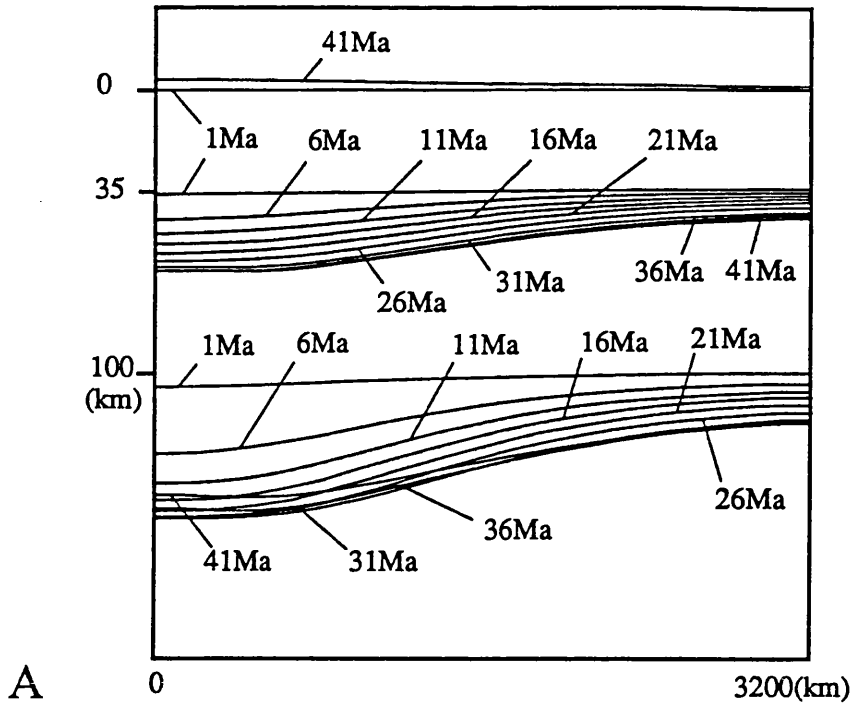

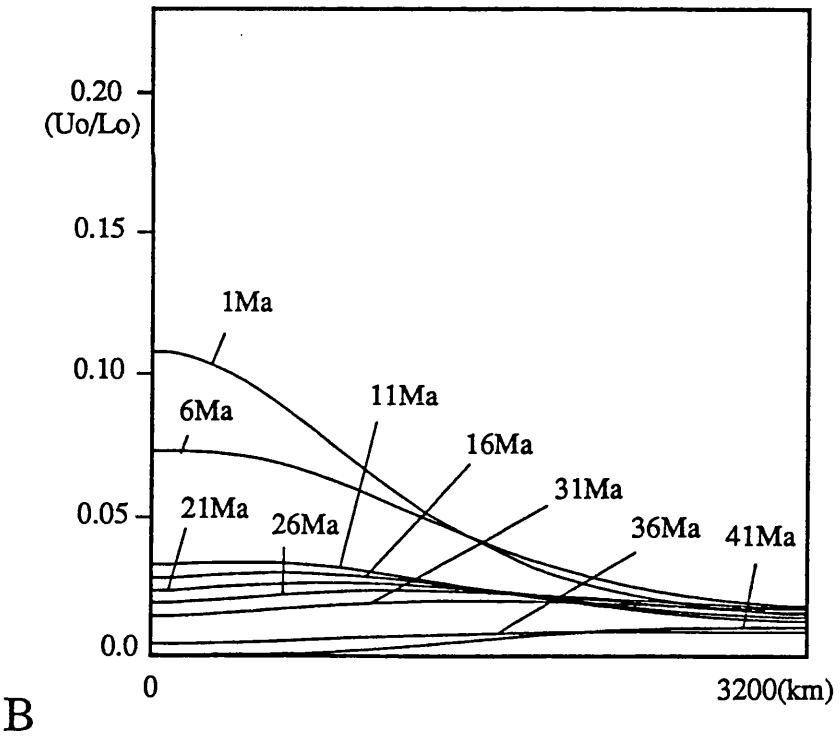

Figure 5.4-11. (A) The evolution of the top surface, the Moho, and the base of the indented lithosphere with decreasing rate of boundary displacement shown as solid line in Figure 5.4-1, shown on the symmetry plane during deformation. A=50. $\bar{B}=\bar{B}o$. **(Model 5.4I)**
(B). The evolution of the vertical strain rate on the symmetry vertical plane during the deformation in **Model 5.4I.**

It should be mentioned that in the calculation, the lithosphere is elevated by the amount shown in Figure 5.4-9(A) and Figure 5.4-10(A), but its thickness is not reduced accordingly. This is because the strength of the lithosphere lies mainly in the upper part and the detachment has little immediate effect on the strength, while in the thin viscous sheet model, the strength is averaged vertically and therefore a reduction of thickness would reduce the lithosphere's ability to resist deformation.

The evolution of the style of deformation in **Model 5.4I** can also be shown by the axial strain-rates and the deviatoric stresses in the indented lithosphere at 5 Ma, 40 Ma and after detachment in Figure 5.4-12, Figure 5.4-13 and Figure 5.4-14 respectively. At 5 Ma, the North and South compression is the dominant process near the indentation boundary. At 40 Ma, maximum compression is away from the indentation boundary. After detachment, extension is more intensive than the compression over part of the thickened lithosphere. Near the end of the indentation boundary, both compressional and extensional strain remain large, and shearing is the dominant mode of deformation. These Figures also show that the deviatoric stresses associated with the deformation is usually within 0.01 $\rho_c g L_o$, which is about 30 MPa (Note these stresses have been vertically averaged). Differential stresses (horizontal axial stresses minus vertical stress) may be larger than deviatoric stresses because $\sigma_x - \sigma_z = 2\tau_x + \tau_y$ (See § 3.3), but is not larger than 0.02 $\rho_c g L_o$. This implies that with A = 50, the tectonic stresses required to form the Tibetan plateau by indentation (with detachment at a later stage) is within the range that can be accounted for by plate tectonics.

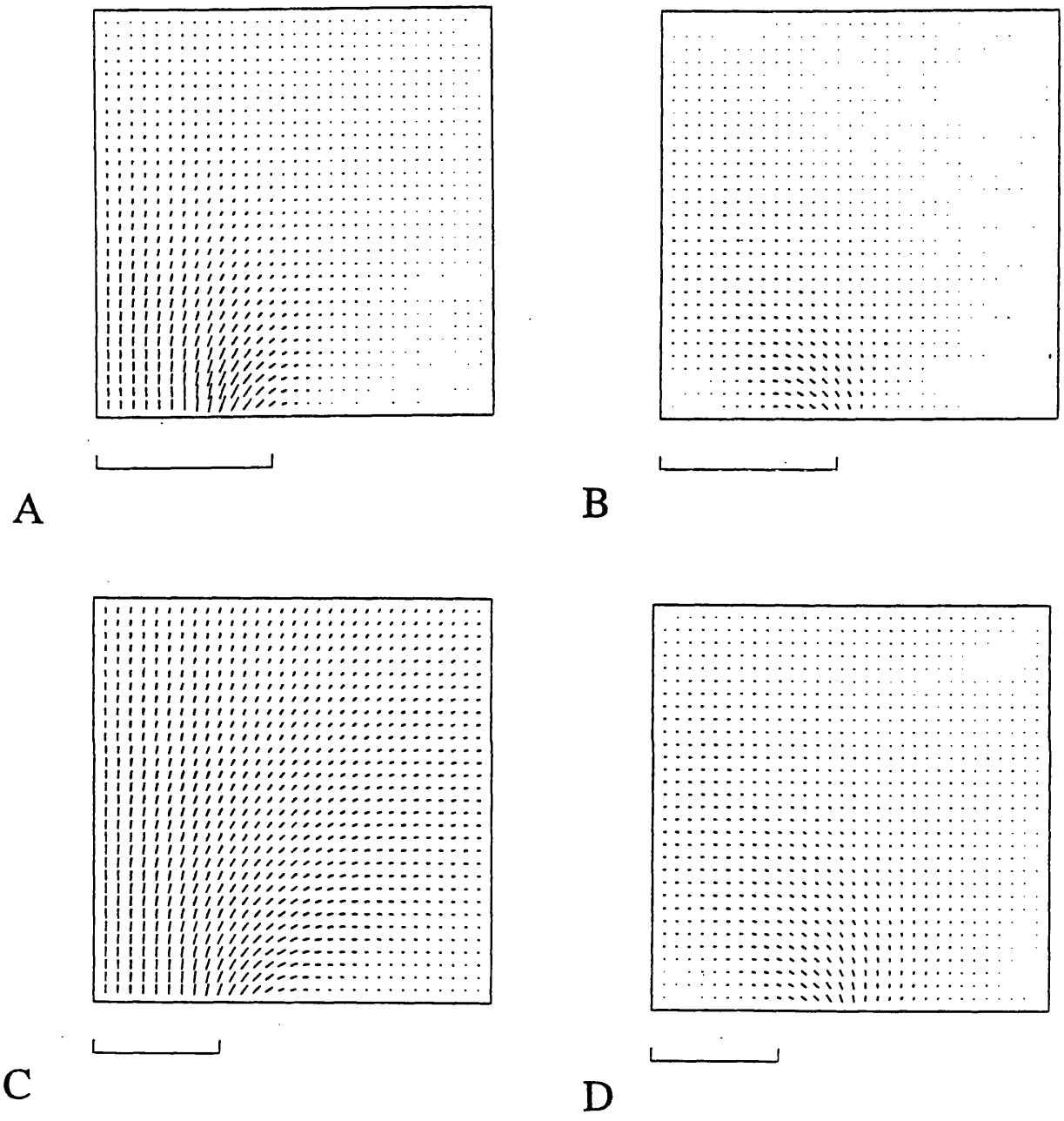

Figure 5.4-12. Axial strain-rates and deviatoric stresses of the indented lithosphere in **Model 5.4I** at 5 Ma. B=Bo. A=50. $\rho_a<\rho_m$. The rate of boundary displacement is shown in Figure 5.4-1. North and South compression is the dominant mode of deformation near the indentation boundary.
A. Compressional axial strain-rate. The scale is Uo/Lo ($\approx 1.7 \times 10^{-14} s^{-1}$).
B. Extensional axial strain-rate. The scale is Uo/Lo.
C. Compressional deviatoric axial stress. The scale is $0.1 \rho_c g Lo$ ($\approx$ 300MPa).
D. Tensile deviatoric axial stress. The scale is $0.1\ \rho_c g Lo$.

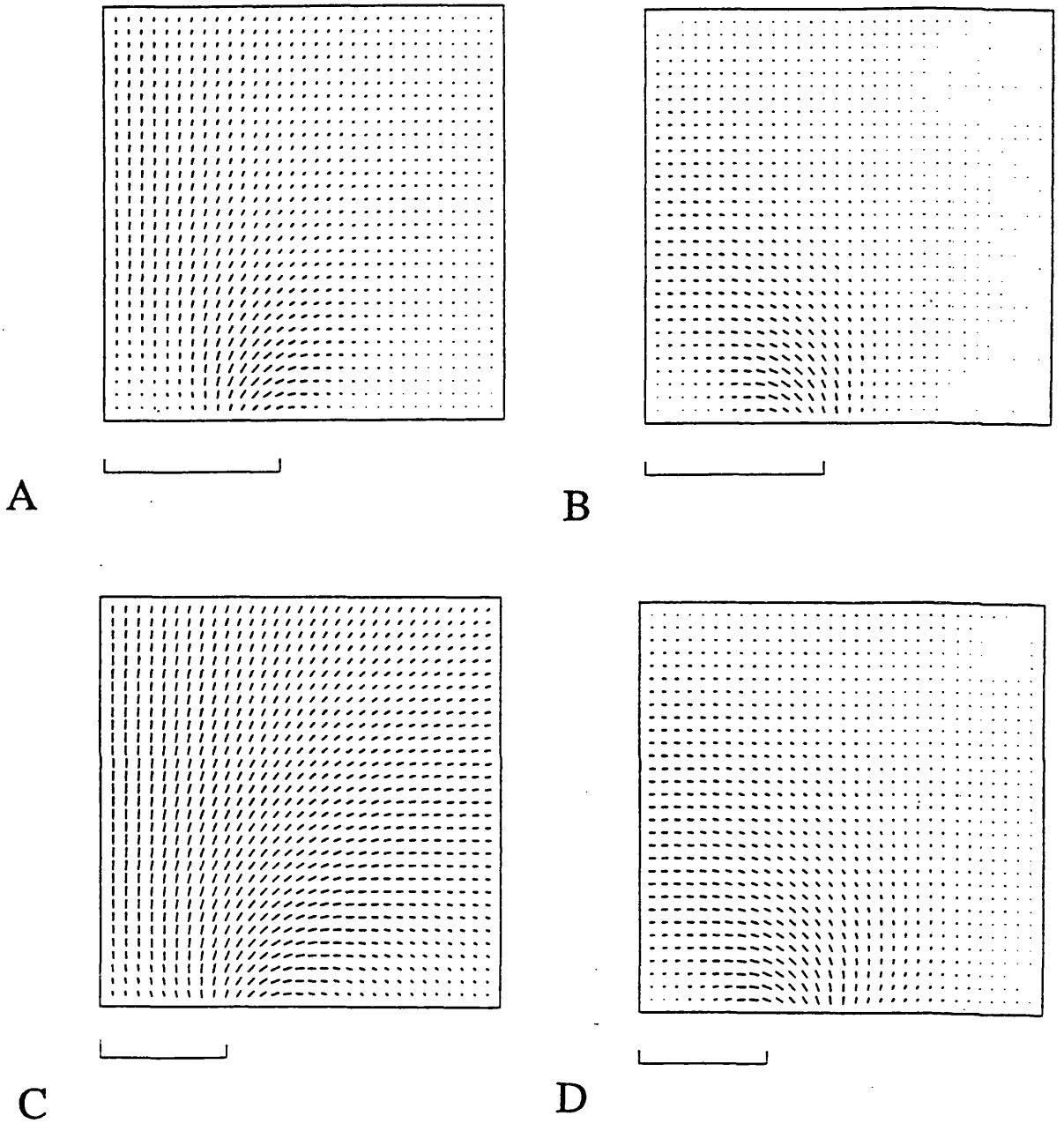

Figure 5.4-13. Axial strain-rates and deviatoric stresses of the indented lithosphere in **Model 5.4I** at 40 Ma. B=Bo. A=50. $\rho_a<\rho_m$. The rate of boundary displacement is shown in Figure 5.4-1. Maximum compression is away from the indentation boundary.

A. Compressional axial strain-rate. The scale is Uo/Lo ($\approx 1.7\text{x}10^{-14}\text{s}^{-1}$).
B. Extensional axial strain-rate. The scale is Uo/Lo.
C. Compressional deviatoric axial stress. The scale is $0.1\rho_c g$Lo ($\approx$ 300MPa).
D. Tensile deviatoric axial stress. The scale is $0.1\ \rho_c g$Lo.

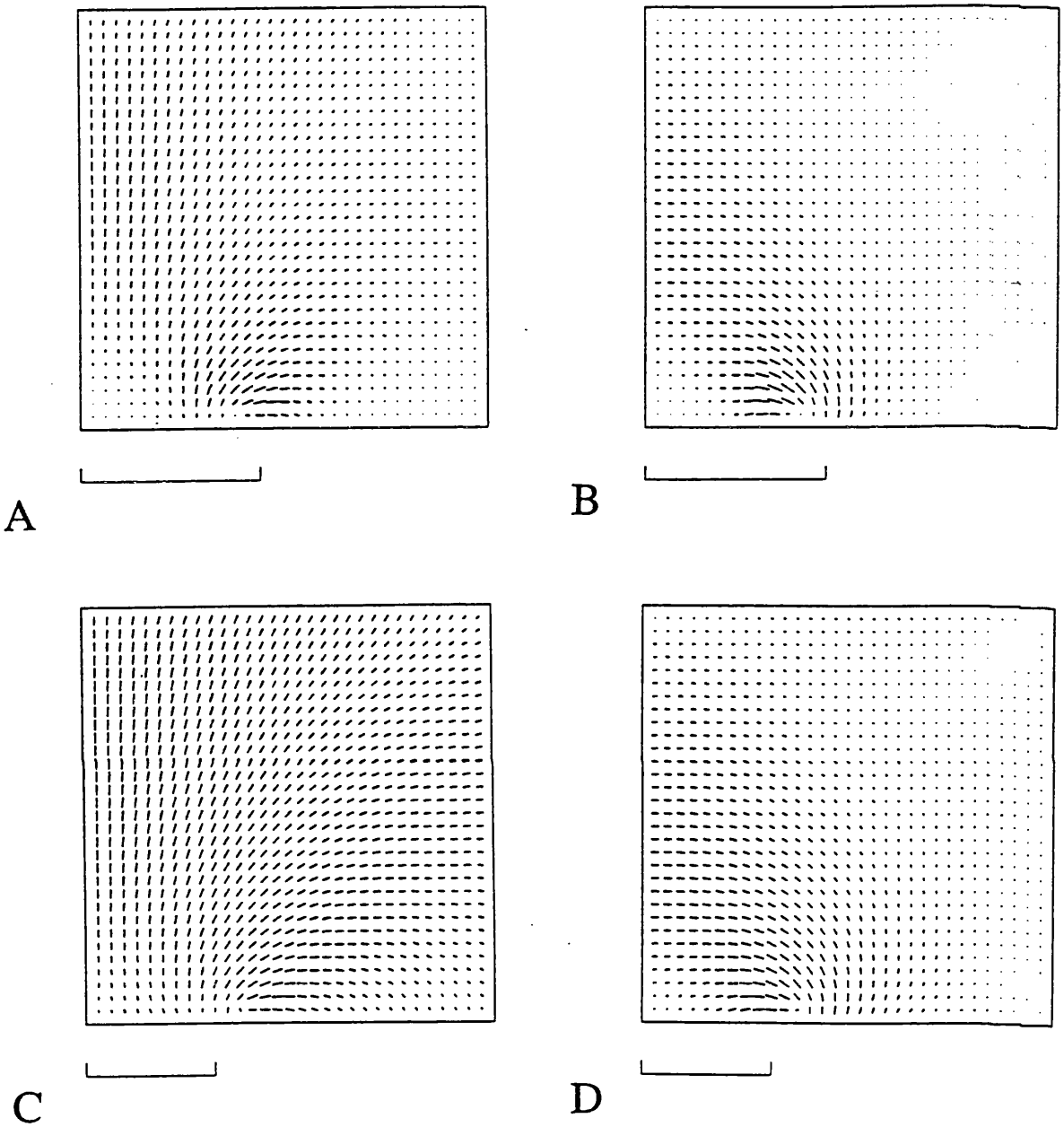

Figure 5.4-14. Axial strain-rates and deviatoric stresses of the indented lithosphere in **Model 5.4I** after detachment. B=Bo. A=50. $\rho_a<\rho_m$. The rate of boundary displacement is shown in Figure 5.4-1. At part of the thickened lithosphere extension is greater than compression.
A. Compressional axial strain-rate. The scale is Uo/Lo ($\approx 1.7\text{x}10^{-14}s^{-1}$).
B. Extensional axial strain-rate. The scale is Uo/Lo.
C. Compressional deviatoric axial stress. The scale is 0.1 ρ_cgLo ($\approx$ 300MPa).
D. Tensile deviatoric axial stress. The scale is 0.1 ρ_cgLo.

In the second case (**Model 5.4II**), the slowing down of indentation follows the detachment. The changing of the maximum boundary displacement rate is shown as in Figure 5.4-1 (dotted line). The crustal thickness and the vertical strain-rate after 32 Ma stable indentation are shown in Figure 5.4-15. At the same time, the top surface, the Moho, the base of the lithosphere, and the vertical strain-rate are shown with isometric plots in Figure 5.4-16. Detachment occurs between 32 and 33 Ma, and the uplift of the lithosphere due to the detachment is shown in Figure 5.4-17. In the mean time, U_{max} remains at 5 cm/year, and the vertical strain-rate at 33 Ma is shown in Figure 5.4-18(A) using a contour map and in Figure 5.4-19(A) using an isometric plot. U_{max} is then reduced from 5 cm/year to 2 cm/year following the uplift, and at 34 Ma, the vertical strain-rate (after the slowing down of indentation) is shown in Figure 5.4-18(B) using a contour map and in Figure 5.4-19(B) using an isometric plot. The detachment, uplift and the slowing down of the indentation occur between 32 Ma and 34 Ma (within 2 Ma) so the warming up of the upper lithosphere (and therefore the weakening of the lithosphere) in the meantime is neglected. The position of the three layers and the vertical strain rate along the symmetry plane during the deformation is shown in Figure 5.4-20.

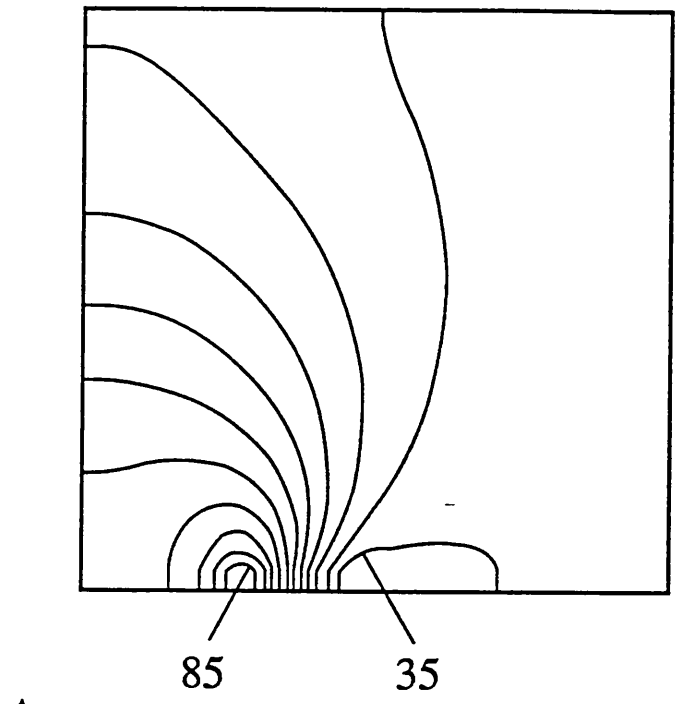

A

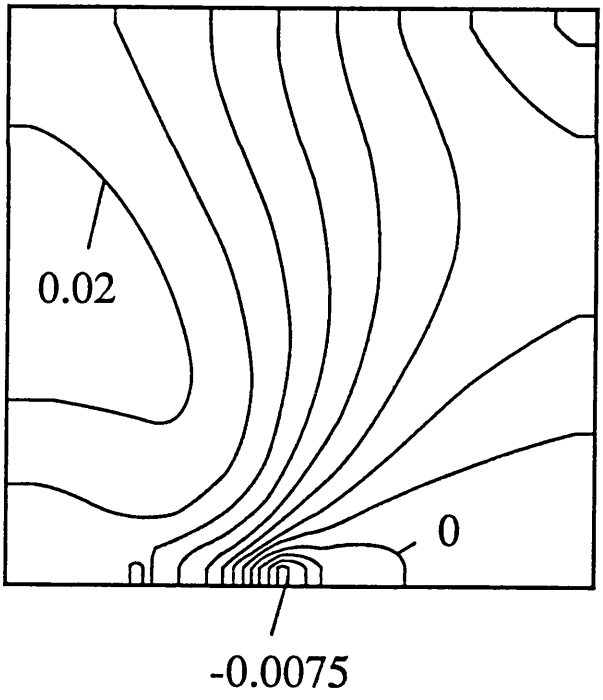

B

Figure 5.4-15. The crustal thickness (A) and the vertical strain rate (B) of the lithosphere after 32 Ma of indentation in **Model 5.4II**. A=50. B=Bo. $\rho_a<\rho_m$. The rate of boundary displacement is shown in Figure 5.4-1 (dotted line).

A. Contours are from 35 by 5 to 85 (km).

B. Contours are from -0.0075 by 0.0025 to 0.02 (Uo/Lo).

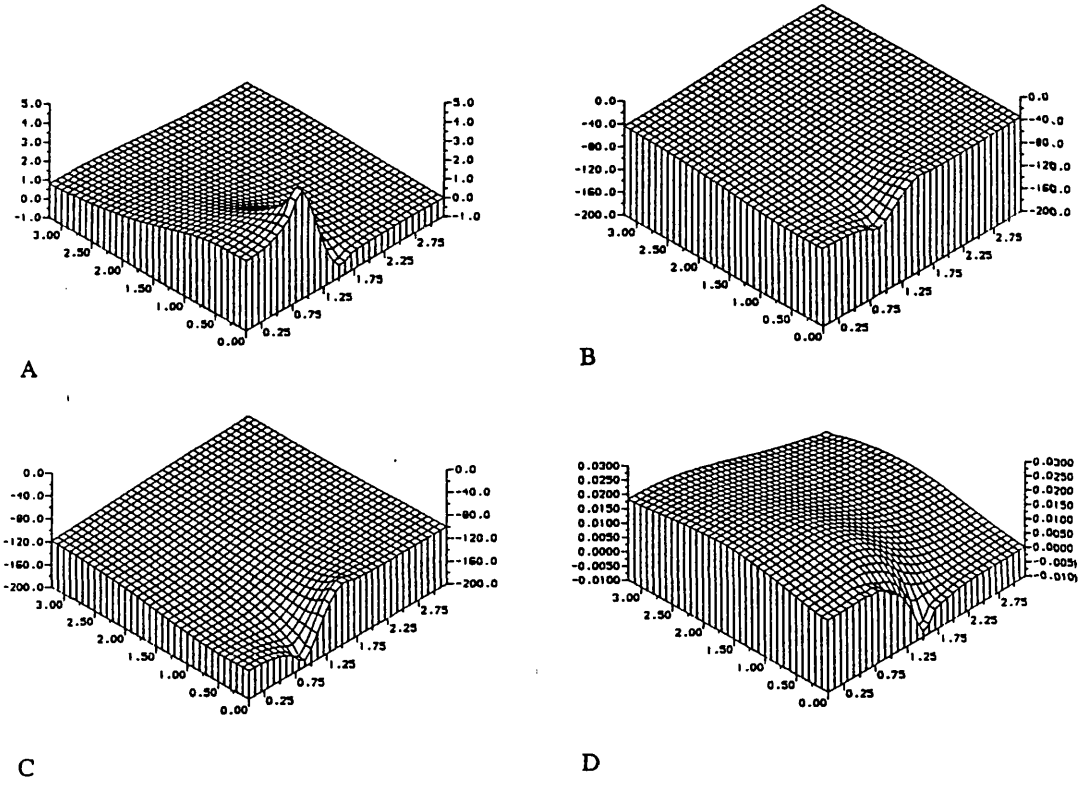

Figure 5.4-16. The isometric plots of the top surface (A), the Moho surface (B), the base of the lithosphere (C), and the vertical strain rate (D) of the indented lithosphere at 32 Ma in **Model 5.4II**. A=50. B=Bo. $\rho_a<\rho_m$. The rate of boundary displacement is shown in Figure 5.4-1 (dotted line). Horizontal unit is 1000km. Vertical unit is km in (A), (B), (C) and Uo/Lo in (D).

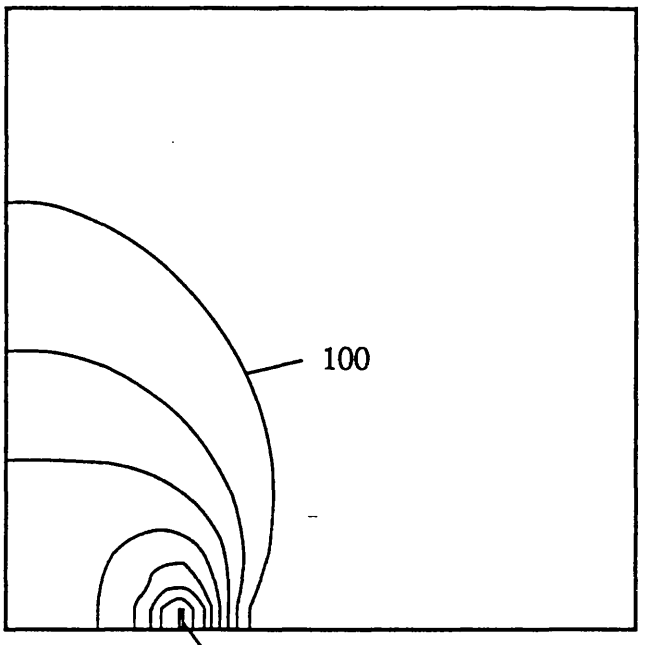

A

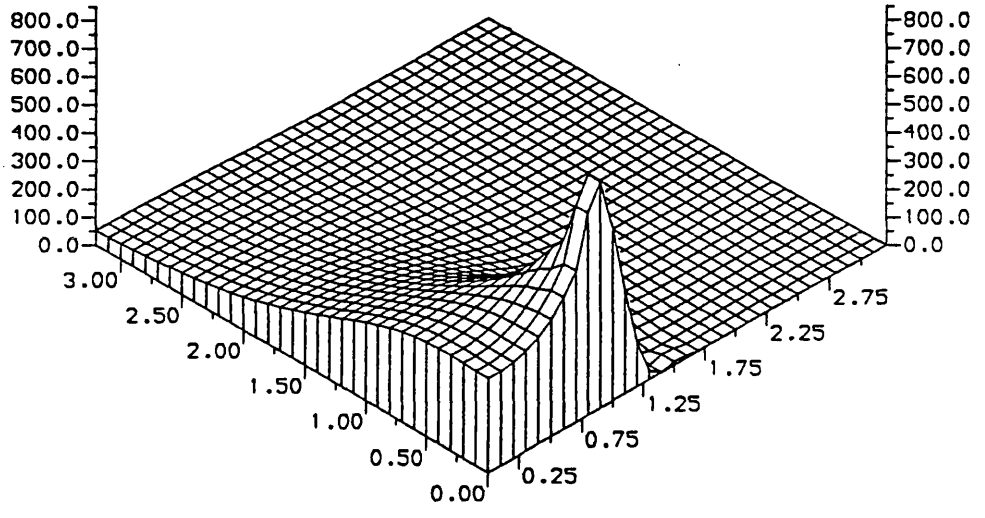

B

Figure 5.4-17. The contour map (A) and the isometric plot (B) of the vertical displacement of the lithosphere **(Model 5.4II)** due to detachment after 32 Ma indentation with rate of boundary displacement shown in Figure 5.4-1 (dotted line). $\bar{B}=\bar{B}o$. A=50. $\rho a<\rho m$. Contours in (A) are from 100 by 100 to 800 (meters). In (B) horizontal unit is 1000km and vertical unit is meter.

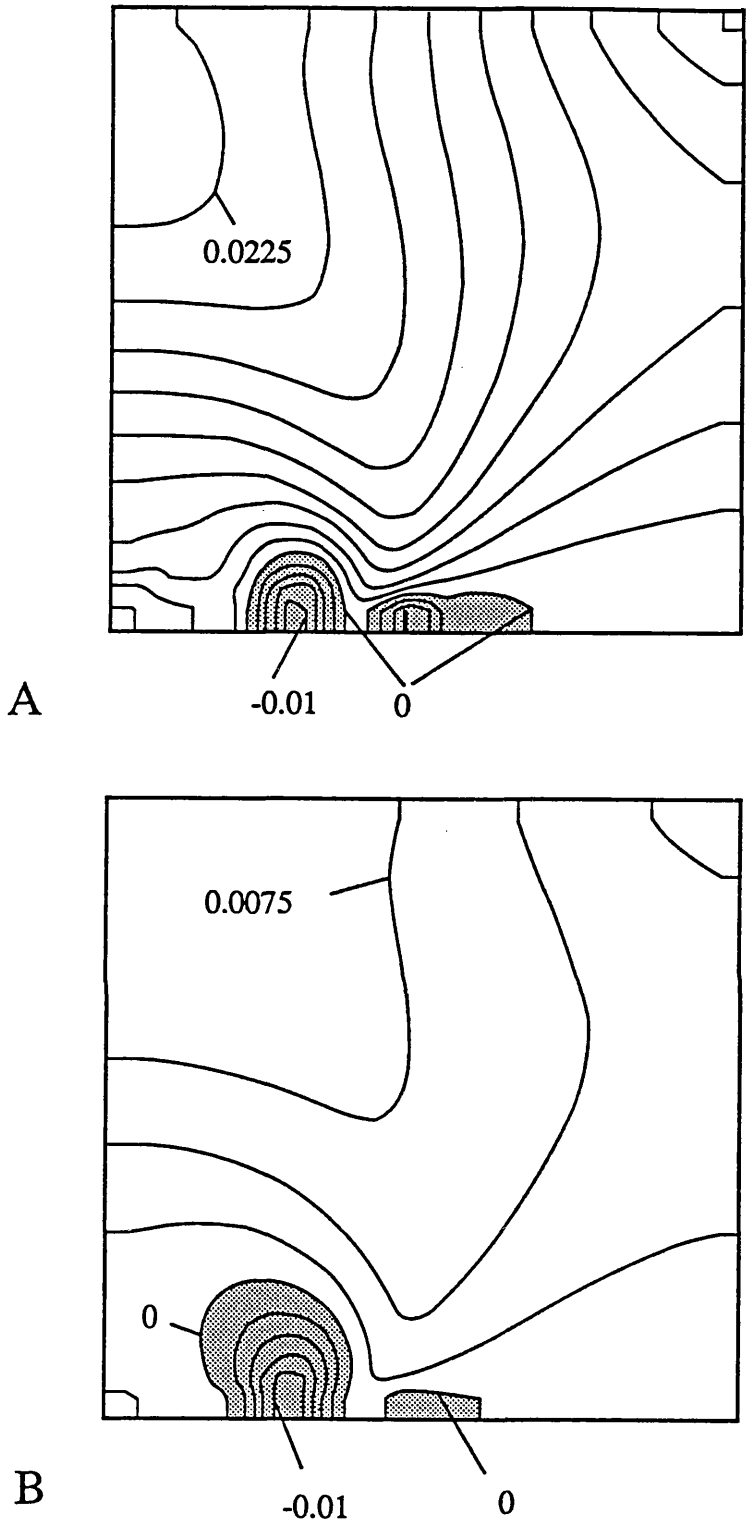

Figure 5.4-18. Contour maps of the vertical strain-rate (A) at 33 Ma (after detachment) and (B) at 34 Ma (after both detachment and the reduction of u_{max} from 5 cm/year to 2 cm/year) in **Model 5.4II.** In the first 32 Ma, the lithosphere has been indented with rate of boundary displacement shown by dotted line in Figure 5.4-1. $\bar{B}=\bar{B}o$. A=50. $\rho_a<\rho_m$.
A. At 33 Ma. Contours are from -0.01 by 0.0025 to 0.0225 (Uo/Lo).
B. At 34 Ma. Contours are from -0.01 by 0.0025 to 0.0075 (Uo/Lo).

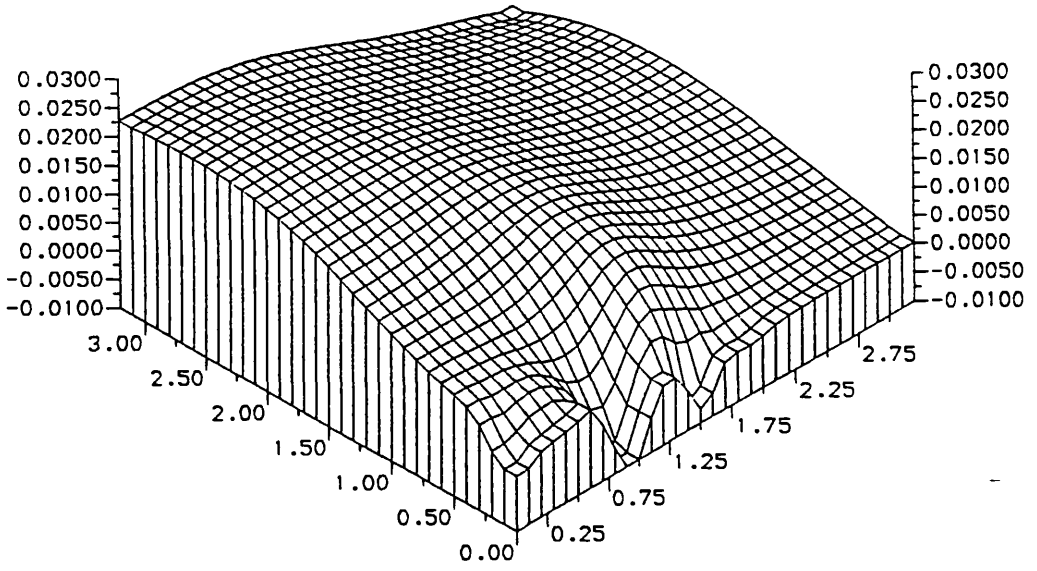

A

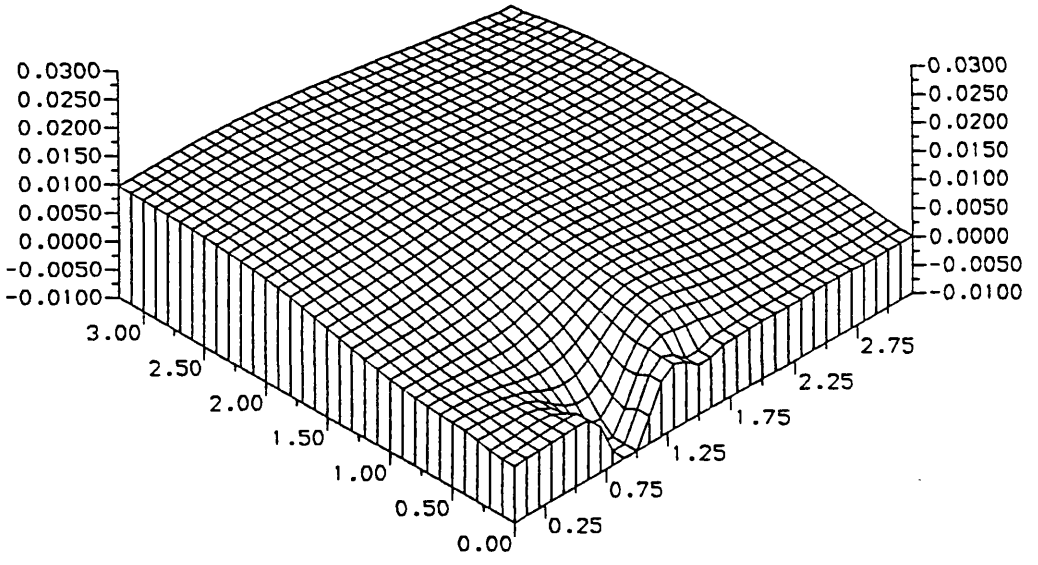

B

Figure 5.4-19. Isometric plots of the vertical strain-rate (A) at 33 Ma (after detachment) and (B) at 34 Ma (after both detachment and the reduction of u_{max} from 5 cm/year to 2 cm/year) in **Model 5.4II.** In the first 32 Ma, the lithosphere has been indented with rate of boundary displacement shown by dotted line in Figure 5.4-1. $\bar{B}=\bar{B}o$. A=50. $\rho_a<\rho_m$.

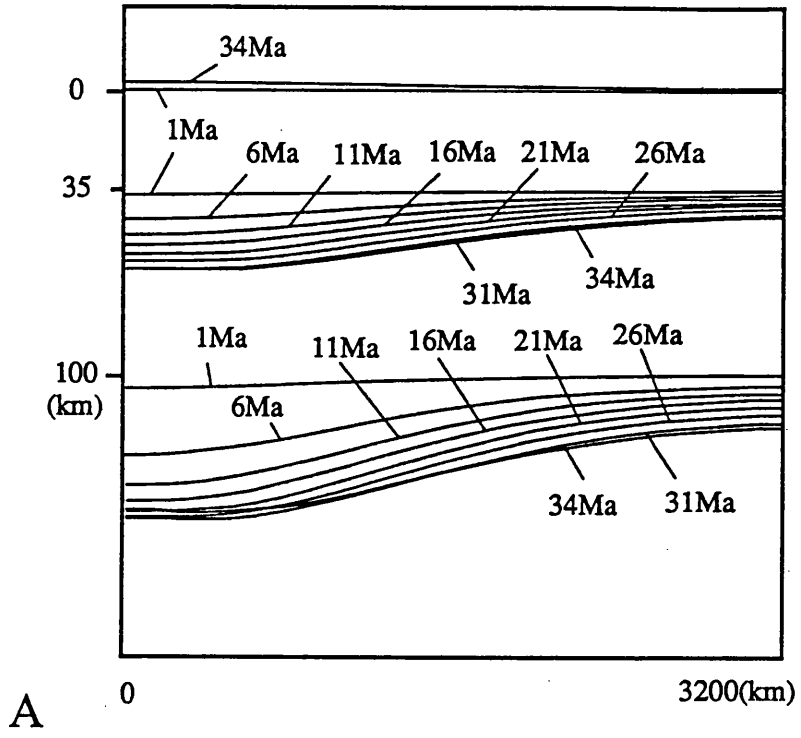

A

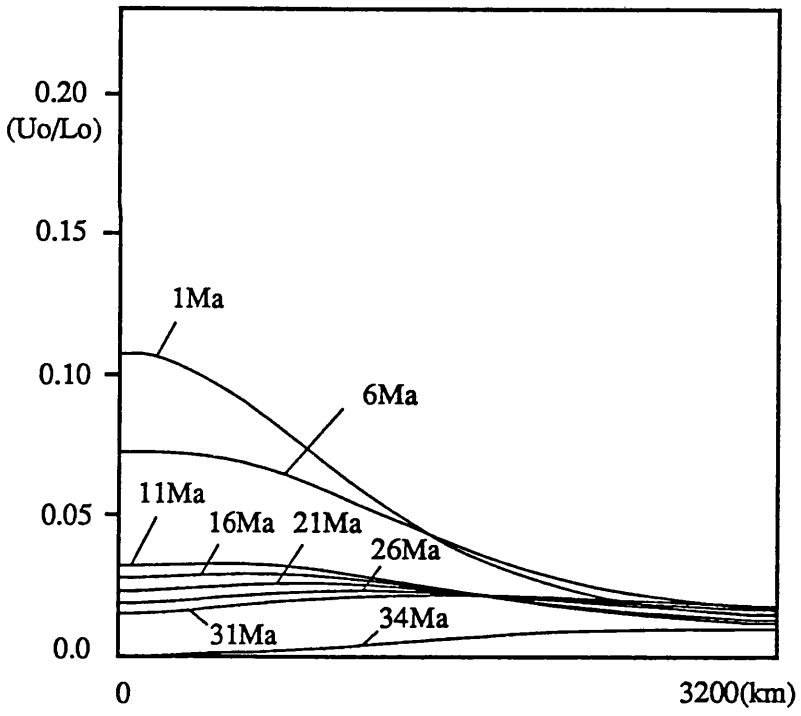

B

Figure 5.4-20. The positions of the three layers (top surface, Moho, and the lithosphere bottom) (A) and the vertical strain rate (B) of the indented lithosphere during deformation in **Model 5.4II**. The rate of boundary displacement is shown in Figure 5.4-1. A=50. $\bar{B}=\bar{B}o$. $\rho_a<\rho_m$. Detachment occurred between 32 and 33 Ma.
Both plots are on the symmetry plane of the studied area (the left margin in Figure 5.1-1).

In the first section of this chapter, an analysis was carried out using the new viscous sheet model and the same boundary conditions and parameters as those of England & McKenzie (1983), and it was found that the results were generally consistent. Three more analyses have been carried out to simulate the evolution of the Tibetan Plateau, with emphasis on the later extension of the plateau, or the transition from phase 2 to phase 3 of plateau evolution.

Analysis of the results showed that the slowing down of the indentation on a reasonable scale could not have caused the late extension of the Tibetan Plateau. The weakening of lithosphere may cause the transition of the Tibetan Plateau from phase 2 to phase 3, if the strength of lithosphere is reduced by a factor of 5. Increased heat conduction from the asthenosphere could not have caused weakening on this scale in 40 Ma, but the increased heat production elements due to crustal thickening may have caused a major rheological change in Tibet.

Uplift of the Tibetan plateau is the more probable cause of the late extension of the plateau. The uplift has been attributed to the mechanical instability at the bottom of the lithosphere, that is the removal of part of the thickened lithosphere the mechanism of which has been simulated by Nataf et al. (1981) and Houseman et al. (1981). It is found that a 600 meter uplift of the plateau at late stage of evolution is probably capable of causing extensional strain-rate of the order of $3 \times 10^{-17} s^{-1}$, which is comparable with the extension rate of the Tibetan Plateau estimated by

Armijo et al. (1986) on the basis of field studies. These results support the suggestion that the Tibetan Plateau has been recently delaminated (England & Houseman, 1988).

The results also clearly demonstrate that the lithosphere root formed during lithosphere thickening tends to cause contraction of the thickened lithosphere, as suggested by Fleitout & Froidevaux (1982). When this effect is included in the modelling, the maximum crustal thickness that can be reached is up to 15 km larger than otherwise. Therefore numerical models assuming simple Airy compensation (e.g., England & McKenzie, 1983) should be used with caution.

Chapter 6. The extensional deformation of continents

Starting in this chapter, I deal with another form of continental deformation — extension. Extensional features are more common than compressional ones because lithosphere is weaker under tension. In studying the Cenozoic extensional tectonics in China, Ma et al. (1987) grouped extensional structures into three styles: a. Linear rift valleys; b. Basin and Range structures; and c. Extensional structures associated with strike-slip faults.

§ 6.1 Linear rifts

Rifts were defined by Gregory (1921) as depressions between long parallel normal faults. In recent years, this definition has been modified so that rifts are now regarded as elongate depressions where the entire thickness of the lithosphere has deformed under the influence of extensional forces (Neumann & Ramberg, 1978; Burchfiel, 1980). This term applies to major lithospheric features. Smaller structures associated with normal faulting are not rifts. Examples of presently active rifts are the East African Rift, the Baikal Rift, the Rhine Graben and the Rio Grande Rift.

§ 6.1.1 Characteristics of continental rifts

The common characteristics of rifts has been summarized by Neumann & Ramberg (1978).

Rifts often contain extensive volcanic rocks (e.g., East Africa Rift), although in some cases few or no volcanics are developed (e.g., Baikal Rift).

Rifts are commonly spatially associated with domal uplifts. They may form an inter-linked network apparently dividing a continental plate (East Africa Rift), or they may be isolated and situated far from any plate margin (Baikal Rift).

The location of rifts is often controlled by existing zones of crustal weakness (Sykes, 1978). These zones should be of high angle to the regional extensional stress system.

The amount of horizontal extension required to form present day rifts is relatively small (Logatchev & Florensov, 1978), being less than 10 km for the Baikal Rift, 4.5-5 km for the Upper Rhine Graben and 8-10 km for the Kenya Rift.

Earthquake focal mechanisms, geological investigations and gravity and seismic reflection surveys have demonstrated that the bounding faults of rift valleys are of normal type (e.g., Brown et al., 1980).

Seismic reflection experiments have shown that the crust underlying many rifts is significantly thinner than beneath adjacent regions, and gravity anomalies indicate that the whole of the lithosphere is thinned (Searle, 1970). Seismological data using both natural and artificial sources have shown that a zone of anomalously low seismic velocities occurs in the upper mantle beneath most rifts and is commonly two to three times wider than the rift zone.

§ 6.1.2 Development of rifts

Although rifts have been extensively studied their origin is still the subject of controversy. Mechanisms of rift formation generally fall into two classes: active and passive (Sengör & Burke, 1978). Active and passive rifts are also called mantle-activated and lithosphere-activated rifts respectively (Condie, 1982).

Active mechanisms for rift formation associate the surface rifting with mantle convection. It has been suggested that mantle plumes impinge on the base of the continental lithosphere at rift-rift-rift triple junctions (Burke & Dewey, 1973). The ascending convection is responsible for pressure release melting and the resulting rift volcanism. The plume flow thins the lithosphere causing isostatic uplift. The doming associated with uplift and the traction forces on the base of the lithosphere contribute to the tensional failure of the lithosphere (Neugebauer, 1978).

The uparching throws the overlying crust into tension, but if the whole crust acts elastically the stresses generated would be too small to cause faulting. However, Bott & Kusznir (1979) have shown that if only the upper crust behaves elastically, with the lower crust acting in a ductile manner, the tensional stresses become confined within the upper crust and amplified to magnitudes at which crustal rupture can take place.

Many rifts are associated with broad domal uplifts as suggested by the Burke and Dewey model, but there are arguments as to whether these are a consequence or a cause of the rifting, or whether both are aspects of a more

fundamental driving mechanism.

Passive mechanisms for continental rifting generally relate the tensional failure of the lithosphere to pre-existing tensional stresses (Turcotte & Oxburgh, 1973). These stresses may be generated by plate boundary forces or by plate incompatibilities. They may be thermal stresses or membrane stresses generated by the ellipticity of the earth. Or they may be due to the variations in the thicknesses of the crust and lithosphere. According to the passive hypothesis the crustal doming and volcanic events are secondary processes.

There is no general consensus as to which model is more realistic. Two examples of linear rifts are given in the following part of this section. Neither of them can be convincingly classified into either mantle-generated (active) or lithosphere-generated (passive) types.

§ 6.1.3 Kenya Rift

The structure of this rift is summarized by Baker & Wohlenberg (1971). It is part of the Eastern African Rift system. It extends from north Tanzania through Kenya and Ethiopia to join the Red Sea and Gulf of Aden rifts at the Afar triple junction. It crosses the Kenya domal uplift, which is elliptical in plan and about 1000 km in length along its major axis parallel to the rift. The well-defined central graben (the Gregory Rift) traverses the elliptical uplift and, at its northern and southern ends, is replaced by less well-defined broad depressions marked by splay faults. The main graben is 60-70 km wide and 750 km long, and is bounded by normal faults (Figure 6.1.3-1). The rift closely follows the axis of a regional

negative Bouguer anomaly interpreted as a zone of thin lithosphere (Figure 6.1.3-2)). Focal mechanism solutions of earthquakes along the rift indicate mainly WNW-ESE to NW-SE extension (Fairhead & Girdler, 1971).

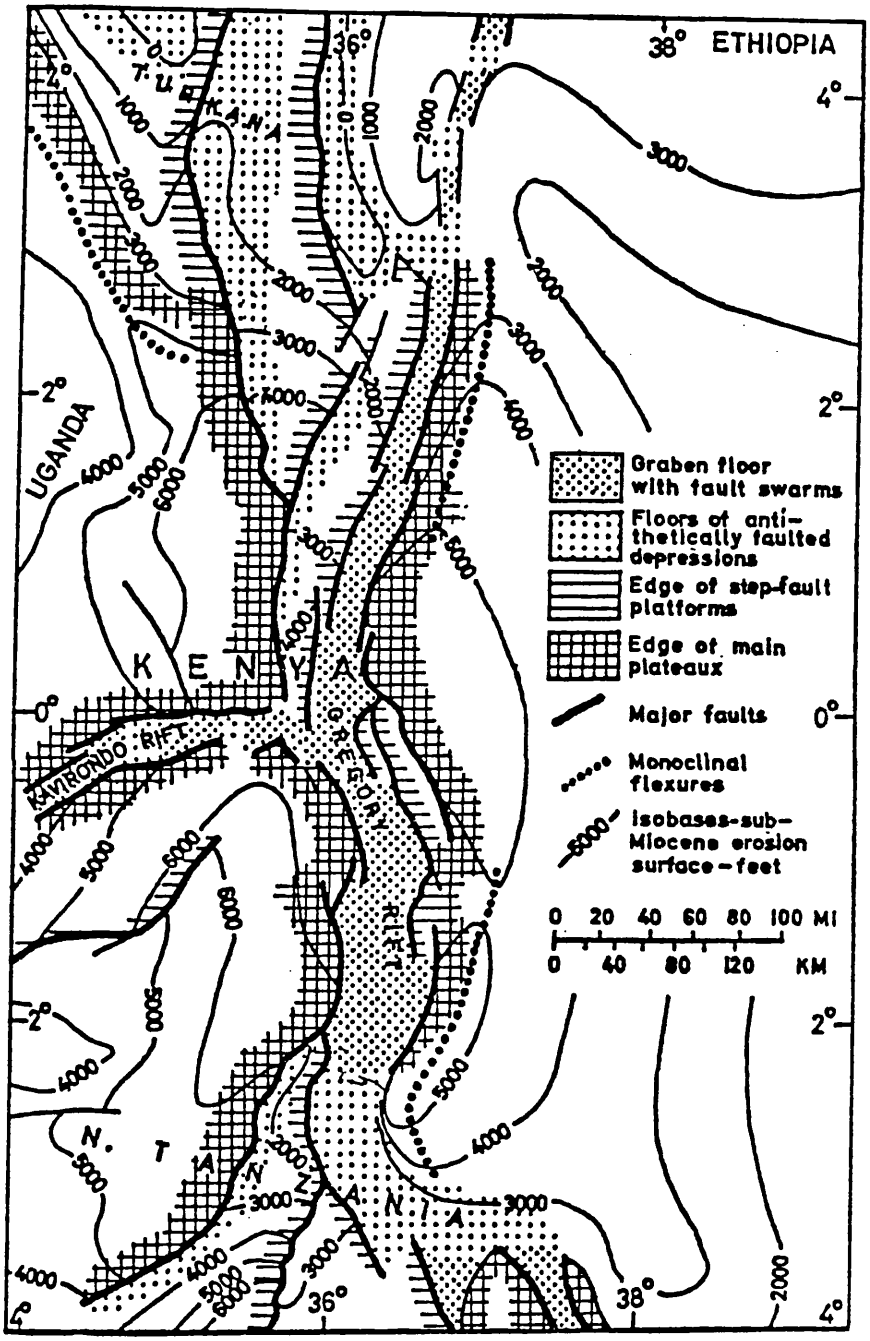

Figure 6.1.3-1 Structure of the Kenya rift zone. The contours indicate the amount of crustal uplift since the mid-Tertiary in feet. From Baker & Wohlenberg (1971).

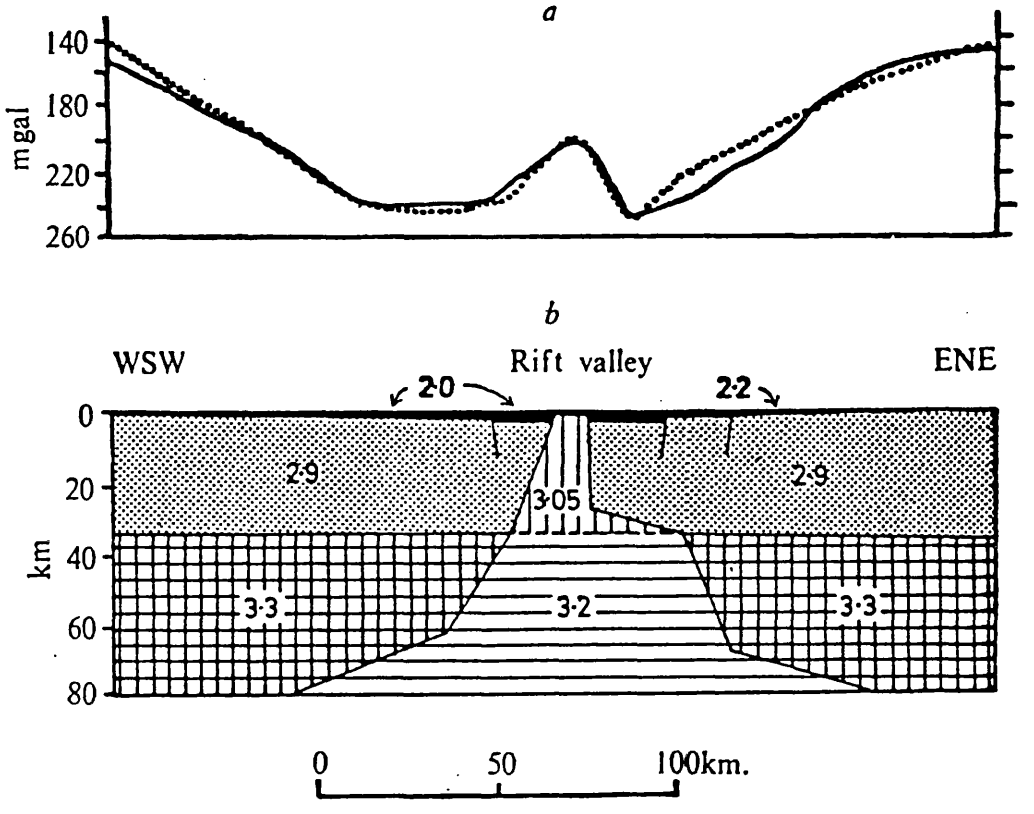

Figure 6.1.3-2 *a*. Bouguer gravity profile across the Gregory rift, oriented ENE-WSW. The continuous line is the observed Bouguer gravity anomaly and the dotted line is the computed anomaly for the crustal model shown in *b*. From Baker & Wohlenberg (1971).

The earliest rift-related structure is a mid-Cenozoic (pre-Miocene) monoclinal flexure along the western rift flank. During the Miocene, extensive vulcanicity occurred, and the first extensive rift faults developed in the early Pliocene. Voluminous vulcanicity characterized the period from the Pliocene to the present, accompanied by periodic fault movements. The crustal extension (or separation) is about 10 km (between 5 to 25 km) in the central sector of the Gregory Rift. If 10 km of crustal extension across the Kenya Rift is assumed since the Miocene, this represents a strain-rate of $10^{-15}s^{-1}$. In summary, it seems that the formation of the Kenya rift valley is the result of phases of epeirogenic uplift, volcanism and faulting since lower Miocene times.

The Kenya Rift, with its abundant vulcanicity, although exhibiting extensional stress locally, exists within a continental plate in a state of general compression. Therefore it may be a good candidate for the mantle-generated (or mantle activated) category. However, the East African Rift is connected via the Afar triple junction with the Red Sea-Gulf of Aden constructive plate boundary, and the whole network needs to be considered in its entirety.

The Gulf of Suez is the northwestern branch of the Red Sea (Figure 6.1.4-1). The rift is 60-100 km wide and extends for 400 km, separating Africa from the Sinai Peninsula. Rifting is post-Eocene and was underway by the start of the Miocene (Robson, 1971; Garfunkel & Bartov, 1977).

The early history of rifting indicates that the large uplifts bordering the rifts were not formed as a precursory doming event, but developed during the main phase of development of the rift (Steckler, 1985). During the Eocene, the entire Gulf of Suez region was a shallow water carbonate platform. When rifting commenced, with the development of tilted fault blocks and minor basalt activity, major erosion of the Eocene and older rocks occurred only on the high ends of the fault blocks. The opposing ends experienced deposition of marine carbonates with local conglomerates. The simultaneous subaerial erosion and marine deposition on the same tilted blocks are clear evidence that the rift was initiated near sea level.

Fault movements and limited tilting appear to have taken place throughout the Miocene and continue to the present. This has been studied in detail by Angelier (1985). Fault displacements are predominantly normal dip-slip with a small dextral component. The fault geometry indicates an extensional horizontal stress oriented at 045°. The amount of extension is estimated at 20-30 percent based on fault movement, and 45-50 percent based on the amount of subsidence over the entire width of the 80 km rift section. It is likely that the fault reconstruction method underestimates the extension. The evolution of the structure of the Gulf of Suez rift is illustrated in Figure 6.1.4-2.

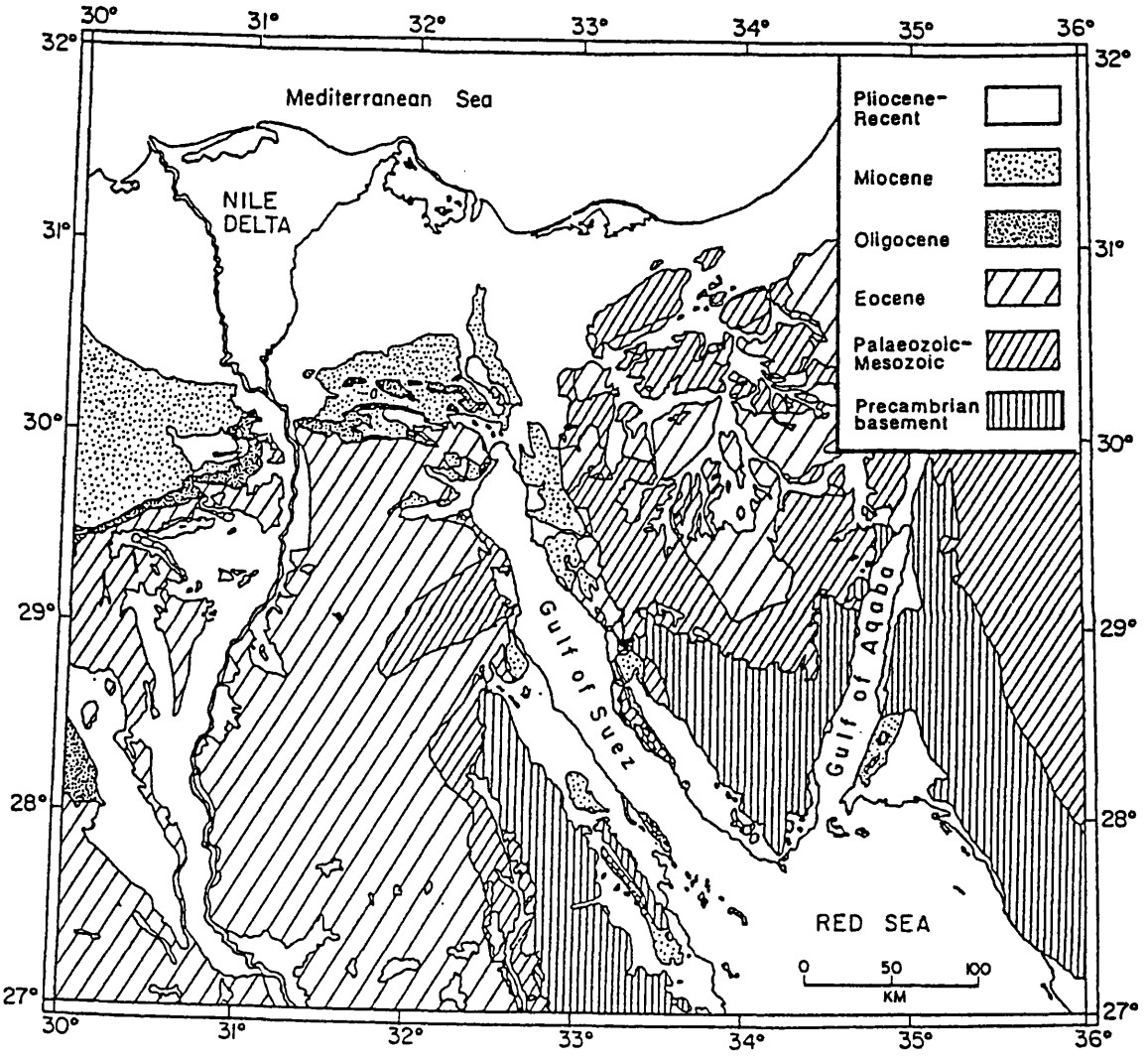

Figure 6.1.4-1 Geological map of the Gulf of Suez region. From Steckler (1985).

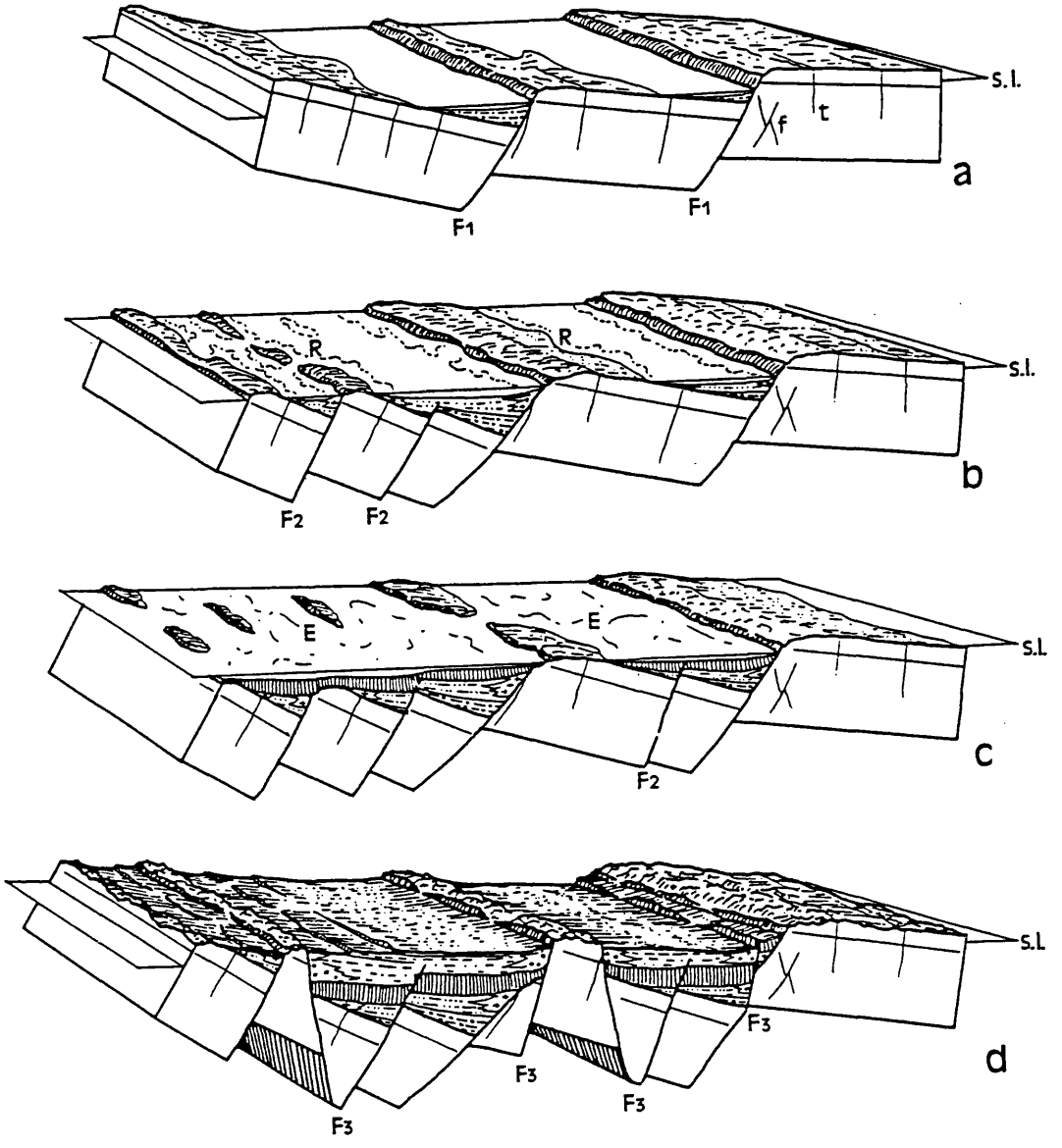

Figure 6.1.4-2 Structure of the Gulf of Suez rift. Block diagrams *a* - *d* show the evolution of tilted blocks accommodating to gradually increased extension: (*a*) late Oligocene-early Miocene; (*b*) early Miocene; (*c*) mid-Miocene; (*d*) Present. F1-3 indicate successive generations of faults; *f*, early conjugate normal fault system; *t*, early tension fractures; *R*, reefs; *E*, evaporite basins (vertical ruling in section); *sl*, sea level. From Angelier (1985).

Basin and range structures are commonly inferred to represent either (a) blocks tilted along downward-flattening (listric) faults in which the upslope part of an individual rotated block forms a mountain and the downslope part a valley or (b) alternating downdropped blocks (grabens) that form valleys and relatively upthrown blocks (horsts) that form mountains (Stewart, 1978). Basin and range structures are sometimes taken as rifts as well (wide rift). The best example is the Basin and Range province in North America, which is introduced below. This introduction is mostly based on the summaries by Stewart (1978), Zoback et al. (1981) and Eaton (1982).

The basin and range structure in North America

Along the western Cordillera of North America, late Cenozoic extensional faulting has produced block-faulted basin and range structures characterized by alternating elongate mountain ranges and alluviated basins. The structure extends from Canada to northern Mexico, with a total distance of 1500 km, and is 500 to 800 km in width (Figure 6.2-1). Generally, the structure is about 500 to 3000 meters above sea level, the valleys are approximately 700 meters lower than the mountains.

Basin and range structures consist of a system of normal faults along which movement has resulted in the relative uplift of linear segments of the crust to form mountains and the relative sinking of adjacent segments to form valleys. The mountains are usually about 15 to 20 km across and are separated by alluviated valleys of comparable width.

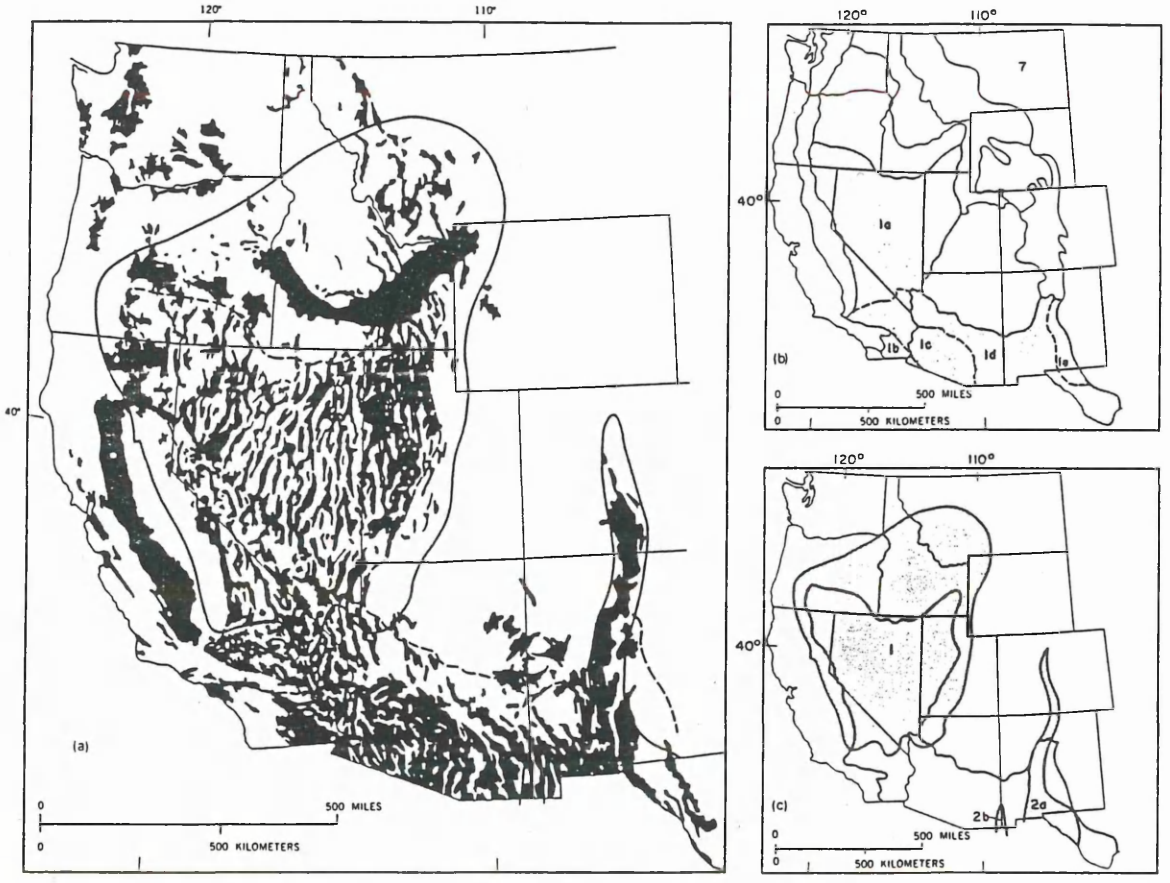

Figure 6.2-1 Maps of the Basin and Range province: (a) Distribution of grabens and other structural basins in the western United States containing Miocene, Pliocene, and Quaternary sedimentary rocks, as well as Quaternary volcanic rocks; (b) Map of physiographic subdivisions of the western United States, with sections of Basin and Range province as follows—— 1a, Great Basin; 1b, Salton Trough; 1c, Sonoran Desert; 1d, Mexican Highland; 1e, Sacramento; (c) Map of regions tectonophysically active in Quaternary time, exclusive of coastal California.

The formation of the Basin and Range province started approximately 17 Ma ago, but the earliest Cenozoic extensional deformation in this region may have begun as early as 37 Ma ago. The amount of extension is estimated to be from 10 percent to 35 percent of the original width of the province and as much as 100 percent in specific areas. According to some authors (e.g., Hamilton, 1987) extension has about doubled the pre-Oligocene width of the province. The crust has been thinned to less than normal (25 km), and heat flow is high.

Cenozoic extension was predated by compression. Northeast-directed compression was aligned in a direction approximately normal to the oceanic trench that existed through late Mesozoic and early Tertiary time at the western margin of North America. The Mesozoic and early Tertiary events produced folding, thrusting, uplift, and the emplacement of plutons and dikes of calc-alkaline magma. Crustal thickness had been increased to probably 35-40 km, or even 50 km, before extension.

Stewart (1978) grouped the early theories on the origin of Basin and Range structure into four main categories. In the first, the structure is presumed to be related to oblique tensional fragmentation within a broad belt of right-lateral movement and distributed extension along the west side of the North American lithospheric plate. The second theory relates extension to spreading caused by upwelling from the mantle behind an active subduction zone (back-arc spreading). The third theory relates the Basin and Range structure to spreading that resulted from presumed subduction of the East Pacific Rise beneath part of North America. The fourth theory relates the Basin and Range structure to plate motion caused by deep-mantle convection in the form of narrow mantle plumes.

Later a more "passive" cause for the formation of Basin and Range has been suggested (e.g., Molnar & Chen, 1983; Coney & Harms, 1984; Coney, 1987; Sonder et al., 1987). Regions of isostatically compensated overthickened crust may be in a state of extensional deviatoric stress (if lithosphere root does not exist below, see Fleitout & Froidevaux [1982]) and this provides the basis for alternative mechanical explanations of continental extension in the Basin and Range. As reviewed above, the Basin and Range province had a crust ranging from 35 to 50 km in thickness before Cenozoic extension. Molnar & Chen (1983) suggest that extension of the Basin and Range Province resulted from such stresses in a manner analogous to the present extension of the Tibetan Plateau. According to Froidevaux & Ricard (1987), the Basin and Range is in the last stage of the evolution of a high plateau.

A plateau with thickened crust cannot collapse without an increase in the vertical compressional stress or a decrease in horizontal compression (Froidevaux & Ricard, 1987). The reduction in boundary compression in Cenozoic North America may have resulted from changes in plate kinematics in the Pacific realm, from a drop in North America's westward motion, and/or from the steepening of the previously flat-dipping Laramide subducting slab after the Eocene (Coney, 1978; Coney, 1971; Coney & Reynolds, 1977). The Cenozoic Cordilleran tectonic evolution of the region and possible forces at work is illustrated in Figure 6.2-2. The Basin and Range may be an example of "oregenic collapse".

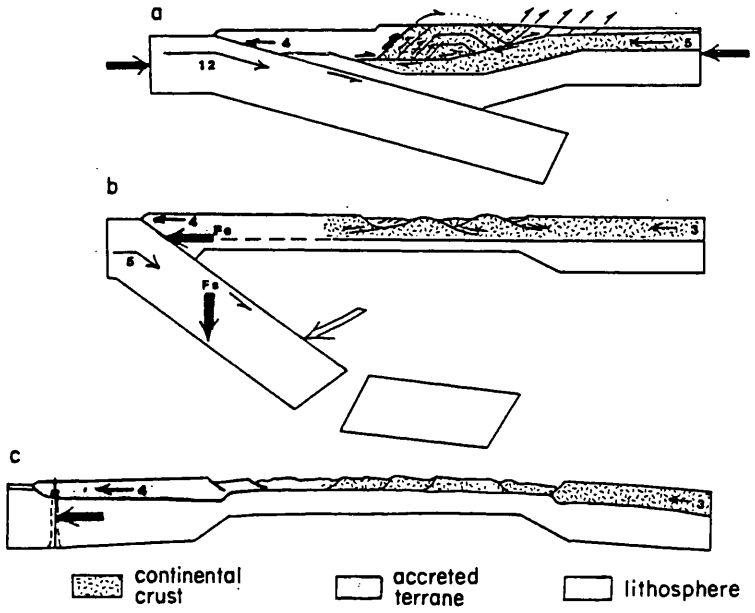

Figure 6.2-2. Possible forces at work during Cenozoic Cordilleran tectonic evolution. (a) Late-Mesozoic/early-Cenozoic Laramide compression. The North America Plate moves westward at 5 cm/year while the Farallon Plate moves eastward at 12 cm/year and subducts at a shallow angle. The opposed forces produce intraplate telescoping during Laramide times at about 1 cm/year. (b) Mid-Tertiary extension. North America Plate westward motion falls to 3 cm/year and Farallon Plate eastward motion falls to 5 cm/year. The crustal welt spread westward at a rate of about 1 cm/year. (c) Late-Tertiary Basin and Range extension. The North America Plate continues to move westward at 3 cm/year while the Pacific Plate moves in the figure and away on the other side of the San Andreas Fault at the left. From Coney (1987).

§ 6.3 Extensional structures associated with strike-slip faults

Strike-slip faults can also accommodate extension. For example, part of the northward convergence of the Indian plate with Tibet is taken up by strike-slip displacement, thus causing E-W extension of the plateau (Armijo et al., 1989). Strike slip faults develop when the vertical stress is σ_2, and are therefore associated with compression in one direction and extension in the other. Extensional features in this case are not dealt with in this thesis.

§ 6.4 Numerical analysis of continental extension

The processes of continental extension have been studied by many authors. It is not possible to review all the important numerical analyses in this area. Only some of the more typical studies are introduced here, and it is not my intention to include all those cited in the following chapter.

A. Stresses responsible for lithosphere failure

The tectonic stresses generated by plate boundary forces and buoyancy forces are usually less than 50 MPa vertically averaged across the lithosphere. If the whole lithosphere behaved elastically, failure would not occur and continental extension would not be possible. However, if the lithosphere is subdivided into upper elastic and lower visco-elastic layers, under constant boundary forces the stress decay in the lower layer will lead

to the amplification of stress in the upper layer to a value which is large enough for failure to occur (Kusznir & Bott, 1977). It has been shown that, through this process a compensated plateau with 2 km uplift can generate sufficient stress for failure to occur in the elastic layer (Bott & Kusznir, 1979). This process is dependent on the thickness of the brittle layer and the viscosity of the lower layer. A further study by Kusznir & Park (1984) shows that the deformation of the lithosphere and the magnitude of the applied stress required for Whole Lithosphere Failure is critically dependent on the thermal structure of the lithosphere as represented by the surface heat flow. Significant strains of 1 percent or more may be produced over times of the order of 1 Ma by an applied stress of 20 MPa in lithosphere with an average heat flow (60 mWm^{-2}). The model predicts extensional failure for areas of moderate heat flow (e.g. Central Europe, Northern China) as well as for areas of high heat flow like the Basin-and -Range Province.

B. Constraint on and the mode of continental extension

When lithosphere thinning occurs, all portions of the lithosphere move to shallower depths. If the thinning takes place rapidly enough, this motion is accomplished isothermally and no increase in the strength of the lithosphere should be expected. However, if thinning is slow enough, temperature within the lithosphere will fall and its strength will rise due to the heavy temperature dependence of the earth materials. This puts a limit to the lithosphere extension. England (1983) considered the extension of the continental lithosphere in terms of the deformation of a thin viscous sheet with a temperature-dependent rheology which is governed primarily by the strength of the upper mantle. He found that the progress of the

extension is influenced by the decrease in strength of the lithosphere, due to its attenuation, and by an increase in strength resulting from cooling. The relative importance of these two effects depends on two parameters, a dimensionless strain rate and the total strain. For a given strain rate the extending lithosphere goes through two phases as the strain increases: in the first, the effect of thinning the lithosphere is predominant and the strength of the lithosphere remains close to, and perhaps slightly below, its original strength; in the second, the effect of cooling of the lithosphere leads to very rapid increase in strength resulting in an effective limit on the degree of stretching that the lithosphere experiences. At strain-rate of $10^{-15}s^{-1}$, this maximum extension is between 100 percent and 150 percent, and it takes about 30 to 50 Ma for thermal cooling to cause the strength to increase. Once the strength starts to rise, it rises rapidly. In this study, when the strength rises to ten times its initial value, it is taken that extension stops.

The change in strength during the extension of continental lithosphere was also studied by Kusznir & Park (1987), incorporating the elastic, plastic and brittle behaviour of lithosphere material. It was found that the rate of extension was critical in determining whether the lithosphere strength would increase or decrease during extension. Fast strain rates (> $5x10^{-15}s^{-1}$) produced a weakening of the lithosphere causing intense localized lithospheric extension with high β values (narrow rift), while slower strain rates led to strengthening of the lithosphere, causing broader regions of lithosphere extension (wide rift) with finite β values of the order of 1.5.

The effects of temperature-dependent rheology of lithosphere on

large-scale continental extension have been modelled by Sonder & England (1989) in the Aegean area. It was observed in their simulation that the locus of extension migrated from the more deformed region to the less deformed area at a later stage of stretching, due to increasing strength in the more deformed area. Because I have some reservations about that work, and because it makes use of the thin viscous sheet model, the work is introduced separately in the next section.

In the work of England (1983) and Kusznir & Park (1987), the mode of lithosphere extension (intense localized rifting or extension in a broad region) is related to changing strength during extension, and strain rate is the key factor. At slow strain rates, deformed regions get stronger causing the strain to migrate to the undeformed area. Another mechanism for producing a wide rift is gravitational collapse. In this mechanism, gravitational stresses produced by crustal thinning resist further extension more strongly than lithospheric thinning promotes it. This is thought to occur where thick crust and high heat flow make the lithosphere very weak. This mechanism has been invoked to explain the flatness of topography across Tibet (Molnar & Chen, 1983) and the small gradients in crustal thickness across the Basin and Range (Sonder et al., 1987; Hamilton, 1987). Buck (1991) combined the two mechanisms in a model, and found that the mode of extension is linked to the crustal thickness and the thermal structure of the lithosphere. Normal heat flow (60 mWm^{-2}) corresponds to a narrow rift, High heat flow (80 mWm^{-2}) corresponds to a wide rift mode, and very high heat flow (100 mWm^{-2}) corresponds to a core complex rift mode. Christensen (1992) reached similar conclusions using more developed techniques.

C. The process of rifting

Rifting is examined by Zuber & Parmentier (1986) in terms of the growth of a necking instability in a lithosphere consisting of a strong plastic or viscous surface layer of uniform strength overlying a weak substrate in which strength is either uniform or decreases exponentially with depth. As the lithosphere extends, deformation localizes about a small imposed initial perturbation (i.e., a pre-existing weakness) in the strong layer thickness. A power law viscous rheology was used, and n=10000 was treated as perfectly plastic. The uplift flanks were argued to be supported dynamically by a periodic deformation process. Lin & Parmentier (1990) improved the above work, describing the formation of a rift as the finite amplitude necking of an elastic-plastic layer overlying a fluid substrate. The major difference in the conclusion in this case is due to the different explanation for the flank uplift. In the latter work, it is found that vertical forces due to the mass deficit of the rift depression will flex the elastic layer outside the yield zone, creating flanking uplifts. These analyses are two dimensional in the vertical cross section of the rift, and the buoyancy force due to the gravity potential has been neglected.

In the last two studies, a perturbation in the thickness of the strong layer always amplifies. This is attributed to the fast deformation assumed, and thermal processes are neglected.

Necking of the strong layer can occur simultaneously. Fletcher & Hallet (1983) treated the lithosphere as a strong surface layer of uniform strength and density overlying a weaker substrate of the same density, showing that unstable extension, or boudinage, results in the concentration

of extension into regions with a regular spacing determined primarily by the thickness of the strong layer. Zuber et al. (1986) assumed two strong layers, upper crust and upper mantle, separated by a weak lower crust, in the lithosphere, and found that necking instability of two wavelengths will arise. They applied this to Basin and Range, and found that the horizontal scale of short wavelength necking is consistent with the spacing of individual basins and ranges, while that of the longer wavelength necking is consistent with the width of tilt domains.

Rifting is affected by preexisting weakness in the lithosphere. Dunbar & Sawyer (1989) studied the passive rifting of lithosphere in which the position of a dominant preexisting weakness varies. In this work, continental lithosphere is viewed as a composite material consisting of two strong layers, one in the upper mantle and one in the middle crust. Extensional failure at weaknesses in the mantle causes concentrated extension in the mantle and diffuse extension in the crust. Failure at weaknesses in the crustal strong zone causes focused extension in the crust and diffuse extension in the mantle. When mantle weakness and crustal weakness are not on the same vertical line, simple shear develops (a vertical reference line is rotated during deformation). Otherwise pure shear dominates (a vertical reference line remains vertical during deformation). Lynch & Morgan (1990) studied the effect of thermal, mechanical, and compositional heterogeneities, and found that thermal heterogeneities are most effective in controlling deformational style.

Sonder & England (1989) extended the work of England & McKenzie (1982, 1983) to study the extension of continental lithosphere. The assumptions and the mechanical equations are the same as before. But this time the effect of temperature on the average rheology of the lithosphere is considered. The behaviour of the model depends principally on two parameters: the Peclet number, which describes the relative rates of advection and diffusion of heat, and a dimensionless activation energy, which controls the temperature dependence of the rheology. Numerical calculation of the deformation of such a thin sheet subjected to an extensional boundary condition shows the following results: at short times following the beginning of extension, deformation occurs with negligible change in temperature, so that only small changes in lithospheric strength occur due to attenuation of the lithosphere, and maximum rates of deformation are located close to the extensional boundary. However, after a certain time interval, thermal diffusion results in lowered temperatures in the lithosphere, strongly increasing lithospheric strength and slowing the rate of extension. This critical time depends principally on the Peclet number and is short compared with the thermal relaxation time constant of the lithosphere. The changes in strength cause the locus of high extensional strain rates to shift with time from regions of high strain to regions of low strain. Results of the calculations are compared with observations from the Aegean, where maximum extensional strains are found in the south, near Crete, but the largest present-day extensional strain rates occur about 300 km further north. The comparisons support the hypothesis that the observed separation of the loci of maximum strain and maximum present-day strain rates in the Aegean may be the consequence of changes in

lithospheric strength arising from the temperature-dependent mechanical properties of lithospheric materials.

There are, however, some problems to this work:

A. The mechanical equations are adopted from the previous studies proved above to be wrongly derived.

B. The mechanical equations assume that compensation is reached within the lithosphere mantle. In another words, the asthenosphere and the mantle lithosphere are of the same effective density, which is not so reasonable in the case of lithosphere extension where the mantle could play at least a secondary role and may play a primary role.

C. The effect of gravity has not been systematically studied. It was mentioned that when $Ar > 0$, gravitational forces resist deformation, and when $Ar < 0$, gravitational forces augment deformation. It is hard to understand how Ar can be negative, given its definition, if the crust is not denser than the mantle.

D. The Aegean area is under water. It is shown in § 3.5 that this does not influence horizontal deformation very much but no discussion is given of this.

E. The most controversial feature is the calculation of temperature. It was assumed that the average rheology is sensitive to the temperature of the strong layer which is near the Moho surface. To calculate temperature variation at the Moho surface during the extension, an analytic solution by

Carslaw & Jaeger [1959, equation(2.4)(1)] was used. However, the cited solution is for the temperature in a half space with zero surface temperature and initial temperature $f(z)$, without deformation. The formula for the change of Moho temperature derived by Sonder & England (1989) is

$$\Delta T_M \approx - \frac{T_L \beta^2}{2\sqrt{\pi}} \frac{\kappa t_B}{Z_L(Z_L - Z_M)} \frac{e^{-x^2}}{x}$$

where $x = (Z_L - Z_M)/\beta\sqrt{2\kappa t_B}$, T_L is the temperature at the bottom of lithosphere, κ is the thermal diffusivity, β is the amount of strain, t_B is the time after a quick stretching which causes the amount of strain β, Z_L and Z_M is the depth of the bottom of lithosphere and of the Moho surface respectively.

If we test the above formula, we see that ΔT_M is always negative whether β is larger, equal or smaller than 1. That is to say, the temperature at the Moho surface is always decreasing whether the lithosphere has been stretched, shortened or not deformed at all. Such a formula might be a practical approximation in the case of lithosphere stretching, but it certainly exaggerates the cooling effect. According to this work, at an extensional strain rate of $10^{-15}s^{-1}$, the strength starts to increase after about 15-20 Ma of extension (Sonder & England 1989, Fig.2a). But according to England (1983), this time span is 30 to 40 Ma (England 1983, Fig.3). There is considerable discrepancy between these two results and I believe the earlier result is more reliable. Without the exaggeration of the cooling process, the migration of the high extension locus observed in this work can probable not be repeated, and comparison with Aegean becomes problematic.

In the next chapter, the viscous sheet model derived in Chapter 3 is applied to continental extension and in particular the mode of extension. It takes into account buoyancy forces and the effect of thermal cooling on lithosphere thickness. The model is suitable for pre-rifting deformation of the lithosphere. Compared with the work of Sonder & England (1989), this model includes the role of the asthenosphere more clearly. Compared with other studies, this model is in the horizontal domain and therefore can include the effect of non-uniform boundary condition.

Chapter 7. Application of the model to continental extension

In this chapter, I apply the thin viscous model to the study of continental extension. It would be over ambitious to analyze continental extension fully at this stage, especially when using such a simple model. The purpose of this study is to add to our understanding of some of the physics in continental extension processes, as many of the previous authors have done. The Finite Difference Method I have used makes it difficult to define the problem in terms of boundary forces or stresses, and I will therefore concentrate on the distribution of extension under boundary displacements, and try to identify the factors affecting the style of deformation.

§ 7.1 Factors affecting the extension of continental lithosphere

The extension of continental lithosphere is a complex process and the development of deformation is affected by several factors.

A. Stretching causes lithosphere thinning, and if thinning is not uniform, deformation will tend to concentrate to the thinner and hence weaker part, and this positive feedback may result in instability (failure, in which most of the deformation is taken up by a narrow zone), which is narrow rift.

There may be two reasons for non-uniform thinning. First, the lithosphere is not uniform. There are weak belts either because of the properties of rocks or because of the variation of the lithosphere thickness. Second, the boundary conditions and intra-plate body forces may

cause non-uniform thinning in uniform lithosphere.

B. On the other hand, if the lithosphere before stretching is in a thermally static state, then the stretching and thinning will cause faster dissipation of heat and this thermal process tends to restore the thickness to its previous state. This has a double effect. First, it makes up part of the thickness by affixing cooled asthenosphere to the bottom of the lithosphere, thus making up part of the lost strength of the thinned lithosphere. Second, if the strength of the lithosphere is controlled by a strong layer, since the thinning causes the ascending of this strong layer, thermal processes will cool this strong layer and therefore strengthen the lithosphere. The first effect can be described by the thermal restoration formula given in § 3.1 (eq.3.1-4 or eq.3.1-5). The second is not included in this model. This will be justified later.

C. The gravitational force due to density variation may have some effect on the development of continental extension. This effect has been largely neglected in numerical analyses by several authors. It was referred to by Sonder & England (1989) who claimed that the gravitational force either resists (when $Ar > 0$) or augments (when $Ar < 0$) deformation. However, given its definition, Ar is always positive as long as the crust has lower density than the mantle. In fact, their equations containing Ar are valid only if the elevation or subsidence of the top of the crust is totally compensated by the subsidence or elevation of the Moho surface, or in other words, the lithosphere mantle and the asthenosphere have the same equivalent density. In that case, as we will see later, the gravitational force always resists localization of deformation. The value of the asthenosphere density is critical in the analysis of continental rifting, because it controls the

elevation or subsidence of the top surface of thinned lithosphere which in turn affects the distribution of the amount of extension. The sedimentation process augments the subsidence of the lithosphere and therefore is a potential factor affecting the gravitational forces, but as long as the lithosphere is a in regional state of isostatic equilibrium, the influence of sedimentation is found to be small in respect of horizontal deformation of the lithosphere. This has been proved in § 3.5 by mathematical arguments and will be tested by an example in this chapter.

§ 7.2 Choice of boundary conditions and parameters

Before going into the details of the calculation, a brief introduction to the boundary conditions and parameters involved needs to be given.

a. The boundary conditions are classified into two kinds: partial stretching, and uniaxial stretching. With partial stretching, a uniform lithosphere is stretched at part of its boundary, which causes uneven thinning and attenuation. With uniaxial stretching, the lithosphere has a long weak belt, achieved by reducing the lithosphere thickness locally, and is stretched uniformly along its boundary.

b. The potential effect of buoyancy forces is indicated by the A number, which is dependent on the average strength of the lithosphere. Since there are great uncertainties concerning the average strength of the lithosphere, A is given three possible choices in the following analysis: (a) low, 0, (b) intermediate 30 to 50 and (c) large, 90 to 100. With A = 0, the lithosphere is so strong that there is no effect of the buoyancy forces.

c. Two possible values of crustal density are considered, 2.95 or 2.8.

d. Two possible values of equivalent asthenosphere density are considered, 3.3, which is the same as that of the lithosphere mantle, and 3.2, which corresponds to a hot spot.

e. There may or may not be an initial elevation. When there is, it corresponds to active rifting, as initial doming should precede rifting in a classical active rift; when there is not, it corresponds to passive rifting.

f. The maximum rate of boundary displacement may take a range of values: 0.5 cm/year, 1cm/year, 2 cm/year, 5 cm/year and 10 cm/year in the calculation.

g. There are two forms of rheology formulation: thickness-related strength, which partly takes into account the strength of the brittle and brittle -ductile transition zone, or constant strength.

It is neither logistically possible nor necessary for the purpose of this thesis to consider all the possible combinations. Here only the results of typical examples are given and discussed. They are put into several groups in which the mantle plays an increasingly greater role.

§ 7.3 Partial Stretching with a completely passive mantle

Suppose normal uniform lithosphere is stretched at part of its boundary. This causes uneven thinning, and deformation may localize into the more deformed part. If the lithosphere mantle and the asthenosphere have the same equivalent density, as treated in the work of Sonder & England (1989), then the subsidence of the top surface is totally balanced by the

elevation of the Moho. In other words, the compensation level is within the lithosphere. In this situation, the mantle is completely "passive".

The boundary conditions used in this model are shown in Figure 7.3-1. Symmetrical deformation is assumed so that only the right-hand side of the stretched area is shown.

The average strength is thickness related, i.e., $\bar{B}=\bar{B}_o L/L_o$. This has the effect of promoting the effect of thickness differences in the lithosphere.

The parameters are listed below.

Initial thickness of the lithosphere	L_o=100 km
Velocity scaling factor	U_o=5 cm/year
Density of crust	ρ_c=2.95 g/cm^3
Density of lower lithosphere	ρ_m=3.30 g/cm^3
Density of asthenosphere	ρ_a=3.30 g/cm^3
Temperature at lower boundary of lithosphere	T_L=1200°C
Temperature at lower boundary of asthenosphere	T_A=1300°C
Power law exponent in rheological equation	n =3
Thermal diffusivity of the lithosphere	κ =3.54×10^{-6}m^{2}s^{-1}

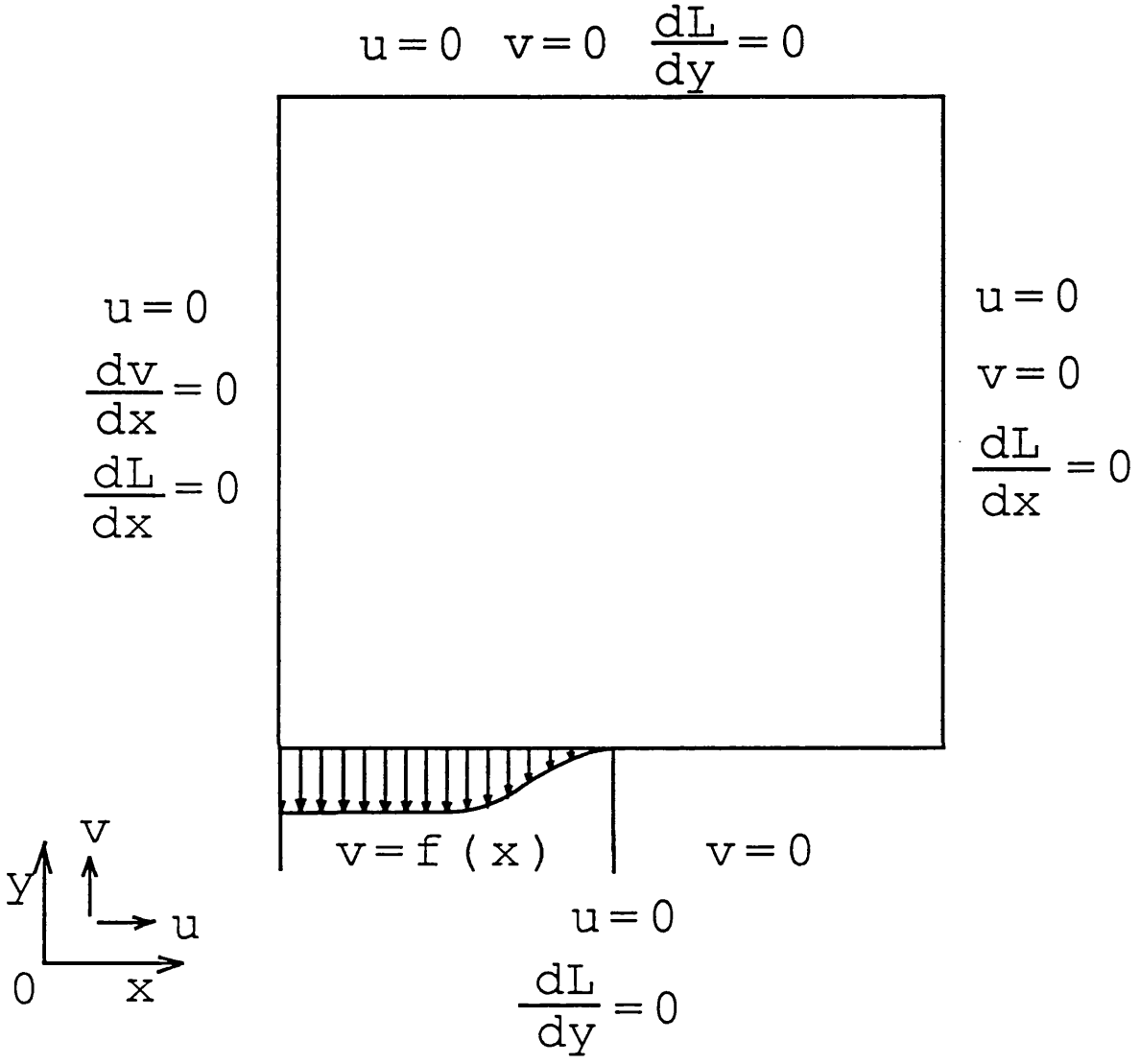

Figure 7.3-1. The boundary conditions used in studying lithosphere extension are similar to those used in the study of lithosphere shortening (see Figure 5.1-1), except that the direction of the boundary velocity is reversed. The function f(x) has the form:

$f(x)=u_{max}$ $\quad 0 \le x \le 8Lo$

$f(x)=u_{max}\cos^2[\frac{\pi}{2}(\frac{x}{8Lo} - 1)]$ $\quad 8Lo \le x \le 16Lo$

The area is meshed by 32x32Lo.

A group of calculations have been carried out with the maximum boundary velocity as 10 cm/year, 5 cm/year, 2 cm/year and A as 0, 50, and 90. In some cases, the deformation accelerates and results in instability after a time span T_{ins}, which is listed in Table 7.3-1, together with the corresponding amount of boundary displacement. In some cases, the deformation is stabilized by the thermal restoration process, and the deformation is stable for an indefinite period. Although the calculation with the maximum boundary velocity of 1 cm/year is not shown, it can be expected that the deformation in that case would be distributed and stable.

Table 7.3-1 Time to extensional instability and corresponding boundary displacement for various boundary velocities and A numbers.

T_{ins} / A / U_{max}	0	50	90
10cm/year	5.6 Ma	7.2 Ma	15.2 Ma
5 cm/year	10 Ma	19.2 Ma	Infinite
2 cm/year	Infinite	Infinite	Infinite

Figure 7.3-2 and Figure 7.3-3 show the crustal thickness and the vertical strain rate of the stretched lithosphere near the onset of instability (failure). Figure 7.3-4 shows the crustal thickness and the vertical strain rate of the steadily stretched lithosphere after 24 Ma of stretching.

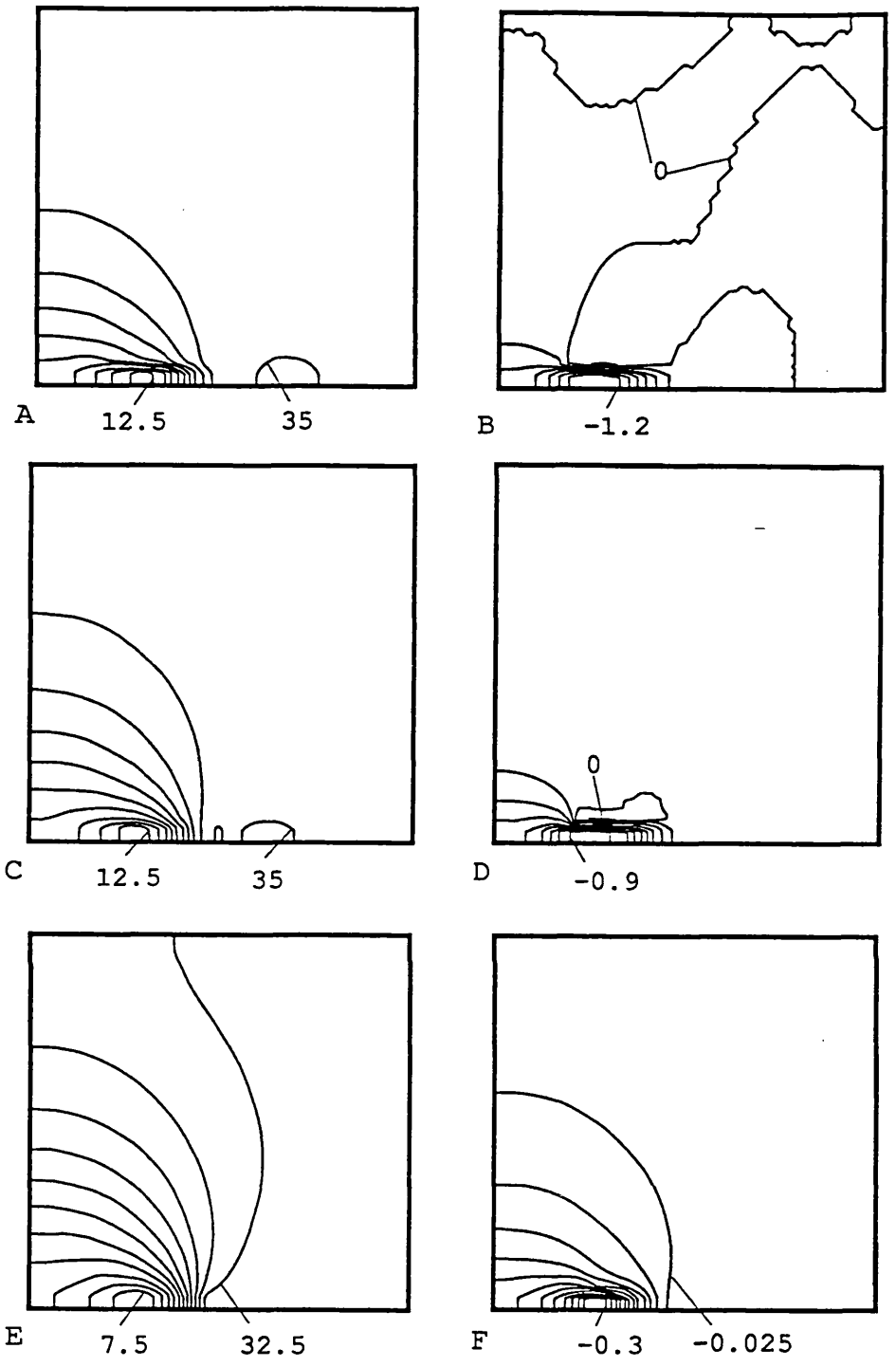

Figure 7.3-2. Contour maps of crustal thickness (A, C, E) and vertical strain rate (B, D, F) of a lithosphere under stretching, near the onset of instability, with u_{max} = 10 cm/year. $\bar{B} = \bar{B}oL/Lo$. $\rho_m = \rho_a$. Boundary conditions are shown in Figure 7.3-1.

A. A = 0. Time is 5.6 Ma. Contours are from 12.5 by 2.5 to 35 (km).
B. A = 0. Time is 5.6 Ma. Contours are from -1.2 by 0.2 to 0.2 (Uo/Lo).
C. A = 50. Time is 7.6 Ma. Contours are from 12.5 by 2.5 to 35.
D. A = 50. Time is 7.6 Ma. Contours are from -0.9 by 0.1 to 0.
E. A = 90. Time is 15.2 Ma. Contours are from 7.5 by 2.5 to 32.5.
F. A = 90. Time is 15.2 Ma. Contours are from -0.3 by 0.025 to -0.025.

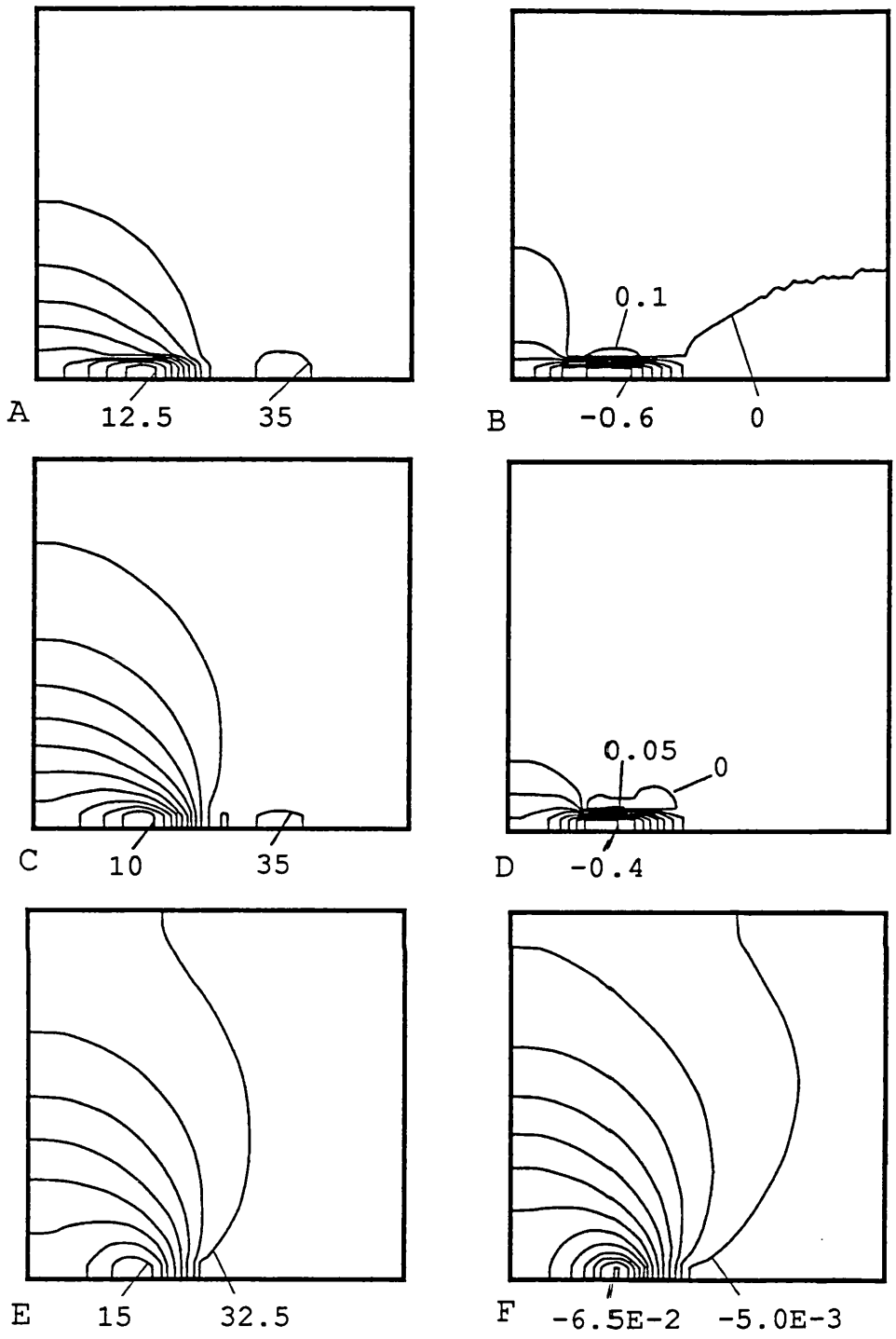

Figure 7.3-3 Contour maps of crustal thickness (A, C, E) and vertical strain rate (B, D, F) of a lithosphere under stretching, with u_{max} = 5 cm/year. $\bar{B} = \bar{B}oL/Lo$. $\rho_m = \rho_a$. Boundary conditions are shown in Figure 7.3-1.
A. A = 0. Time is 10 Ma. Contours are from 12.5 by 2.5 to 35.
B. A = 0. Time is 10 Ma. Contours are from -0.6 by 0.1 to 0.1.
C. A = 50. Time is 19.2 Ma. Contours are from 10 by 2.5 to 35.
D. A = 50. Time is 19.2 Ma. Contours are from -0.4 by 0.05 to 0.05.
E. A = 90. Time is 24 Ma. Contours are from 15 by 2.5 to 32.5.
F. A = 90. Time is 24 Ma. Stable deformation. Contours are from -6.5E-2 by 5.0E-3 to -5.0E-3.

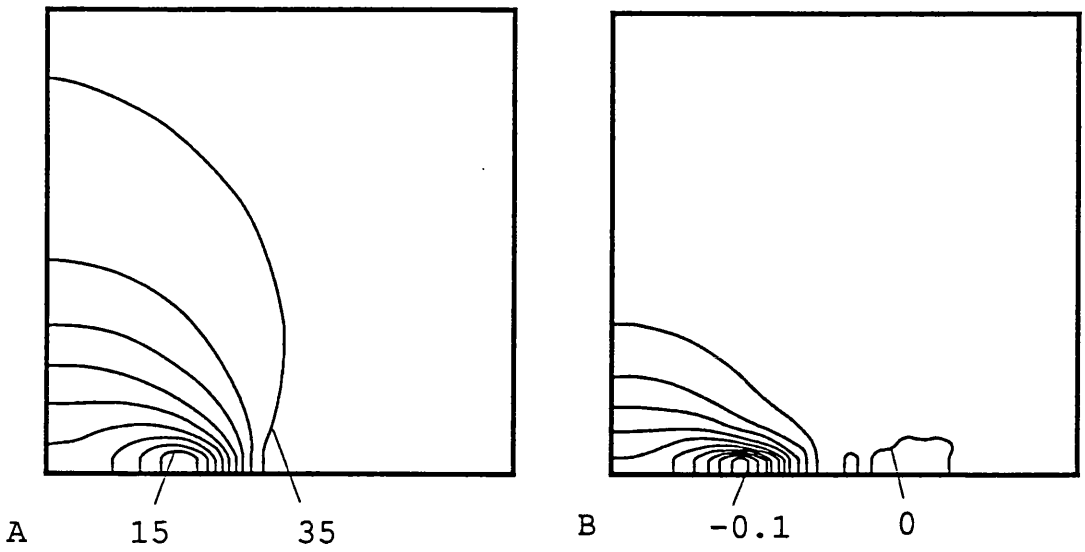

Figure 7.3-4. Contour maps of crustal thickness and vertical strain rate after 24 Ma stretching, with u_{max} = 2 cm/a, and A = 0. Boundary conditions are shown in Figure 7.3-1. $\bar{B}=\bar{B}oL/Lo$. $\rho_m=\rho_a$. Further stretching is stable.
A. Crustal thickness. Contours are from 15 by 2.5 to 35.
B. Vertical strain rate. Contours are from -0.1 by 0.01 to 0.

Discussion

a. The role of gravity flow

It can be seen from the above results that low gravity flow (stronger lithosphere) favours stretching instability and the localization of extension. The stretching causes thinning and subsidence in the more deformed areas, and the gravity flow from the less deformed to the more deformed and subsided area causes the thinning to be distributed to wider areas, so that large gravitational flow acts against the concentration of deformation. A large A number corresponds to weak lithosphere, as indicated

by high heat flow. Therefore the diffuse extension of the Tibetan Plateau and the Basin and Range is very likely to be due to a weak lithosphere and high gravitational flow (or collapse). This has been suggested by Molnar & Chen (1983) and Sonder et al. (1987), and modelled by Buck (1991) in another way. Lower gravity flow corresponds to a stronger lithosphere. Since it is more difficult to deform a stronger lithosphere, it is an inevitable conclusion that rifting occurs only along a preexisting weak belt in a strong lithosphere under stretching when the mantle plays a completely passive role.

b. Thinning and thermal restoration

Generally, slow stretching causes widespread thinning and subsidence, and deformation will not be concentrated into a weak belt. This is partly because the thermal process has the effect of restoring thinned lithosphere to its normal thickness. However, if the stretching and resulting thinning in the weak belt is quick enough, then the thermal thickening can not keep up with the mechanical thinning, and the thinner and weakened belt causes thinning to occur even faster. Finally, the deformation becomes unstable, and continental breakup occurs. This has been suggested by Kusznir & Park (1987) when studying the changing of rheology during lithospheric extension. The critical value of strain rate determining strain-hardening or strain -softening is given as $5x10^{-15}s^{-1}$ by these authors.

In the above numerical analyses, although the thermal restoration process on the lithospheric thickness has been included, the possible rheological change during deformation has not been considered. Therefore a thinned lithosphere is taken to be weaker than a normal one. This is not

always true. During slow and stable extension, if there is enough time, the thinned lithosphere may grow stronger than it used to be because of the subsequent cooling of the strong layer following stretching (England, 1983; Kusznir & Park, 1987), which is sometimes called "strain-hardening". However, this is a slow process. According to England (1983), the duration of extension is 20 Ma, 15 Ma, 11 Ma and 9 Ma at strain rate of $3.6 \times 10^{-15} s^{-1}$ (0.22 Uo/Lo), $6.3 \times 10^{-15} s^{-1}$ (0.38 Uo/Lo), $1.3 \times 10^{-14} s^{-1}$ (0.78 Uo/Lo), and $1.7 \times 10^{-14} s^{-1}$ (1.02 Uo/Lo) respectively. England (1983) took the duration of extension to be the time before lithospheric strength increased to ten times its initial value. Since strength increases sharply once it starts to increase, the duration of extension can also be taken as the time before strain-hardening takes place. Comparing the above data with the results presented in Figures 7.3-2 to 7.3-4, it can be seen that strain-hardening could not have occurred in any of the cases. Therefore I am confident that the omission of a strain-hardening mechanism does not affect the results in this section. In fact this is true throughout this chapter.

In the above analysis, the average strength is related to the lithosphere thickness. If the average strength remains constant, the attenuation of the lithosphere thickness caused by uneven boundary stretching would be much smaller, and deformation has been found to be generally in a stable and distributed mode.

§ 7.4 Uniaxial stretching with a completely passive mantle

In this case, the lithosphere is stretched uniaxially and there is a weak belt in the lithosphere, transverse to the direction of stretching, as shown in Figure 7.4-1. When this lithosphere extends under stretching, the thinner part deforms more than the rest. The contrast may or may not develop to an extent that the thinner part accommodates most of the extension.

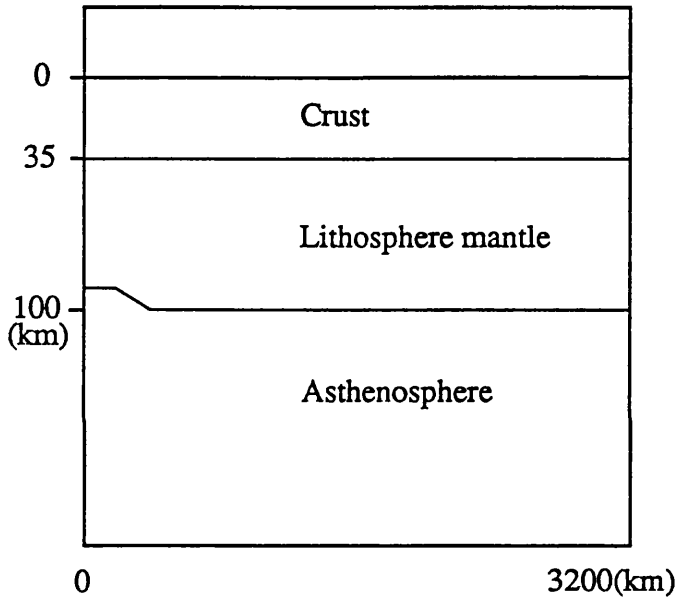

Figure 7.4-1 The vertical section of a lithosphere with weak belt normal to the direction of stretching.

Two sets of calculations were done concerning this.

A. In the first calculation, all the parameters are the same as in § 7.3. The average lithosphere strength is thickness-related, i.e., $\bar{B}=\bar{B}_o L/L_o$. The boundary velocity is 5 cm/year. The A number is 0, 30 and 100 respectively.

According to the results of the calculations, with A=0, the extension goes unstable after 12.4 Ma (Figure 7.4-2) and the total displacement before that is 620 km. With A=30 and A=100, the extension remains stable and widely distributed for at least 24 Ma.

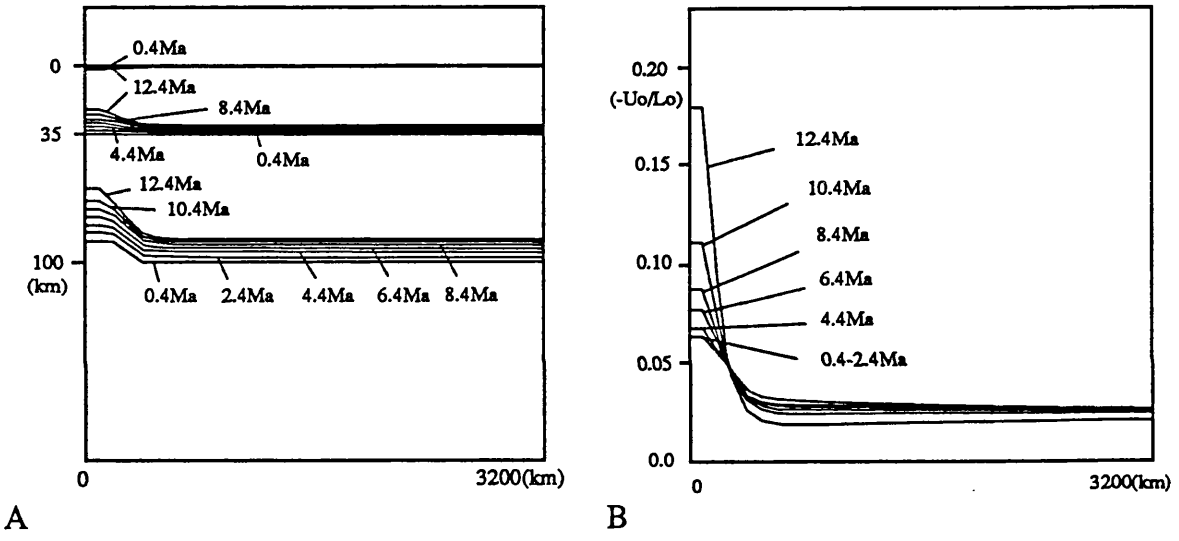

Figure 7.4-2 The deformation history of a uniformly stretched lithosphere with existing weak belt as shown in Figure 7.4-1. A=0. u_{max}=5 cm/year. $\bar{B} = \bar{B}oL/Lo$. $\rho_m = \rho_a$.
A. The position of the three layers during the extension.
B. The rate of thinning.

B. In the second calculation, all the parameters are the same as in the previous case. The difference is in the formulation of strength: the average strength of the lithosphere remains constant. With the boundary velocity no larger than 5 cm/year, the deformation is always in stable and

distributed forms. So with constant average strength, moderate perturbation in the lithosphere thickness does not amplify fast enough to form narrow rifts. To find out under what conditions extension will localize in a lithosphere with constant average strength, I relax the conditions of the calculation in favour of extension localization in two ways: firstly the maximum value of the defect at the bottom of the lithosphere is increased from 10% to 20% so that there is a greater perturbation to amplify; and secondly, the thermal restoration process is neglected so that the attenuation of the lithosphere thickness is not offset by the cooling process. With these conditions, rifting does occur, if A=0, in a period of 15.2 Ma (Figure 7.4-3). However, if A=30, rifting does not occur (Figure 7.4-4); if A=100, the perturbation can not even amplify (Figure 7.4-5). Again the effect of gravitational force is to prevent the localization of the deformation.

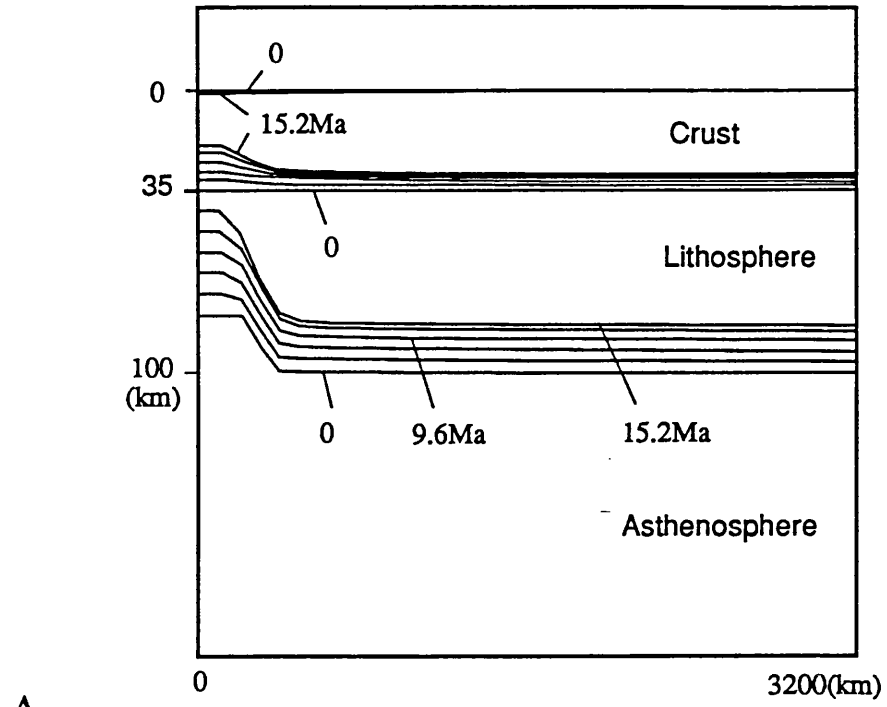

A

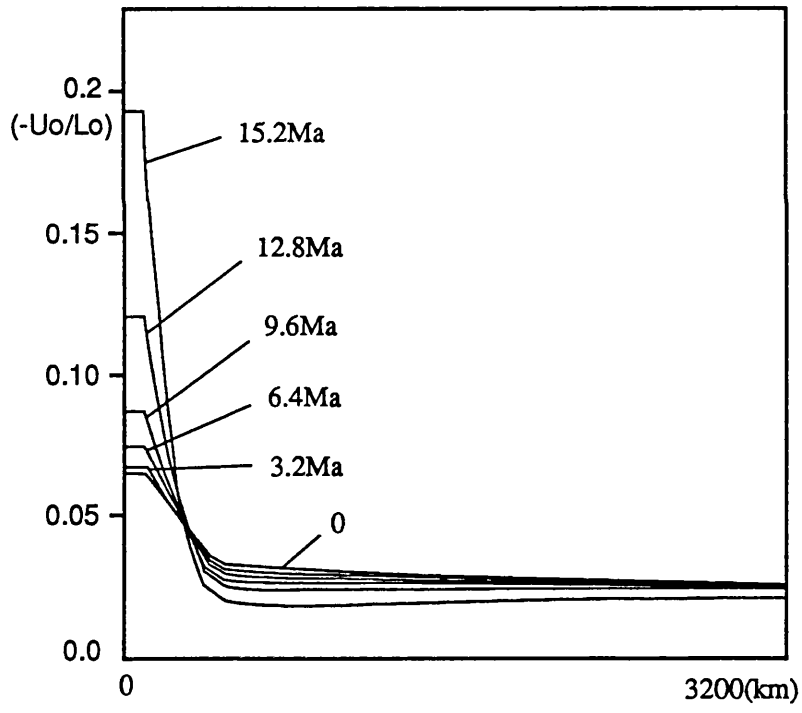

B

Figure 7.4-3. Uniaxial extension with A=0, $\bar{B}=\bar{B}o$, $\rho a=\rho m$, and u=5cm/year. Thermal restoration process has been neglected in favour of localizing deformation.
A. The top surface, Moho surface and the lower boundary of the lithosphere.
B. The vertical strain rate distribution during the extension.

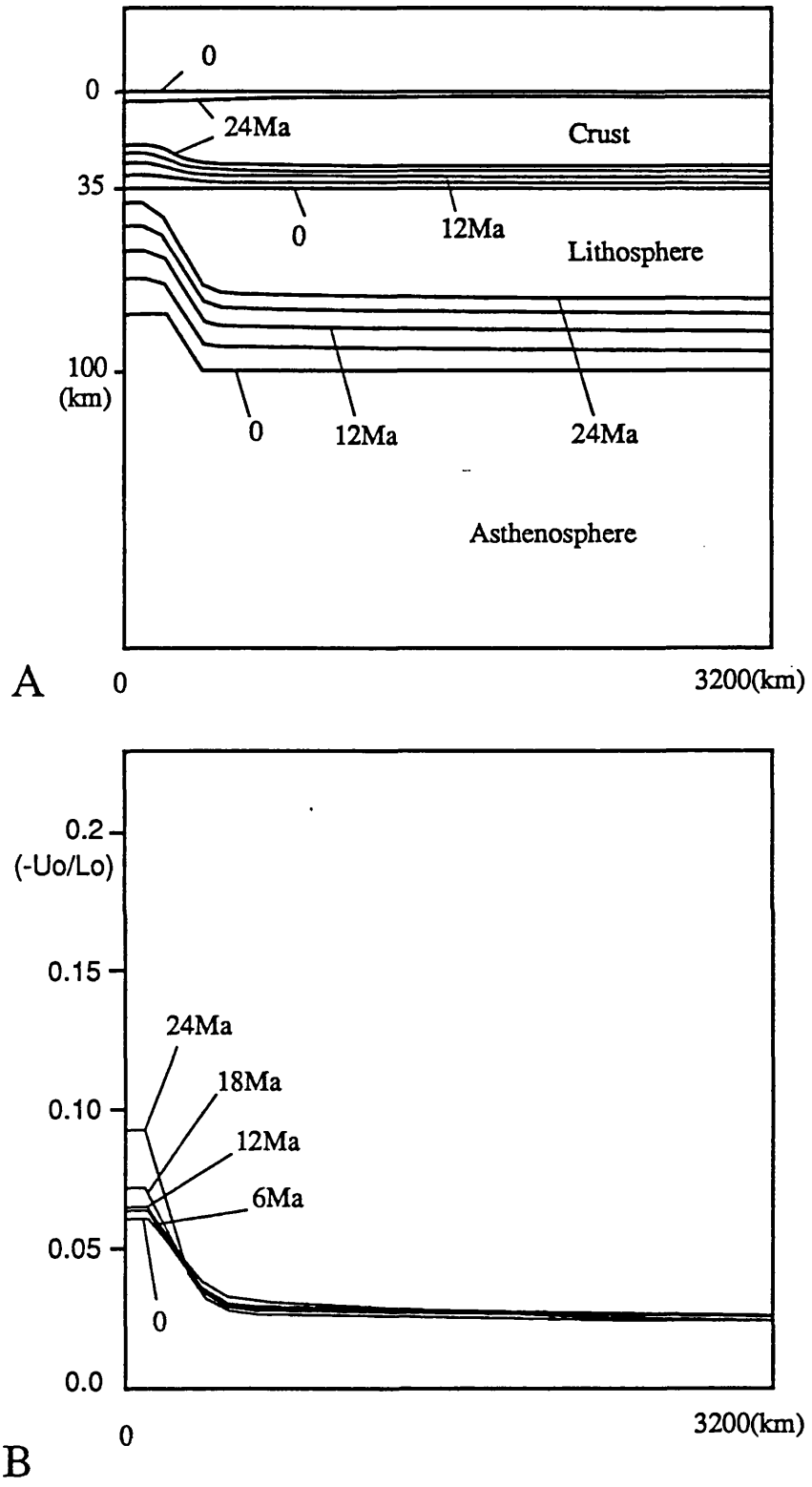

Figure 7.4-4. Uniaxial extension with A=30, $\bar{B}=\bar{B}o$, and U_{max}=5cm/year. Thermal restoration process is neglected in favour of localizing deformation. $\rho_a=\rho_m$.
A. The top surface, Moho surface and the lower boundary of the lithosphere.
B. The vertical strain rate distribution during the extension.

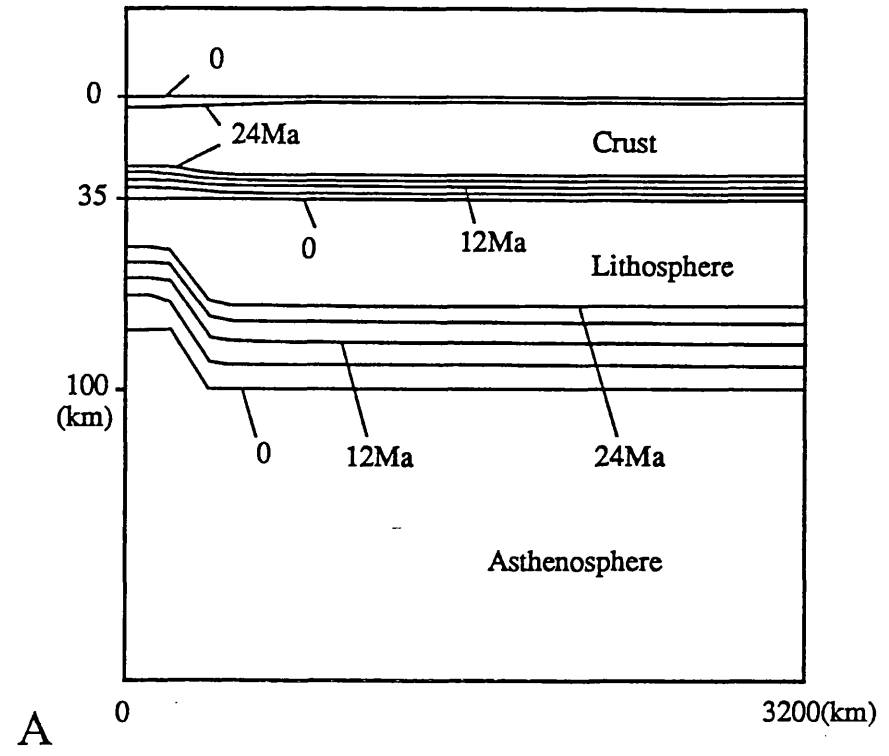

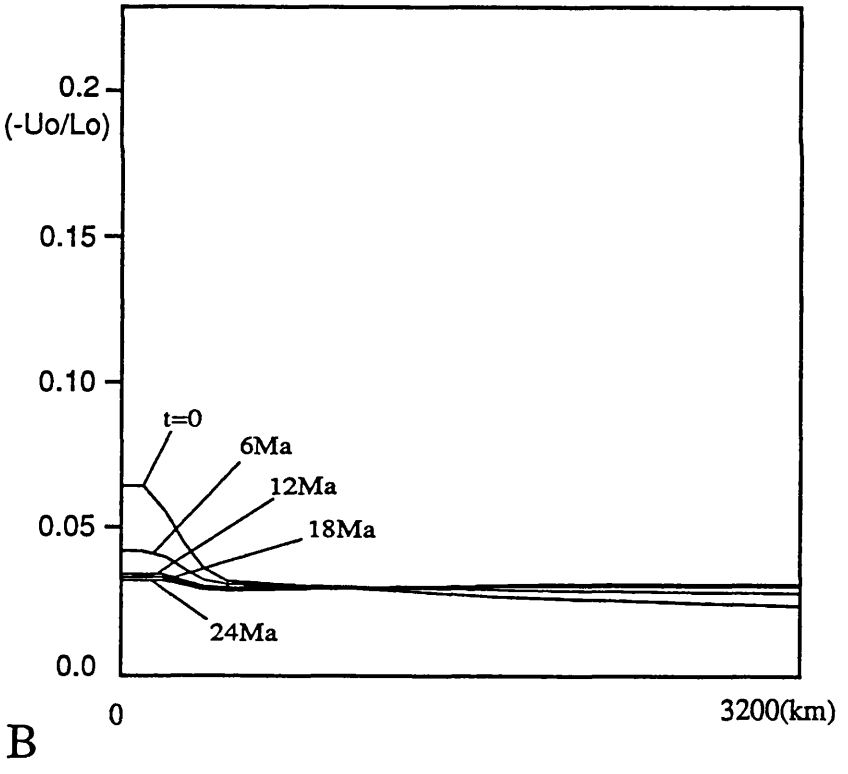

Figure 7.4-5. Uniaxial extension with A=100, $\bar{B}=\bar{B}o$, and U_{max}=5cm/year. Thermal restoration process is neglected in favour of localizing deformation. $\rho_a=\rho_m$.
A. The top surface, Moho surface and the lower boundary of the lithosphere.
B. The vertical strain rate distribution during the extension.

Discussion

The results in this section are in line with the results in § 7.3. Generally, the extension and thinning always results in the subsidence of the top surface, and as a result gravitational forces always tend to distribute extension over wide areas. Although 5 cm/year and 10 cm/year stretching rates have been used in the numerical experiment, they are usually not valid in geological circumstances. In fact, the rate of extension is mostly smaller than 2 cm/year over a distance of 3000 km within a continental plate. With $u_o \leq 2$ cm/year, the calculations show that the extension and thinning caused by stretching is always widely distributed and rifting is not possible. Also the amount of boundary displacement required before localized extension takes place is too great compared with currently active narrow (or linear) rifts.

§ 7.5 Partial Stretching with the mantle playing secondary role

In the previous two sections, the mantle has a completely passive role during the deformation. In this and the next section, the asthenosphere plays a secondary role. The asthenosphere has a lower equivalent density than the mantle lithosphere because of its higher temperature. This difference is around 0.05 g/cm^3, depending on the vertical thermal gradient (see § 3.4 and § 5.4). The ascending of the hot asthenosphere under the thinner part of the lithosphere (or, the anti-root of lithosphere) has a tendency to elevate the lithosphere (also the top surface of the lithosphere will elevate rather than subside, if the crustal thickness of the stretched lithosphere is initially less than 18 km, see § 3.4 and McKenzie [1978]), which may change the magnitude or even nature of the effect of the gravitational force on horizontal deformation. The value of the asthenosphere density is given as 3.2 g/cm^3, 0.1 g/cm^3 lower than that of the mantle lithosphere, 3.3 g/cm^3. This difference (0.1) is definitely an upper limit.

In the previous two sections, the thinning of the lithosphere disturbs the equilibrium of heat transfer through the asthenosphere and the lithosphere, and therefore the thermal diffusion tends to restore the thinned lithosphere to its normal thickness. In this section the asthenosphere is no longer treated as a passive layer to conduct heat; as mantle rises, the melting temperature is lowered because of the decrease of the pressure, which affects the thermal restoration process. These processes are too complicated to be represented by the thermal restoration equations. So in this and the following sections, the thermal process is neglected for simplicity. In fact, since the development of rifting is a

relatively short process, the omission of thermal restoration processes on crustal thickness should not affect the conclusions too much, as long as the rheological change due to cooling does not occur.

The value of parameters used in calculation are listed below

Thickness of normal lithosphere	Lo=100 km
Velocity scaling factor	Uo=5 cm/year
Density of crust	ρ_c=2.95 g/cm^3
Density of lower lithosphere	ρ_m=3.30 g/cm^3
Density of ascending asthenosphere	ρ_a=3.20 g/cm^3
Power law exponent in rheological equation	n =3

The boundary conditions are of the same form as in Figure 7.3-1.

Two groups of calculations were carried out. One with thickness related average strength ($\bar{B}=\bar{B}_oL/L_o$), another with constant average strength.

A. $\bar{B}=\bar{B}_oL/L_o$

A range of analysis have been carried with different value of u_{max} and A. The results from the analysis can be generalized as listed in Table 7.5-1 in terms of the time and displacement required in each case before localized extension takes place. If the deformation remains distributed after 24 Ma, localized extension will not occur and the deformation remains distributed for an indefinite period.

Table 7.5-1. Time and the boundary displacement before localized extension. $\bar{B}=\bar{B}_0 L/L_0$. $\rho_a<\rho_m$.

U max \ A	0	30	100
5 cm/year	9.2Ma,460km	6.8Ma,340km	4.4Ma,220km
2 cm/year	22Ma,440km	15.2Ma,304Km	9.2Ma,184km
1 cm/year	infinite	infinite	16Ma,160km

The calculated results at the later stage of deformation for two examples are shown in Figure 7.5-1 and Figure 7.5-2 respectively.

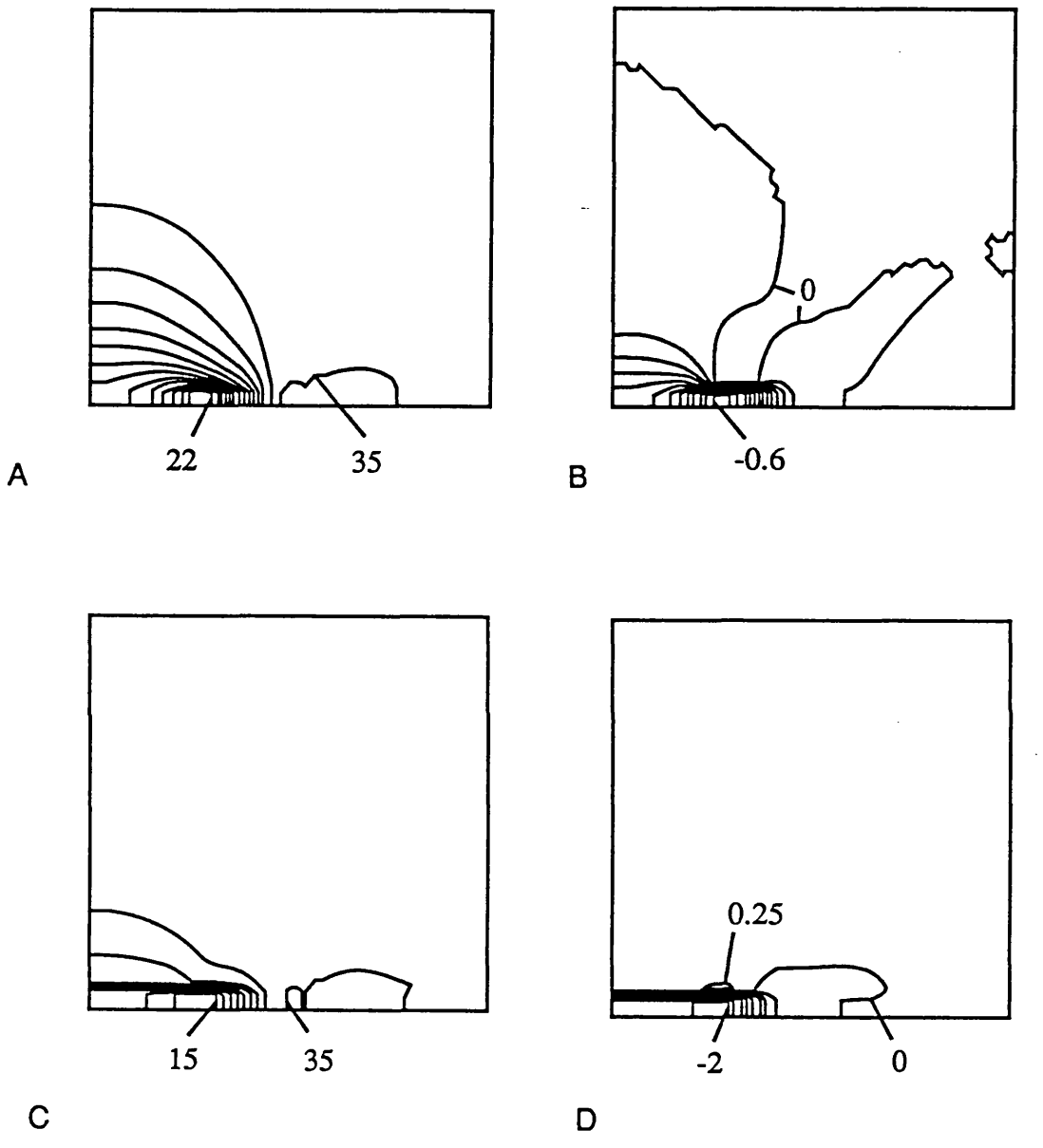

Figure 7.5-1. Contour maps of crustal thickness (A, C) and vertical strain rate (B, D) of a lithosphere under stretching, at the later stage of extension, with u_{max} = 5 cm/year and A=100. $\bar{B}=\bar{B}oL/Lo$. $\rho_a < \rho_m$.
A. Time is 4.4 Ma. Contours are from 22 by 1 to 35 (km).
B. Time is 4.4 Ma. Contours are from -0.6 by 0.05 to 0 (Uo/Lo).
C. Time is 5.2 Ma. Contours are from 15 by 2.5 to 35 (km).
D. Time is 5.2 Ma. Contours are from -2 by 0.25 to 0.25 (Uo/Lo).

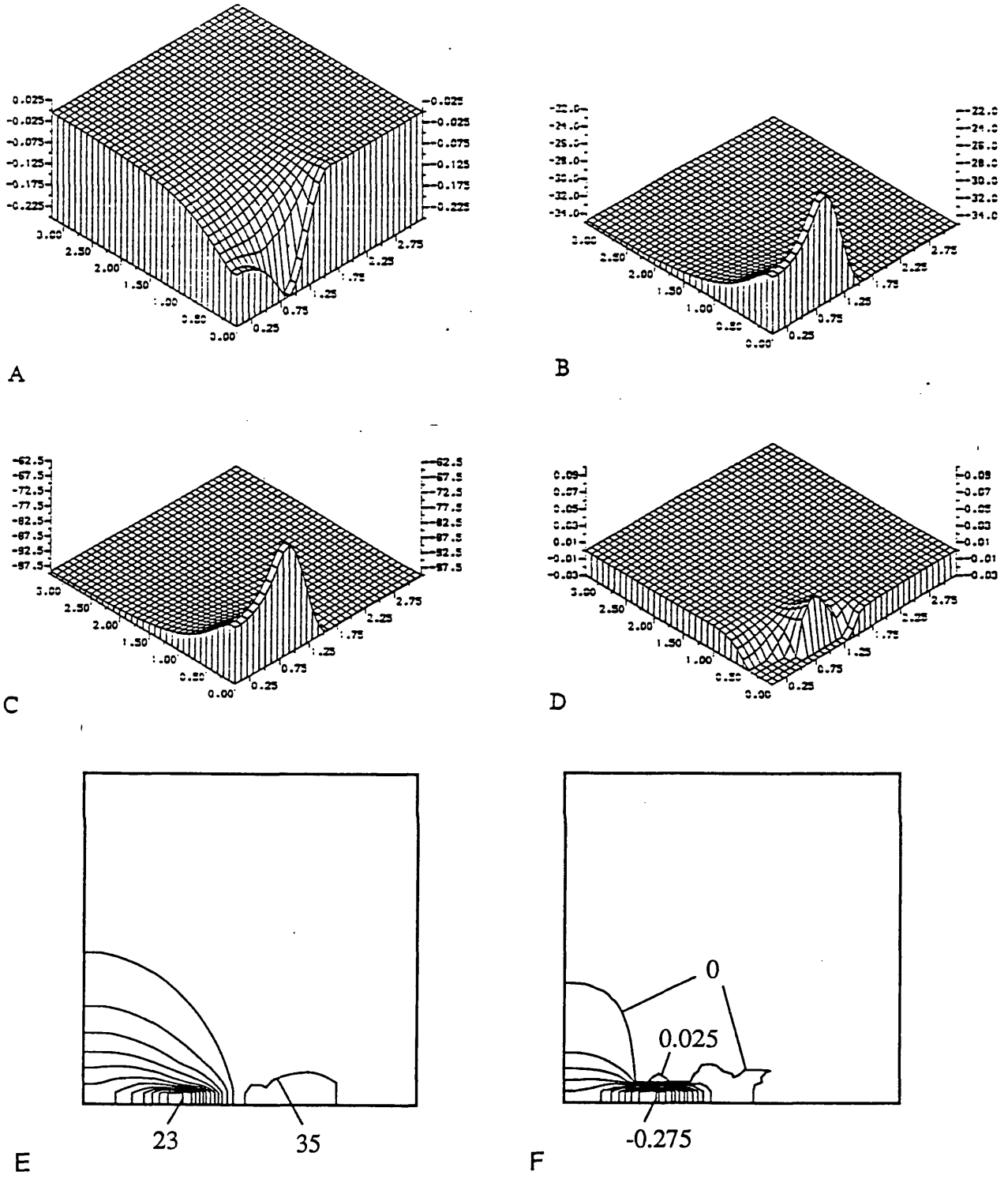

Figure 7.5-2. Results at the later stage of stretching of lithosphere near the onset of instability, with u_{max} = 2 cm/year. $\bar{B}=\bar{B}oL/Lo$. $\rho_a<\rho_m$. A=100. Time is 9.2 Ma.

A. Isometric plot of the top surface. Vertical units in km.
B. Isometric plot of the Moho surface. Vertical units in km.
C. Isometric plot of the base of lithosphere. Vertical units in km.
D. Isometric plot of the vertical strain rate. Vertical units in Uo/Lo.
E. Contour map of crustal thickness. Contours are from 23 by 1 to 35 (km).
F. Contour map of vertical strain rate. Contours are from -0.275 by 0.025 to 0.025 (Uo/Lo).

B. $\bar{B}=\bar{B}_o$

The following calculations use a constant average strength. Because of this, the result is less sensitive to the thickness attenuation and rifting takes longer time to develop. u_{max} ranges from 1 cm/year to 5 cm/year. A ranges from 0 to 100. The time and boundary displacement before localized extension are generalized in Table 7.5-2.

Table 7.5-2. Time and the boundary displacement before localized extension. $\bar{B}=\bar{B}_o$. $\rho_a<\rho_m$.

U max \ A	0	30	100
5 cm/year	16.4Ma,820km	10.4Ma,520km	5.6Ma,280km
2 cm/year	infinite	24Ma,480km	10Ma,200km
1 cm/year	infinite	infinite	20Ma,200km

Results from one of the analysis are shown in Figure 7.5-3.

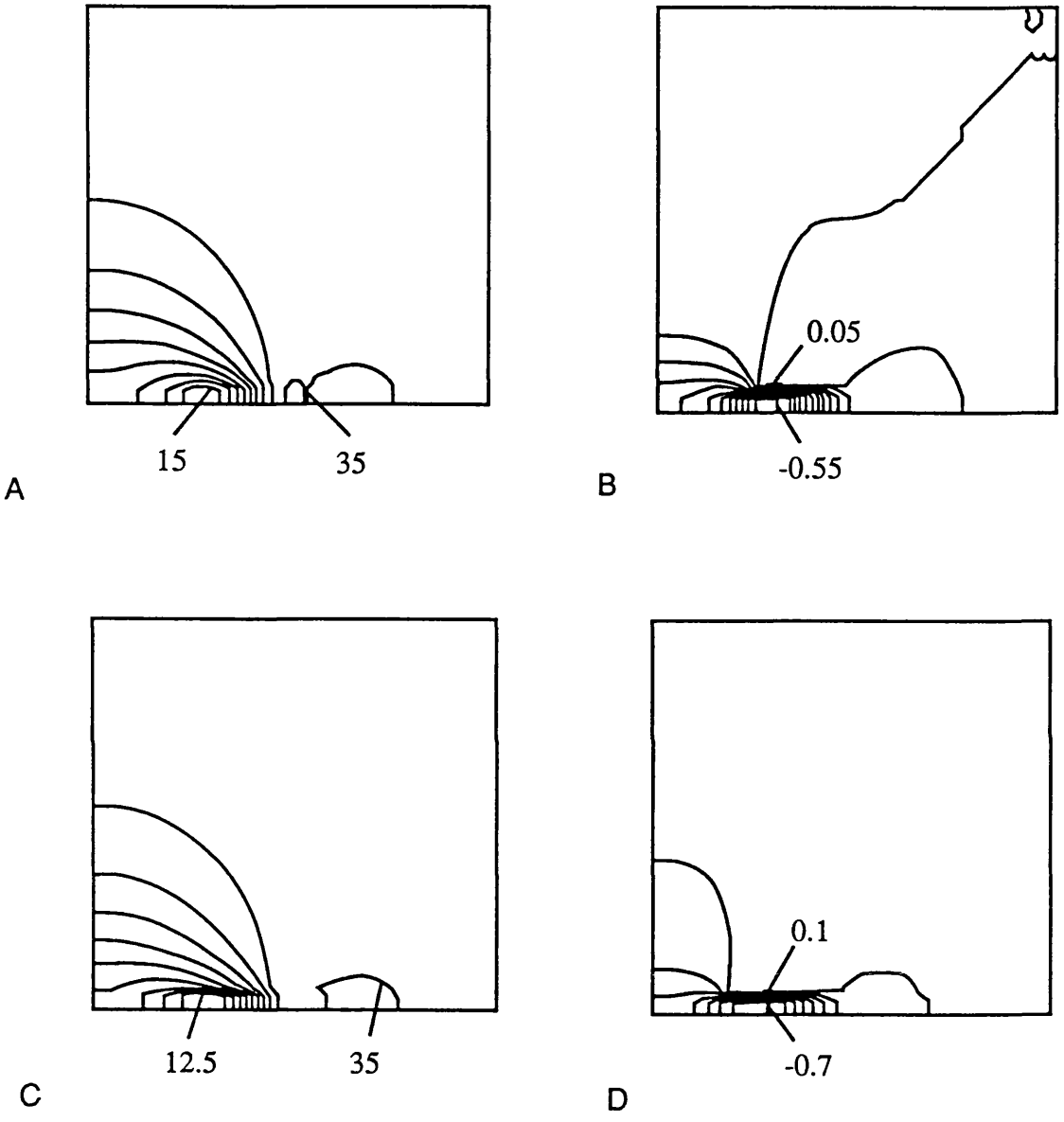

Figure 7.5-3. Contour maps of crustal thickness (A, C) and vertical strain rate (B, D) of a lithosphere under stretching, with u_{max} = 5 cm/year and A=30. $\bar{B}=\bar{B}o$. $\rho_a < \rho_m$.
A. Time is 10.4 Ma. Contours are from 15 by 2.5 to 35 (km).
B. Time is 10.4 Ma. Contours are from -0.55 by 0.05 to 0.05 (Uo/Lo).
C. Time is 11.2 Ma. Contours are from 12.5 by 2.5 to 35 (km).
D. Time is 11.2 Ma. Contours are from -0.7 by 0.1 to 0.1 (Uo/Lo).

Table 7.5-1 and Table 7.5-2 show that, contrary to the results in the previous two sections (§ 7.3, § 7.4), the buoyancy force augments the concentration of deformation to local belt. However, in all the cases, the top surface of the lithosphere still subsides during the stretching, and the effect of buoyancy force is mainly the result of the elevation of the Moho surface. Compared with the last two cases in § 7.3 and § 7.4, the same amount of thinning of the lithosphere causes less subsidence of the top surface and more elevation of the Moho surface because of the ascent of low density asthenosphere below the thinned lithosphere. These results are apparently dependent on the choice of the density contrast between the asthenosphere and the lithosphere. The analysis in § 7.3 and § 7.4 is one extreme, where the asthenosphere and the lithosphere have the same equivalent density, and the analysis in this section (and also the next section) is another.

As buoyancy forces augment the localization of deformation the thinned lithosphere will tend to generate tensile stress. This has been predicted by Fleitout & Froidevaux (1982) and Turcotte & Emerman (1983), through static rather than dynamic analysis. But Turcotte & Emerman (1983) do not accept lithospheric stretching as a viable mechanism for lithospheric thinning. They prefer either the penetration of an asthenospheric diapir through the mantle part of the lithosphere or erosion by hot plumes.

In this section, all the treatments are biased in favour of the localization of extension (e. g., the high rate of boundary displacement, the omission of the thermal cooling process, the low value given to the

equivalent density of the asthenosphere). Even so, the amount of extension required for the initiation of linear rifts by stretching is still too large compared with currently active linear rifts on Earth. Apparently, with more realistic conditions, the pre-rifting extension would be even larger. Hence the currently active linear rifts could not have been formed by stretching a viscous lithosphere with moderate perturbation (either non-uniform boundary conditions or a preexisting weak belt).

So far all the analysis has been for the case in which the basin formed by the subsidence of the surface of the lithosphere is not filled by water or sediment. It is predicted in § 3.5 by mathematical arguments that the filling of a basin by water and sediments does not appreciably influence the process of horizontal deformation, although the vertical displacement is dependent on it. To verify this prediction, one calculation has been performed. Suppose the initial top surface of the lithosphere is at sea level, and hence the subsided part is fully covered by water. This is an exaggeration because in reality, the top surface of the stretched lithosphere is well above the sea level and the formed basin is only partly covered by water. The boundary conditions are the same as above. The maximum boundary displacement rate is 5 cm/year. The results are shown in Figure 7.5-4 and Figure 7.5-5. Compared with Figure 7.5-3, the difference is negligible.

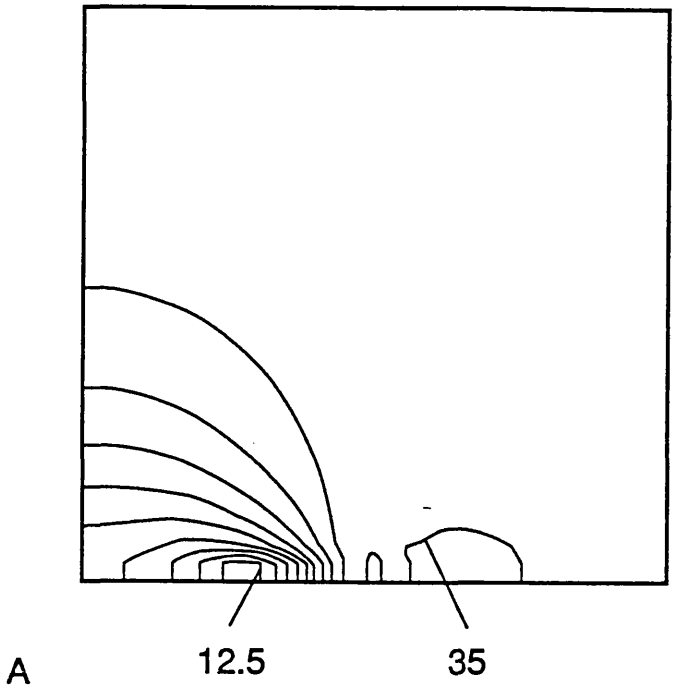

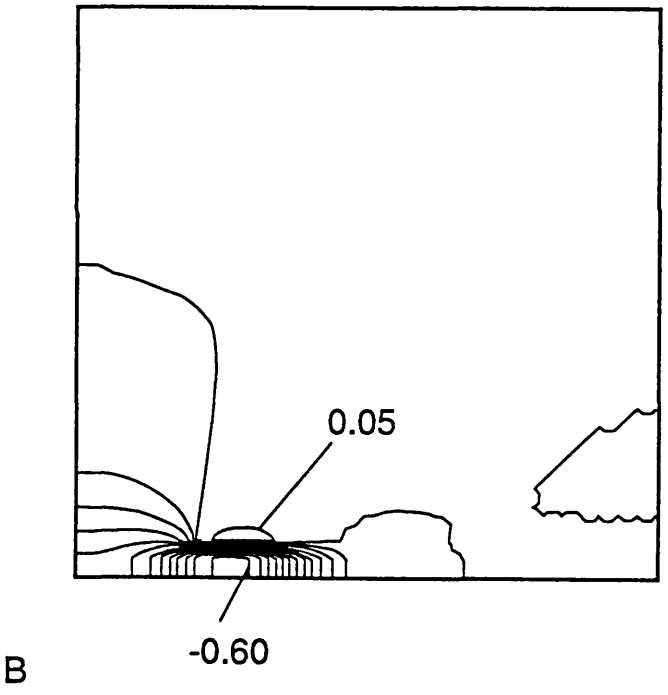

Figure 7.5-4. Contour maps of crustal thickness (A) and vertical strain rate (B) of a lithosphere having been stretched for 10.8 Ma, with u_{max} = 5 cm/year and A=30. $\bar{B}=\bar{B}o$. $\rho_a < \rho_m$. The depression formed by stretching is totally covered with water.
A. Contours are from 12.5 by 2.5 to 35 (km).
B. Contours are from -0.60 by 0.05 to 0.05 (Uo/Lo).

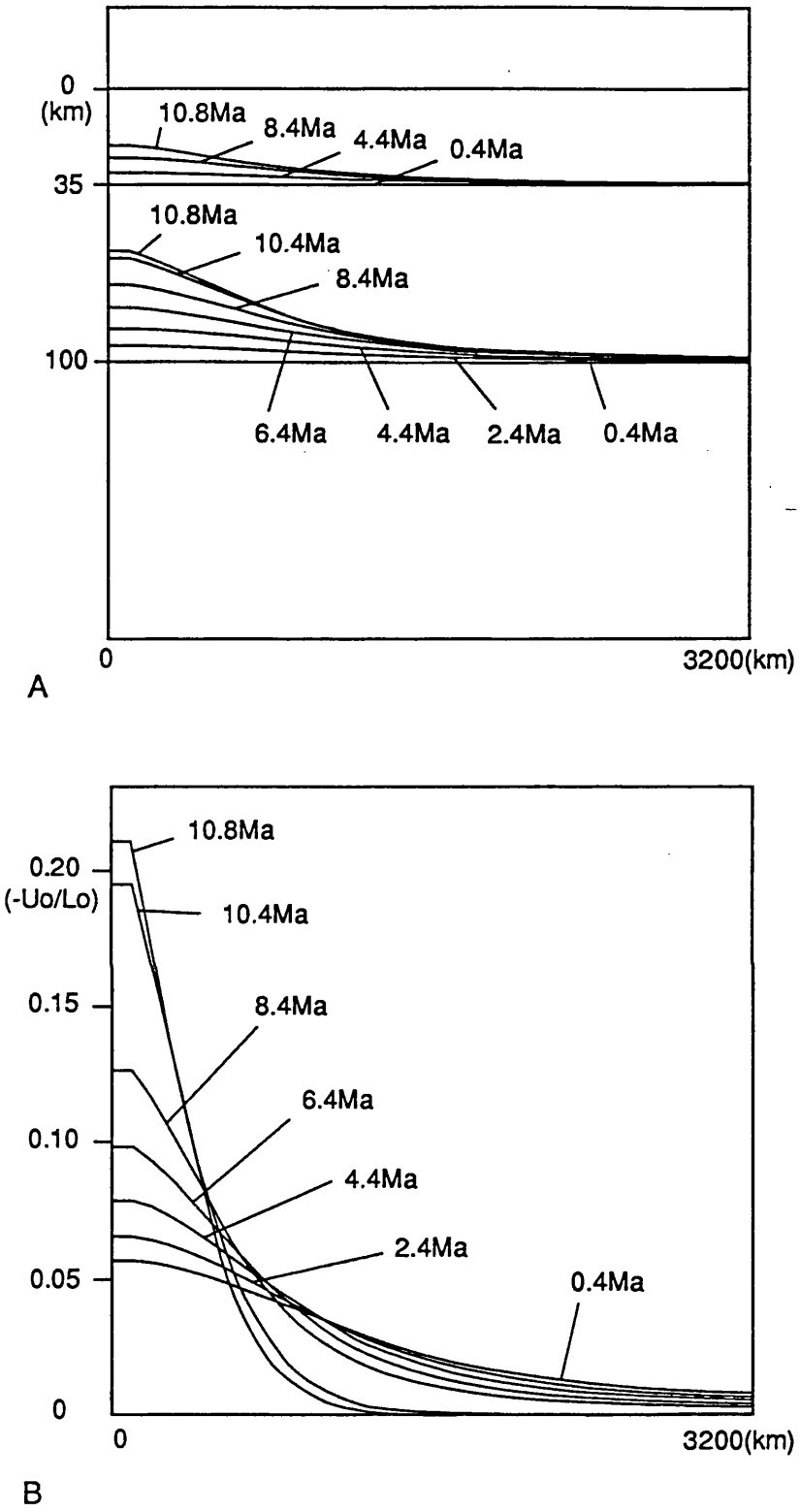

Figure 7.5-5. Vertical sections on the symmetry plane showing (A) the position of the top surface, the Moho and the base of the lithosphere, and (B) the vertical strain rate of a lithosphere during deformation, with u_{max} = 5 cm/year and A=30. $\bar{B}=\bar{B}o$. $\rho_a < \rho_m$. The depression formed by stretching is totally covered with water.

§ 7.6 Uniaxial stretching with secondary thermal anomalies

The analysis in this section is parallel with the one in the last section. In this case we have a lithosphere under uniaxial stretching, with a weak belt (20 percent weaker than the neighbouring lithosphere) transverse to the direction of extension (Figure 7.6-1). The weak belt in the figure is due to the local reduction of the lithosphere thickness, but it can also be the result of weak lithosphere material. The thinning and extension may or may not localize at the weak belt. As in the last case, the ascending lithosphere has lowered density. The parameters are similar to those of the last section, listed below.

Thickness of normal lithosphere	Lo=100 km
Velocity scaling factor	Uo=5 cm/year
Density of crust	ρ_c=2.80 g/cm^3
Density of lower lithosphere	ρ_m=3.30 g/cm^3
Density of ascending asthenosphere	ρ_a=3.20 g/cm^3
Power law exponent in rheological equation	n =3

The average strength of the lithosphere is taken as constant.

Some typical results are shown in Figure 7.6-2 to Figure 7.6-4 with the boundary rate of displacement u as 5 cm/year. With u=2cm/year or less, the deformation is always distributed.

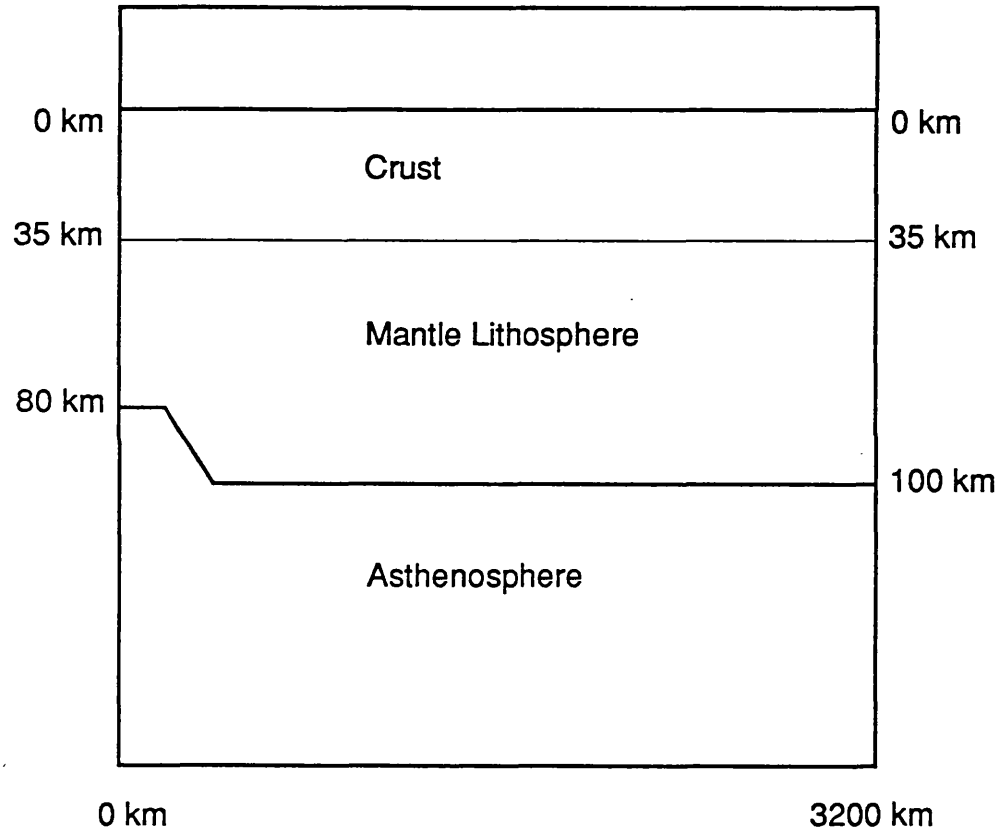

Figure 7.6-1. The lithosphere with a weak belt (20 percent weaker) transverse to the direction of stretching.

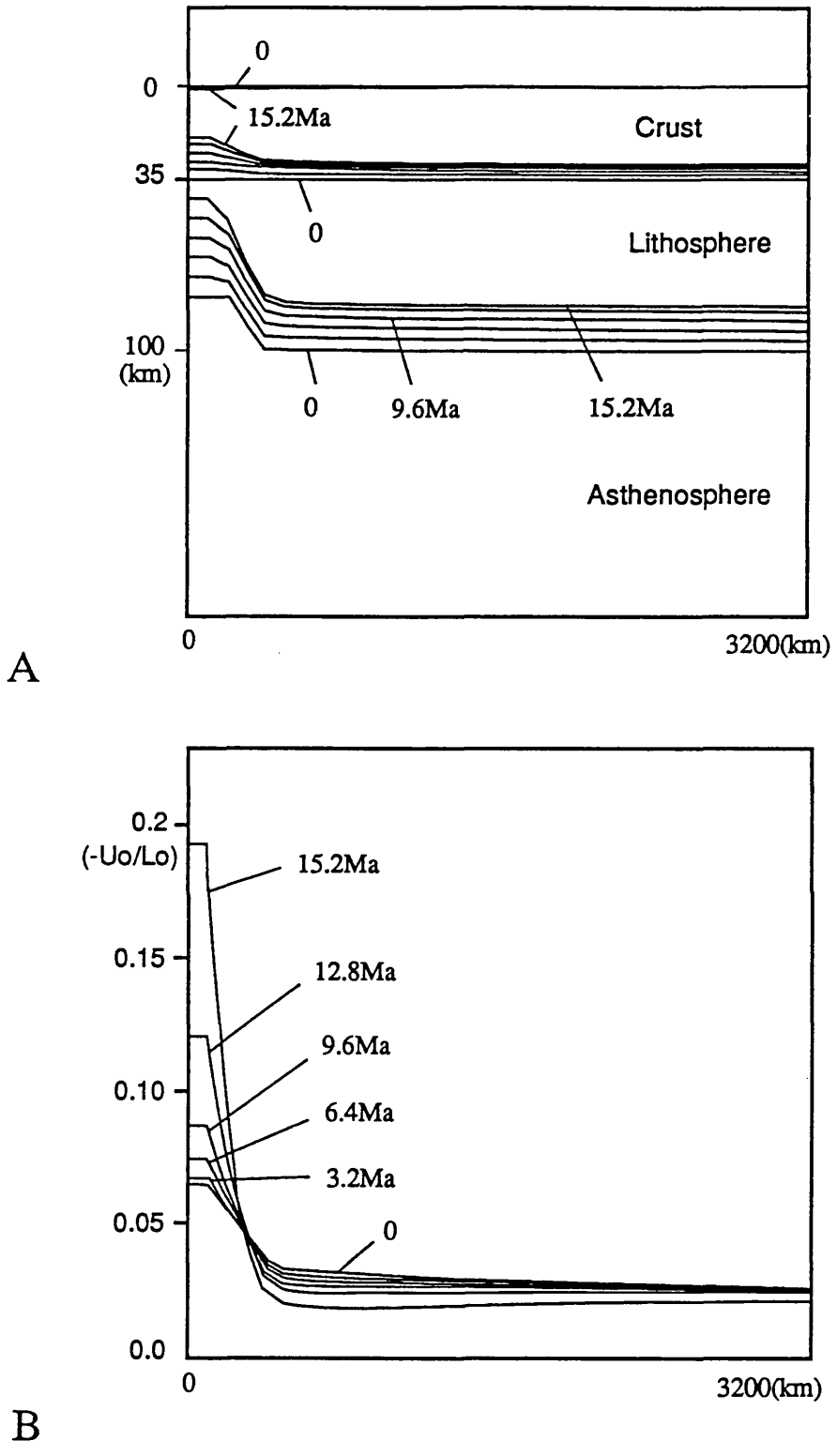

Figure 7.6-2. The position of the top surface, Moho surface, and the base of the lithosphere (A) and the vertical strain rate (B) during the uniaxial stretching of a lithosphere with weak belt as shown in Figure 7.6-1. u = 5 cm/year. $\bar{B}=\bar{B}o$. $\rho a<\rho m$. A=0. This result is the same as Figure 7.4-3. Although the vertical displacement is different between these two cases, it does not affect horizontal deformation because A=0.

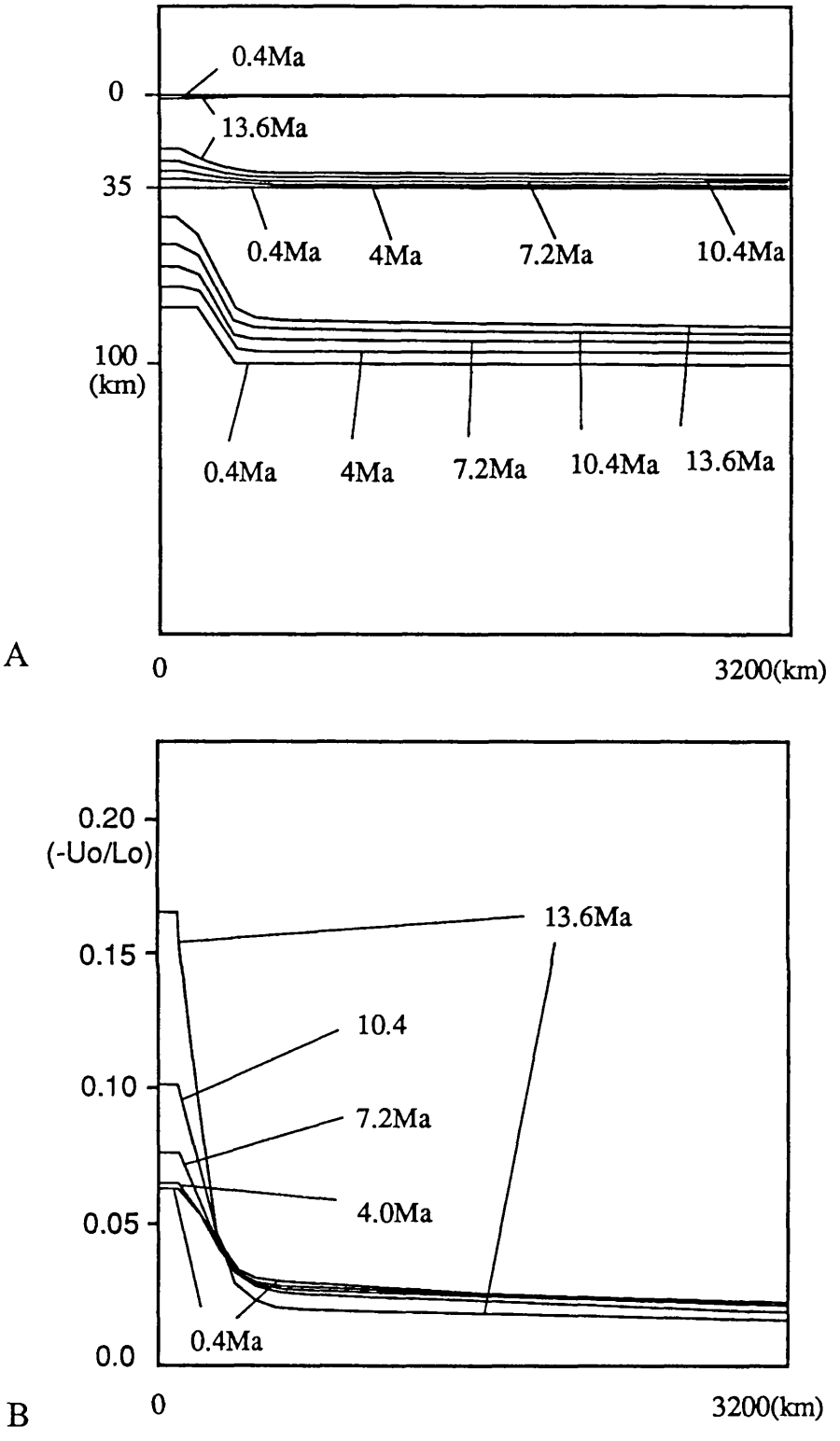

Figure 7.6-3. The position of the top surface, Moho surface, and the base of the lithosphere (A) and the vertical strain rate (B) during the uniaxial stretching of a lithosphere with weak belt as shown in Figure 7.6-1. u = 5 cm/year. $\bar{B}=\bar{B}o$. $\rho_a<\rho_m$. A=30.

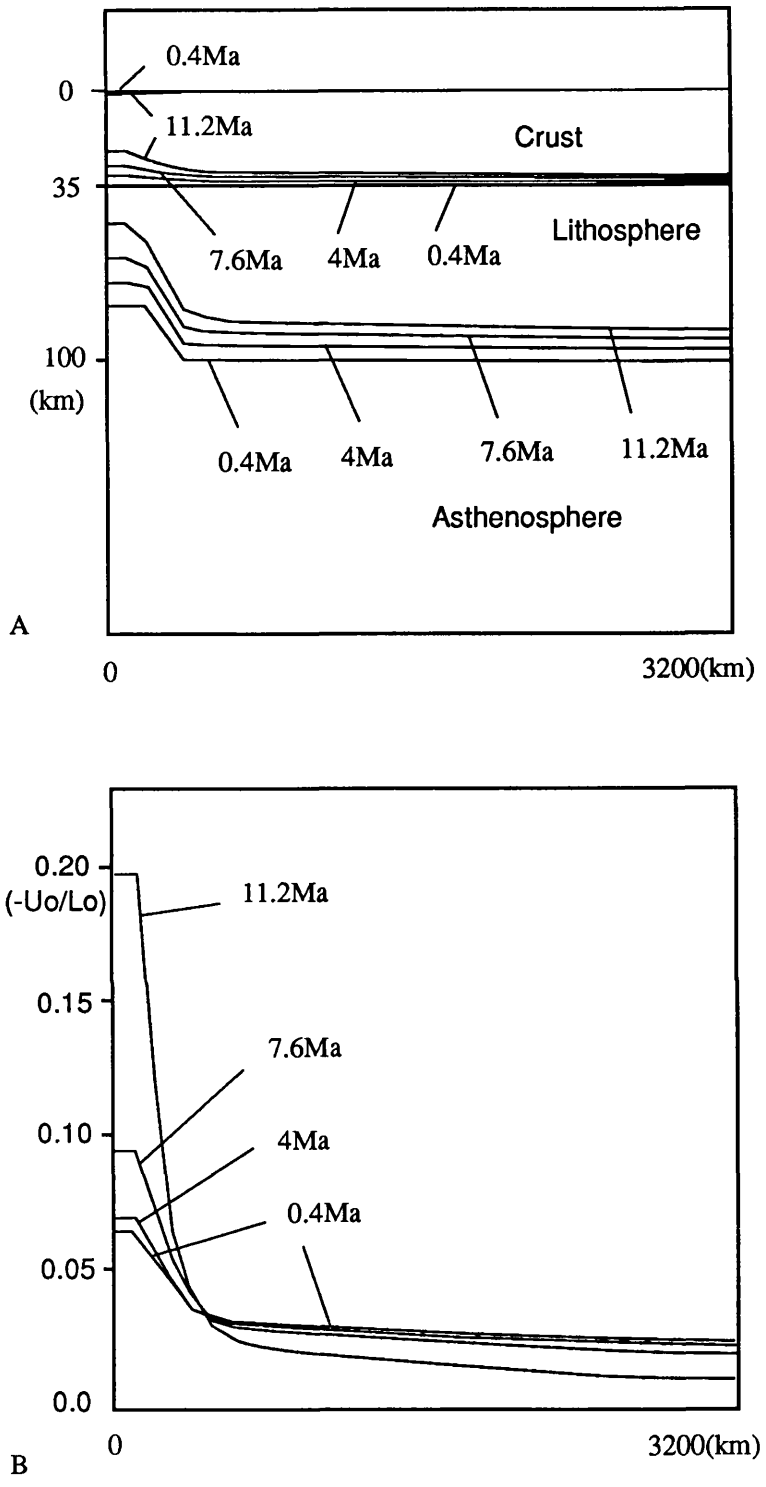

Figure 7.6-4. The position of the top surface, Moho surface, and the base of the lithosphere (A) and the vertical strain rate (B) during the uniaxial stretching of a lithosphere with weak belt as shown in Figure 7.6-1. u = 5 cm/year. $\bar{B}=\bar{B}o$. $\rho_a<\rho_m$. A=100.

The time and the amount of displacement before most deformation occurs at the weak belt through the uniaxial extension of a stretched continent with a secondary asthenosphere effect can be generalized as in Table 7.6-1.

Table 7.6-1. Time and the boundary displacement before localised deformation by uniaxial stretching. $\bar{B}=\bar{B}_o$. $\rho_a<\rho_m$.

U max \ A	0	30	100
5 cm/year	15.2Ma,760km	13.2Ma,660km	11.2Ma,560km
2 cm/year	infinite	infinite	infinite

Again, as in § 7.5, the amount of boundary displacement before the localization of deformation is found to be too large to be comparable with currently active linear rifts on Earth. With a smaller rate of boundary stretching and/or the addition of thermal cooling processes, narrow rifts would be even less likely to occur. So stretching of a lithosphere with a moderate weak belt could not have caused the linear rifts currently active on Earth.

In the modelling of this section, the displacement during the deformation is calculated using the formula given in § 3.4, so that isostasy is maintained in that the weight of column over the compensation level is kept constant with time. However, since the initial lithosphere thickness is reduced locally to simulate the effect of weak belt and the top surface and the Moho are still flat (Figure 7.6-1), there is lack of compensation at

the weak belt and this lack of compensation is preserved all through the process. If isostasy is maintained from the beginning, there will be initial elevation due to the extra hot asthenosphere at the base of the thinner lithosphere. This is studied in the next section.

§ 7.7 Uniaxial extension with initial doming

In this section, the lithosphere is underlain by anomalously hot mantle. The thermal anomaly has two effects. Firstly, it removes part of the lithosphere at its bottom (or elevates the asthenosphere-lithosphere boundary). Secondly, the thermal anomaly causes the elevation (or doming) of the lithosphere, which tends to "flow" laterally under gravity and concentrates the extension to the elevated part. Figure 7.7-1 shows a lithosphere which is invaded 20 km at the bottom by the asthenosphere. If the invading asthenosphere has a density of 3.2 g/cm^3, 0.1 g/cm^3 lighter than the lithosphere mantle, the lithosphere would be elevated by 625 meters maximum due to isostasy.

The value of the parameters are listed below

Thickness of normal lithosphere	Lo=100 km
Velocity scaling factor	Uo=5 cm/year
Density of crust	ρ_c=2.8 g/cm^3
Density of lower lithosphere	ρ_m=3.30 g/cm^3
Density of invaded asthenosphere	ρ_a=3.20 g/cm^3
Power law exponent in rheological equation	n=3

With constant average strength, two calculations have been done with the boundary velocity as 5 and 0.5cm/year respectively. The value of A is 30

in both calculations. Figure 7.7-2 and Figure 7.7-3 show the development of the deformation, and Figure 7.7-4 shows the evolution of the topography for both cases. In both cases, the deformation in the thinner part accelerates fast and in a very short time (<3.2 Ma) the thinner and elevated part (rift) accommodates most (when u=5cm/year) or all (when u=0.5cm/year) of the extension of the lithosphere and there is even thickening at the side of the rift (Figure 7.7-3B). This thickening may be partly attributed to the doming which causes the material to flow laterally but it is also observed in the cases where there is no doming as in the analysis in the previous sections of this chapter. This thickening near the thinning belt seems to be characteristic of a non-linear viscous fluid, and has been used by Zuber and Parmentier (1986) to explain the shoulders of rift valleys. Another possible explanation for the rift shoulders is that the central part of the domed weak belt thins faster (Figure 7.7-2 and Figure 7.7-3) and therefore subsides faster than the less weak part of the weak belt (Figure 7.7-4). Unfortunately, this cannot be proved by field observation. For example, the rift shoulders in the Gulf of Suez formed at the same time as rift faulting and there seems to have been no initial doming prior to rifting. Steckler (1985) and Buck (1986) attribute the uplift of rift shoulders to small-scale convection induced by rifting.

At the time of rifting, the amount of boundary displacement in the case where u = 0.5 cm/year is only 16 km, consistent with the fact that all the existing narrow rifts have developed with a relatively small amount of lateral displacement. Although a boundary velocity of 0.5 cm/year has been assumed in the simulation, it can be seen from Figure 7.7-3B that the lithosphere is generally under compression and thickening, except at the location of rifting. This compares well with the Kenya Rift which is in a

plate under general horizontal compressional stresses.

If the role of the brittle layer is considered by using a thickness -related average strength, the rifting would develop more quickly with the same boundary and initial conditions.

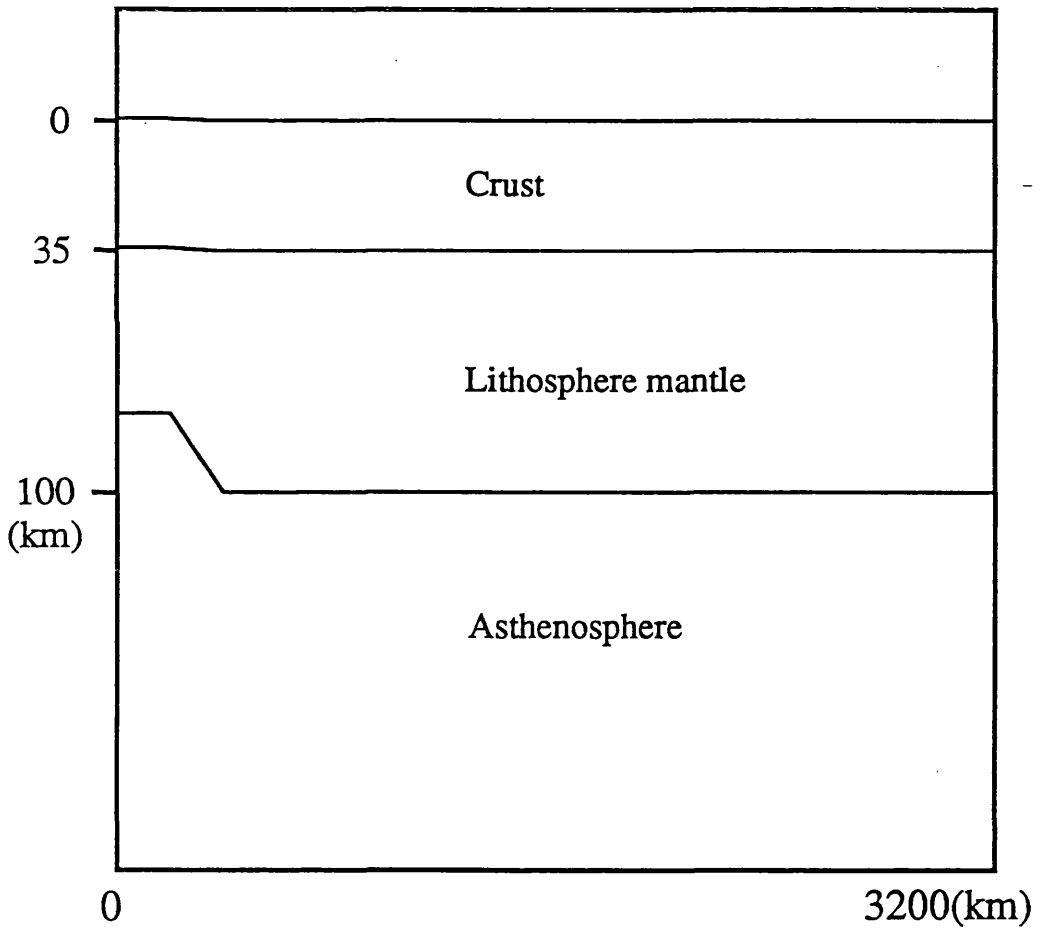

Figure 7.7-1. The lithosphere with initial doming due to hot mantle below.

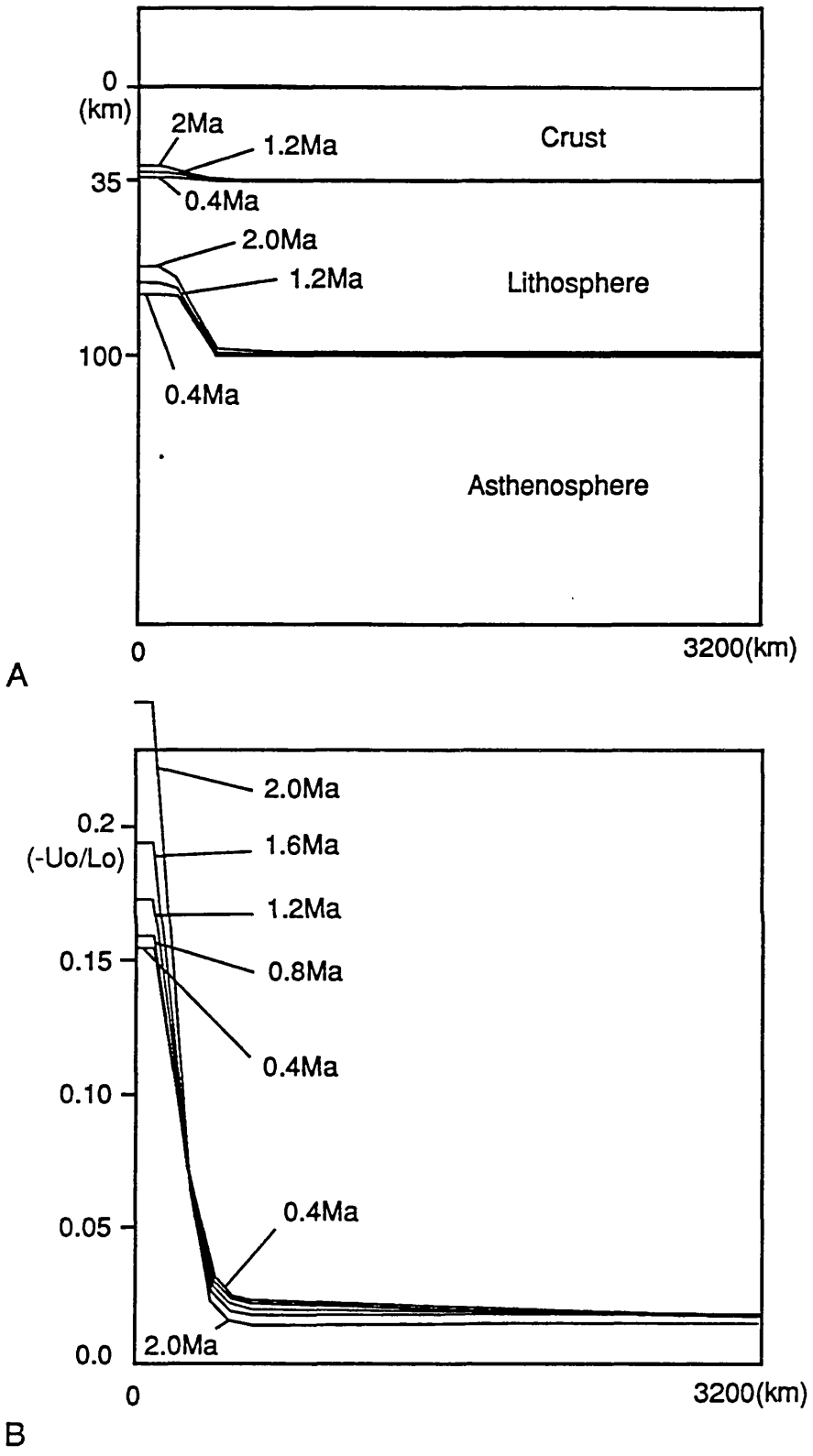

Figure 7.7-2. The deformation history of rifting with initial doming (see Figure 7.7-1). A=30. $\bar{B}=\bar{B}o$. u = 5 cm/year. $\rho_a < \rho_m$.
A. The position of the top surface, Moho and the base of the lithosphere.
B. The vertical strain-rate.

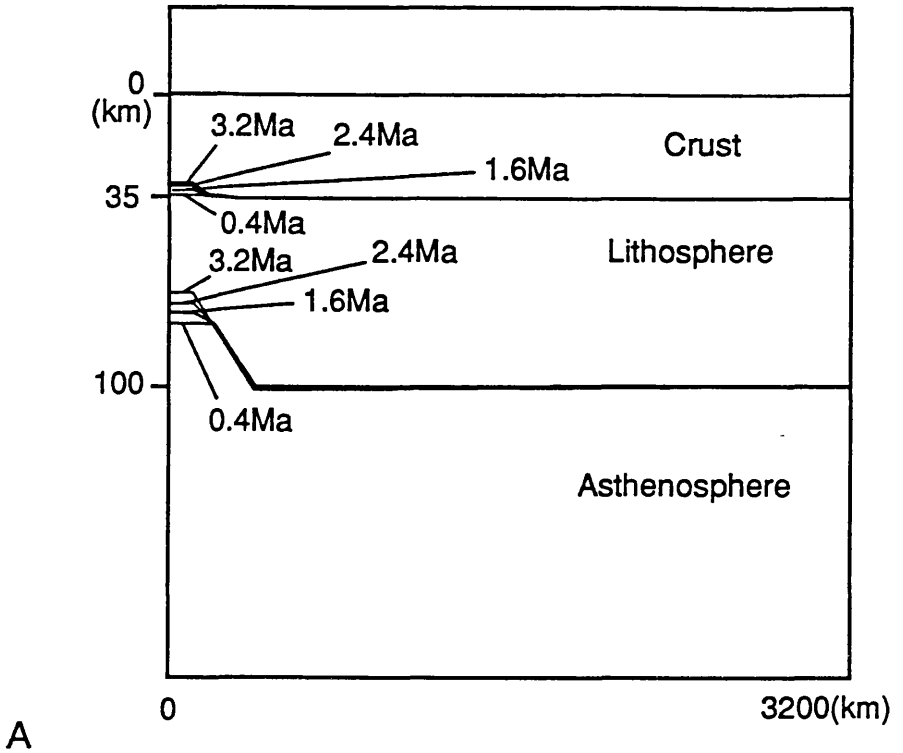

A

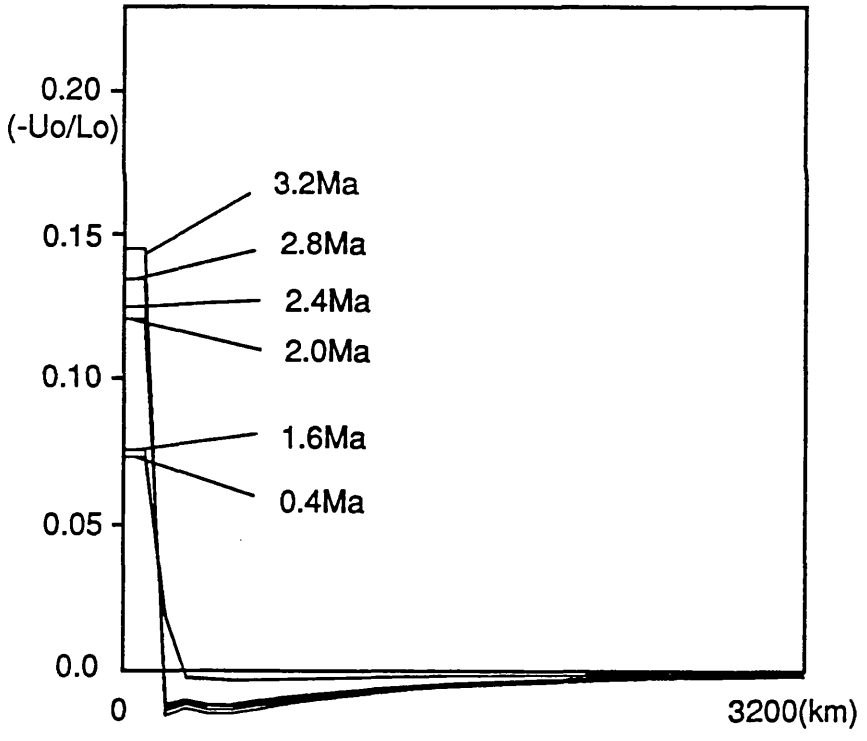

B

Figure 7.7-3. The deformation history of rifting with initial doming (see Figure 7.7-1). A=30. $\bar{B}=\bar{B}o$. u = 0.5 cm/year. $\rho_a < \rho_m$.
A. The position of the top surface, Moho and the base of the lithosphere.
B. The vertical strain-rate.

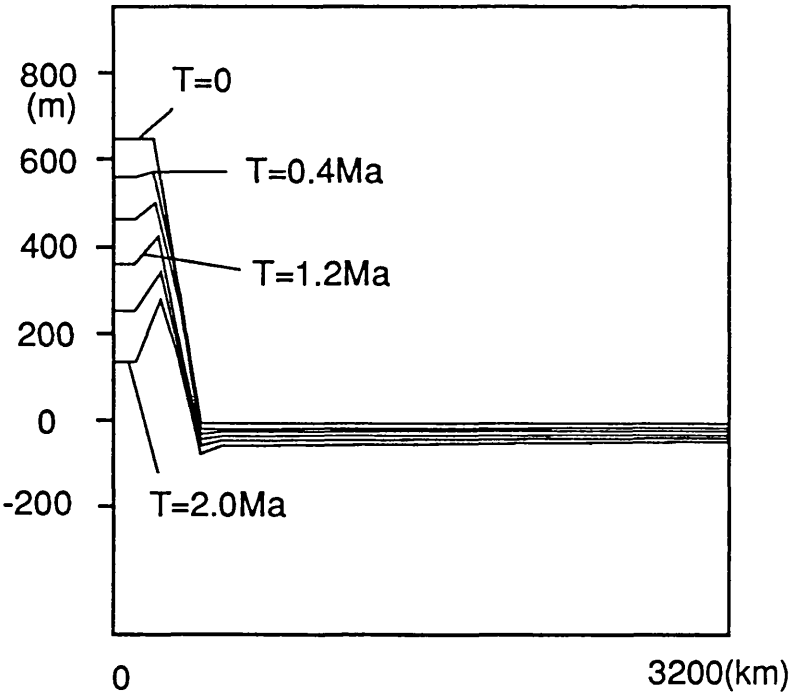

A

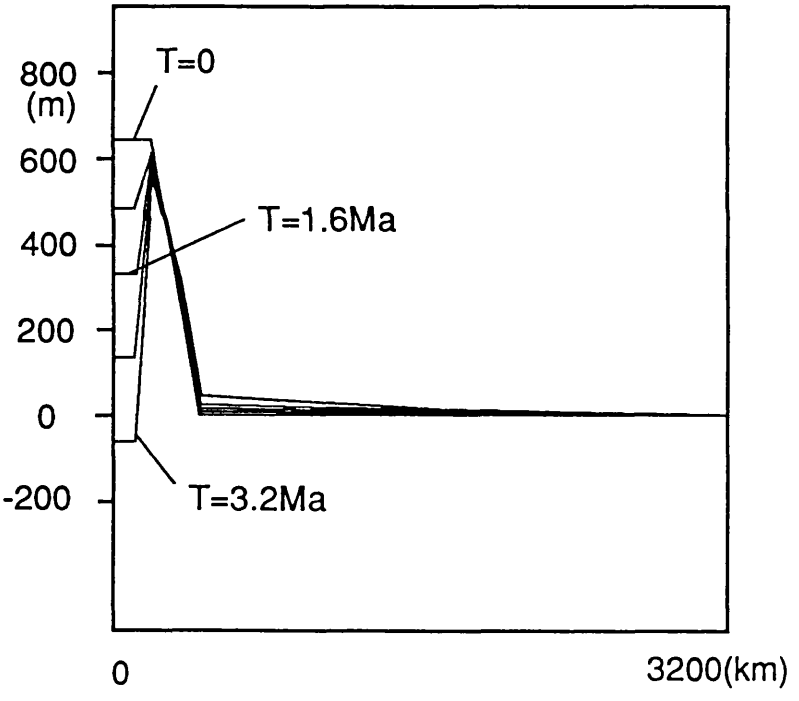

B

Figure 7.7-4. The evolution of the topography of rifts formed by stretching with initial doming (see Figure 7.7-1). A=30. $\bar{B}=\bar{B}o$. $\rho_a < \rho_m$.
A. u = 5 cm/year.
B. u = 0.5 cm/year.

Two points have been demonstrated through the analyses in this chapter.

First, the gravitational forces (or buoyancy forces) either resist or augment the localization of deformation, depending on the equivalent density contrast between the lithosphere mantle and the asthenosphere, which is in turn determined by the geotherm. If the lithosphere mantle is hot, then this contrast is small, and buoyancy forces distribute deformation over large areas in favour of wide rifts. And since the lithosphere mantle is hot, the lithosphere is weak, and the effect of buoyancy forces is significant. This mechanism may be operating in the evolution of Basin and Range province in the United States, as suggested by Molnar & Chen (1983). If the lithosphere mantle is cold, then this contrast is large, and thinned lithosphere generates tensile stresses as suggested by Turcotte & Emerman (1983), augmenting extension localization. The trouble is that lithospheres with cold mantle are strong and commonly resist deformation, so this mechanism is not very realistic.

Second, from the analyses in this chapter, it is clear that stretching does not cause localized deformation in the lithosphere without large amount of distributed extension, unless there is local initial doming. The basin and range structure in North China may be an example of distributed extension under boundary stretching. However, one should not jump into conclusion that all the currently active linear rifts have been formed with initial doming. Because a) the effect of initial doming in the above analyses is actually to provide a localized force or stress which makes the local style of deformation different from the regional one. This local

stress does not has to be produced by initial doming. It can be due to the variation of crustal thickness, diapiric penetration of the asthenosphere mantle into the lithosphere (Turcotte & Emerman, 1983), or other processes; b) in all the analyses in this chapter, perturbations in lithosphere, either through non-uniform thinning or from initial weak belt, are moderate. If the strength of the weak belt is initially lowered by a factor of say 3, stretching should cause localized deformation right from, or soon after, the beginning of stretching. The second reason is more probable. Therefore, in the absence of initial doming, a linear narrow rift can only be caused along a belt which is significantly weaker than the surrounding region. In fact, many rifting events are predated by thermal events as indicated by volcanism or magma activity (e.g., Sengör & Burke, 1978) which serves to weaken the lithosphere since the rheology of the lithosphere is sensitive to the geotherm (e.g., Morgan et al., 1986). Another possible cause of the weak belt is the crustal thickness. With the same geotherm, the lithosphere with thicker crust has lower strength, therefore a suture zone is a likely location for rifting to occur when under tension (Vink et al., 1984). That rifts tend to develop along preexisting weak belt is a sensible idea and has been suggested by some authors (e.g., Wilson, 1968; Vink et al., 1984). This analysis adds more support to it from the point view of the distribution of extension.

Chapter 8 Summary, discussion and suggestions for future research

I have derived a new thin viscous sheet model for lithosphere deformation and applied it to the investigation of the shortening and extension of continental lithosphere.

In the case of continental shortening, the study has shown that, under a specified set of boundary conditions and parameters, the conclusions of England & McKenzie (1982, 1983) still hold despite the errors involved in their derivation of the governing equations. This also suggests that the later studies (e.g., England, Houseman & Sonder, 1985, Cohen & Morgan, 1986, Sonder & England, 1989), which still use the erroneous equations, again gave results which were broadly correct.

Next I applied the model to investigate the evolution of the Tibetan Plateau. In particular I investigated the three possible causes for late extension of the Tibetan Plateau, namely the decreased boundary displacement, a possible rheological change, and a possible detachment of part of the lithospheric mantle into the asthenosphere at a late stage in deformation. It was found that a detachment in the last several million years can very well explain recent E-W extension and the uplift of the Tibetan plateau, as suggested by England & Houseman (1988). The detachment causes uplift of the lithosphere and hence increases the gravity potential to drive the plateau to flow laterally.

One possible problem relating to the detachment hypothesis is that the

detached lithosphere mantle should still have some effect on the upper lithosphere. The fact that the datached lithosphere mantle sinks implies that it has lost the support of the upper lithosphere, which is equivalent to saying that the upper lithosphere has lost some of its burden and will rise in consequence. In addition the detached lithosphere mantle may sink rapidly deep into mantle, so that its effect on the lithosphere is minor; alternatively the detached lithosphere mantle migrates laterally, exerting its weight elsewhere. Lateral migration of the detached mantle can be likened to a sheet of paper being dropped in air (or a piece of foil in water?). The paper does not drop vertically, but moves obliquely. Detailed numerical or experimental simulations need to be done to justify or reject this speculation.

It was also clearly demonstrated that the lithosphere root formed during lithosphere shortening tends to augment further shortening, as predicted by Fleitout & Froidevaux (1982). In the case of Tibet, when this effect is included, the maximum crustal thickness due to lithosphere shortening can be up 15 km larger than otherwise. Thus models assuming simple Airy compensation (e.g., England & McKenzie, 1983) should be used with caution.

On the basis of this analysis and other lines of evidence, a likely sequence of events is:

a. About 40 Ma ago, the India subcontinent collided with Asia.

b. Continued convergence of the two plates caused crustal thickening. The thickening resulted in the elevation of the top surface, which opposed further thickening. The rate of boundary indentation decreased due to this opposition.

c. As the crust thickened, so did the lithosphere mantle. The elevation of the top surface was balanced not only by the crustal root but also by the lithospheric root. The effect of the lithospheric root is to reduce the elevation of the top surface during thickening, and favours lithosphere thickening. If a lithosphere of 100 km thickness with a 35 km thick crust is thickened by 100 percent, and the crust has a density of 2.95 g/cm^3, the elevation of the top surface is only 2.53 km. If the density of the crust is 2.8 g/cm^3, the elevation is 4 km.

d. Finally, in the course of the last several million years, detachment occurred at the base of the lithosphere. Replacement of part of the relatively cold lithosphere mantle by the relatively hot asthenosphere mantle beneath the plateau caused swift uplift of the lithosphere, by an amount of around 1 km, which is responsible for the late E-W extension of the Tibetan plateau and may also have caused further slowing down of the boundary indentation.

One of the problems with the results from this analysis is that crustal thickness decreases from the indenting boundary to the inside of the continent and there is no clear boundary with the region of crustal thickening, while geological and geophysical evidence shows that crustal thickness in the Northern Tibetan plateau is not less than that of the Southern Tibetan plateau and the plateau has a relatively clear boundary. This is probably because the lithosphere has been assumed to be homogeneous in the analysis. If the plateau is very weak, lateral flow under gravity would flaten both the top surface and the Moho, as suggested by Molnar & Chen (1983). Another possible cause for the flat plateau is the channel flow in the lower crust under differential pressure, which tends to smooth the Moho topography and also the top surface (e.g., Bird, 1991).

In the case of continental extension, three predictions can be made. First, from both analytical discussion and numerical analysis, it is found that the filling of a sedimentary basin with water and sediment does not appreciably influence the style of horizontal deformation of the stretched lithosphere. Second, the gravitational forces (or buoyancy forces) either resist or augment the localization of deformation, depending on the geotherm. If the lithosphere mantle is hot, then buoyancy forces distribute deformation over large areas in favour of wide rifts. This may be partly responsible for the distributive style of deformation in the Basin and Range province in the United States, as suggested by Molnar & Chen (1983) and others. If the lithosphere mantle is cold, then thinned lithosphere generates tensile stresses as suggested by Turcotte & Emerman (1983), augmenting extension localization. However, lithospheres with cold mantle are strong and commonly resist deformation, so that this mechanism is not very realistic. Third, without initial doming, currently active narrow linear rifts have to be formed along belts significantly weakened prior to rifting. The weakness may be due to previous geologic events such as suturing or due to thermal anomalies indicated by volcanism or magmatic activity.

Although continental shortening and extension have been investigated in two separate chapters, the two processes are actually related to each other. In both the Tibetan Plateau and the Altiplano of South America extension occurs in one direction while the area is under compression in another direction. In the Basin and Range province of the United States, Cenozoic extension follows Mesozoic and early-Cenozoic lithosphere shortening and thickening, which provides a high gravity potential and makes the

lithosphere tend to spread when boundary compression is reduced or removed.

I have made some progress with this model, but the work needs improvement in several respects. The first is the calculation of the thermal process. I have given a formula to describe this process, based on some assumptions, but because of the assumption of linear vertical distribution of temperature, it is too crude for accurate calculation of the rheological change of the lithosphere during deformation. An analytical solution has been given for stretched lithosphere (Jarvis & McKenzie, 1980), but there is no such solution for thickened lithosphere. A very important improvement required is the inclusion of heat production within the crust in equations describing thermal processes, especially in the case of lithosphere shortening, because it appears that rheological change in the Tibetan Plateau is not due to heat conduction from the asthenosphere but to the increased heat-producing elements in the thickened crust.

Another improvement concerns the solution of the mechanical equation. The Finite Difference Method has been used to solve the problem because I was eager to compare the results from the new model with those of England & McKenzie (1982, 1983). This took more than a year to carry out and there was not enough time left when I realized the limitations of the FD method. This mistake does not affect the conclusions, but because of it, I was forced to define the boundary conditions in terms of displacement and concentrate on the pattern of deformation, and could not give enough attention to the boundary forces and stresses in the lithosphere. Any further modelling with this scheme should make use of the Finite Element Method.

The model contains some weaknesses which are difficult to overcome. The major one is the thin sheet assumption. Thin sheet model is in effect pure-shear model. There is considerable concern that simple-shear rather than pure-shear dominates in some circumstances (e.g., Wernicke, 1984). This does not pose a problem in an analysis in the scale of thousands of kilometers, but many analyses are not carried out over such a large scale.

Finally, improved numerical analysis, like our general understanding of the Earth, depends on the data available. No matter how refined a model is, without data of equivalent quality to test it, the effort to build the model may not be rewarded. In fact, one should construct the numerical model according to the available data. A mistake I made in this work was that I made the model before sufficient data had been gathered. This lesson I shall remember throughout my career.

References

Allègre C. J. et al., 1984, Structure and evolution of the Himalaya-Tibet orogenic belt, Nature, Vol.307, 17-22.

Angelier, 1985, Extension and rifting: the Ziet region, Gulf of Suez, J. Struct. Geol., Vol.7, 605-612.

Armijo, R., P. Tapponnier and T. Han, 1989, Late Cenozoic right-lateral strike-slip faulting in Southern Tibet, J. Geophys. Res., Vol.94, 2787-2838.

Armijo, R., P. Tapponnier, J. L. Mercier and T. Han, 1982, A field study of Pleistocene rifts in Tibet, EOS, 51-A02, 1093.

Armijo, R., P. Tapponnier, J. L. Mercier and T. Han, 1986, Quaternary extension of Southern Tibet: field observations and tectonic implications, J. G. R., Vol.91, 13803-13872.

Baker, B.H. and J. Wohlenberg, 1971, Structure and evolution of the Kenya Rift valley, Nature, Vol.229, 538-542.

Barazangi, M. and J. Ni, 1982, Velocities and propagation characteristics of Pn and Sn beneath the Himalayan Arc and Tibetan Plateau: possible evidence for underthrusting of Indian continental lithosphere beneath Tibet, Geology, Vol.10, 179-185.

Bird, P., 1989, New finite element techniques for modeling deformation histories of continents with stratified temperature-dependent rheology, J. Geophys. Res., Vol.94, 3967-3990.

Bird, P., 1991, Lateral extension of lower crust from under high topography, in the isostatic limit, J. Geophys. Res., Vol.96, 10275-10286.

Bird, P. and X. Kong, 1991, First accurate thin-plate models with faults, in AGU 1991 Fall Meeting Program & Abstracts, pp.121.

Bird, P. and K. Piper, 1980, Plane-stress finite element models of tectonic

flow in southern California, Phys. Planet. Intern., Vol.21, 158-175.

Bolt, B.A. and R.A. Uhrhammer, 1975, Resolution techniques for density and heterogeinity in the Earth, Geophys. J. R. Astron. Soc. Vol.42, 419-435.

Bott, M.H.P., 1982, The Interior of the Earth: Its Structure, Constitution and Evolution, Edward Arnold, London, 403 pp.

Bott, M.H.P. and N.J. Kusznir, 1979, Stress distribution associated with compensated plateau uplift structures with application to continental splitting mechanism, Geophys. J. R. Astron. Soc., Vol.56, 451-459.

Bott, M.H.P. and N.J. Kusznir, 1984, The origin of tectonic stress in the lithosphere, Tectonophysics, Vol.105, 1-13.

Brown, L. D., C. E. Chapin, A. R. Sanford, S. Kaufman and J. Oliver, 1980, Deep structure of the Rio Grande Rift from seismic reflection profiling, J. Geophys. Res., Vol.85, 4773-4800.

Buck, W.R., 1986, Small-scale convection induced by passive rifting: the cause for uplift of rift shoulders, Earth Planet. Sci. Lett., Vol.77, 362-372.

Buck, W.R., 1991, Modes of continental lithospheric extension, J. Geophys. Res., Vol.96, 20161-20178,

Burchfiel, B. C., 1980, Tectonics of non-collisional regimes — the modern Andes and the Mesozoic Cordilleran orogen of the Western United States, In: B. C. Burchfiel (ed) Continental Tectonics, 65-72, National Academy of Sciences.

Burke, K. and J. F. Dewey, 1973, Plume generated triple junctions: key indicators in applying plate tectonics to old rocks, J. Geol., Vol.81, 406-433.

Carslaw, H. S., and J. C. Jaeger, 1959, Conduction of Heat in Solids, Oxford.

Carson, M. A. and M. J. Kirkby, 1972, Hillslope Form and Processes, Cambridge University press, New York, 475pp.

Chang, C. et al., 1986, Preliminary conclusions of the Royal Society and Academia Sinica 1985 geotraverse of Tibet, Nature, Vol.323, 501-507.

Cohen, S. C. and R. C. Morgan, 1986, Intraplate deformation due to continental collision: a numerical study of deformation in a thin viscous sheet, Tectonophysics, Vol.132, 247-259.

Condie, K.C., 1982, Plate Tectonics and Continental Drift, Pergamon Press, Oxford.

Coney, P.J., 1971, Cordilleran tectonic transitions and motion of the North American plate, Nature, Vol.233, 462-465.

Coney, P.J., 1978, Mesozoic-Cenozoic Cordilleran plate tectonics, In: Smith, R.B. & G.I. Eaton (eds) Cenozoic Tectonics and Regional Geophysics of the Western Cordillera, Mem. Geol. Soc. Am., Vol.152, 33-50.

Coney, P.J., 1987, The regional tectonic setting and possible cause of Cenozoic extension in the North American Cordillera, From: Coward, M.P., J.F. Dewey and P.L. Hancock (eds), Continental Extensional Tectonics, Geological Society Special Publication No.28, 177-186.

Coney, P.J. and T.A. Harms, 1984, Cordilleran metamorphic core complexes: Cenozoic extensional relics of Mesozoic compression, Geology, Vol.12, 550-554.

Coney, P.J. and S.J. Reynolds, 1977, Cordilleran Benioff zones, Nature, Vol.270, 403-406.

Christensen, U.R., 1992, An Eulaerian techneque for thermomechanical modelling of lithospheric extension, J. Geophys. Res., Vol.97, 2015-2036.

Dalmayrac, B., P. Molnar, 1981, Parallel thrust and normal faulting in Peru, and Constraints on the state of stress, Earth Planet. Sci. Lett., Vol.55, 473-481.

Davy, P., A. Sornette and D. Sornette, 1990, Some consequences of a proposed fractal nature of continental faulting, Nature, Vol.348, 56-58.

Dewey, J. F. and K. C. A. Burke, 1973, Tibetan, Variscan, and Precambrian basement reactivation: products of continental collision, J. Geol., Vol.81, 683-692.

Dunbar, J.A. and D. Sawyer, 1989, How preexisting weaknesses control the style of continental breakup, J. Geophys. Res., Vol.94, 7278-7292.

Eaton, G.P., 1982, The Basin and Range province: Origin and Tectonics significance, Ann. Rev. Earth. Planet. Sci., Vol.10, 409-440.

Ekström, G. and P. England, 1989, Seismic strain rates in regions of distributed continental deformation, J. Geophys. Res., Vol.94, 10321- 10257.

Elsasser, W.M., 1971, Sea-floor spreading as thermal convection, J. Geophys. Res., Vol.76, 1101-1112.

England, P., 1983, Constraints on extension of continental lithosphere, J. Geophys. Res., Vol.88, 1145-1152.

England, P. and G. Houseman, 1988, The mechanics of the Tibetan Plateau, In R. M. Shackleton, J. F. Dewey and B. F. Windley (eds), Tectonic evolution of the Himalayas and Tibet, Phil. Trans. R. Soc. Lond. A326, 301-318.

England, P., G. Houseman and L. Sonder, 1985, Length scales for continental deformation in convergent, divergent, and strike-slip environments: analytical and approximate solutions for a thin viscous sheet model, J. Geophys. Res., Vol.90, 3351-3357.

England, P. and J. Jackson, 1989, Active deformation of the continents, Ann. Rev, Earth Planet. Sci., Vol.17, 197-226.

England, P. C., and D. P. McKenzie, 1982, A thin viscous sheet model for continental deformation, Geophys. J. R. Astron. Soc., Vol.70, 295-321

England, P. C., and D. P. McKenzie, 1983, Correction to: A thin viscous sheet model for continental deformation, Geophys. J. R. Astron. Soc., Vol.73, 523-532

England, P. and S. W. Richardson, 1977, The influence of erosion upon the mineral facies of rocks from different metamorphic environment, J. Geol. Soc. London, Vol.134, 201-213.

Fairhead, J.D. and R.W. Girdler, 1971, The seismicity of Africa, Geophys. J. R. Astron. Soc., Vol.24, 271-301.

Fleitout, L. and C. Froidvaux, 1982, Tectonic and topography for a lithosphere containing density heterogeneities, Tectonics, Vol.1, 21-56.

Fleitout, L. and C. Froidevaux, 1983, Tectonic stresses in the lithosphere, Tectonics, Vol.2, 315-324.

Fletcher, R.C. and B. Hallet, 1983, Unstable extension of the lithosphere: A mechanical model for Basin and Range structure, J. Geophys. Res., Vol.88, 7457-7466.

Forsyth, D. and S. Uyeda, 1975, On the relative importance of the driving forces of plate motion, Geophys. J. R. Astron. Soc., Vol.43, 163 -200.

Froidevaux C. and B. Isacks, 1984, The mechanical state of the lithosphere beneath the Altiplano-Puna segment of the Andes, Earth Planet. Sci. Lett., Vol.71, 305-314.

Froidevaux, C. and Y. Ricard, 1987, Tectonic evolution of high plateaus, Tectonophysics, Vol.134, 227-238.

Garfunkel, Z. and Y. Bartov, 1977, The tectonics of Suez Rift, Bull. Geol. Surv. Israel, Vol.71, 1-44.

Gregory, J. W., 1921, The rift valleys and geology of East Africa, Macmillian, New York, 479pp.

Hamilton, W., 1987, Crustal extension in the Basin and Range province,

southwestern United States, From Coward, M.P., J.F. Dewey and P.L. Hancock (eds), Continental Extensional Tectonics, Geological Society Special Publication No.28, 155-176.

Haskell, N. A., 1935, The motion of a viscous fluid under a surface load, Physics, Vol.6, 265-269.

Hirn, A. et al., 1984a, Crustal structure and variability of the Himalayan border of Tibet, Nature, Vol.307, 23-25.

Hirn, A. et al., 1984b, Lhasa block and bordering sutures - a continuation of a 500 km Moho traverse through Tibet, Nature, Vol.307, 25-27.

Houseman, G. and P. England, 1986, Finite strain calculation of continental deformation 1: method and general results for convergent zones, J. Geophys. Res., Vol.91, 3651-3663.

Houseman, G. and D. McKenzie and P. Molnar, 1981, Convective instability of a thickened boundary layer and its relevance for the thermal evolution of continental convergence belts, J. Geophys. Res., Vol.86, 6115-6132.

Jackson, J. and D. P. McKenzie, 1988, The relationship between plate motions and seismic moment tensors, and the rates of active deformation in the Mediterranean and Middle East, Geophys. J. R. Astron. Soc., Vol.93, 45-71.

Jacobs, J.A., R.D. Russell, and J.T. Wilson, 1974, Physics and Geology, 2nd ed., McGraw-Hill, New York.

Jarvis, G. and D. McKenzie, 1980, Sedimentary basin formation with finite extension rates, Earth Planet. Sci. Lett., Vol.48, 42-52.

Jeffreys, H., 1924, The Earth, Cambridge University Press.

Kruse, S., M. McNutt, J. Phipps-Morgan, and L. Royden, 1991, Lithospheric extension near Lake Mead, Nevada: a model for ductile flow in the lower crust, J. Geophys. Res., Vol.96, 4435-4456.

Kusznir, N.J. and M.P. Bott, 1977, Stress concentration in the upper

llithosphere caused by underlying visco-elastic creep, Tectonophysics, Vol.43, 247-256.

Kusznir, N.J. and D.H. Matthews, 1988, Deep seismic reflections and the deformational mechanics of continental lithosphere, J. Petrl., Special Lithosphere Issue, 63-87.

Kusznir, N.J. and R.G. Park, 1984, Intraplate lithosphere deformation and the strength of the lithosphere, Geophys. J. R. Astron. Soc., Vol.79, 513-536.

Kusznir, N.J. and R.G. Park, 1987, The extensional strength of the continental lithosphere: its dependence on geothermal gradient, and crustal composition and thickness, From Coward, M.P., J.F. Dewey and P.L. Hancock (eds), Continental Extensional Tectonics, Geological Society Special Publication No.28, 35-52.

Lin, J. and Parmentier, E. M., 1990, A finite amplitude necking model of rifting in brittle lithosphere, J. Geophys. Res., Vol.95, B4, 4909-4923.

Lin, J. and D. R. Watts, 1988, Palaeomagnetic constraints on Himalayan Tibetan tectonic evolution, In R. M. Shackleton, J. F. Dewey and B. F. Windley (eds), Tectonic evolution of the Himalayas and Tibet, Phil. Trans. R. Soc. Lond. A326, 177-188.

Logatchev, N. A. and N. G. Florensov, 1978, The Baikal system of rift valleys, Tectonophysics, Vol.45, 1-13.

Lynch, H. and P. Morgan, 1990, Finite-element models of continental extension, Tectonophysics, Vol.174, 115-135.

Ma, X. and D. Wu, 1987, Cenozoic extensional tectonics in China, Tectonophysics, Vol.133, 243-255.

McKenzie, D. P., 1969, Speculations on the consequences and causes of plate motion, Geophys. J. R. Astron. Soc., Vol.18, 1-32.

McKenzie, D. P., 1978, Some remarks on the development of sedimentary

basins, Earth Planet. Sci. Lett., Vol.40, 25-32

Mercier, J., R. Armijo, P. Tapponnier, E. Carey-Gail and T. Han, 1987, Change from late Tertiary compression to Quaternary extension in Southern Tibet during the India-Asia collision, Tectonics, Vol.6, 275-304.

Molnar, P., 1984, Structure and tectonics of the Himalaya, Ann. Rev. Earth Planet. Sci., Vol.12, 489-512.

Molnar, P. and W. Chen, 1982, Seismicity and mountain building, In: Hsu, K. G. (ed) Mountain Building Processes, 41-57, Academic Press, London.

Molnar, P. and W. Chen, 1983, Focal depths and fault plane solutions of earthquake under the Tibetan plateau, J. Geophys. R., Vol.88, 1180-1190.

Molnar, P. and Tapponnier, 1975, Cenozoic tectonics of Asia: Effects of a continental collision, Science, Vol.189, 419-426.

Molnar, P. and P. Tapponnier, 1978, Active tectonics of Tibet, J. Geophys. Res., Vol.83, 5361-5375.

Morgan, P., W.R. Seager and M.P. Golombek, 1986, Cenozoic thermal, mechanical and tectonic evolution of the Rio Grande Rift, J. Geophys. Res., Vol.91, 6263-6276.

Murrell, S.A.F., 1986, Mechanics of tectogenesis in plate collision zones, from Coward, M.P. & Ries, A.C.(eds), Collision Tectonics, Geological Society Special Publication No.19, 95-111.

Nataf, H., C. Froidevaux, J. Levrat, and M. Rabinowicz, 1981, Laboratory convection experiments: effect of lateral cooling and generation of instabilities in the horizontal boundary layers, J. Geophys. Res., Vol.86, 6143-6154.

Neugebauer, H. J., 1978, Crustal doming and the mechanism of rifting, Tectonophysics, Vol.45, 159-186.

Neumann, E. R. and I. B. Ramberg, 1978, Paleorifts — concluding remarks, In

Neumann, E. R. and I. B. Ramberg (eds) Tectonics and Geophysics of Continental Rifts, 409-424, D. Reidel, Dordrecht, Holland.

Patriat, P. and J. Achache, 1984, India-Eurasia collision chronology has implications for crustal shortening and driving mechanism of plates, Nature, Vol.311, 615-621.

Powell, C., 1986, Continental underplating model for the rise of the Tibetan Plateau, Earth Planet. Sci. Lett., Vol.81, 79-94.

Powell, C.McA. and P. J. Conaghan, 1973, Plate tectonics and the Himalayas, Earth Planet. Sci. Lett., Vol.20, 1-12.

Powell, C.McA. and P. J. Conaghan, 1975, Tectonic models of the Tibetan Plateau, Geology, Vol.20, 727-731.

Price, N. J., G. D. Price and S. L. Price, 1988, Gravity glide and plate tectonics, In Audley-Charles, M. and A. Hallam (eds) Gondwana and Tethys, Geological Society Special Publication No.37, 5-21.

Ranalli, G., 1987, Rheology of the Earth: deformation and flow processes in geophysics and geodynamics, Allen & Uwin, Boston, 366pp.

Richardson, R. M., S. C. Soloman and N. H. Sleep, 1979, Tectonic stress in the plates, Rev. Geophys. Space Phys., Vol.17, 981-1019.

Robson, D.A.Q., 1971, The structure of the Gulf of Suez (Clysmic) rift, J. Geol. Soc. Lond., Vol.127, 247-276.

Searle, R. C., 1970, Evidence from gravity anomalies for thinning of the lithosphere beneath the rift valley in Kenya, Geophys. J. R. Astron. Soc., Vol.21, 13-31.

Sengör, A.M.C., and K. Burke, 1978, Relative timing of rifting and volcanism on earth and its tectonic implications, Geophys. Res. Lett., 5(6):419-421.

Sengör, A.M.C., and W. S. F. Kidd, 1979, Post-collisional tectonics of the Turkish-Iranian Plateau and a comparison with Tibet, Tectonophysics,

Vol.55, 361-376.

Sonder, L. and P. England, 1986, Vertical averages of rheology of the continental lithosphere: relation to thin sheet parameters, Earth Planet. Sci. Lett., Vol.77, 81-90.

Sonder, L. J., and England, P. C., 1989, Effects of a temperature dependent rheology on large scale continental extension, J. Geophys. Res., Vol.94, No.B6, 7603-7619.

Sonder, L.J., P. England, B.P. Wernicke and R.L. Christiansen, 1987, A physical model for Cenozoic extension of western North America, From Coward, M.P., J.F. Dewey and P.L. Hancock (eds), Continental Extensional Tectonics, Geological Society Special Publication No.28, 187-201.

Steckler, M.S., 1985, Uplift and extension at the Gulf of Suez: indications of induced mantle convection, Nature, Vol.317, 135-139.

Stewart, J. H., 1978, Basin-range structure in western North America: A review, Geol. Soc. America Mem. 152:1-30.

Stuwe, K., 1991, Flexural constraints on the denudation of asymmetric mountain belts, J. Geophys. Res., Vol.96, 10401-10408.

Sykes, L. R., 1978, Intra-plate seismicity, reactivation of pre-existing zones of weakness, alkaline magmatism and other tectonism post-dating continental fragmentation, Rev. Geophys. Space Phys., Vol.16, 621-688.

Tapponnier, P., J. L. Mercier, R. Armijo, T. Han and J. Zhou, 1981, Field evidence for active normal faulting in Tibet, Nature, Vol.294, 410-414.

Tapponnier, P. & Molnar, P., 1976, Slip-line field theory and large-scale continental tectonics, Nature, Vol.264, 319-324.

Tapponnier, P. & Molnar, P., 1977, Active faulting and tectonics in China, J. Geophys. Res., Vol.82, 2905-2930.

Tapponnier, P., Peltzer, G. & Armijo, R., 1986, On the mechanics of the

collision between India and Asia, from Coward, M.P. & Ries, A.C.(eds), Collision Tectonics, Geological Society Special Publication No.19, 115-157.

Tapponnier, P., C., Peltzer, A. Y. Le Dain, R. Armijo and P. Cobbold, 1982, Propagating extrusion tectonics in Asia: new insights from simple experiments with plasticine, Geology, Vol.10, 611-616.

Taylor, F. B., 1910, Bearing of the Tertiary mountain belt on the origin of the earth's plan, Bull. Geol. Soc. Amer., Vol.21, 179-226.

Toit, A., 1937, Our Wandering Continents, Oliver and Boyd, Edinburgh.

Turcotte, D., and S. Emerman, 1983, Mechanisms of active and passive rifting, Tectonophysics, Vol.94, 39-50.

Turcotte, D. L. and E. R. Oxbough, 1973, Mid-plate tectonics, Nature, Vol.244, 337-339.

Vilotte, J.P., M. Daignieres, R. Madariaga, 1982, Numerical modeling of intraplate deformation: Simple mechanical models of continental collision, J. Geophys. Res., Vol.87, 10709-10728.

Vilotte, J.P., R. Madaraga, M. Daignieres, and O. Zienkiewicz, 1986, Numerical study of continental collsion: Influence of buoyancy forces and an initial stiff inclusion, Geophys. J. R. Astron. Soc., Vol.84, 279-310.

Vink, G.E., W. Morgan and W. Zhao, 1984, Preferential rifting of continents: A source of displaced terranes, J. Geophys. Res., Vol.89, 10072-10076.

Vita-Finzi, C., 1991, Holocene deformation chronology of the Arabian plate, In IUGG 20th General Assembly Program and Abstracts (IASPEI), pp.163.

Wang, C., Y. Shi and W. Zhou, 1982, Dynamic uplift of the Himalaya, Nature, Vol.298, 553-556.

Wdowinski, S., R. O'Connell and P. England, 1989, A continuum model of continental deformation above subduction zones: Application to the Andes and the Aegean, J. Geophys. Res., Vol.94, 10331-10346.

Wdowinski, S. and R. O'Connell, 1991, Deformation of the Central Andes (15 -27 S) derived from a flow model of subduction zones, J. Geophys. Res., Vol.96, 12245-12255.

Wegener, A., 1912, The origin of continents, Petermanns Geog. Mitteilungen, Vol.58, pp 185-195, 253-256, 305-309.

Wernicke, B., 1984, Uniform-sense normal simple shear of the continental lithosphere, Can. J. Earth. Sci., Vol.22, 108-125.

Wilson, J.T., 1968, Static or mobile earth: the current scientific revolution, Am. Philos. Soc. Proc., Vol.112, 309-320.

Windley, B. F., 1985, The Himalayas, Geology Today, Vol.1, 169-173.

Zhao, L. and D. Helmberger, 1991, Geophysical implications from relocations of Tibetan earthquakes: Hot lithosphere, Geophys. Res. Lett., Vol.18, 2205-2208.

Zhu, J., 1991, Evidence from lithosphere structure studies for plates in China, In IUGG 20th General Assembly Program and Abstracts (IASPEI), pp.79.

Zoback, M.L., R.E. Anderson, and G.A. Thompson, 1981, Cainozoic evolution of the state of stress and style of tectonism of the Basin and Range province of the western United States, Philos. Trans. R. Soc. London Ser., Vol.A300, 407-434.

Zuber, M.T. & Parmentier, E.M., 1986, Lithosphere necking: a dynamic model for rift morphology, Earth Planet. Sci. Lett., Vol.77, 373-383.

Zuber, M.T., E.M. Parmentier, and R.C. Fletcher, 1986, Extension of continental lithosphere: A model for two scales of Basin and Range deformation, J. Geophys. Res., Vol.91, 4826-4838.

Suppose a lithosphere is stretched (or shortened) instantaneously by a factor β. The temperature of the lithosphere increases linearly with depth before and after the instantaneous deformation. The temperature of the asthenosphere is constant. The temperature and pressure of the lithosphere and the asthenosphere are illustrated in Figure A-1.

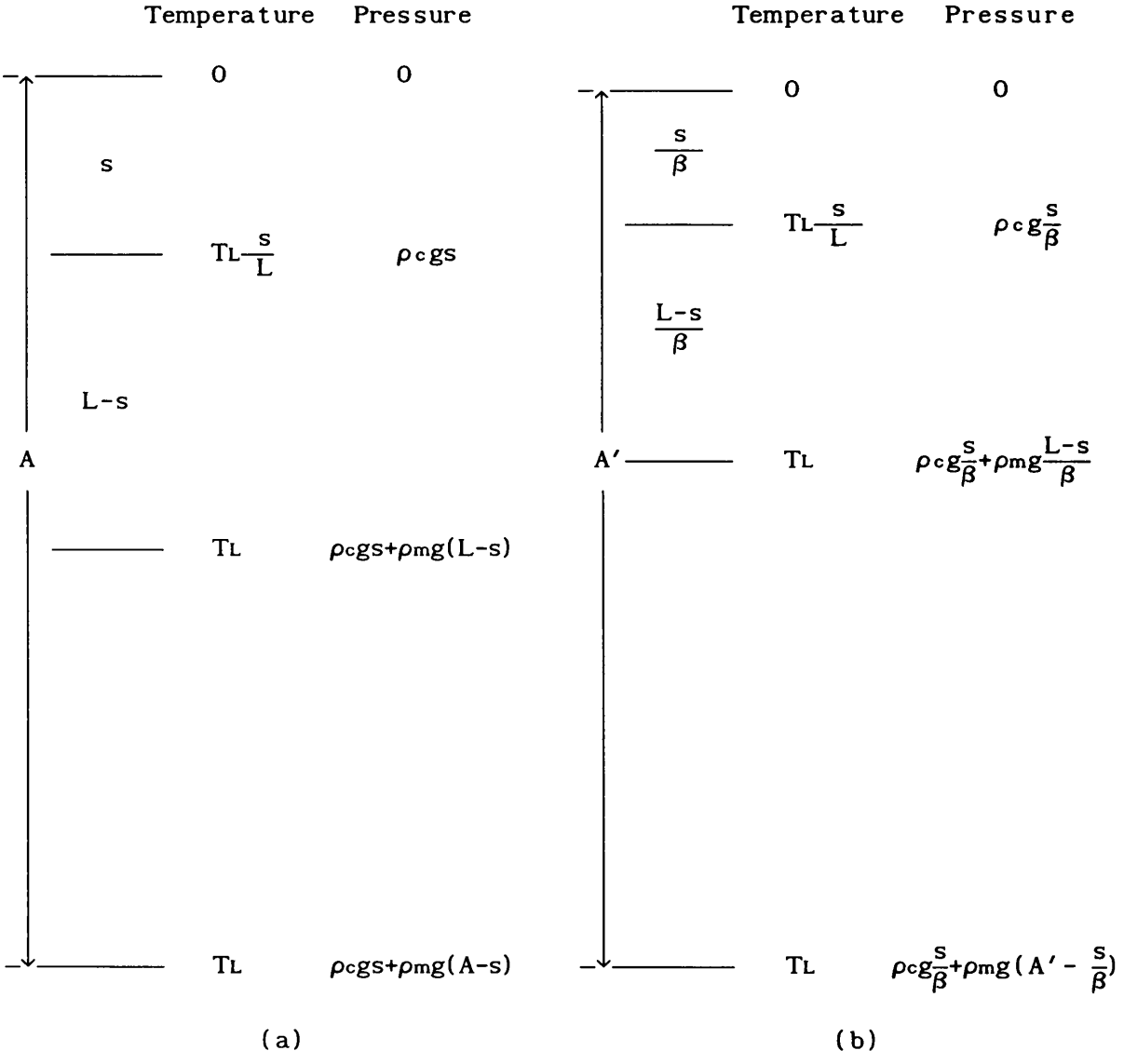

Figure A-1. The temperature and pressure in the lithosphere and the asthenosphere (a) before and (b) after instantaneous deformation.

Before stretching, the density of the crust at the top surface is ρ_c, the density of the crust at the Moho is

$$\rho_{cM} = \rho_c(1-\alpha T_m+\lambda\rho_c gs)$$

$$= \rho_c(1-\alpha T_L\frac{s}{L} + \lambda\rho_c gs)$$

in which T_m is the temperature at the Moho surface, T_L is the temperature at the bottom of the lithosphere, s is the thickness of the crust, L the thickness of the lithosphere, α the thermal expansion coefficient, λ the coefficient showing the change of density under pressure.

The density of the lithosphere mantle at the Moho is

$$\rho_{mM} = \rho_m(1-\alpha T_L\frac{s}{L} + \lambda\rho_c gs)$$

where ρ_m is the density of the mantle material at the temperature and pressure of the top of the lithosphere.

And the density of the lithosphere mantle (and also the density of the asthenosphere) at the bottom of the lithosphere is

$$\rho_{mL} = \rho_m[1-\alpha T_L + \lambda\rho_c gs + \lambda\rho_m g(L-s)]$$

The density of the asthenosphere at the compensation depth is

$$\rho_{mA} = \rho_m[1-\alpha T_L + \lambda\rho_c gs + \lambda\rho_m g(A-s)]$$

where A is the level of the surface relative to the compensation depth.

The mass of the column above the compensation level is then

$$M = \frac{s}{2}(\rho_c + \rho_{cM}) + \frac{L-s}{2}(\rho_{mM} + \rho_{mL}) + (A-L)\frac{1}{2}(\rho_{mL} + \rho_{mA})$$

$$= \frac{s}{2}\left[\rho_c + \rho_c(1-\alpha T_L\frac{s}{L} + \lambda\rho_c gs)\right]$$

$$+\frac{L-s}{2}\left[\rho_m(1-\alpha T_L\frac{s}{L}+\lambda\rho_c gs)+\rho_m(1-\alpha T_L+\lambda\rho_c gs+\lambda\rho_m gL-\lambda\rho_m gs)\right]$$

$$+(A-L)\frac{1}{2}\left[\rho_m(1-\alpha T_L+\lambda\rho_c gs+\lambda\rho_m gL-\lambda\rho_m gs)+\rho_m(1-\alpha T_L+\lambda\rho_c gs+\lambda\rho_m gA-\lambda\rho_m gs)\right]$$

After stretching by an amount β, the density of the crust at the Moho is

$$\rho'_{cM}=\rho_c(1-\alpha T_L\frac{s}{L}+\lambda\rho_c g\frac{s}{\beta})$$

The density of the lithosphere mantle at the Moho is

$$\rho'_{mM}=\rho_m(1-\alpha T_L\frac{s}{L}+\lambda\rho_c g\frac{s}{\beta})$$

The density of the lithosphere mantle at the bottom of the lithosphere (and also that of the asthenosphere) is

$$\rho'_{mL}=\rho_m(1-\alpha T_L+\lambda\rho_c g\frac{s}{\beta}+\lambda\rho_m g\frac{L-s}{\beta})$$

The density of the asthenosphere at the compensation depth is

$$\rho'_{mA}=\rho_m\left[1-\alpha T_L+\lambda\rho_c g\frac{s}{\beta}+\lambda\rho_m g(A'-\frac{s}{\beta})\right]$$

where A' is the new level of the top surface relative to the compensation level.

The mass of the column above the same compensation level is then

$$M'=\frac{s}{\beta}\frac{1}{2}(\rho_c+\rho'_{cM})+\frac{L-s}{2\beta}(\rho'_{mM}+\rho'_{mL})+(A'-\frac{L}{\beta})\frac{1}{2}(\rho'_{mL}+\rho'_{mA})$$

$$=\frac{s}{\beta}\frac{1}{2}\left[\rho_c+\rho_c(1-\alpha T_L\frac{s}{L}+\lambda\rho_c g\frac{s}{\beta})\right]$$

$$+\frac{L-s}{2\beta}\left[\rho_m(1-\alpha T_L\frac{s}{L}+\lambda\rho_c g\frac{s}{\beta})+\rho_m(1-\alpha T_L+\lambda\rho_c g\frac{s}{\beta}+\lambda\rho_m g\frac{L}{\beta}-\lambda\rho_m g\frac{s}{\beta})\right]$$

$$+(A'-\frac{L}{\beta})\frac{1}{2}\left[\rho_m(1-\alpha T_L+\lambda\rho_c g\frac{s}{\beta}+\lambda\rho_m gA'-\lambda\rho_m g\frac{s}{\beta})+\rho_m(1-\alpha T_L+\lambda\rho_c g\frac{s}{\beta}+\lambda\rho_m gA'-\lambda\rho_m g\frac{s}{\beta})\right]$$

The masses of the two columns are equal, $M = M'$, so

$$\frac{s}{2}\left[\rho_c + \rho_c(1-\alpha T_L\frac{s}{L} + \lambda\rho_c g s)\right]$$

$$+ \frac{L-s}{2}\left[\rho_m(1-\alpha T_L\frac{s}{L} + \lambda\rho_c g s) + \rho_m(1-\alpha T_L + \lambda\rho_c g s + \lambda\rho_m g L - \lambda\rho_m g s)\right]$$

$$+(A-L)\frac{1}{2}\left[\rho_m(1-\alpha T_L + \lambda\rho_c g s + \lambda\rho_m g L - \lambda\rho_m g s) + \rho_m(1-\alpha T_L + \lambda\rho_c g s + \lambda\rho_m g A - \lambda\rho_m g s)\right]$$

$$= \frac{s}{\beta}\frac{1}{2}\left[\rho_c + \rho_c(1-\alpha T_L\frac{s}{L} + \lambda\rho_c g\frac{s}{\beta})\right]$$

$$+ \frac{L-s}{2\beta}\left[\rho_m(1-\alpha T_L\frac{s}{L} + \lambda\rho_c g\frac{s}{\beta}) + \rho_m(1-\alpha T_L + \lambda\rho_c g\frac{s}{\beta} + \lambda\rho_m g\frac{L}{\beta} - \lambda\rho_m g\frac{s}{\beta})\right]$$

$$+(A' - \frac{L}{\beta})\frac{1}{2}\left[\rho_m(1-\alpha T_L + \lambda\rho_c g\frac{s}{\beta} + \lambda\rho_m g A' - \lambda\rho_m g\frac{s}{\beta}) + \rho_m(1-\alpha T_L + \lambda\rho_c g\frac{s}{\beta} + \lambda\rho_m g A' - \lambda\rho_m g\frac{s}{\beta})\right]$$

After some algebra, the above equation can be rewritten as

$$A' - A = \frac{(1-\frac{1}{\beta})\left[s(\rho_c-\rho_m)(1-\frac{\alpha}{2}T_L\frac{s}{L}) + \frac{\alpha}{2}\rho_m L T_L + (1+\frac{1}{\beta})\frac{1}{2}\lambda g s^2(\rho_c-\rho_m)^2 + A\rho_m\lambda(\rho_c-\rho_m)gs\right]}{\rho_m\left[1-\alpha T_L + \frac{1}{2}\lambda\rho_m g(A+A') + \frac{1}{\beta}\lambda(\rho_c-\rho_m)gs\right]}$$

From this formula, with reasonable values for λ, it can be easily found that terms involving λ are of secondary importance and are therefore negligible. Hence, in calculating the vertical displacement due to stretching or shortening, the lithosphere and the asthenosphere can be treated as incompressible.

Stretching occurring over a finite time, rather than instantaneously, can be divided into a number of steps. In each step instantaneous stretching is followed by thermal contraction or expansion. Thus the above

conclusion still holds.

If $\lambda = 0$, i.e., the effect of pressure is neglected, there is

$$A'-A = \frac{(1-\frac{1}{\beta})\left[s(\rho_c-\rho_m)(1-\frac{\alpha}{2}T_L\frac{s}{L})+\frac{\alpha}{2}\rho_m L T_L\right]}{\rho_m(1-\alpha T_L)}$$

which is actually the formula given by McKenzie (1978) to calculate basin subsidence (without water filling) due to stretching.